2008

FABRICATION AND CHARACTERIZATION OF MOLECULAR SPINTRONICS DEVICES

Pawan Tyagi
University of Kentucky, tyagi.pawan@gmail.com

ABSTRACT OF DISSERTATION

Pawan Tyagi

The Graduate School

University of Kentucky

2008

FABRICATION AND CHARACTERIZATION OF MOLECULAR SPINTRONICS DEVICES

ABSTRACT OF DISSERTATION

A dissertation submitted in partial fulfillment of the
requirements for the degree of Doctor of Philosophy in the
College of Engineering
at the University of Kentucky

By
Pawan Tyagi

Lexington, Kentucky

Director: Dr. Bruce J. Hinds, William Bryan Professor of Materials Engineering

Lexington, Kentucky

2008

ABSTRACT OF DISSERTATION

FABRICATION AND CHARACTERIZATION OF MOLECULAR SPINTRONICS DEVICES

Fabrication of molecular spin devices with ferromagnetic electrodes coupled with a high spin molecule is an important challenge. This doctoral study concentrated on realizing a novel molecular spin device by the bridging of magnetic molecules between two ferromagnetic metal layers of a ferromagnetic-insulator-ferromagnetic tunnel junction on its exposed pattern edges. At the exposed sides, distance between the two metal electrodes is equal to the insulator film thickness; insulator film thickness can be precisely controlled to match the length of a target molecule. Photolithography and thin-film deposition were utilized to produce a series of tunnel junctions based on molecular electrodes of multilayer edge molecular electrodes (MEME) for the first time. In order to make a microscopic tunnel junction with low leakage current to observe the effect of ~10,000 molecules bridged on the exposed edge of a MEME tunnel barrier, growth conditions were optimized; stability of a ~2nm alumina insulator depended on its ability to withstand process-induced mechanical stresses. The conduction mechanism was primarily 1) tunneling from metal electrode to oranometalic core by tunneling through alkane tether that acts as a tunnel barrier 2) rapid electron transfer within the oranometalic Ni-CN-Fe cube and 3) tunneling through alkane tether to the other electrode. Well defined spin-states in the oranometalic Ni-CN-Fe cube would determine electron spin-conduction and possibly provide a mechanism for coupling.

MEME with Co/NiFe/AlOx/NiFe configurations exhibited dramatic changes in the transport and magnetic properties after the bridging of oranometalic molecular clusters with S=6 spin state. The molecular cluster produced a strong antiferromagnetic coupling between two

ferromagnetic electrodes to the extent, with a lower bound of 20 erg/cm,^{2} that properties of individual magnetic layers changed significantly at RT. Magnetization, ferromagnetic resonance and magnetic force microscopy studies were performed. Transport studies of this configuration of MEME exhibited molecule-induced current suppression by ~6 orders by blocking both molecular channels and tunneling between metal leads in the planar 25μm^2 tunnel junction area. A variety of control experiments were performed to validate the current suppression observation, especially critical due to observed corrosion in electrochemical functionalization step. The spin devices were found to be sensitive to light radiation, temperature and magnetic fields.

Along with the study of molecular spin devices, several interesting ideas such as ~9% energy efficient ultrathin TaOx based photocell, simplified version of MEME fabrication, and chemical switching were realized. This doctoral study heralds a novel molecular spin device fabrication scheme; these molecular electrodes allow the reliable study of molecular components in molecular transport.

KEYWORDS: Molecular Spintronics; Magnetic Tunnel Junctions; Molecular Electronics; Photovoltaic Cell; Spin Transport; Magneto Resistance.

Pawan Tyagi

10th April, 2008

FABRICATION AND CHARACTERIZATION OF MOLECULAR SPINTRONICS DEVICES

By

Pawan Tyagi

Lexington, Kentucky

Dr. Bruce J. Hinds
Director of Dissertation

Dr. Douglass Kalika
Director of Graduate Studies

Date: 10th April, 2008

RULES FOR THE USE OF DISSERTATIONS

Unpublished dissertations submitted for the Doctor's degree and deposited in the University of Kentucky Library are as a rule open for inspection, but are to be used only with due regard to the rights of the authors. Bibliographical references may be noted, but quotations or summaries of parts may be published only with the permission of the author, and with the usual scholarly acknowledgements.

Extensive copying or publication of the dissertation in whole or in part also requires the consent of the Dean of the Graduate School of the University of Kentucky.

A library that borrows this dissertation for use by its patrons is expected to secure the signature of each user.

Name	Date

DISSERTATION

Pawan Tyagi

The Graduate School
University of Kentucky
2008

FABRICATION AND CHARACTERIZATION OF MOLECULAR SPINTRONICS DEVICES

DISSERTATION

A dissertation submitted in partial fulfillment of the
requirements for the degree of Doctor of Philosophy in the
College of Engineering
at the University of Kentucky

By
Pawan Tyagi

Lexington, Kentucky

Director: Dr.Bruce J. Hinds, William Bryan Professor of Materials Engineering

Lexington, Kentucky

2008

This doctoral study is dedicated to my beloved family members:
My grand father late Ramanand Tyagi

My father Raj Bahadur Tyagi

My mother Chanderwati Tyagi

& my wife Punam Tyagi

ACKNOWLEDGEMENTS

This doctoral study has been possible due to many persons who directly and indirectly helped me progress in the right direction. In the first place, I am deeply grateful to Prof. Bruce J. Hinds for granting me an exciting PhD topic and for mentoring the subsequent research efforts. I respectfully appreciate his role in honing my experimental and analytical skills, giving me freedom to try new ideas and patiently supporting me during numerous struggles. I had a deeply satisfying learning period in his lab. I am thankful to the Air Force Office of Scientific Research and Kentucky Science and Engineering Foundation (KSEF-621-RDE-006 and KSEF-992-RDE-008) for funding this thesis work.

Thanks are due to administrators and staff of Center of Nanoscience and Engineering. I am grateful to an accomplished technician late Mr. George Spiggle, for his invaluable role in accomplishing the critical experiments.

I would like to take the opportunity to thank Prof. Stephen Holmes and Dr. Dong Feng Li for the synthesis of excellent molecular compounds. I am indebted to my lab mate, Mr. Bing Hu, for his conscientious help and camaraderie. I am grateful to Prof. Gang Cao, Dr. Vinobalan Durairaj and Ms. Shalinee Chikara for help with insightful magnetization studies. It is an immense pleasure to thank Prof. A.F. Miller for training me on FMR setup and giving me access to her lab. Appreciations are due to Dr. Hequing Huang and Dr. Song for equipping me with much needed knowledge of AFM. I am indebted to Prof. J. Todd Hasting for numerous insightful suggestions and help with spectroscopic ellipsometry. I like to thank Mr. Peng-Leen Ong for help with the transport and capacitance study. Sincere thanks are due to Prof. Kwok Wei Ng for guidance with low temperature studies and for sparing time to visit our lab to check our setup. I wish to thank Prof J. K. Lumpp for numerous insightful suggestions about wire-bonding. I express my thanks to Prof. John Balk for several astute suggestions about mechanical stress measurements and for giving me access to his sputtering machine.

I express my thanks to the writing center staff at W.T.Young library for refining the quality of this dissertation.

I gratefully acknowledge time spared by Prof. Ganpathy Murthy, Prof. Lance DeLong, Prof. Bruce Apanhar, Prof. Supriyo Datta, Prof. Mark Ratner, Prof. Christian Joachim, Prof Matthew Foulkes, Prof. David Cepereley, Prof. Mark S. Hybertsen, Prof. Igor Zutic, Prof. Sam Bader, Prof. Ivan Schuller, Prof. J.M.D. Coey and Prof. Arthur J. Epstein for giving their opinions and suggestions about some of the complex results we observed during this doctoral study.

I am thankful to former lab mate Dr. Nitin Chopra for introducing me to Prof. Hinds. Much assistance and a vibrant lab environment produced by the company of Mr. Dinesh Kalyansundaram, Dr. Mainak Mazumdar, Dr. Kerin Keis, Dr. Wu Ji, Ms. Karen Gerstandt, Mr. Xin Zhan, and Mr. Xin Xu are much appreciated.

I take pleasure in acknowledging Dr. Anjali Mishra, Dr. Mridu Pawan Deka, Ms. Shalinee Chikara, and Mr. Rupak Datta for making mine and my family's stay in Lexington during this Ph.D a pleasant experience.

I am indebted to a number of friends who have assisted me in several crucial stages. I thank Rahul Kasat for his moral boosting and practical suggestions. I am honored to acknowledge my friends Mr. Amit Guliani, Dr. Prashant Salwan, Mr. Anand Tiwari, Mr. Ravi Yadav and Mr. Vivek Bhatnagar for their support during my trying time. I thank Mr. Rahul Srivastava for helping me get a great learning opportunity at Midhani. I am grateful to Mr. and Mrs. Srivastava, and their family for providing me a home away from home during my stay in Hyderabad.

It is an immense delight for me to express gratitude to my past teachers who played key roles in motivating me to choose a research career. Firstly, I would like to thank my high school teacher, Mr. Bansi Lal Bagla, for showing me the right direction. I am deeply grateful to the late Prof. A.K. Patwardhan for restoring my interest in research through his excellent teaching and encouragement during my undergraduate study. I thank Prof. A. K. Pant for helping me to explore my potential. I would like to thank the mentors of my master program, Prof. R. Balasubramanium and Prof. Deepak Gupta, for their role in improving my writing and experimental skills. These skills provided a strong foundation I always benefited from.

I wish to thank my special friend and wife, Dr. Punam Tyagi, for her continuous support, understanding and taking extra burden; without her mental and emotional support. I am thankful to my little angel Pranshu Tyagi to bear my long absence from home. I could have not progressed significantly. I thank my in-laws, Mr. Nakli Ram Tyagi and Mrs. Rajeshwari Tyagi, for their mental support and blessings.

I wish to express my respect and gratitude to my grandfather and my childhood friend, Mr. Ramanand Tyagi, who helped me secure my first book for the engineering entrance exam. Finally, I thank my revered father, Mr. Raj Bahadur Tyagi, and my beloved mother, Mrs. Chanderwati Tyagi. I express my gratefulness towards my parents for the struggle they encountered in getting me this far.

TABLE OF CONTENTS

LIST OF TABLES

LIST OF FIGURES

LIST OF FILES

File name	Size
PawanTyagi_Dissertation.pdf	4.0 MB

PREFACE

The central theme of this dissertation is the study of interaction between high spin molecular clusters and the magnetic tunnel junction based multilayer edge molecular electrode (MEME). A MEME is essentially a customized tunnel junction with the desired metal electrodes (ferromagnetic metals for the molecular spin devices) and the exposed sides. Exposed sides, where the molecular dimension distance between two metal electrodes is set by the robust insulator, enable the bridging of molecular channels across insulator. The covalently bridged multiple molecular channels then become the dominant current and spin channels. Molecular channels are found to produce dramatic change in transport and magnetic characteristics of a tunnel junction. Tunnel junctions, utilized as MEME electrode, were produced by the optimization of photolithography and thin film sputter deposition. Few specific tunnel junctions, based on tantalum oxide tunnel barrier, exhibited photovoltaic effect. Findings of the present doctoral study are organized in the form of eight chapter and appendicies. Following is the brief listing of hypothesis and content of individual chapters.

Chapter 1 reviews the molecular conduction mechanisms. Since we studied a number of combinations of new molecule and various electrodes, it was important to understand the various aspects of charge and spin transport through various molecules for the deciphering of results we obtained. Molecule between two metal electrodes can behave like a tunnel barrier or quantum dot.. Due to the electrostatic effects molecular levels undergo significant rearrangement after being between two metal electrodes. How the details of molecular levels, molecular coupling, and charge state of the molecule affect the molecular transport is discussed here.

Chapter 2 discusses the optimization efforts to produce robust alumina to form multilayer edge molecular electrodes. Effect of tensile and compressive stresses on the morphology and tunnel barrier device life was studied. Here we also demonstrated the realization MEME electrode. The exposed side of MEME was produced by the ion milling.

Chapter 3 elaborates photolithography-thin film based molecular electrode fabrication scheme. Molecular clusters produced the similar change in transport of photolithography-liftoff produced MEME as seen with ion milled MEME. Molecular junctions were formed with NiFe, Ni, Au and Ta metals. Number of control experiments, the reversible effect of molecular cluster on MEME transport, effect of the barrier thickness and the effect of unbridgeable-short molecules, were performed. Transport analysis of MEME before and after molecule attachment was performed using Simmons model.

Chapter 4 shows how we further simplified the molecular electrode fabrication scheme. To produce molecular dimension gap between two metal electrodes a segment of Ta electrode was oxidized to form TaOx barrier. Using this approach deposition of alumina insulator, requiring stringent control over deposition parameters, was skipped. In this chapter we present number of molecular electrodes based on Ta/TaOx/Metal configuration.

Chapter 5 is dedicated to the significantly high photovoltaic effect observed on Ta/TaOx/Ta. It was found that TaOx barrier is endowed with atomic defects. Due to the presence of atomic defects ~3nm TaOx was found to absorb light radiation producing electron-hole pair suitable for producing photovoltaic effect. In this chapter we illustrate a number of experiments which were performed to understand the unusually high photovoltaic effect arising from an ultrathin layer TaOx.

Chapter 6 illustrates the effect of magnetic molecular cluster on the magnetic properties of the ferromagnetic- multilayer edge molecular electrode (F-MEME). Molecular clusters produced unprecedented strong antiferromagnetic coupling between two magnetic layers of F-MEME with Co/NiFe/AlOx/NiFe configuration. In this chapter we discuss the magnetization, ferromagnetic resonance and magnetic force microscopy results on F-MEME before and after the bridging of molecular clusters. Understanding about the interaction between molecular clusters and the the magnetic electrodes of F-MEME is helpful in explaining results of chapter 7.

Chapter 7 is about the dramatic change in transport of F-MEME, with Co/NiFe/AlOx/NiFe configuration, after the bridging of magnetic clusters between two ferromagnetic layers. To validate the observation of current suppression by ~6 orders over the complete molecular device (F-MEME +molecular channels) large number of control experiments was performed. In this chapter we describe the details of control experiments. Effect of light radiation, heat and magnetic field on molecular device is also furnished. We present plausible reason behind the current suppression in terms of the equally dramatic change in magnetic ordering of F-MEME produced by the magnetic clusters.

Chapter 8 is the conclusion of this dissertation. Key advantages, major findings and future directions are presented in this chapter.

Chapter 1
Introduction

For the ultimate device miniaturization,[4,5] the few atoms dimensions molecular devices[6,7] have attracted world wide attention. Because of the fact that electronic, optical, and magnetic properties of molecules are easily controlled via synthesis rout,[8,9] new generation devices aim to use a molecule as an active device element.[10] The electric field,[10,11] light radiation[8,12] and magnetic field[13,14] are the promising for controlling the transport of a molecular device. Magnetic field controlled[14] bi-stable molecular devices[15] are being researched extensively due to their possible application in the quantum computation[8] and spin valves.[16] The success and limitations of the conventional spin valves (ferromagnet-nonmagnetic spacer-ferromagnet)[17,18] further emphasize the need of molecular spin valves.[19]

Conventional spin devices, mainly magneto resistance devices,[18] have successfully journeyed from the laboratory to the commercial fabrication stage in an impressively short spell.[20] The irreproducible quality of nm thick nonmagnetic spacers,[17] interface-roughness[21] induced high spin scattering[18] and relatively small spin polarization[17] of ferromagnetic metals are the major hurdles in the advancement of conventional spin devices. There is a growing hope that the replacement of the nonmagnetic spacer with the organic molecule,[22] exhibiting reproducible length[23] and well defined metal-molecule coupling,[11,24] will be helpful in improving the performance of magneto resistance devices.[25] Other striking features, which favor the application of the molecule, in spin devices are the small spin-orbit coupling and hyperfine splitting.[26] Due to this attribute of the molecules, a spin can travel without getting flipped for a longer time and distance,[27] as compared to inorganic counterparts, e.g. metal, insulator and semiconductors.[26] There are various candidate molecules. Impressive success in producing molecular magnets with the wide spectrum of spins states[28] controllable via light radiation[8] and the magnetic field,[29] has fueled the motivation to employ the molecular magnets in the novel molecular devices.[30]

To date only few experimental attempts have been made to produce magnetic-molecular devices.[13,16] In these devices the spin state of the molecule[31] and/or electrode(s)[13] influenced the spin transport of a molecular device. However, there has been a large number of theoretical calculations[20] and good reviews[20] on the scope of molecular spin devices. Theoretical studies have exhibited the possibility of achieving very high magneto resistance.[19] A number of theoretical calculations also suggests the possibility of realizing exotic phenomena[14,32,33] with the advent of advance magnetic molecular junctions.

In this literature review, we begin with the analysis of molecular transport mechanisms,[34,35] especially independent of the spin state of the molecule.[36] In this part there are two sections: the first one considers the molecule as a pure tunneling medium[37] while the second section treats the molecule as a quantum dot.[38] Next, spin dependent transport through a molecular channel[33] and the studies where a spin state of molecular channel actively participated in the molecular transport[39] have been reviewed. We briefly discuss the molecular electrodes design deemed suitable for fabrication of magnetic molecular junctions.[40] Based on this discussion, we tender the rationale behind the molecular electrode fabrication approach taken in present work. Lastly, we present a brief introduction of the research work performed during the present doctoral study.

1.1 Spin-independent molecular conduction mechanisms:

In charge transport though molecules generally molecules act as barriers for incoming electrons from the metal electrode.[41] A great deal of molecular electrodes have been made using alkane molecular channels,[42] which are good examples of the tunneling barriers.[36] In the event that a resourceful molecular channel with conjugated bonds,[23] functional groups,[43] optically active center[8] and magnetic field activated spin states[33] are bridged between the two metal electrodes, molecules are much more than tunnel barriers.[35] In such cases, molecules are akin to quantum dots.[35] However, unlike quantum dots molecules are smaller, and their electronic, optical and magnetic properties are reproducible through a well established synthetic chemistry route.[11] Due to the small size, producing large charging energy and large gaped molecular energy levels, number of phenomenon, such as single electron tunneling,[31] Coulomb blockade[44] and Kondo effect[45] are observable at much higher temperature than that of various quantum dots.[46] In the many cases of the molecular quantum dot, the thermal broadening of the Fermi energy levels and ambience thermal energy do not mask the exotic phenomenon at relatively high temperatures.[35] Another important advantage associated with the use of the molecule as a quantum dot is the ability to tune the molecule-metal electrode coupling strength through the length of linker tethers and the chemistry of anchoring groups.[31] Tethers and anchoring groups help covalently, attaching the molecules to the metal electrodes.[40] The illustration of the coupling energy effect on the molecular transport is presented elsewhere in this review.

The formulation for the molecular conduction mechanism was first introduced by Marcus for a system of donor-bridge-acceptor (DBA) molecular configuration.[34] We begin understanding the molecular transport mechanism with Marcus's expression. This expression provides a helpful conceptual foundation for the deciphering of several complex systems.[36] Here the main

assumption is that the donor and the acceptor are weakly coupled via a molecular bridge.[23] In an adiabatic regime the electron transfer event produces a change in the charge state of the donor (D) and the acceptor (A).[36] The complete electron transfer event can be expressed by DA=> D^+A^-. The corresponding rate, k_{ET}, for this reaction is the following[36]:

$$k_{ET} = \frac{2\pi}{h} |T_{DA}|^2 F_{DA} \quad (1.1)$$

T_{DA} = electronic coupling between donor and acceptor sections

F_{DA} = Frank-Condon factor.

h = Plank constant

The above expression relies on the Fermi-Golden rule and holds good when D and A are weakly coupled. $|T_{DA}|^2$ represents the coupling between D and A. F_{DA} represents the reorganization of the bond length and bond angle necessitated by the donor moiety to loose its electron to become D^+ and for acceptor moiety to become A^- in their equilibrium geometry.[36] In the classical limits F_{DA} can be written as follows[36]:

$$F_{DA} = \frac{e^{-(\lambda + E_{AD})^2 / 4\lambda k_B T}}{\sqrt{4\pi\lambda k_B T}} \quad (1.2)$$

$E_{AD} = E_A - E_D$, is electronic energy gap between the donor and acceptor states,

k_B = Boltzmann constant

T = Temperature

λ= molecular reorganization energy

Reorganization energy (λ) is a measure of the electronic energy that would be dissipated after a sudden jump from the electronic states of a donor to the electronic states of an acceptor.[36]

Most molecular devices are prepared by covalently attaching the molecular bridges between two metal electrodes.[42] To make a transition from the DBA system to the metal-molecule-metal-junction system, one should replace the discrete energy levels of donors and acceptor moiety with the continuum of electronic states of metals[36], figure 1.1. In figure 1.1 the bridge segment of DBA is analogous to the active molecule under study.

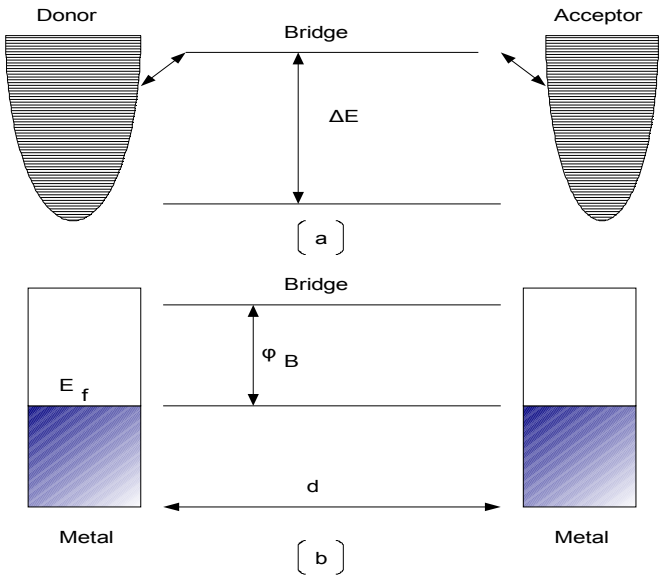

Figure 1.1: (a) DBA system, where donor and acceptor possess discreet energy levels and molecular bridge is an energy barrier. (b) Metal-molecule-metal system realized by replacing the donor and acceptor of DBA with metal electrodes.

1.1.1 Molecules behaving as tunnel barriers between two electrodes:

Molecular bridges producing extremely weak interaction between the two metal electrodes can be considered as tunneling barriers.[37] In this case the transport mechanism is predominantly a coherent tunneling and controlled by the barrier height[42] and barrier thickness of a molecular barrier.[37] For such a system, transparency (T_{Trans}) of the tunneling barrier is an important parameter; it is a measure of the inter-electrode electronic coupling introduced by the molecular bridge, as compared to the competing coupling process through the vacuum gap.[4] The transparency of a rectangular barrier, assuming this is the shape of a molecular barrier, of barrier height (φ_B) and barrier thickness (d), with respect to an impinging electron of energy E (E< φ_B), can be given by following expression[47] eq.(3):

$$T_{Trans} = \left[1 + \frac{\varphi_B^2}{4E(\varphi_B - E)}\sinh^2(kd)\right]^{-1} \tag{1.3}$$

Here, $k = \sqrt{\frac{2m(\varphi_B - E)}{\hbar^2}}$

m = effective mass of electron

$\hbar$=h/2π= Planck's constant

Transparency can also be calculated from the macroscopically measurable Ohmic resistance (R) of a molecular junction ($T_{Trans} = h/2e^2 \ R^{-1}$).[4] However, this approach includes the resistance of contacts and leads along with the molecule.[48] The most popular approach to measure the electron transparency or transmission rate due to the molecular barrier is to utilize the tunneling decay factor[37] (β) and barrier thickness(d).[4] Transmission of an electron in a non resonant tunneling regime through a rectangular barrier exhibits the following form.[42]:

$$T_{Trans} = exp(-\beta.d) \tag{1.4}$$

The tunneling decay factor, given by the following expression, depends on the barrier height, φ_B, and the applied bias, V, across the molecular junction[42].

$$\beta = 2\frac{\sqrt{m.(2\varphi_B - eV)}}{\hbar^2} \tag{1.5}$$

The charge transfer rate or electronic coupling strength between the donor and the acceptor, or two metal electrodes via molecular tunneling bridge, is dependent on the molecule length and tunneling decay factor β.[42] It is noteworthy that β is a function of the barrier height. In other words, β is the characteristic of a medium between the two metal electrodes. For instance, $\beta = 2.8$ Å^{-1} for vacuum and $\beta = 0.27 - 1$ Å^{-1} for covalent molecular bridges.[37] Interestingly, for the given thickness, a barrier with the β=0.5 Å^{-1} exhibited > 20,000 fold higher electron transfer rate as compared to $\beta = 1$ Å^{-1}.[37] Moreover, β is governed by the atomic orbital arrangement on the molecular bridge. Faster tunneling via the molecular bridge as compared to tunneling through the vacuum is due to the super-exchange of atomic orbitals.[10] Interaction of the tunneling electron with orbitals and molecular electronic structures enhances the tunneling rate.[37] This process makes through bond tunneling more efficient than the through space tunneling.[42] Joachim et al.[49] have also shown theoretically that the molecular channels facilitate efficient tunneling through them.[4] Molecular bridges increase the size of the quantum state space for the quantum trajectory describing the charge transport via molecule as compared to the quantum trajectory through space.[49] A detailed description of the tunneling decay factors for the various molecular channels is given elsewhere.[42]

In order to calculate the barrier transparency and tunneling decay factor, effective barrier height and barrier thickness for the molecular tunnel barrier is required. The common way to extract barrier height and barrier thickness is to fit the measured current–voltage data with

Simmons model.[37] Current (J)-voltage (V) characteristics of a molecular junction exhibiting pure coherent tunneling can be expressed by the following Simmons model expression for a medium voltage range ($V < \varphi_B/e$), eq.1.6.[50]

$$J = \left(\frac{e}{4\pi^2 \hbar d^2}\right)\left\{\left(\varphi_B - \frac{eV}{2}\right)\times \exp\left[-\frac{2(2m)^{1/2}}{\hbar}\alpha\left(\varphi_B - \frac{eV}{2}\right)^{1/2} d\right] - \left(\varphi_B + \frac{eV}{2}\right)\times \exp\left[-\frac{2(2m)^{1/2}}{\hbar}\alpha\left(\varphi_B + \frac{eV}{2}\right)^{1/2} d\right]\right\} \quad (1.6)$$

where m is the mass of an electron, d is barrier thickness, φ_B is barrier height, V is applied bias, and α is a unitless adjustable parameter, accommodating the deviations from a simple rectangular barrier and effective mass of the electron.[51]

1.1.2 Molecule behaving as a quantum dot:

The situation changes when a molecule provides molecular level(s) close to the metallic Fermi levels, or molecular energy level(s) are coupled to the metallic levels. Molecules behave more like a quantum dot.[38] Molecular levels are interacting with the continuums of metal density of states via tunneling barriers; tunneling is the dominant transport mechanism in alkane tethers, anchoring ligands and/ or vacuum gap.[52] A simple tunneling picture through molecular barrier falls short in capturing the accurate physics of the molecular transport; generally, molecular transport becomes a thermally activated process.[37] It is worth noticing that electronic properties of the isolated molecule significantly change after being placed between the two metal electrodes,[53] separated by an nm scale gap.[38] Details of the charge state of the molecule, coupling of molecular level to the electrodes and relative gap between the Fermi level and the molecular level after the equilibration process in the metal electrode environment pronouncedly affect the molecular transport.[35]

1.1.2.1 Effect of molecular electrode environment on molecular energy level:

Before delving into the specific molecular conduction mechanisms, it is worth discussing the changes in the electronic properties of the molecule[53] which are directly associated with the molecular transport.[54] Generally, insertion of molecule between the two metallic electrodes leads to: (a) reduction in e^- charging energy, (b) loss of the charge neutrality, (c) broadening of the molecular levels due to their overlap with metallic wave-functions.

1.1.2.1.1 Reduction in the charging energy:

It was observed that a molecule placed between two electrodes exhibited smaller e^- charging energy.[35] This is due to the change in electrostatic nature of the ambience. For instance, C_{60} molecule experienced a reduction of 1.4 eV after being inserted between two metal electrodes. This change in the charging energy ($E_C = e^2/C$) is due to the increase in the effective capacitance, figure 1.2. The capacitance of a C_{60} molecule increased from isolated molecule capacitance, C_{iso}, to the capacitance of the molecule in the new environment (metal electrodes at nanogap), C_{MJ}. Expressions for the C_{iso} and C_{MJ} are following:

$$C_{iso} = \frac{4\pi\varepsilon_0}{\frac{1}{R_1}} \tag{1.7}$$

$$C_{MJ} = \frac{4\pi\varepsilon_0\varepsilon}{\left(\frac{1}{R_1} - \frac{1}{R_2}\right)} \tag{1.8}$$

Here

R_1 = effective diameter of C_{60} molecule

R_2 = distance of metal electrode from the center of molecule.

ε_0 and ε = are the dielectric constants of vacuum and the medium between molecule and metal electrode, respectively.

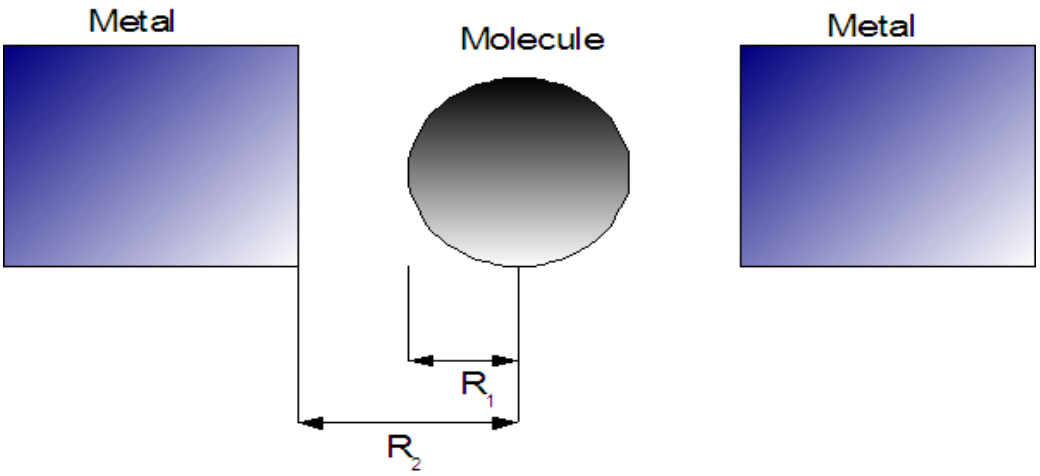

Figure 1.2: Surrounding of metallic electrode environment increase the effective capacitance of a molecule.

It is noteworthy that molecules separated from the electrode by the high dielectric constant insulating medium will exhibit smaller reduction in the charging energy.[35] In other words, dielectric constant is a measure of the degree of delocalization of molecular levels; higher dielectric constant is indicative of the localization of molecular wave-functions.[35]

1.1.2.1.2 Loss of charge neutrality:

Relative position of the active molecular level(s) with respect to metallic Fermi level is important in defining the charge state of the molecule.[9,38] The Fermi level of metallic electrode, electrochemical potential, lies somewhere within the HOMO-LUMO gap.[55] In the equilibrium, a number of molecular states below Fermi-level must be filled with electrons, while the molecular state above Fermi-level should be empty. Molecules between the two electrodes are generally charged; the amount of the charge on a molecule can vary from -1e to +1e. Metallic Fermi-level is found to stay close to the LUMO of +1e charged molecules, figure 1.3(a). But the Fermi-level positioned in the vicinity of HOMO of molecule induces -1e charge state[35], figure 1.3(b). In the first case (+1e charged) Fermi level attempts to remove electrons from the molecule, whereas, in the second case (-1e charged) the Fermi level loads charge on to the molecule. One spectroscopic study on C_6F_6 chemisorbed metal surface has shown that the LUMO of C_6F_6 shifted by 0.7eV towards the center of the HOMO-LUMO gap; this event leads to the charge transfer event producing an ionized molecule.[54] It has also been observed that the charge state of the molecule, which is not possible in their isolated state, becomes feasible after being attached to molecular electrodes. Liang et al.[39] found that the divanadium complex exhibited +1 ionic state, or S=1/2 spin state, after being attached to gold leads. This charge state has not been isolated with bulk divanadium complex, used in their study.

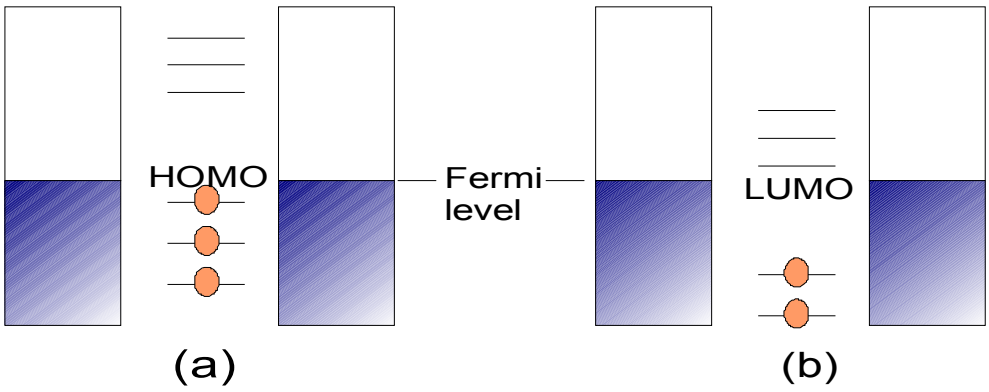

Figure 1.3: Molecule looses its charge neutrality when connected two metal electrodes. (a) HOMO level (b) LUMO level of a molecule staying close to the metal Fermi level for the -1 and +1 charge states, respectively.

1.1.2.1.3 Broadening of molecular levels:

It has been reported that a molecular level looses its discreteness after being placed between the two metal electrodes.[35,55] Because of the coupling due to the finite delocalization of the metal and molecular energy levels, molecular level broadening occurs. When a molecular state is coupled to the metal states both types of states leak towards each other. Due to this molecule losing part of its state at a fixed energy, it simultaneously gains metallic states spilling on it at various energy levels, figure 1.4. This tradeoff transforms a discrete molecular energy level into a diffused or broadened energy level and ultimately produces broadened molecular level.[55] The larger the energy level broadening, the faster will be the transport through that level. It is noteworthy that irrespective of the magnitude of the broadening, only one electron at a time can occupy the broadened level.[55] The simple case of the expression for the density of states, D(E), resulting from the broadening of a single molecular level(ε) can be expressed in the form of a Lorentzien function as given below:[35,55]

$$D(E) = \frac{\Gamma/2\pi}{(E-\varepsilon)^2 + (\Gamma/2)^2} \tag{1.9}$$

Here, Γ is total energy level broadening and is the sum of broadenings due to source Γ_S and draining of Γ_D electrodes. It is noteworthy that if level broadenings are energy dependent, then Lorentzien function is not a suitable choice.[35] The situation becomes more intriguing and challenging when the localized spin state of a molecular level interacts with delocalized spins of the electrode to engender additional exchange coupling.[56] A brief discussion on interaction between molecule and electrode's spin state is given elsewhere in this review.

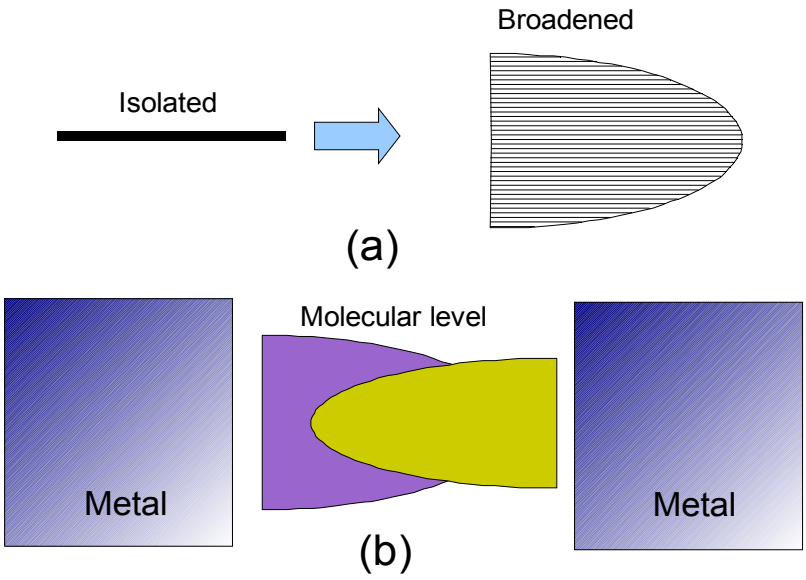

Figure 1.4: Interaction of a molecular level with metallic continuum of energy levels produces broadened molecular level (a). Difference in coupling strength of molecular level to the metal electrode will produce difference in molecular level broadening (b).

1.1.2.2 Electron dynamics through molecular quantum dots:

To consider the charge transport through a molecular junction, it is instructive to begin with a molecule whose only energy level, which is E eV above the Fermi level of metal electrodes, takes part in the transport. Net equilibrium charge flux under the effect of the applied bias V can be written in the following manner:[35,55]

$$I_S = \left(\frac{e}{\hbar}\right)\frac{\Gamma_S\Gamma_D}{(\Gamma_S+\Gamma_D)}(f_S - f_D) \tag{1.10}$$

Here, f_S and f_D are Fermi functions of electron density of states at source and drain and are given by,

$$f_S = \frac{1}{1+\exp\left(\frac{E-\mu_S}{k_BT}\right)} \tag{1.11}$$

$$f_D = \frac{1}{1+\exp\left(\frac{E-\mu_D}{k_BT}\right)} \tag{1.12}$$

Here μ_S and μ_D are the electrochemical potentials of the source and drain, respectively. Applied potential, V_{SD}, between source and drain can be given by:

$$\mu_S - \mu_D = eV_{SD} \quad (1.13)$$

In the above equation Γ, the energy level broadening, controls the current amplitude. Energy level broadening also accounts for the charging energy for the molecular quantum dot. The difference in the density of states at Fermi energy levels of source and drains, i.e. $(f_S - f_D)$, dictates the direction of charge transport.[35] The above given description is generic in nature; features and characteristics of molecular transport depend on the specificity of both, the molecule and the electrode.[38] In order to encompass the important aspects of the molecular transport, it is worth studying the various transport mechanisms.

1.1.2.2.4 **Weak molecule-metal electrode coupling:**

For the molecular junction where molecular levels weakly interact with electrodes, coupling energies Γ_S and Γ_D are small and negligibly broadened ($\Gamma << k_BT$).[35] This condition suggests that the molecular wave function is highly localized. Any exchange of charge between metallic electrodes and molecular level requires a large charging energy, figure 1.5.[57] Furthermore, for a molecule to be in single electron transport (SET) regime the following assumptions have to be satisfied:

$E_C + E >> k_BT$ (for single electron transport)

$E >> k_BT$ (for quantum dot regime)

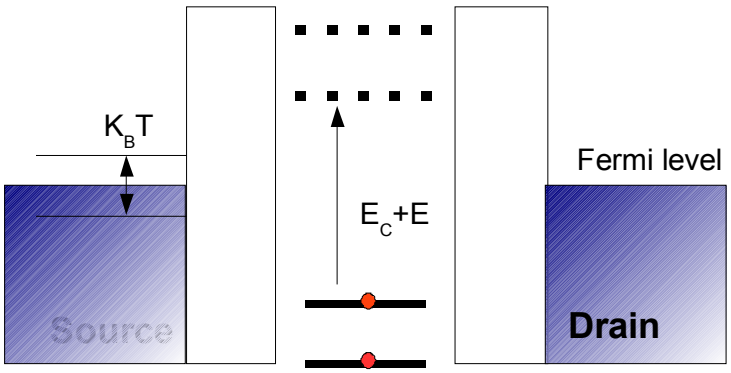

Figure 1.5: Molecule weakly interacting with metal electrodes is behaving like a quantum dot. Figure design adopted from ref. [32].

In general I –V of such a system is expected to show a non-conductivity region up to certain bias and then the start of a conducting regime for the higher bias with a current of eΓ magnitude.[35] A non-conducting regime of this type has been observed in a STM (scanning

tunneling microscope) based transport study of 2,2,6,6-tetramethyl-1-piperidinyloxy (TEMPO) molecules, assembled on Si substrate.[58] In an elegant STM study of double-ended thiol molecule p-xylene-α, ά-dithiol room temperature coulomb blockade was observed.[44] This result asserts the fact that the smaller size of molecular quantum dot leads to a higher charging energy which in turn prevents masking of the coulomb blockade phenomenon due to the ambient thermal energy.[59] Park et al.[31] have also observed the signature of single electron transistor in the transport characteristic of a cobalt complex, bonded to the metal electrodes by relatively longer alkane tethers. Reducing the alkane tether length produced Kondo resonance, a signature of strong coupling between molecular level and metallic density of state.[31] For low bias regime, a dearth of charging energy results in a non-conducting region, also called a Coulomb blockade regime. It is noteworthy that the width of the Coulomb blockade regime is directly affected by the gate voltage; gate voltage is capable of moving the active molecular level with respect to E_F.

1.1.2.2.5 **Strong molecule-metal electrode coupling:**

Delocalization due to the strong coupling between the molecular energy level and metallic density of state produces a broadened molecular level; delocalization effect also reduces the charging energy. As a consequence, transport through the molecular level enhances significantly.[55] In the strong coupling regime, molecular transport is a dephasing process[60] between molecular resonance levels and the continuum of the metallic states around the Fermi level. Broadening and the coupling strength depend on the details of the metal electrode, the anchoring group, e.g. thiol group, and the molecular structure.[35] Seminaro et al.[61] have shown that the nature of the metal of the anchoring group dramatically affected the molecular conductance.[61] Popular thiol functional groups is not the best choice as an anchoring group, figure 1.6.

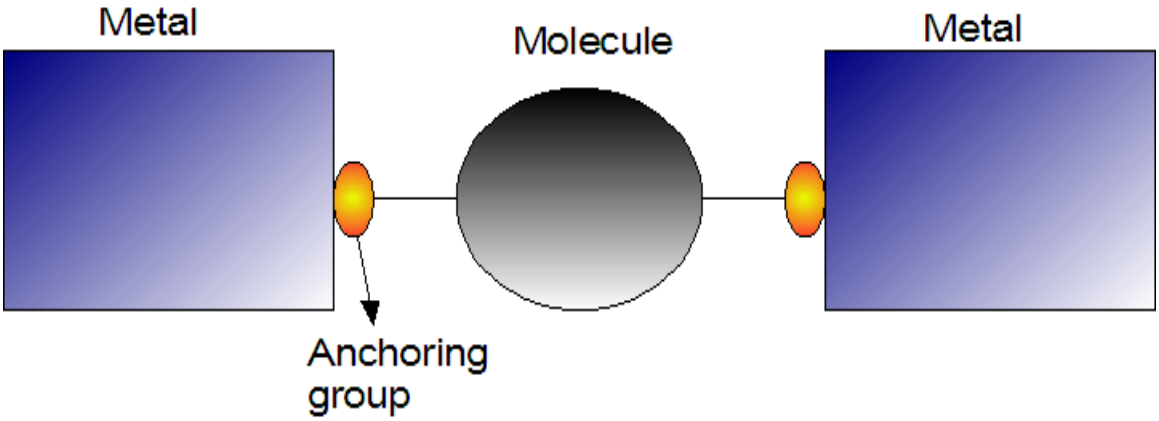

Figure 1.6: Molecule attached to the two electrodes via anchoring group.

To understand the role of the metal anchoring group on the metal-molecular coupling, it is instructive to consider the following examples. It was found that a hydrogen molecule bridging the gap between the two platinum electrodes produced a conductance plateau at $1G_0$ in an energy window of 4eV around the Fermi level.[62] It is due to the availability of the antibonding level, with 4eV energy level broadening around the Fermi level. Such a huge broadening arises from the hybridization of s (hydrogen) and d (Platinum) orbitals.[35] The bonding level is almost completely dormant in the conduction process. In another case, when a CO molecule was introduced on a gold (Au) atom chain, connected to the two Au electrodes, a localized resonance level was observed.[63] This effect was attributed to the misalignment of the energy levels between the CO affected Au atom chain and the Au electrode.[63] Consequently, conductance of the Au chain reduced dramatically for a wide energy range.[35]

In several studies, molecular break junctions a molecule, between the two metal electrodes at ~1nm gap, exhibited a strong coupling with the two metal electrodes.[31] These junctions exhibited the Kondo resonance;[31] Kondo resonance is caused by the strong exchange coupling between the localized electron at the molecular level and the itinerant electrons of the metal electrodes. Martineck et al. have shown that if two electrodes are spin polarized and strongly coupled to a quantum dot, analogous to a molecule[13], additional coupling will arise due to the spin dependent exchange.

1.1.2.2.6 **Effect of the molecular structure on the molecular transport mechanism:**

Molecular structure imparts a profound effect on the molecular transport[10,64-66]. However, reviewing all the molecules used in a molecular junction is beyond the scope of this study; we examined the representative cases only.

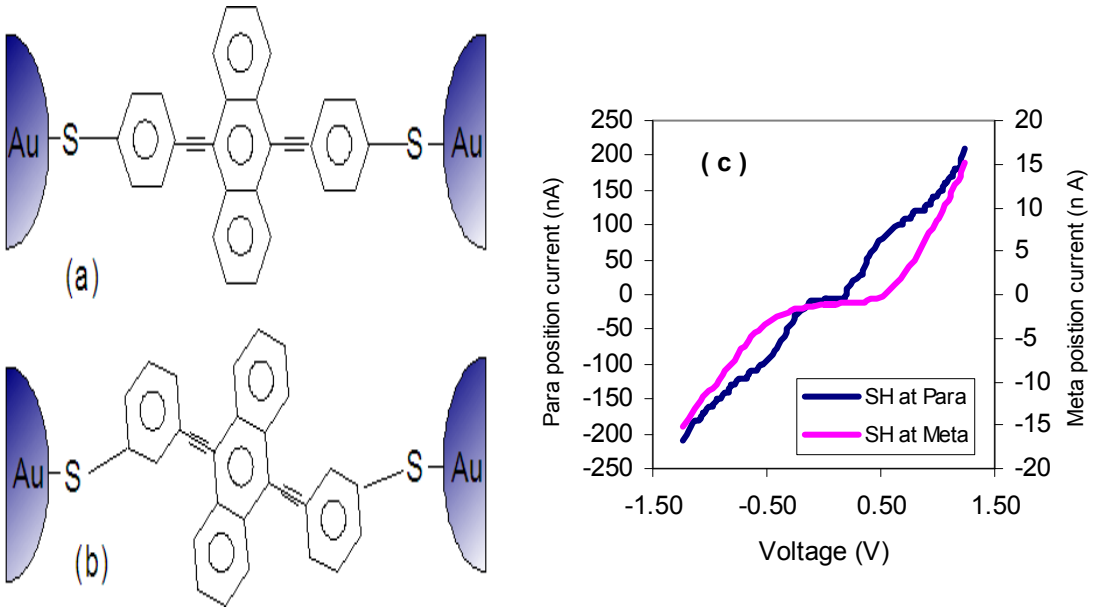

Figure 1.7: The change in anchoring group position from para (a) to meta (b) state produce the significant change in the molecular junction transport(c). Adapted from ref. [65]

In the previous section, we briefly studied the effect of the molecule-metal bonding on the molecular transport.[61] Interestingly, it was also observed that the position of anchoring group on the molecular bridge also played a crucial role with regards to molecular transport.[67,68] The fact that the structural changes directly affect the delocalization of the charge over the molecular bridge is supported by the following examples. In a transport study,[68] the effect of an anchoring SH group position with respect to a molecule[68], figure 1.7, was studied. When the SH group is attached to benzene rings at the two ends of the molecule in a para position, conductance was higher than the case when the SH group is in a meta position on the same benzene rings.[68] It has been observed that I-V curves are generally symmetric for symmetric molecules.[67] In a similar study, delocalization over the molecular bridge was significantly affected when molecular configuration was changed from 1,4-benzenedimethylthio to 1,4-dibenzenethiol.[66] In the latter case conductance was found to be two orders higher.

The molecular conduction has been found to occur via multiple charge states. Some molecules produce multiple levels around Fermi levels and have multiple charge states (>2). To access more than two charge states of the molecule, electron charging energy has to be minimized[69]. One way to reduce the charging energy is to have multi-unit molecules with the delocalized orbitals[23]. It is noteworthy that we are primarily seeking the delocalization on the molecular bridge; delocalization between molecular levels and metal Fermi level, defining the

broadening of an energy level, is less important. For a single conjugated oligomer of p-phenylene vinylene with 5-benzene rings, as many as six charge states partake in conduction,[69] figure 1.8. Here molecular orbitals are closely spaced- that becomes possible if different molecular units are strongly coupled together or their atomic orbitals are delocalized over the molecule.[69]

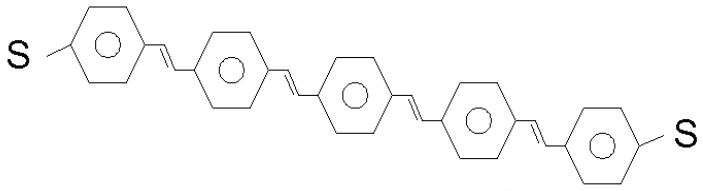

Figure 1.8: Conjugated oligomer of p-phenylene vinylene with 5-benzene rings. Adapted from ref. [66].

It is noteworthy that the molecule between two metal electrodes experiences the dramatic reduction in the HOMO-LUMO gap. It was suggested that the image charge generated in the source and drain electrodes, induced by the charge on the molecule, produces apposite electrostatics to shift the HOMO-LUMO gap.[69] The main effect of the presence of image charge is to reduce the effective barrier height.[70] In an experimental study, it was shown that for the C_6F_6 molecule, chemisorbed on metal surface,[54] LUMO shifted by 0.7eV towards the center of the HOMO-LUMO gap.

Excited state assisted resonant-inelastic conduction has been observed in a number of molecular transport studies. To understand the role of the excited states in the molecular transport, we consider a molecular quantum dot with only one excited state for the N+1 electron state. It is noteworthy that the molecular quantum dot has only one ground state for the N electron state; however, when there are N+1 electrons in this state, one excited state is located ΔE above the N+1 electron state.[35] Hence the availability of an excited state is specific to a charge state of the molecule, figure 1.9. It is assumed that the charge transfer rate from the excited state to the electrode is faster than the charge relaxation rate to the ground state.[35] Since for the N+1 state both excited and ground states are coupled to the source and drain, net transport rate will be faster. The cumulatively following expression can define the net current (note g and e stand for ground state and excited state, respectively):[35]

$$I = |e| \frac{\Gamma_S{}^g \Gamma_D{}^g (f_S^g - f_D^g)[\Gamma_S^e(1-f_S^e)+\Gamma_D^e(1-f_D^e)]+\Gamma_S{}^e \Gamma_D{}^e (f_S^e - f_D^e)[\Gamma_S^g(1-f_S^g)+\Gamma_D^g(1-f_D^g)]}{(\Gamma_S^g+\Gamma_D^g)(\Gamma_S^e+\Gamma_D^e)-(\Gamma_S^g f_S^g+\Gamma_D^g f_D^g)(\Gamma_S^e f_S^e+\Gamma_D^e f_D^e)} \quad (1.14)$$

During molecular transport, several features at low source voltage can be observed as an example of the excited state assisted transport.[71] For instance, in the case of the charge transport through the C_{60} molecule,[72] excitation modes at 35 meV and 5 meV were observed. The excitation mode at 35 meV is believed to be due to an internal mode stemming from the change in the shape of the C_{60} molecule from sphere to prorate ellipsoid.[72] However, a 5 meV feature was assigned to the oscillating center of mass of C_{60}, within the confinement potential responsible for the binding of the C_{60} molecule to a metallic surface.[72] In another transport study through the C_{140} molecule, the signature of an internal mode was clearly observed in transport spectra.[73] This vibrational mode at ~ 11 meV was assigned to the stretching mode of the spring between the two C_{70} subunits. These illustrations comply with the Frank-Condon processes occurring during the charge transport through the molecular bridge.[73]

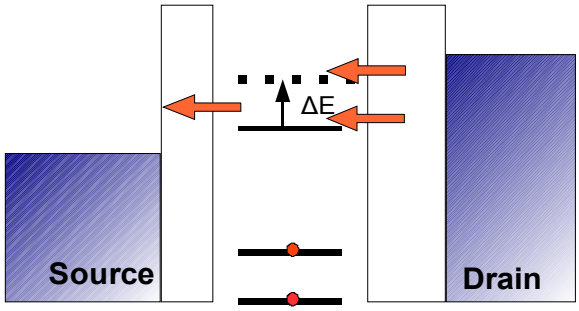

Figure 1.9: Simultaneous coupling to the excited state producing enhanced transport. Adapted from ref. [32].

In a number of molecular conduction studies clear signatures of inelastic nonresonant-tunneling (cotunneling) were detected. In several cases coupling of the excited level, mainly due to the molecular vibrations,[74,75] to the electrode is weak. Due to this, charge transfer rate of an electron reaching the excited energy level to the metallic electrodes is smaller.[10] In this case charge prefers to relax to the lower molecular level and then subsequently move to the metal electrode, figure 1.10. These events cumulatively represent an inelastic non-resonant tunneling process.[76]

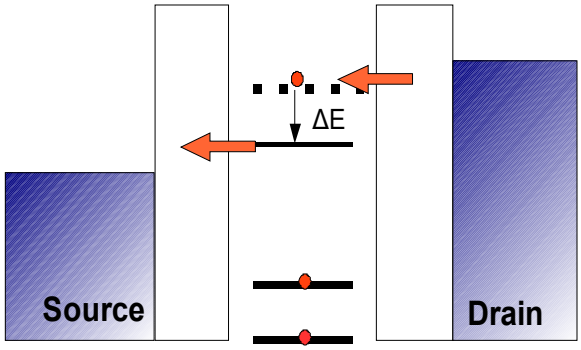

Figure 1.10: Inelastic transport through a vibrational state.

Due to weaker coupling of the excited states, it is expected that the signature of the vibrational levels, producing an excited state, will be observed when bias is far away from the prime molecular level, figure 10. Another important consequence of the inelastic tunneling is that a finite charge transport will always be possible through the vibrational levels, even when transport though the main molecular channel is insignificant or blocked.[35] Common signatures of the inelastic tunneling are observed in d^2I/dV^2 vs. V spectra.[49] A comparison of the d^2I/dV^2 peaks position[74] on the energy scale with the IR and RAMAN spectra for a molecule under study proves that d^2I/dV^2 peaks correspond to the vibrational excitations. The d^2I/dV^2 features in the blockade region occurred essentially at a constant value of V_{SD} until gate voltage was varied.[35] It is noteworthy that when the conductance gap is large, d^2I/dV^2 peaks are rather easily observed. Otherwise, these features may be masked by the dominant transport through the main molecular level(s). It is logical to say that vibrational states in the present case, promoting co-tunneling and corresponding conductance, can be given by the following equation:[35]

$$G^{CO} = \frac{\pi\hbar}{3e^2}\left(\frac{\Gamma}{E_C}\right)^2 G_S G_D \qquad (1.15)$$

E_C = charging energy, G_S and G_D are conductance through the barrier adjacent to source and drain, respectively. At low temperature, as sequential tunneling reduces exponentially, co-tunneling which scales as the square of the temperature prevails.

According to the study of the number of molecular junctions, the transport mechanism was found to be switching between coherent (tunneling) and incoherent (hopping) with respect to temperature.[35] Such observations were mainly prevalent in the events when molecular backbone

possessed a functional group with the rotational freedom.[60] Rotation of the functional group, a thermally activated process, significantly changes the electronic coupling between the two nearest molecular segments. A decrease in electronic coupling increases the molecular barrier height and coherent tunneling mechanism prevails. However, larger electronic coupling decreases the molecular barrier height, leading to the hopping type mechanism. As an example, a single molecule of oligothiophene, possessing a rotatable NO_2 group, is worth considering,[60] figure 1.11(a). This molecule exhibited a thermally activated transport mechanism up to 100 K; below this temperature coherent tunneling prevailed, figure 1.11(b). A similar study of the oligophenylene molecules grafted on a glassy carbon substrate McCreery group obtained the thermal signature of the change in the transport mechanism.[10]

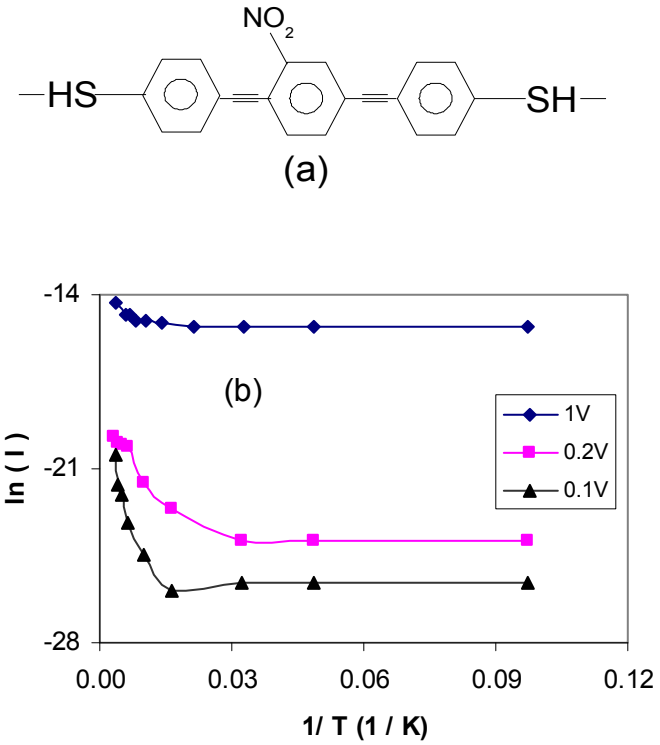

Figure 1.11: Molecule backbone with a functional group with rotational freedom (a) experience change transport mechanism with temperature (b). For higher bias, transition point between two mechanisms is smearing out. Adapted from ref. [57].

The above mentioned case is possible when a tunneling electron strongly interacted with the molecular environment, leading to decreased coherence and mechanism switching to thermally activated transport.[10] Such interaction mainly depends on the interaction time, for the

duration of which an electron remains in the molecular environment. The conduction time, according to Landaur -Buttiker treatment,[77] can be given by $\tau = Nh/2\pi\Delta E$, where ΔE is the energy gap between the Fermi energy level and active molecular orbitals, N = no. of molecular subunits.[10,64] A longer time for the electron to stay on the molecule promotes mixing up of vibration with the transfer matrix elements, governing the transport.[10] It is noteworthy that for the shorter molecule, with a large energy barrier and a smaller barrier height, tunneling rate is fast. However, for a long molecule with multiple subunits, barrier height is relatively small and hopping is the dominant charge transport mechanism.

1.2 Spin-valves and role of the spin in the molecular transport:

The primary interest of incorporating the spin in the molecular electronic devices is to form a molecular spin valve.[16] Since most of the molecules exhibit non linear transport characteristics, if one connects them with two ferromagnetic electrodes, the whole device will be equivalent to a magnetic tunnel junction (MTJ) device.[78] A MTJ structure possesses two ferromagnetic (FM) electrodes separated by nm thick insulating spacer, figure 1.12.[78]

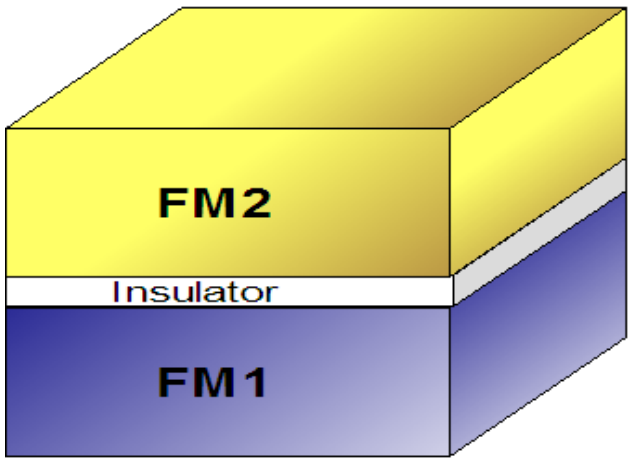

Figure 1.12: Typical stack of a magnetic tunnel junction.

The performance of a spin valve is mainly described in terms of the tunneling magneto resistance ratio (TMR),[79] a function of resistance values of spin valves in parallel (Rp) and antiparallel (Rap) states of the two magnetic electrodes.[78]

$$TMR = \frac{(Rap - Rp)}{Rap}.100 = \frac{2.P_1.P_2}{1 + P_1.P_2}.100 \qquad (1.16)$$

P_1 and P_2 are the degree of spin polarization[80] of the first and second electrode, respectively. It is instructive to consider the Rp and Rap in terms of the DOS[81] of up ($D_\uparrow$) and down ($D_\downarrow$) spin of the FM electrode, according to the following expressions.

$$Rp \propto 1/(D_\uparrow^2 + D_\downarrow^2) \tag{1.17}$$

$$Rap \propto 1/(2.D_\uparrow.D_\downarrow) \tag{1.18}$$

TMR originates from the difference in the density of states (DOS) of the spin up $D_\uparrow(E_F)$ and the DOS for the spin down $D_\downarrow(E_F)$ near Fermi energy (E_F) level.[18,81] To abide with the conservation of spin orientation during tunneling, electrons are only permitted to move between the subbands of the similar spin orientation, as depicted in figure 1.13. The magnetization of electrodes controls the DOS of spin in subbands; tunneling rate for a specific spin is proportional to the product of the DOS of this spin in the respective spin subbands of the two FM electrodes at E_F.

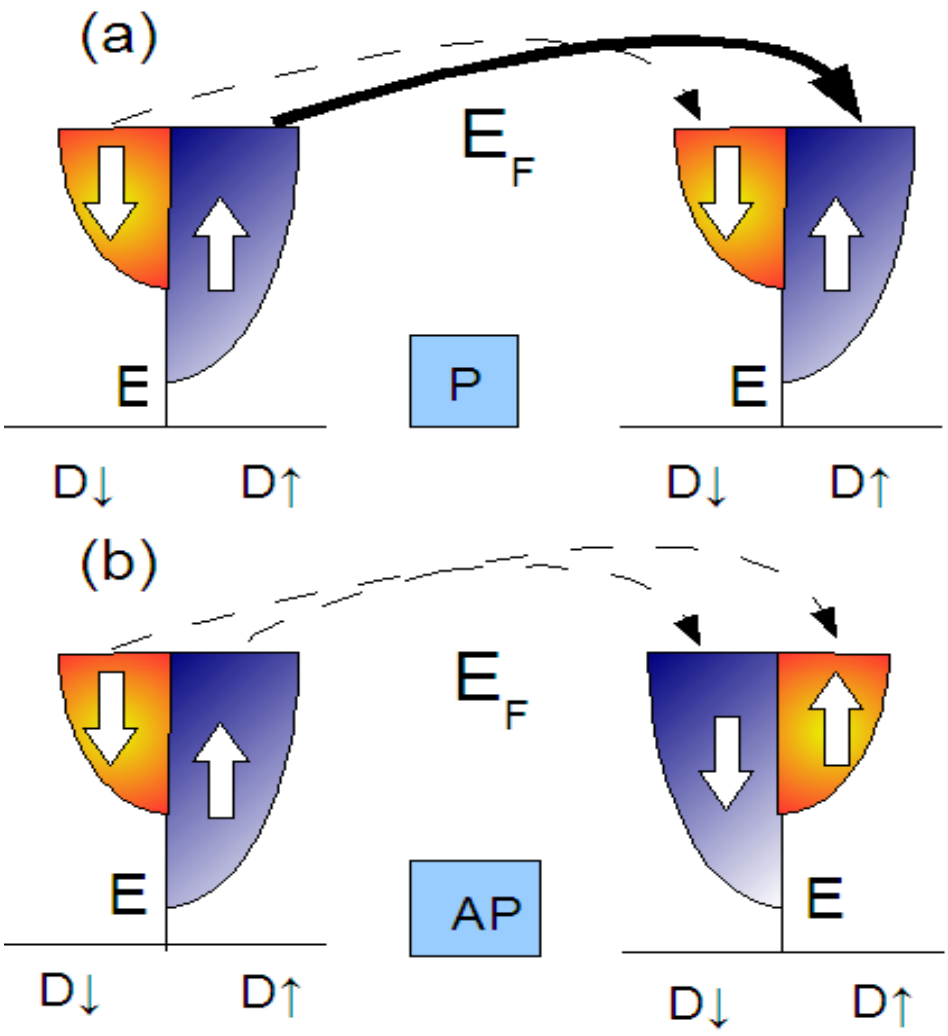

Figure 1.13: Transport between spin subbands of the two ferromagnetic electrodes in the parallel (a) and antiparallel state (b). Thick line (thin dashed line) shows the high (low) spin current. Adapted from ref. [23].

How a MTJ works as a spin valve can be described in the following manner. For a typical ~2nm thick insulator, two FM electrodes are antiferromagnetically coupled via insulator, e.g alumina and exhibit high resistance state (Rap).[17] Application of the magnetic field, strong enough to overcome the antiferromagnetic coupling between the two electrodes, aligns the magnetization of the two electrodes parallel to each other and hence produces smaller device resistance, (Rp). An example[82] of a TMR ratio for the MTJ with CoFe/Al_2O_3/NiFe configuration is given in figure 1.14. It is noteworthy that the TMR peak is slightly shifted from the zero point on field scale; it is attributed to the stray field arising from the MTJ stack itself producing a non

zero field even in the absence of an external field.[83] In a more popular scheme, the magnetization direction of one FM electrode is pinned and magnetization of the other electrode is freely switched with magnetic field. In the later case, the least exchange coupling energy is desirable to do switching with a smaller magnetic field. To flip the spin orientation of two ferromagnetic layers, it is quite reasonable to assume that the amount of energy produced by the corresponding magnetic field should be more than the exchange coupling energy. On energy scale, 1Tesla magnetic field is equal to ~1K temperature. A smaller switching field (> ~100Gauss) is aimed to produce integrable spin devices.

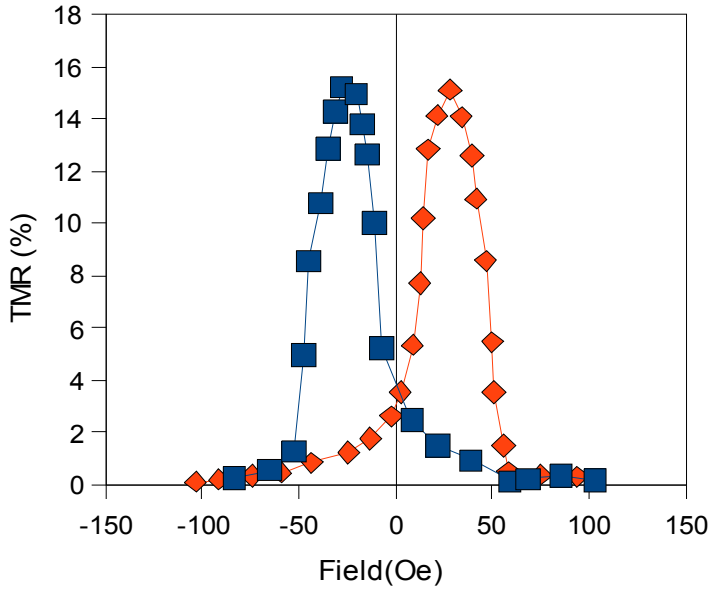

Figure: 1.14 Percent tunneling magneto resistances versus applied field curve for the CoFe/AlOx/NiFe MTJ. Adapted from ref. [79].

The degree of spin polarization of the FM electrode significantly affects the TMR of a MTJ.[18] According to Julliere[78], considering that spin polarization is a material constant, TMR should always be less than 50%. This is close to the best TMR obtained with an alumina insulating barrier.[17] Attempts to use 100% spin polarized to increase TMR did not yield significant change.[17] The reason is mainly due to the strong interface associated with spin scattering, precluding the transfer of 100% spin polarized current from one electrode to another[17]. Another plausible reason may be that the band structure of a spin polarized material at interface is significantly different from the bulk material.[83]

Replacing an alumina barrier with magnesium oxide (MgO) yielded as high as 250% TMR.[18] This study suggests that spin-polarization near FM-insulator interface is not a material constant;[18] spin polarization can be significantly different from the bulk. Tsymbal and coworkers have theoretically shown that the spin polarization of ferromagnetic metal changed due to the absorption of oxygen atoms on the surface of a ferromagnetic metal.[84] Moreover, in the case of the gold nanoparticles, the evolution of ferromagnetism was found to be the direct corollary of change in surface chemistry using thiol terminated alkanes.[85] These observations open doors for the manipulation of spin polarization through the change in surface chemistry and then applying them for the spin valve fabrications.

Major hurdles in the advancement of MTJ development are specific to material. Insulator and FM-insulator interface roughness significantly contribute to the spin flip events precluding the realization of the full potential of a MTJ device. Irregular insulator thickness between two FM electrodes produces orange peel effect, disabling the independent switching of ferromagnetic layer.[17] Another tantalizing issue is to produce the same thickness and quality of ultrathin insulator[17].

Organic molecules are highly competent to replace inorganic insulators.[26] Organic molecules are known to exhibit long spin coherence length due a relatively small spin-orbit coupling and hyperfine splitting.[26] Organic molecules also possess fixed length and readily make well defined chemical bonds with the metal surface once functionalized appositely. Molecules are supposed to attach to the ferromagnetic electrodes through self assembly chemistry, which in turn may also affect the degree of spin polarization of FM near interface,[84] at least, to yield higher effect on TMR than expected. Recent theoretical work showed the possibility of achieving ~600% TMR with 1, 4 tricene-dithiolate molecules between Ni contacts, and rekindled the interest in molecular Spintronics.[19] In a little more radical prediction, Petrov et al. quoted that "In the case of antiferromagnetically ordered molecular wires, the inter electrode tunnel current may be changed up to 7-8 orders of magnitude if a magnetic field has been applied".[30] In addition, a low dimensional electronic system with molecular magnets, akin to single molecular magnets with insulating alkane tethers, etc. was considered promising to realize their prediction.[14]

Petta et al.[16] have prepared a nickel-octane thiol-nickel spin valve in a nanopore geometry. These molecular spin valves were reported to exhibit as high as ~17% magneto resistance ratio at 4.2 K. Because the octane-thiol molecule behaved as a tunnel barrier between two ferromagnetic electrodes, the overall device is one form of the tunneling magneto resistance (TMR) devices and is expected to follow the mechanism of conventional MTJ.[18] However, large scatter in transport data, the need of cryogenic temperature, and insufficiently characterized metal

molecule interfaces are suggestive of the long way ahead for making molecular spin valves, which can at least compete with conventional MTJ spin valves.[25] Pasupati et al. have prepared a molecular spin valve by inserting a C_{60} molecule between the nm gap of Ni breakjunction.[13] This study reports ~17% TMR but more interesting is the observation of Kondo splitting. We discuss the Kondo level splitting observation elsewhere in this review. Break junctions are highly irreproducible and poorly characterized.[86] Due to a low yield complex fabrication scheme, break junctions are apparently unsuitable for the molecular spin valve structures.

The dearth of sufficient successful experimental attempts to form molecular spin devices has not given requisite boost to the much vaunted field of molecular Spintronics.[20] However, a number of magnificent observations have surfaced due to the role of the spin state of molecules in the molecular transport. The Kondo effect,[31] complete charge suspension, negative differential conductance,[33] Zeman splitting,[39] and exchange interaction produced an extremely high exchange field.[13] The impressive experimental observation strongly indicates that studying the role of spin in molecular transport with a variety of electrodes which can reveal a treasure of new scientific phenomenon.

The C_{60}[13] molecules and divanadium complexes,[39] physiosorbed on the gold electrodes of a break junction, have shown the Kondo phenomenon. The Kondo effect in molecular junctions is a coherent many-body state,[87,88] which evolves due to the antiferromagnetic exchange between the localized spin of the molecule and the spins of the conduction electrons of the lead. Kondo resonance[89] brings about an enhanced density of the states at the metal electrode that leads to the zero bias conductance peaks.

A molecule generally acquires a net spin after being connected to two model electrodes through tunneling barriers. When these tunneling barriers are reasonably transparent, the wave function of the unpaired electron at the molecular level can leak out through barriers to hybridize with the delocalized electrons in the contact. If the hybridization step makes the spatial wave functions of the localized electron on a molecular level and delocalized electrons at the metal electrode symmetric, then the spin part of the wave functions for the electron at the molecule. The interacting electron of the electrode has to be the anti-parallel of the antiferromagnetically coupled. According to the Pauli rule,[47] the overall wave function of the interacting fermions have to be antisymmetric. The coupling energy of interacting electrons at the molecule and at the lead can be defined in terms of a characteristic temperature, popularly known as Kondo temperature (T_{Kondo}).[39]

$$T_{Kondo} = \frac{\sqrt{\Gamma E_C}\,\exp(-\pi.\varepsilon/\Gamma)}{2} \qquad (1.19)$$

Ec = charging energy

ε = difference between localized state and the Fermi level

Γ = summation of coupling strengths of energy level with two electrodes, Γ_S and Γ_D are the coupling strength of energy level with source and drain respectively.

The Kondo state is stable for ε/Γ >> 1. It is noteworthy that non-uniform source-drain coupling can bring about a higher Kondo temperature[39]. Interestingly, Kondo resonance in bulk metals due to dilute magnetic impurities enhances scattering events for conduction electrons. Scattering due to the antiferromagnetic interaction between the localized spin of impurity and delocalized spins of conduction electrons increases resistivity.[90]

Liang et al.[39] have studied the Kondo resonance with the divanadium molecular complex. The choice of the divanadium molecule was based on the control of its spin degree of freedom in a predictable manner. As high as 30 K Kondo temperature was realized. Interestingly, the application of a magnetic field was found to produce a 230 μV/T splitting in Kondo resonance level.[39] This splitting magnitude of Kondo level was consistent with the Zeeman splitting calculated by $2g\mu_B B/e$, where g=2 is the g factor for the molecule, and μ_B is the Bohr magnetron. It was also observed that the vanadium complex possessed a V_2^+ ion state, producing a spin doublet (s = ½) state between the two electrodes. It is noteworthy that the V_2^+ ion state was not realized in the bulk state.[39]

Numerous studies showing Kondo resonance[39] have been reported with the physio-sorbed molecule(s) in the gap of the break junction electrode. Here metal molecule contacts are far from being robust[90]. Netlson and coworkers have encountered the irreversible switching from Kondo resonance mode to Coulomb blockade[90]. This change can be associated with the change in the physical coupling between the metal and the molecule; this event hints towards the instability of the metal-molecule bond.

A plausible way to tackle the instability of the metal-molecule contact is to use molecules with organic tethers ending with a metal affinitive functional group.[33] Using alkane molecules is apparently a good choice over the conjugated tethers[91]. A π bond misalignment, producing a high resistive state, may mask the true properties of the core molecule[23]. Bond tunneling via alkane tethers, even though they exhibit insulating attributes, is much more efficient than the tunneling

through space. Another clear advantage is that metal molecule coupling can be easily tailored to be weak to strong by changing the length of the alkane tethers.

Park et al.[31] have given an excellent demonstration of imparting a control on the molecular transport mechanism by controlling the metal molecule coupling with the help of alkane tethers of different lengths. It is noteworthy that metal molecule coupling is exponentially dependent on metal molecule separation. It was found that changing the tether lengths attached to a cobalt coordination complex changed the transport mechanism from the single electron transistor regime to the Kondo regime. It has also been observed that alkane tethers work as a guiding channel for electron transport so that it tunnels to the molecule core, interacts with it, and then tunnels to the other electrode via another tether. For the longer molecule, molecular devices showed a strongly suppressed transport to a threshold voltage, which depended on the gate voltage. Beyond the threshold voltage, the current increased in step. This transport characteristic is of a single electron transistor device. For a larger gate voltage, cobalt with a paired electron and with s = 0 spin state resulted. However for a smaller negative gate voltage, cobalt with an unpaired electron and with s = ½ spin state was active. In the latter case i.e., a higher spin state current through the molecule would be suspended by a Clebsh-Gordan coefficient.

The smaller molecular [Co(tpy-$SH)_2$] was shown to exhibit a Kondo resonance at zero bias[31]. Since a smaller molecule metal gap produces a stronger wave function delocalization through barriers, the existence of a high exchange coupling between molecular spin state and electrode spin become viable. The application of the magnetic field was found to split the Kondo resonance peak. This is expected due to the Krammer degenerate Co^{2+} charge state ($3d^7$) with an unpaired electron that splits in the magnetic field. Another possible charge state, i.e., Co^{3+} ($3d^6$) has paired electrons and s = 0 spin state, will not undergo Zeeman splitting[31].

In the aforementioned cases, Kondo resonance was observed when a molecule with a low spin state (s = ½)[31] interacted with the nonmagnetic gold electrode. Typical level splitting under the effect of the magnetic field was ~200 $\mu V/T$[31], which is consistent with the typical Zeeman splitting.

A striking observation of Kondo resonance and its splitting was observed when a C_{60} molecule was placed between the two ferromagnetic electrodes of a Ni break junction.[13] Interestingly, the experimental realization shown here[13] was found to be in close agreement with the prediction of Kondo level splitting, even in the absence of a magnetic field for the system of a quantum dot coupled to magnetic electrodes.[92] In this study,[13] the shape of the two electrodes were designed to give them different shapes in order to induce magnetic anisotropies, figure 1.15(a). Different magnetic anisotropies allowed the magnetic reversal of the two electrodes at

dissimilar magnetic fields. Kondo resonance is generally suppressed by ferromagnetic ordering;[88] hence, it is rather surprising to see the existence of the Kondo resonance peaks in the present case.[13] Even more intriguing is the observation of as much as 16 meV Kondo level splitting, which is likely to occur under the application of a ~70 T field,[13] figure 1.15(b). Such a large splitting can not be due to the Zeeman splitting of the Kondo level in the external field.[56]. The Zeeman splitting observed on a junction comprising a C60 molecule and gold break junction was found to be ~230μV/T, [39] figure 1.16.

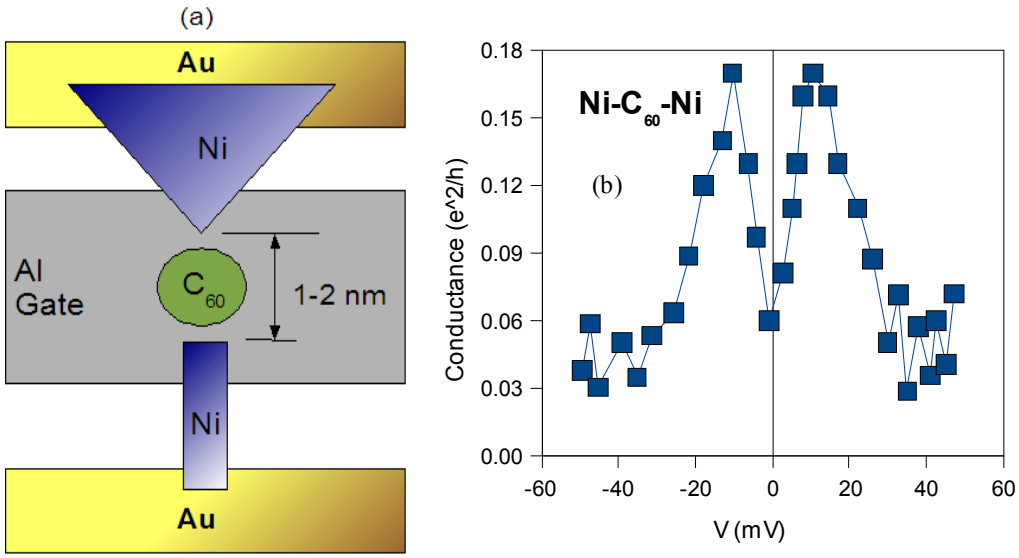

Figure 1.15: Schematic of Ni break junction with C_{60}[1] molecule (a). Splitting of Kondo resonance level by ~16mV due to the effect of exchange induced high magnetic field on C_{60} molecular level. Adapted from ref [10].

The extent of the splitting was found to be tunable by the application of an external magnetic field, aiming to set the magnetization of the two electrodes parallel and anti-parallel with respect to each other. For the parallel (anti-parallel) orientation of electrodes, Kondo level splitting was found to be 16 meV (7.5 meV)[13].

In the present case, it is apparent that the two many-body-correlated states[88,93] are in competition. First, correlated state occurs due to the coupling between the localized spin of the molecule and the itinerant spins of the electrode(s); the second correlated state is associated with the itinerant electron ferromagnetism of the electrodes.[88] A strong coupling between the molecule and metal electrode, presumably via electron transparent barriers, creates a strong magnetic exchange coupling.[93] Due to the spin polarization of electrodes and a strong exchange coupling of

molecular levels with metallic states, an exchange field arises which contributes to the Zeeman splitting.[39] In this case modified expression for the Zeeman splitting is following:[13,92]

$$e\Delta V = 2g.\mu_B B + a\sum_{m=R,L} P_m \Gamma_m \qquad (1.20)$$

It is believed that due to quantum charge fluctuations, the spin asymmetry in the coupling of the molecular level to the ferromagnetic electrodes, produces a spin dependent renormalization of the molecule's level in the proximity of the Fermi level.[13,92] The spin dependent renormalization breaks the spin degeneracy for the spin up and spin down states to bring about a splitting of the conductance curve, as expected from an external magnetic field.[92] It is important to note that if $\Gamma_L = \Gamma_R$, then for the anti-parallel magnetization of leads the effects of exchange interactions of molecular level with the two electrodes will cancel each other.[56] Kondo resonance will occur without splitting.[13] It can be inferred that the utilization of magnetic leads with dissimilar magnetization attributes will produce Kondo splitting rather easily.

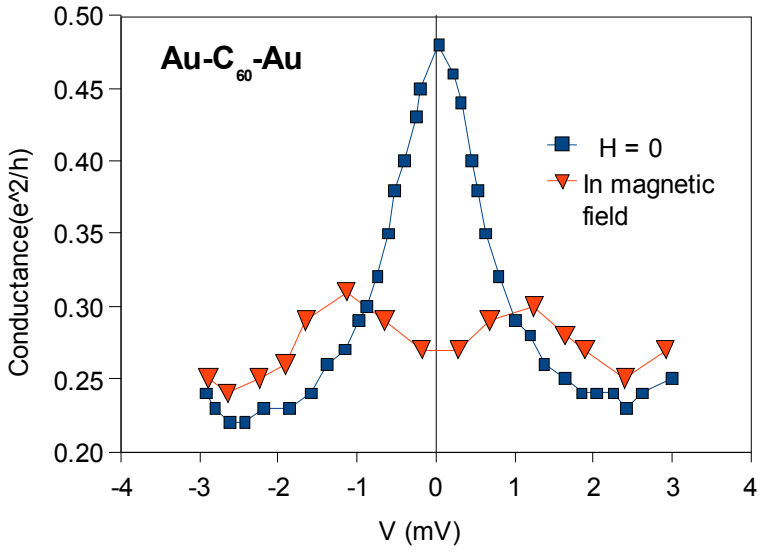

Figure 1.16: Kondo resonance peak for the C_{60} molecule between the two electrodes of gold break junction. Kondo resonance peak undergo Zeeman splitting when external magnetic field (H) is applied. Adapted from ref. [10].

We observed how a C_{60} molecule mediated to produce extremely strong exchange coupling between the two Ferromagnetic electrodes. In a relevant theoretical study it was found that impurities, considering them analogous to molecule, within the tunnel barrier of a magnetic tunnel junction can enhanced exchange coupling[94] by ~3 orders in magnitude.[95] It was calculated that an impurity level close to the Fermi energy level and physically present at the center of the tunnel barrier were highly influential, figure 1.17(a), in increasing the inter-electrode exchange coupling, figure 1.17(b). Strength of impurity assisted exchange coupling was shown to directly depending upon their concentration.

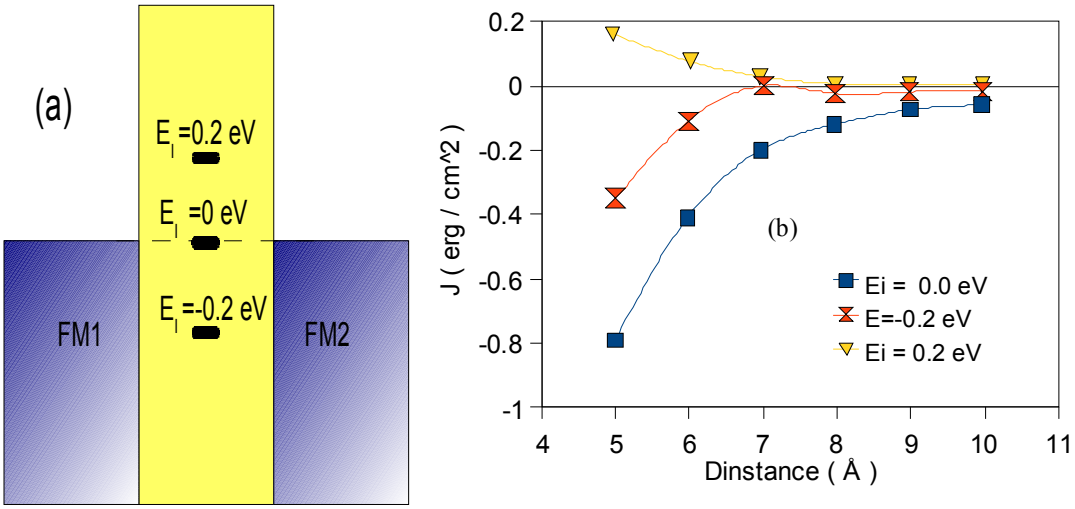

Figure 1.17: Band diagram of a MTJ showing the position of the impurity levels within the tunnel barrier (a) enhancing the exchange coupling energy between two FM electrodes. Exchange energy versus impurity position in tunnel barrier for the three energy levels with respect to Fermi energy level. Exchange coupling energy via impurity free barrier is ~$1x10^{-3}$ erg/cm^2. Adapted from ref. [92].

It is evident that molecule or strongly coupled quantum dots to the ferromagnetic electrodes[96] can produce an extraordinarily strong exchange field,[56] which is not attainable within a laboratory. This magnetic field, around the junction, has been experimentally seen to influence the molecular levels.[13] Can the same strong exchange field[97] also affect the band structure of the ferromagnetic metals by producing Zeeman like splitting? If so then band offset for the spin up and spin down DOS is going to be more than the Stoner splitting.[46] Zeeman splitting for an electron level and the shift in Fermi level of a ferromagnetic metal (ΔH), due the application of magnetic field H, are $\pm 0.5(g\mu_0\mu_B H)$ and $\pm 0.5(Pg\mu_0\mu_B H)$, respectively[46].

A direct consequence of the larger band offset will be the larger difference in the spin populations of a ferromagnetic metal (FM), figure 1.18. In the conductance versus magnetic field study of ferromagnet-quantum dot-ferromagnet system observed conductance fluctuations were attributed to the Zeeman splitting of ferromagnetic metals.[98] This study insinuates that the molecule induced strong exchange field between two FMs has the potential to dramatically affect the molecular junction transport. Moreover, recent theoretical study on the strongly coupled quantum dot to the magnetic electrode considered various forms of the band diagrams of the ferromagnetic metals to capture the precise physics of strongly coupled ferromagnetic electrode system.[99]

Since atom(s) of the FM metal experiencing the molecule/quantum dot mediated field are also coupled to the atoms of the bulk via Heisenberg exchange coupling,[99] localized effect can give rise to a long range magnetic ordering. However, the experimental study of the change in the magnetic properties of the ferromagnetic electrode(s) due to molecules, quantum dots and impurity would need sample size much bigger than the brekjunctions.[13]

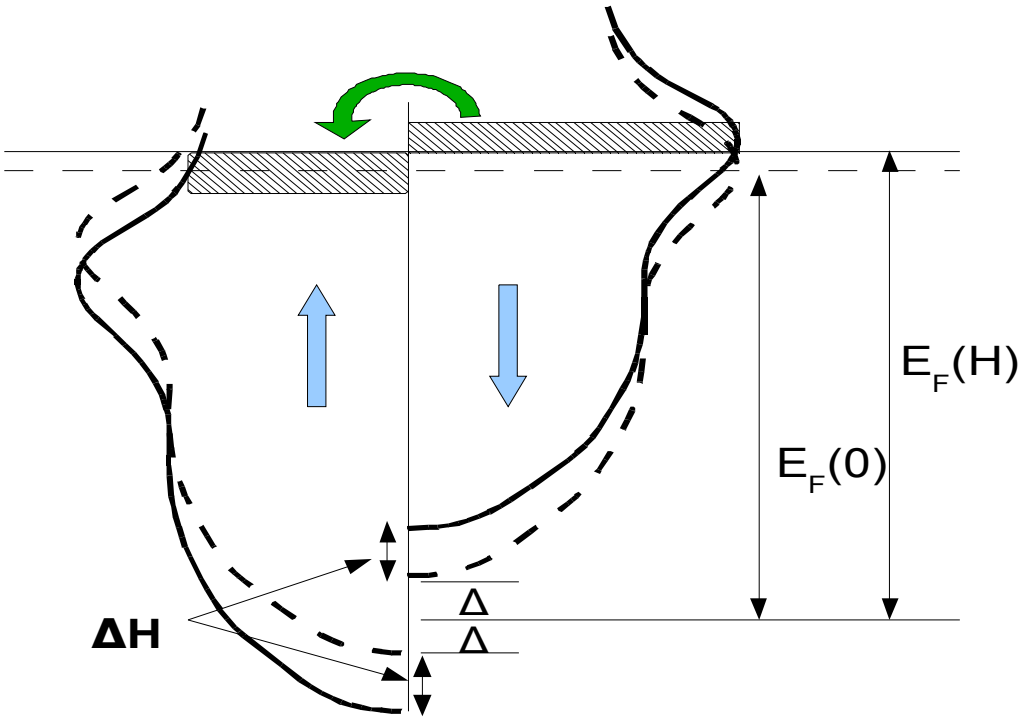

$E_F(0)$= Fermi energy in zero magnetic field
$E_F(H)$=Fermi Energy in H magnetic field
Δ= Stoner splitting
ΔH= Zeeman splitting energy

Figure 1.18: External magnetic field producing redistribution of spin density and shift in Fermi energy level of in ferromagnetic band. Adapted from ref. [53].

By now we have seen the effect of molecular spin state on the molecular transport in mainly s = ½ or low spin states. Utilization of the high spin state molecules[33] such as single molecular magnets (SMM) in molecular junction can be very interesting; SMMs are promising candidates for producing molecular spin devices which are switchable due to light and magnetic field.[8] Heersche et al.[33] produced gold break junction based molecular junction by bridging $[Mn_{12}O_{12}(O_2C\text{-}R\text{-}SAc)(H_2O)_4]$ molecules, described as Mn_{12}. Here R refers to alkane tethers. It helps SMM binding to metal electrodes, separated by a nanogap, to create robust bond, which also serves as tunnel barrier. It was reported that a SMM based molecular junction exhibited negative differential conductance (NDC) and total charge current suppression phenomenon. Interestingly, a single SMM based molecular junction was reported to show three different charge transport regions in the conductance-bias voltage-gate voltage spectra. “This kind of behavior is

otherwise expected to arise from three different quantum dots".[33] This result hints towards the possibility of using same molecular junction for the different device characteristics. These different charge transport regions were assumed to be associated with there different states of the same molecule.

Authors have summarized that CCS and NDC in SMM molecular junction is due to the intrinsic characteristic of molecules. For the quantitative explanation of experimental results a sequential tunneling model with spin Hamiltonian of SMM has been considered. The spin Hamiltonian is believed to capture the effect of the high spin ground state of SMM and its ladder of spin excited states in transport of SMM junction.[33] From the analysis it is apparent that a sequence of tunnel processes can yield a non-equilibrium population of certain excited states. Subsequent depopulation from these excited states will occur slowly by violating the spin selection rule, due to quantum tunneling of magnetization.[29] In this event transport of charge was shown to be hampered to produce CCS and NDC observations. In a theoretical study of a system of SMM attached to two ferromagnetic electrodes, it was calculated that interference between different tunneling paths within the molecule can produce a dramatic current suppression. Interference between molecular states lead to Berry phase.[32] With the aim of studying SMM based molecular junctions in magnetic field thoroughly, similar SMM functionalized[100] and unfunctionalized[39] has been utilized. The device instabilities, potential damage to SMM, irreproachability appear to plague the further progress.[101] Moreover, STM study, in which it is quite easy to controllably address single SMM, could reveal that the SMM has ~1.0 V HUMO – LUMO gap.[102]

From the above given discussion it is clear that molecule based spin devices are promising for the making of spin-valve devices. Utilizing molecular bridges between two metallic electrodes allows exploring of new spin dependent phenomenon in metal-molecule systems. A more interesting, yet challenging idea is to attach high spin state molecular complex[3] to ferromagnetic leads to produce molecular spin valves.[40] Advancement of molecular spin device would ultimately rely on their functioning at room temperature. For this devices do not have to be based on single molecule.

1.3. Molecular electrode design for molecular spintronics:

Fabrication of molecular spintronics devices[13] is expected to be more challenging than that for molecular electronics devices and magnetic tunnel junctions[18]. Producing reproducible molecular device with ferromagnetic electrodes, functioning at RT, is a daunting task. On the other hand fabrication of a MTJ with a metal oxide insulator that possesses the virtue of molecules (long spin coherence, reproducible fixed length to atomic dimensions and well defined metal/molecule interface) is apparently implausible. A practical molecular spin device is expected to unite attributes of a MTJ[17] and molecular devices[4].

What can be the suitable device design for molecular spin devices can justified from the following discussion. In one of the pioneering experimental attempt Petta et al.[16] have fabricated molecular magnetic tunnel junction with nanopore geometry. These devices mainly studied at cryogenic temperatures and exhibited large device to device scatter. In order to make the top metal contact with active molecules, physical vapor deposition was performed on the monolayer self-assembled on metallic surface. This scheme is inevitably likely to suffer with the impurities coming arising due to diffused metal atoms and self assembly step[34]. Since device lateral dimensions are very small due to nanopore geometry adverse effects of the impurity and defects could be minimized; as high as 17% TMR could be observed at cryogenic temperature[16]. Moreover, metal deposition steps for nanopore geometry are quite tricky. Such schemes are unlikely to yield reproducible molecular spin devices purely dictated by the attributes of molecules.

Break junctions have been the most popular test pads for studying the influence of molecular magnetic state on molecular transport.[13] Break junctions are rather easy to produce with gold electrodes and have been employed to observe Kondo effect, a magnetic correlated state.[86] In our knowledge only in one study break junction with Ni magnetic electrodes were successfully employed. Break junctions based devices are excellent test pads but suffer with poor reproducibility and very low yield.[86] Every break junction device has dissimilar environment for a molecule. Atomic defects in break junction can also imitate the attribute of a molecule.[86]. For instance a celebrated Kondo effect due to molecules could be seen in bare break junctions;[103] difficulty in studying break junctions before molecule attachment can make any finding questionable.[90] The two metal electrodes of a break junction are of same; molecular spin devices can not use highly refined multilayer configuration of top and bottom electrodes utilized in magnetic tunnel junctions.

Magnetic tunnel junctions having the possibility of attaching molecules between two metallic electrodes similar to the break junction device can be the basis of successful molecular spin devices. By default magnetic tunnel junction utilizes molecular dimension metal oxide insulators. An ion milled MTJ stack, with sharp vertical cut, reveals the sharp edges where looking from the side one finds that the top and the bottom electrode possesses the open site for the bridging of molecules between two metal electrodes. This minimum distance between the two electrodes is equal to the insulator film thickness. Since in a typical MTJ lateral dimensions are of few microns to hundreds of nm large, a big population of molecules will have the opportunity to form molecular junction. The large number of molecular channels is expected to dictate the molecular transport. One can imagine this design is akin to break junction. One can consider that break junctions are made perpendicular to the plane of substrate and kept abut to form a parallel array of break junctions. Aim of following work is to realize a tunnel junction based molecular spin device.

Chapter 2

Mechanical Stress Control for the Fabrication of Stable Molecular Electrodes at the Patterned Edges of Metal/Insulator/Metal Junctions

2.1 Introduction

The use of molecules as the primary switching element in logic and memory devices[4] is a highly active research area with difficult technological challenges. The main attributes of molecular electronics are: angstrom level control of structure, cost effective manufacturing, lower power consumption, and high aerial density and flexibility to tailor the electronic properties of a molecule through synthetic chemistry.[9,104] A variety of molecular junctions have been explored and demonstrated at the laboratory scale e.g. metal break junctions,[7] nano-pore junctions,[105] sandwiching the molecule layer between two metal electrodes,[9,106] forming molecular junctions by a scanning tunneling microscope tip[65] and a conducting probe of atomic force microscope[107,108] as a second electrode on the self assembled molecules on metal. There remains a great challenge to make molecular devices that are stable, reproducible, flexible in using different electrode materials, and are suitable for mass production.

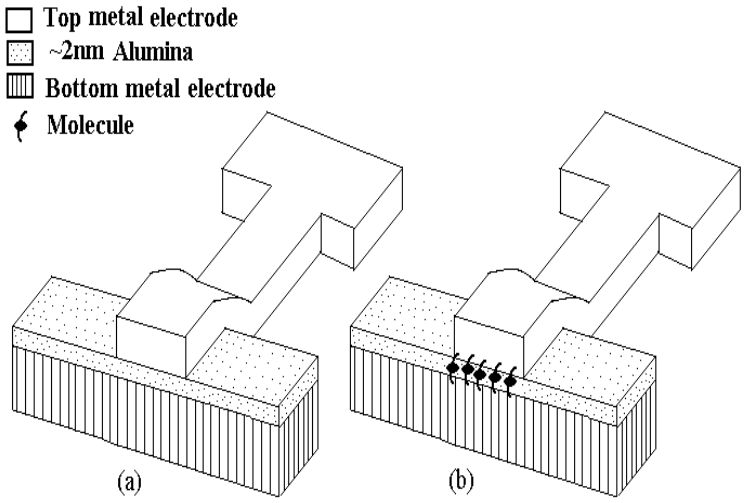

Figure 2.1: Modification of a simple tunnel junction into molecular electrodes. (a) 3D of bare tunnel junction (b) 3D of tunnel junction after attaching molecule by self assembly.

Recently, a new class of molecular electrodes[109,110] has been reported where thin film thickness is utilized to set the nm-scale gap between two electrodes. A key advantage of this approach is that metallic contacts with a wide variety of metals,[9] including ferromagnetics for molecular spin-injection, can be incorporated into the design. One way to make stable molecular electrodes with a large difference between background current (in planar area of electrode) and molecular current (at the edge of the pattern) is to use a thick insulator (4-10nm) and then attach long molecular chains to bridge the insulator gap.[111] Ideally, the separation between two metal electrodes can be set to the dimensions of single molecular clusters offering well-defined molecular conduction paths as schematically shown in figure 2.1. As a practical consideration, the background tunnel current is too high for junctions <~1nm for small molecule conduction, hence the larger molecular dimensions of clusters (~2nm) are favored in this geometry. However, the major challenge even at 2nm thickness is to produce a stable insulator barrier with low leakage current through the planar junction area thus allowing molecular conduction paths at the pattern edge to dominate. Depending upon molecule design, conduction through the molecule can be controlled by the external input such as light, magnetic field, and chemical environment. In this chapter we illustrate the role of mechanical stresses on the tunnel barrier stabilityand insulator deposition methods to counteract the effects of the stresses. Lastly we demonstrate molecular electrode fabrication process.

2.2 Experimental details

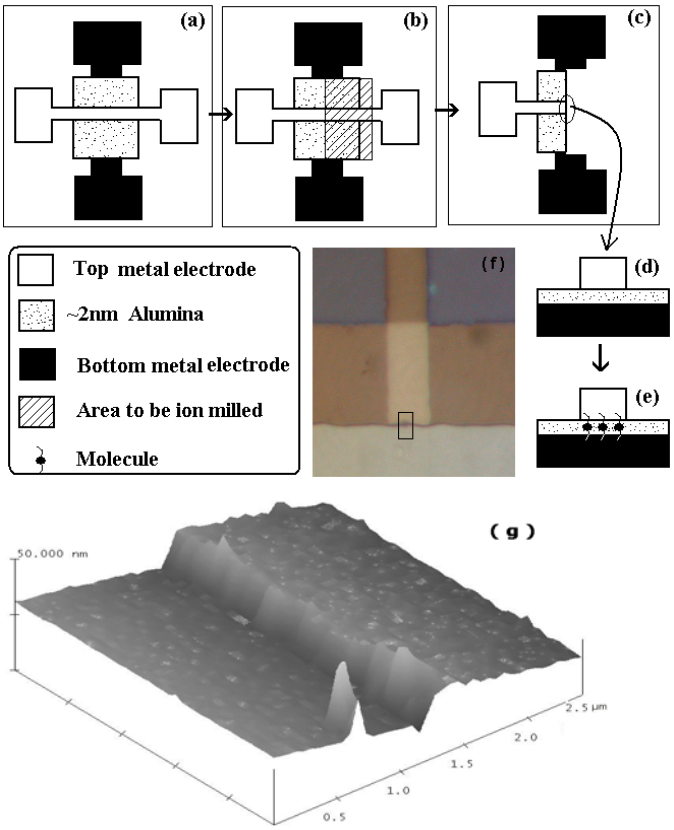

Figure 2.2: (a) Metal-insulator-metal tunnel junction fabricated by sandwiching ~2nm Al_2O_3 between two metal electrodes. Bottom metal electrode (top metal electrode) is produced by depositing 8nm Co and 2nmNiFe (only 10nm NiFe) in photolithographically defined pattern. (b) Created window for ion milling to produce vertically sharp exposed side of tunnel junction, (c) top view of tunnel junction after ion milling (f) optical micrograph from the top side of an actual ion milled TJ (d) side view of sharp and exposed metal-insulator –metal TJ after ion milling (e) ion milled TJ after molecule attachment or bridging the molecule across insulator gap. (g) 3D AFM image of ionmilled TJ in the rectangular are a as shown in (f). Note width of top electrode is 5µm. Bottom electrode dimension used in this study was ~2µm and ~8µm.

To understand the role of the stresses and their effects on tunnel barrier morphology of metal-insulator-metal tunnel junctions utilized in our molecular junction scheme, unpatterned samples without top metal and with metal-insulator configuration were prepared. The bilayers possess a sufficient stress level to bring about similar morphological changes on the ultrathin insulator, alumina in present work, as one would expect with metal-insulator-metal trilayers. This approach made alumina directly accessible for the morphological study by the atomic force

microscope (AFM) and the transmission electron microscope (TEM). <100> Silicon (Si) substrate with 100nm silicon oxide (SiO_2) was utilized. For the TEM study, 50nm thick electron transparent silicon nitride (Si_3N_4) windows on etched Si<100> was used as substrate. Throughout this work, cobalt (Co) and nickel-iron (NiFe), with Ni:Fe::80:20 ratio, metals, and plasma oxidized aluminum was utilized as an alumina (Al_2O_3) insulator. Unpatterned, Si/SiO_2(100nm)/Co(10nm)/Al_2O_3(~2nm) samples, were fabricated for the stress measurement (using Veeco, Dektack 6M profilometer) and morphological study (using Digital Instrument Multimode AFM) in contact mode. It was noted that the sputtering of the thin films inherently produced compressive stresses in the samples and can be termed as a general case. However, tensile stress was only observed after heating and mechanical bending of sample before deposition in the sputtering instrument. The stress measurement was performed by the substrate curvature method.[112] Radius of curvature for the oxidized silicon substrate was obtained before and periodically after the deposition of unpatterned Co(10nm) and then alumina(2nm) on it. The substrate radius was then applied to the Stoney formula to calculate the nature and magnitude of stresses. The Stoney formula connects the radius of curvature *R*, the in-plane component of the stress σ_0, and the thickness of both the bilayer structure (h_l) and the substrate (hs), as given below

$$\sigma_0 = \frac{E_s}{6(1-\nu)} \frac{h^2{}_s}{h_l R} \tag{2.1}$$

Where *Es* and ν are, respectively, the Young's modulus and the Poisson's ratio of the substrate.Values of *Es* and ν*s* for <100> silicon substrate are 130GPa and 0.2783 respectively.[113] Wafer thickness (*hs*) is 400μm and total film thickness (h_l) is 12nm.

A TEM study was also performed on an analogous system but with a different composition. Titanium (Ti), for good adhesion, was placed between Co/Al_2O_3 bilayer and electron transparent silicon nitride substrate present on the TEM grid to form [Si_3N_4(50nm)/Ti(2nm)/Co(10nm)/Al_2O_3(2nm)] structure. For this study a 200 kV field emission analytical transmission electron microscope (JEOL JEM-2010F) equipped with an Oxford energy-dispersive X-ray spectrometer, a scanning (STEM) unit with a high-angle annular dark field (HAADF) detector and a Gatan imaging filter (GIF) system was utilized.

Tunnel Junctions (TJ) [Si/SiO_2(100nm)/Co(8nm)/NiFe(2nm)/Al_2O_3(2nm)/ NiFe(10nm)] for molecular electrodes were prepared following the established magnetic tunnel junction fabrication approach with 1-2 nm thick insulator layers as an active device element.[18] Photolithography (using Karl –Suss mask aligner) for defining the pattern for multilayer deposition, sputtering process (using AJA International Sputtering system) for depositing metal electrodes and Al_2O_3 film, and ion milling (using FISCHIONE 1010 ion mill) for creating a sharp

exposed side edge of TJ, were utilized. NiFe is used on both sides of the Al_2O_3 due to its air and chemical stability[114] and better oxide coverage as compared to Au. From the TEM studies,[115] it is well established that the ion milling process reliably produces sharp vertical cuts on multilayer. To avoid photoresist hardening, the sample was cooled by liquid nitrogen during ion milling. Extra care was taken to avoid ion milling-caused damage to the thin Al_2O_3 barrier by adopting a low angle and a low energy argon ion beam for milling. The molecular electrode fabrication scheme is summarized in figure 2.2. Typical junction areas of a TJ were 10 and 40μm^2 and the effective length of the exposed edge, where molecules were attached, is 5μm.

Base pressure for sputtering was ~2x10^{-7}torr for all the depositions. NiFe and Co films were deposited using a RF-powered gun at 150W power and 1mtorr argon (Ar) pressure. Alumina deposition, for molecular electrodes fabrication, was accomplished in two steps. In the first (second) step 1nm (0.5nm) Al was deposited using a DC-powered gun with 75W power and 2 mtorr Ar pressure. Each Al deposition was followed by plasma oxidation for 30 seconds at 20W RF power and at 60 mtorr pressure of 1:1 argon and oxygen mixture. Details of alumina deposition for stress and morphological studies are described elsewhere in this chapter. It is noteworthy that sputtering parameters for NiFe, Co and Al deposition were individually optimized to produce the least roughness value before the fabrication of molecular devices and samples for the stress study.

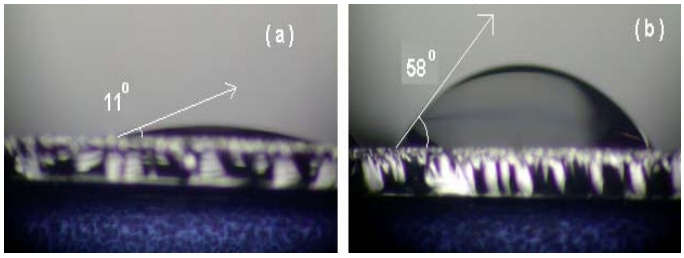

Figure 2.3: Water contact angle was 11º on bare NiFe film(a) but increased to 58º after the functionalization of NiFe metal with organometallic metallic molecules (b) used in this study.

A ~3nm long organometallic cluster (OMC) with thioacetate terminated tethers was synthesized[3] for the attachment across the insulator gap utilized in the present electrode design. Through thiol surface attachment to metal leads, an array of OMC, $[(pzTp)Fe^{III}(CN)_3]_4[Ni^{II}(L)]_4$-$[O_3SCF_3]_4$ [(pzTp) = tetra(pyrazol-1-yl)borate; L = 1-S(acetyl)tris(pyrazolyl)decane], were covalently linked to top and bottom electrodes to span the edge of the insulator film to form a dominant conduction pathways.[116] This molecule essentially comprises a cube of 8 edges of cyanide bridged Ni and Fe atoms (-Ni-N≡C-Fe-). There are four 10 carbon alkane tethers connected to Ni atoms of the molecule's cube at one end and to the metal electrode, with thio-

acetate group, on another end.[3] The thioacetate group is a protecting group to preclude thiol reactions during the formation of an octametalic core. This thiolacetate group is readily removed during an electrochemical molecule attachment process[117] on the device to form thiol-Ni surface bonds. To attach the molecule to electrodes, a 2mM solution of OMC in dichloromethane (CH_2Cl_2) solvent was subjected to the alternating ±100mV biasing between two metal electrodes with a time interval of 0.02 seconds for a period of 2 minutes. After the molecule attachment process samples were rinsed with CH_2Cl_2, iso-propyl alcohol and DI water (18Mohm), the samples were dried. Electrical properties of TJ before and after molecule attachment were studied with Keithley 2430 1KW Pulse Source Meter. Effectiveness of the electrochemical step in making metal-molecule bonds were confirmed by the contact angle measurement on the flat NiFe metal film, used in the actual TJ to interact with molecules. It was found that the water contact angle on NiFe film rose from 11(±1.5)º to 58(± 1.6)º after electrochemistry of molecules, affirming the chemisorptions of the molecules on the metal films, figure 2.3. The reaction between Ni metal and thiol ended molecules are well established. [118]

2.3 Results and discussion

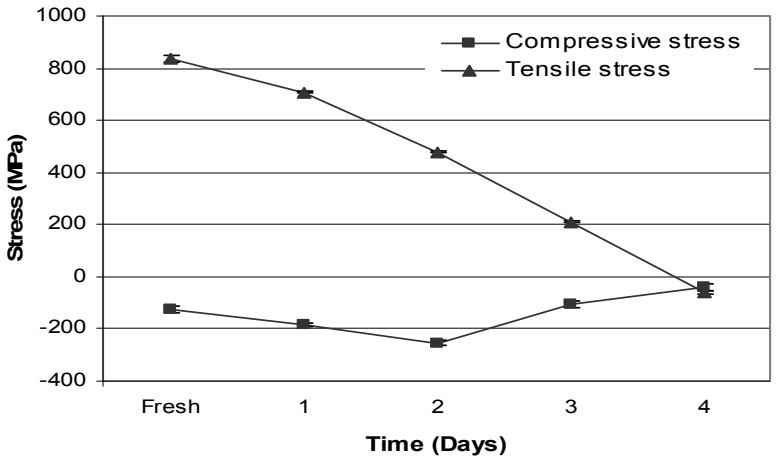

Figure 2.4: Compressive and tensile stresses are relaxing with time on multilayer Si/SiO_2(100nm)/Co(10nm)/ Al_2O_3 (~2nm).

The thin alumina film insulator is the most important part of the Tunnel Junction (TJ)- based molecular electrodes. The stability of a thin alumina film used in TJs has been nearly exclusively characterized in terms of electrical breakdown voltage.[119] Insignificant attention was given to the role of mechanical stresses in the tunnel barrier breakdown. In our studies, we have observed that both tensile and compressive stresses appeared in multilayer samples. First, we studied the stress

evolution and corresponding morphological changes by AFM in the $Si/SiO_2(100nm)/Co(10nm)/Al_2O_3$ (~2nm) samples. Invariably, compressive stresses were observed after sputter deposition of the metal and the insulator at low pressure (0.5-5mtorr). However, to induce arbitrary tensile stress levels in the sample, the substrate was bent to acquire a slightly concave shape on the front side facing the target gun, where Co and Al_2O_3 film were deposited. After deposition, the sample possessed ~830 MPa tensile stresses. It was observed that both tensile and compressive stresses relaxed with time, as shown in figure 2.4, but at the expense of severe morphological changes in an alumina film. However, compressive stress relaxed in a rather complex oscillatory behavior. This is consistent with the continued oxidation of the Co top layer generating compressive stresses that relax by deformation events. It should be noted that deposition of only the Co layer produced nearly 120MPa compressive stress. Stress level generally became more compressive (~150-200 MPa) after the deposition of alumina layer.

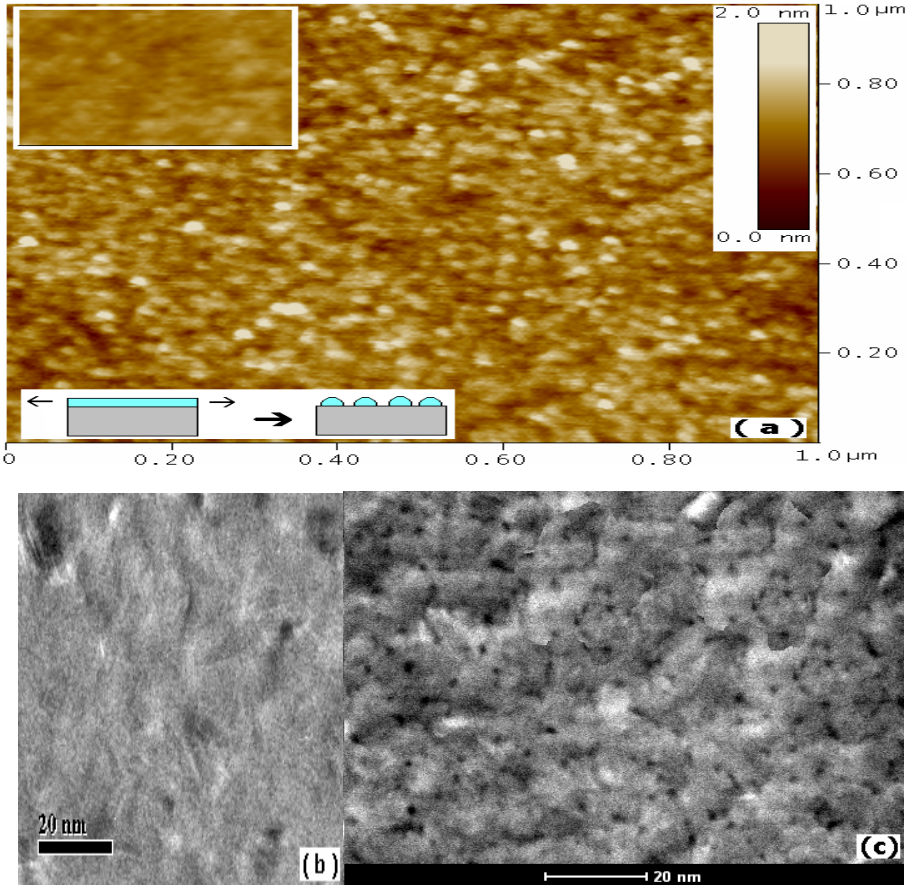

Figure 2.5: Effect of tensile stress relaxation on alumina covered cobalt film. (a)This system was atomically smooth when fresh as shown in inset but surface roughness increased 4-6 fold after tensile stress relaxation. TEM images of similar system before (b) and after (c) tensile stress relaxation.

According to the AFM study, after 3 days of tensile stress relaxation on the bilayer sample (initially with tensile stress), the surface roughness increased by ~6 fold. The Rq roughness of a fresh sample, shown in top inset of figure 2.5(a), and a 3 days old sample, shown in figure 2.5(a), was 0.25±0.05 and 1.5±0.1nm, respectively. We surmise that brittle alumina with poor fracture toughness (3-5 KPa.m$^{1/2}$),[120] as compared with that of ductile Co (>50KPa.m$^{1/2}$),[121] fragmented due to its inability to plastically deform under the tensile stress. However, the cobalt metal film plastically deformed and remained continuous under the tensile stress. A conceptual picture of this mechanism is given in the lower inset of figure 2.5(a). To confirm this hypothesis, a TEM study on Si_3N_4(50nm)/Ti(2nm)/Co(10nm)/Al_2O_3(2nm) sample was performed. It was found that heating by an e-beam during the TEM study[122] itself produced the tensile stress in the Al_2O_3 layer. This tensile stress roughened the initially smooth sample surface, figure 2.5(b), due to the emergence of a dense population of cavities as the Al_2O_3 layer fractured, figure 2.5(c). In bright field imaging, underfocus gives dark contrast for voids. The sample was also rotated to show that the dark contrast was not due to diffraction scattering. Both the TEM and AFM studies of the surface morphology resulting from the tensile stress relaxation are in good agreement and clearly indicate that the fracturing of a 2nm thick Al_2O_3, as depicted in the conceptual picture. For comparison, the oxidation of bare Co film after one week of oxidation in air showed a smooth Rq of <0.3nm). AFM observations of the tensile stress relaxation on the alumina covered Co layer produced nearly 1.5 nm Rq. Alumina barrier thickness, obtained from the AFM-based step height measurement and transport data of a TJ, and confirmed that thickness of alumina was ~ 2nm. This corresponds to the complete oxidation of deposited Al. The ~1.5nm Rq roughness of the sample, following tensile stress relaxation, is consistent with the fracture of alumina layer.

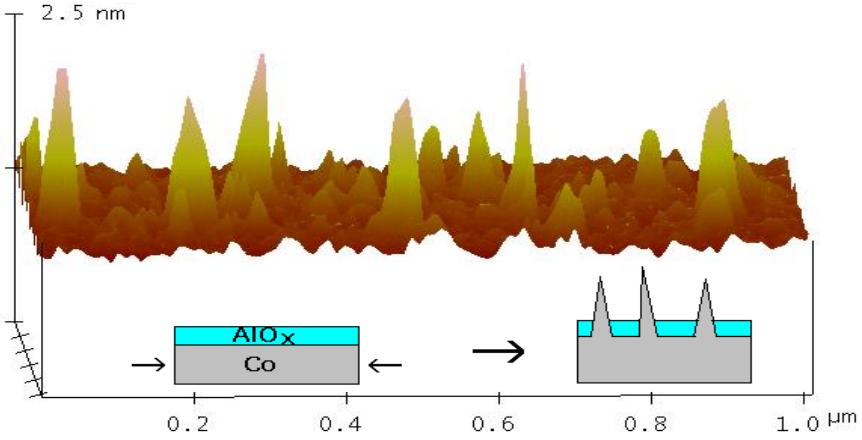

Figure 2.6: 3D AFM image of Si/SiO_2/Co/Al_2O_3 sample after 3 days of compressive stress relaxation shows the hillocks formation. As deposited sample showed negligible hillocks density and surface roughness was 0.2nm.

Compressive stresses showed a different failure mechanism. The AFM study of the Si/SiO_2(100nm)/Co(10nm)/ Al_2O_3(~2nm) sample after 3 days of compressive stress relaxation suggests the evolution of nano-hillocks or nano-coneslike features, figure 2.6. The typical diameter and height of such features was 5-50nm and 0.5-5nm, respectively. We believe that under the effect of compressive stress, hard alumina remains stable while the ductile Co metal extrudes out through the weak points and pinholes in alumina film. A conceptual picture of the related mechanism is shown in the inset of figure 2.6.

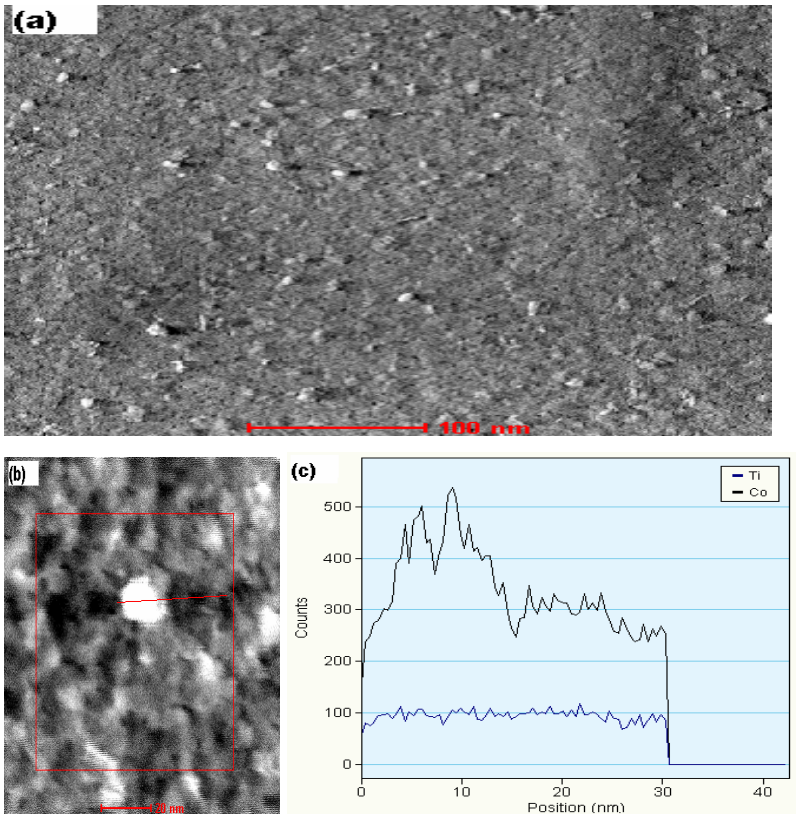

Figure 2.7: (a) TEM study show nano hillocks formation and their shadow on Si/Ti(2nm)/Co/Al_2O_3/alumina multilayer. (b) Magnified version of nanohillock and (c) elemental analysis on hillocks shown in (b) confirm that it is made up of Co, the metal underneath alumina film.

Hillocking and whisker formation under compressive stress is a well established phenomenon that causes failure in interconnect technology.[123] To confirm the nano-hillock formation due to compressive stress, TEM was performed on the Si_3N_4(50nm)/Ti(2nm)/Co(10nm)/Al_2O_3 (2nm) samples with compressive stress from the sputtering of the films. We observed nano-hillocks with a 10-20nm diameter, figure 2.7(a).

Elemental analysis of individual hillocks, figure 2.7(b), strongly suggested that they are made up of Co metal present underneath 2nm alumina, figure 2.7(c). The presence of Ti in element analysis was from the ultrathin adhesion layer. Inability to statistically cut through the nano-hillocks in sample preparation precluded the cross sectional TEM study of hillocks. AFM and TEM study together confirm the nano-hillock formation as a consequence of compressive stress relaxation and fits to the presented conceptual picture. According to an estimate, the amount of compressive stress required to produce a nano-hillock of cobalt with 20nm diameter and 5nm height was 180 MPa.[124] In our study we have found as high as 500MPa compressive stress in the multilayers, which are of the same order of stress required to produce hillocking.[121]

Knowing the role of mechanical stresses, growth conditions were optimized to achieve stable alumina. In order to grow ~2nm alumina, we first deposited Al in one to three steps and after each step 30 seconds plasma oxidation commenced. Motivation for the multistep Al_2O_3 deposition came from the earlier work that reported significant improvement in electrical properties with 2 step Al_2O_3 deposition.[125] Sample names, S15, S10-5, S5-10 and S5-5-5, were selected to clearly indicate the number of steps incorporated and the amount of aluminum (Al), in Å unit, deposited in each step on top of ~10nm thick Co film. For instance, S10-5 would indicate two step processes where a 10 Å Al deposition is followed by the first plasma oxidation, then followed by a 5 Å Al deposition and lastly followed by the second plasma oxidation. Each process would result in ~20 Å of Al_2O_3 after volume expansion by oxidation. Note all the samples are unpatterned unless stated.

Table 2.1: Level of stress, hillocks density, hillocks height, stability of TJ prepared by using S15, S10-5, S5-10 and S5-5-5 alumina growth approaches.

Sample Name	Compressive Stress (MPa)		Hillocks density per μm^2		Average Hillock height (nm)		TJ life (Days)
	As grown	3 days later	As grown	3 days later	As grown	3 days later	
S15	186± 6	20±15	2	37	1.8	2.6	14
S10-5	263± 21	4±21	3	17	0.7	2..2	30
S5-10	348± 7	161 ±13	5	60	1.8	1..9	3
S5-5-5	428± 7	190 ±10	4	9	3	5	0.5

The calculations of average hillocks density and hillocks height from the AFM study and the stress measurement study were carried out on the fresh and the 3 days old S15, S10-5, S5-10 and S5-5-5 samples. S15 samples are comparable to the compressive samples of Figures 2.4, 2.6, and 2.7. Simultaneously, patterned tunnel junctions, with the $Si/SiO_2/Co(10nm0/Al_2O_3(2nm)/NiFe(10nm)$ configuration were also prepared by using these four alumina growth schemes for the electrical and the device life study. Fitting the current voltage data with the Simmons tunneling model[50] provided 2±0.2nm barrier thickness and 0.9±0.1 eV barrier height. In order to determine the device life, a TJ was subjected to periodic low bias (± 50mV) I-V measurement till a TJ started showing instability in the transport. Device failure is determined by the dramatic current increase and I-V curves becoming linear (ohmic) at the observed time. Since the applied bias is only ±50 mV and is far below the breakdown voltage (1.8V), failure is due to the mechanical stress relaxation process. In general, a compressive stress relaxation occurring in such systems leads to nano-hillocks formation. These nanohillocks produce short circuits between the top electrode and bottom electrode, resulting in junction failure. Results of all the studies are tabulated in Table 2.1.

Table 2.1 shows that the compressive stresses, observed in all the samples, significantly relax after 3 days. The AFM study shows that the density and average height of hillocks increased in all the cases. For the S5-5-5 case hillocks density increased minimally but hillocks height, which was already quite tall, have increased drastically. We expect quick development of shorts and hence an unstable TJ, as also suggested by the device life data on TJ prepared with the S5-5-5 approach. The S5-10 sample showed drastic increase in hillocks density but moderate increase in their height. Poor tunnel quality was expected and confirmed by the tunnel device life time data. The S10-5 sample, which exhibited minimum increase in the hillocks density and moderate increase in the average hillocks height, appears to be the most promising alumina growth approach. Tunnel devices prepared with this scheme gave the best performance and the longest device life. Therefore we opted to make our molecular electrodes using S10-5, two steps alumina growth approach.

Next we fabricated the stable molecular electrode with the $Si/SiO_2/Co(8nm)/NiFe(2nm)/Al_2O_3(2nm)/NiFe(10nm)$ configuration and with a vertically sharp exposed edge. We used the optimized 2-step alumina deposition condition, the electrode fabrication scheme shown in figure 2.2 and attached the organometallic molecules electrochemically. NiFe metal surface is known to have elemental Ni (non-oxidized) surface in ambient conditions[114] which facilitate the Ni-S bond formation for the establishment of molecular conduction channels. This is evident in the change in water contact angle shown in figure 2.3.

Current-voltage (I-V) measurement on the tunnel junctions (6 devices) before and after molecule attachment showed a clear current enhancement by ~350±80% (~120±30%) for 10μm^2 (40μm^2) TJ area due to the bridging of molecules forming additional current paths. Representative transport study on TJ before and after molecule attachment is shown in figure 2.8. In the figure 2.8 the current of a bare and molecule attached TJ with 10μm^2 (40μm^2) junction area at 100mV bias are 0.5μA and 2.0μA (1.7μA and 3.32μA) respectively. The additional molecular current at 100mV bias was 1.5 μA and 1.6 μA for the 5um long window cut into each TJ (10μm^2 and 40μm^2). Each sample has nearly the same number of molecular channels since both have 5um long exposed junction area for molecular attachment. Assuming that the molecules bridge densely along the pattern edge (~1nm each) about 5000 molecules are conducting in the device. At 100mV this yields 0.5±0.3 nA current/molecule which is concurrent with previous reports for both ion-milled and photolighography defined junctions.[116]

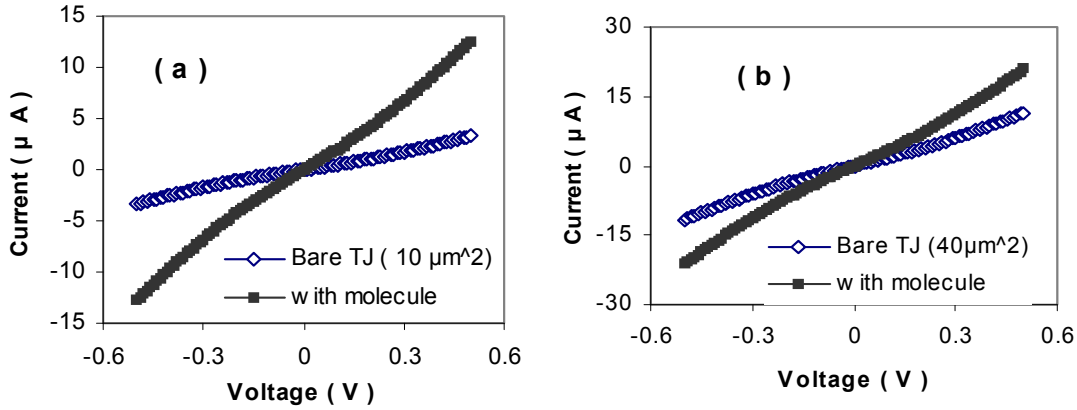

Figure 2.8: I-V study before and after molecule attachment on Co/NiFe/AlOx/NiFe tunnel junctions with (a) 10 μm^2 and (b) 40μm^2 junction area.

In order to prove that current increase for the electrode is only due to the addition of molecular conduction channels, we have performed number of control experiments on the analogous system.[109] In summary these included treatment with neat solvent, binding with non-organometallic di-thiol molecules, non-bridging mono-thiol molecules, insulators too thick for molecular bridging, and reversible binding with an Au top electrode. Results of all control experiments were consistent with the organomettalic complex being the additional conduction path for the molecular electrode. Simmon's analysis of the molecular conduction was consistent with charge tunneling from first electrode through the alkane tether to the organomettalic core, then subsequent tunneling through alkane tether to second electrode.[9] This allows tunneling into

the well-defined electronic states of the organometallic clusters to dominate the macroscopic current of the device.

2.4 Conclusion

By optimization of thin-film stresses and insulator growth a new type of molecular electrodes on the exposed edge of ion milled tunnel junction has been fabricated. A larger contrast between tunnel junction background current (planar area) and molecular current at the pattern edge can be attained by reducing the tunnel junction area by employing commercially available high resolution photolithography process (~50nm). The mechanical stresses were the primary source of instability in the molecular electrodes. The adverse effects of the stresses, mainly compressive hillock formation, were mitigated by using the optimum alumina growth scheme. A double-step alumina deposition was found to be the most stable and reliable for molecular electrodes realization. Understanding of stress induced failure is important for all those devices where ultrathin insulator (<5nm) is utilized as tunnel barrier or gate insulator on diverse materials such as ferromagnetic metals. We have extensively utilized the information furnished in this chapter for the tunnel junctions and molecular electrodes fabrication illustrated in the following chapters.

Chapter 3

Molecular Electrodes at the Exposed Edge of Metal-Insulator-Metal Trilayer Structures

This chapter is based on following manuscript

P. Tyagi, D. F. Li, S. M. Holmes, and B. J. Hinds, "*Molecular Electrodes at the Exposed Edge of Metal-Insulator-Metal Trilayer Structures"* Journal of The American Chemical Society **129,** 4923-4928 (2007).

3.6 Introduction

An ultimate goal of electronics miniaturization is to have discrete molecules act as logic or switching elements. An advantage to this approach is that the molecules can be synthesized reproducibly at the angstrom scale with well-defined electronic states tuned through chemical functionality. Electrical transport through molecules has been investigated via a variety of theoretical[6] and experimental methods, with promising observations such as negative differential resistance[126], spin-state dependent conduction [39,31] and stable memory based on conformational shifts being demonstrated recently.[127] To date, no single fabrication approach has allowed for the facile integration of molecules into circuit architectures. For molecule-based electronics to become a technological reality, electrode architectures must be engineered with nanometer scale dimensions and allow for the incorporation of bistable molecules that can be synthesized and tuned with angstrom level precision.

One of the major challenges in the field has been to reliably integrate molecules into circuit architectures, where mass produced electrodes with gaps at the nanometer scale and angstrom precision are needed. In particular, it has been difficult to reliably make electrodes where electron conduction travels along the length of a molecule. Initial studies of molecular currents through isolated molecules utilized 1,4-benzenedithiols inserted into gold break junctions were prepared via mechanical or electromigration techniques[7], where atomically sharp points terminate each electrode, separated by nanometer-sized gaps. While this is an experimentally attainable process, it is exceedingly difficult to control the dimensions of the gap between electrodes. This requires tedious analysis of the prepared break junction devices, to ensure that conduction through the molecules dominate rather than electron hopping via nanometer-scale metallic islands (Coulomb blockade).[90] A second approach for contacting molecules lengthwise, utilizes densely packed arrays of molecules on metallic surfaces, followed by careful deposition of metal films onto the self-assembled monolayer (SAMs) array. Unfortunately this approach

suffers from electrical shorts through defect areas, which can be minimized through the use of small contact areas located in nanopores,[128] micropatterns, or areas under gold nanocrystals.[129] While these structures are useful for studying molecular conduction processes they do not allow for external gating nor possess exposed regions for chemical sensing.

A third promising approach utilizes molecular wires that require only two metallic terminals, whose logic function is determined by the applied bias and location of a charged rotaxane molecule along the length of a conductive chain. To minimize electrical shorting of the electrical terminals, incorporation of the rotoxane assemblies under the small area (20x20nm) of crossed metallic nanowires, allows for each junction to be addressed and logic architectures formed.[130] However, a significant challenge in this approach is the reliable alignment of nanowires into multi-million node arrays for very large scale integration (VLSI) applications. A technique that utilizes established scalable processes, such as photo lithography and thin film deposition to produce electrodes with gap lengths of molecular dimensions, is critical for the advancement of molecular electronic applications.

Conventional thin film deposition processes can control film thickness with angstrom-level precision; however utilizing this planar dimension offered integration challenges. On the perpendicular surface of the patterned multilayer thin-film structure edge, there are by necessity parallel lines of material that have widths corresponding to the thickness of deposited films. For example selective material etching followed by transfer to imprint lithography masks allow for transfer of the parallel lines with nm-scale pitch.[131] The principle of film thickness for critical dimensional control has also been applied to the formation of vertical transistors with a gate-lengths corresponding to thickness of the thin films.[132] This film thickness approach has been utilized to construct electrode gaps after selective chemical etching of a thin barrier layer, as in the case of thin sections along template-grown nanowires[133] or on patterned $Si/SiO_2/Si$ structures.[134] In the former case, the smallest gap attained was 5 nm which would require relatively long molecules. Integration of these wires without adjustment (mechanical bending of the wire) of the gap width into large scale architecture remains a significant challenge. However, $Si/SiO_2/Si$ gap structures are easily integrated into circuit designs but for films that are ca. $\leq$ 5 nm thick, significant $1/frequency^{-}$ noise after the etching is found.[14,135] Moreover, chemical functionalization of Si surfaces without an intermediate oxide layer also presents great difficulty. Clearly, an alternate scalable approach that can generate electrode gap lengths on the order of large conductive molecules (ca. 2 nm), that allows for a range of metallic contacts, and variety of surface chemistries is required for reliable molecular electronics.

In this chapter an alternative strategy for preparing reliable molecular electrodes is discussed. Under a newly developed approach a metal/insulator/metal multilayer structure was grown, and there was a narrow 'line' of insulator material on the perpendicular plane at the pattern edge. This formed a 'gap' where surface molecules could bridge across the insulator to become the primary current path. Surface molecules that did not bridge across the insulator layer did not contribute to the current between the leads. Critical to the feasibility of this approach was to have the 'background' current of the bare electrode (without molecules) much less than the case after molecular bridging. In general background current is primarily due to tunneling current in the planar area of the electrode through defect free insulator layer. The process was experimentally optimized by the deposition of uniform and nearly defect free insulating oxides, details are in chapter 2. A molecule had to be designed which was large enough to span an experimentally reasonable tunnel barrier thickness, but was sufficiently conducting, readily soluble and had a well defined rigid structure. In this chapter we present a fabrication methodology to prepare Multilayer Edge Molecular Electrode (MEME) geometry by two techniques and offer experimental evidence showing that current conduction is dominated by surface molecules spanning the insulator gap. A sharp exposed edge of multilayer, a critical step in MEME fabrication, was produced by using both ion milling and photolithography-liftoff process. Although both processes resulted in similar molecular transport , the photolithography approach was adopted due to fabrication ease and high device yield (~90%). The photolithography based molecular electrode has been utilized in the other chapters of this dissertation. Control experiments included the reversible binding of a conductive molecule across the insulator gap with consistent changes in current. Phenomenological modeling of electron transport was consistent with tunneling through alkane tethers to and from the core of a metal-cluster molecule.

3.2 Physical Methods

Throughout this work, a thermally grown 100nm silicon oxide (SiO_2) isolation layer was used as the substrate. Prior to every photolithography step, substrates were first sequentially cleaned with acetone (2 x 10mL) , (2 x 10ml) and in de-ionized (DI) water (2 x 10ml), then dried in flowing nitrogen. The pattern areas were defined by a conventional photolithography method using Shipley 1813 positive photoresist and a Karl Suss mask aligner. Photoresist thickness, exposure time and developing steps were optimized to obtain a suitable edge profile. After the required film deposition steps, a gentle liftoff process was carried out with a Shipley 1165 resist remover for 2-4 hours. The liftoff step was critical for the photolithography-liftoff produced

MEME sample because success in exposing the side edge of tunnel junction for molecule hosting depends upon liftoff efficacy. The metal films for multilayer molecular electrode fabrication were sputtered using an AJA International Sputtering system. For all the depositions, base pressure was ~2 x 10^{-7} torr. Top and bottom metal films of all the molecular electrodes were deposited at 2mtorr argon pressure and 150W power with RF sputtering gun. Gold (Au), nickel (Ni), cobalt (Co), nickel-iron (Ni:Fe::80:20) and tantalum(Ta) metals were sputter deposited as top and bottom metal film of different multilayer tunnel junctions. RMS roughness measured by AFM for all the metal films was around ~0.2nm. Deposition of the 2nm thick alumina insulator, the most important step of molecular electrode fabrication scheme, was accomplished using a multi-step process. To have uniform coating of the insulator, aluminum (Al) metal was first deposited on top of the bottom metal electrode, since similar surface energies of metals result in good wetting without island growth. Al metal was deposited from a DC powered gun at 75W power and 2mtorr Ar pressure. The Al film (1nm) was then subsequently plasma oxidized with 60 mtorr of 1:1 Ar and oxygen gas mixture for 30 seconds at 20W substrate bias in sputtering chamber. A second Al deposition (0.5nm) followed by plasma oxidation was performed to give an optimal tunnel barrier quality for a ~2.0 nm thick insulating layer with a breakdown voltage ranging from 1.8 to 2.5V. The typical tunnel junction area and contact resistance were ~10-25μm^2 and ~1MΩ respectively for all the MEME samples. Dimensions of cross junctions were chosen according to our photolithography resolution limit and was optimized to reduce shorting defects in the cross junction area. Particularly intense experimental effort was required to optimize the conditions of deposition (power, pressure and seed layer material) such that the metal surfaces had less than 0.2 nm RMS smoothness as measured by tapping mode AFM (Digital Instruments Multimode). Another critical experimental optimization was to minimize compressive stress in the deposited films. This was because we observed that the stress release mechanism involves the formation of hillocks that short across the tunnel barrier, dramatically reducing the temporal and thermal stability of the device.

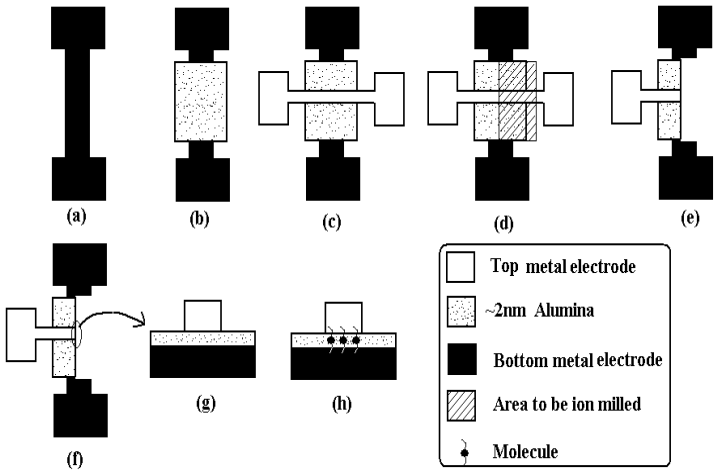

Scheme A

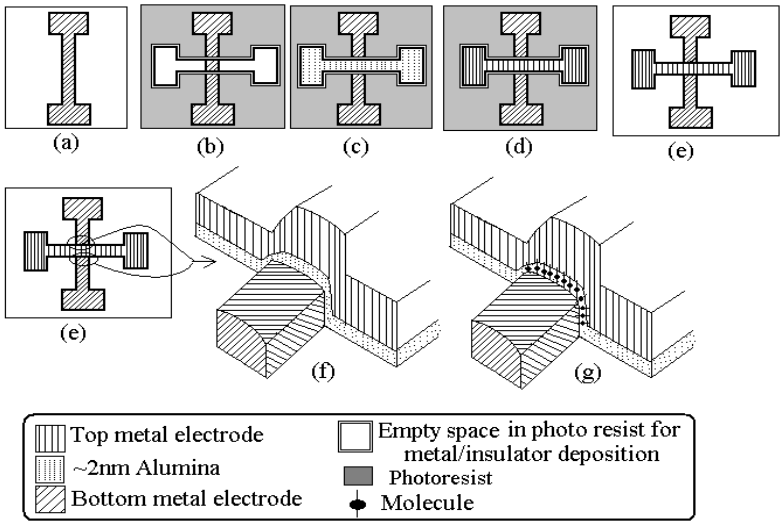

Scheme B

Figure 3.1: Description of electrode fabrication for (A) Ion-milling based molecular electrodes: first a complete metal-insulator-mtal tunnel junction is prepared (a-c) followed by ion milling in specified area (d) to produce sharp exposed edge of MEME (e-g) and then molecule attachment commenced on the exposed edge (h). (B) Photolithography-pattern based molecular electrodes: Bottom metal eceltode deposition (a) followed by the photoresist window generation for the alumina and top metal electrode deposition (b). Deposition of ~2nm alumina (c) top metal electrode film deposition (d) followed by liftoff (e) produced tunnel junction with exposed side edges where separation between two metal electrode is controlled by the insulator thickness (f). Finally molecule attachment on the exposed side complete molecular junction fabrication (g).

The exposed pattern edges were produced by two fabrication approaches. In the first approach, shown in figure 3.1 Scheme A, ion beam milling (FISCHIONE 1010 ion mill) was employed to produce the edge, a well established method to produce atomically sharp and exposed side edges of tunnel junctions.[115]

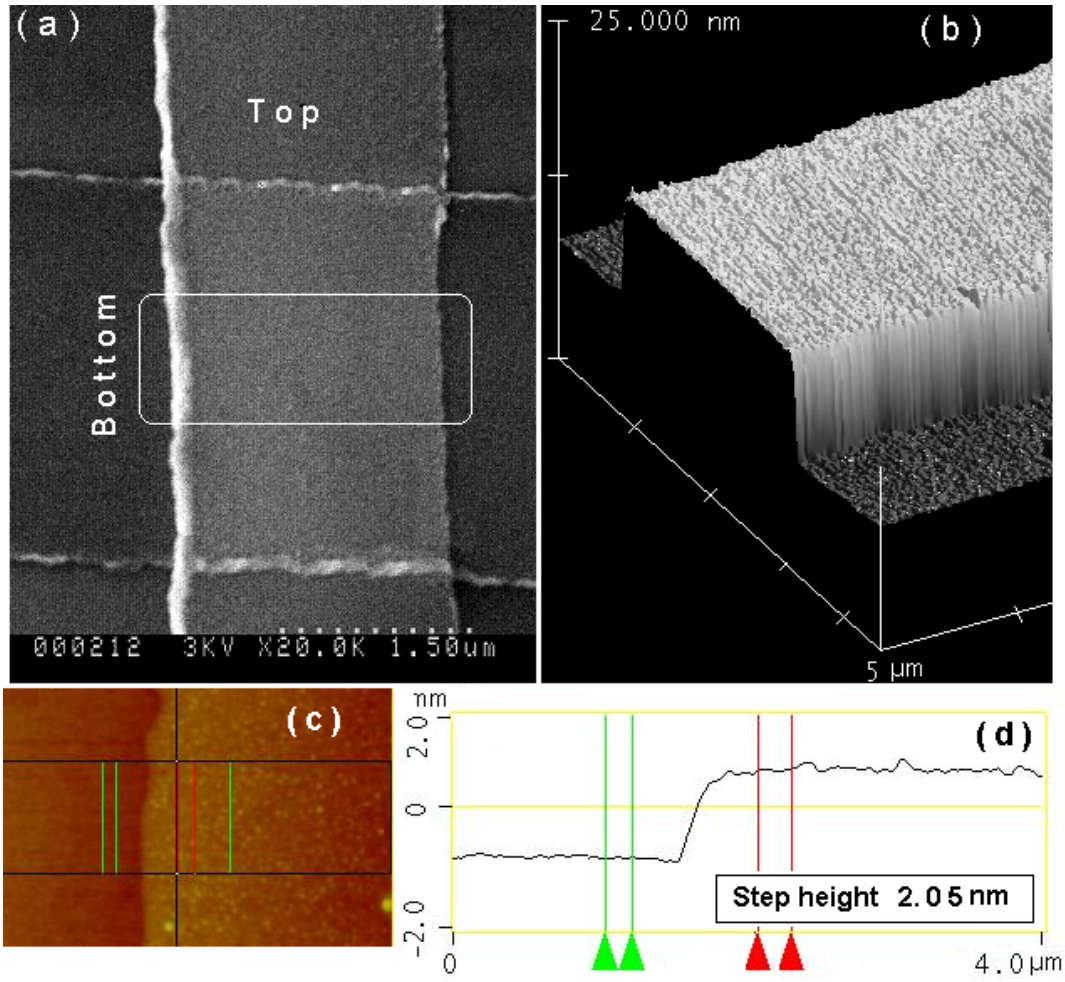

Figure 3.2: (a) SEM micrograph of a photolithography-liftoff produced tunnel junction with exposed metal-insulator-metal side edges. (b) 3D view from AFM study of exposed side edge in the box of Fig (a), 2nm thick alumina deposited before top metal electrode is not resolved. (c) topography and (d) step height measurement of alumina grown in a typical photoresist cavity is continuous and appears with exposed sides after clean liftoff.

The ion-milled samples were cooled by liquid nitrogen during ion milling to minimize photoresist hardening, however thermal stresses introduced tunnel junction instabilities and a short device life. To overcome the limitations of ion milling, a MEME fabrication scheme based

on liftoff photolithography to define the pattern edge (figure 3.1 Scheme B) was adopted. Initial sputter deposition of metal (a) onto an oxidized silicon surface in patterned window, followed by (b) photoresist window definition of cross-junction window (c) sputter deposition of aluminum metal and subsequent plasma oxidation (O_2), with repeated cycles to give a ca. 2 nm thick alumina (Al_2O_3) film; (d) top contact metal sputter deposition final and (e) liftoff removal of metal layer to leave exposed edge. 3-D perspective before (f) and after (g) molecular attachment. In this scheme, a key step is the deposition of ~2nm insulator and top metal electrode in the positive photo resist window. The advantage of this method is that the planar dimension of the alumina barrier and top metal electrodes are controlled by the same photoresist boundaries. At the length scales involved in the normal direction (~3nm) the photoresist is essentially atomically flat (0.2 nm RMS for 50nm x 50nm area AFM scans) providing a sharp pattern. Scanning electron microscope (SEM) and AFM study of a typical cross junction produced by scheme B are given below figure 3.2.

A molecule that can chemically link and bridge both electrodes has been developed by Holmes and co-workers.[3] To date only microcrystalline powders of **1**, $\{[(pzTp)Fe^{III}(CN)_3]_4$-$[Ni^{II}(L)]_4]_4[O_3SCF_3]_4\}$ (pzTp = tetra(pyrazol-1-yl)borate; L = 1-S(acetyl)tris(pyrazol-1-yl)decane), have been available, precluding X-ray structural studies; a structural analogue (**2**), where L = 1-S(acetyl)tris(pyrazol-1-yl)hexane, is illustrated in figure 3.3.[3] In **2** the Fe^{III} and Ni^{II} centers reside in alternate corners of a slightly distorted box and are linked via cyanides (figure 3.3). The cluster core contains coordinated tris(pyrazolyl)decyl- chains that are terminated with S(acetyl) groups at alternate corners (Ni^{II} centers) of the cubic cluster.[3] The S(acetyl) groups were chosen for several reasons: (1) there is ample literature precedence in self-assembled monolayer (SAM) literature, (2) acetyl protection prevents sulfur atom coordination to transition metal centers during complexation, (3) circumvents the use of air sensitive thiols, and (4) acetyl groups are easily removed by electrochemical or chemical means. Electrochemical attachment of the clusters to the MEME electrodes via the thiolacetyl terminii[136,117] was accomplished via immersion of the electrodes in a dichloromethane solution of **1**, followed by alternating a ±100 mV bias between the two metal electrodes, at a time interval of 0.01 seconds, for 2 min. Subsequently, the assembled devices were rinsed with dichlromethane, 2-propanol, and deionized water and dried under a nitrogen gas stream. Immersion of the MEMEs in a dichloromethane solution of **1** without the performing of electrochemical step did not affect transport properties of exposed edge tunnel junctions. We surmise that the use of alternating voltage during electrochemical step helped in conditioning the metal electrode surface by reducing it and subsequently favored the metal-thiol bonding.

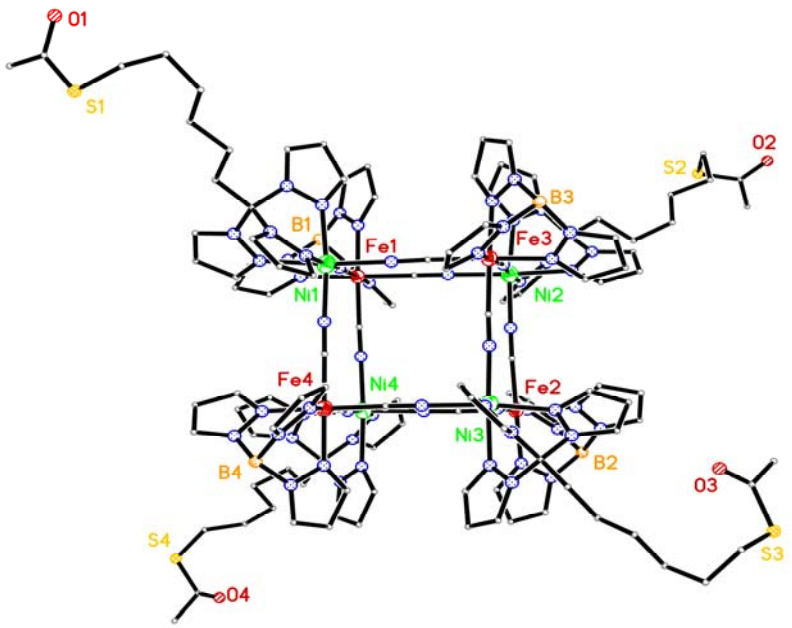

Figure 3.3: X-ray crystal structure of a structural analogue of **2**. Cubic cluster consists of alternating Fe^{III} and Ni^{II} centers (corners) bridged by cyano groups (edges). All anions, hydrogen atoms, pendant pyrazoles, and disordered S(acetyl)hexyl- chains are removed for clarity. Note: 1-S(acetyl)tris(pyrazolyl)decane was used in all electrode studies.

Transport measurements of the tunnel junctions were obtained before and after attachment of molecules. The current was measured while the voltage was swept between ±100 mV for normal transport measurements, while a ±500mV range was chosen for determining the the tunnel barrier properties; these voltage ranges are far below the breakdown voltage potentials (ca. 2 V) of the devices. Typically 3-5 measurements per each I-V plot, using a 5 mV voltage and 0.5 to 1 second time steps were collected for each sample, to minimize possible scan to scan variation error.

3.3 Results and Discussions

3.3.1 Molecules on Ion-Milled Molecular Electrodes with Atomically Sharp Exposed Edges. To probe our hypothesis that the perpendicular plane of a tunnel junction at a pattern can be used for molecular electrode formation, we begin with MEMEs prepared via ion-milling methods (figure 3.1, Scheme A). For our comparative studies, film thicknesses (from bottom to top) were utilized: Si/SiO_2 (100 nm), Co (8 nm), NiFe (2 nm), Al_2O_3 (2 nm), and NiFe (10 nm).

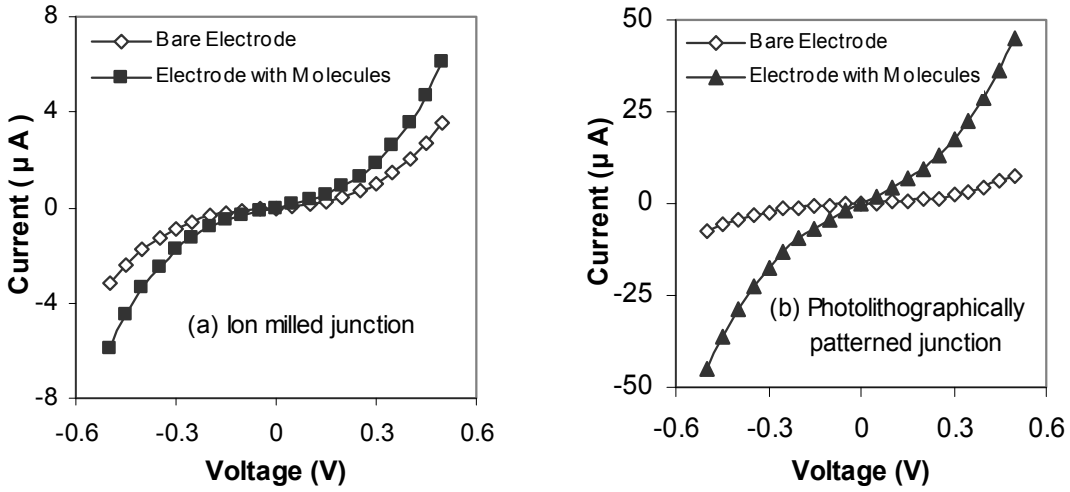

Figure 3.4: Current-Voltage characteristics of multilayer edge molecular electrodes before and after molecular attachment for (a) Co/NiFe/Al_2O_3/NiFe (Figure 2, Scheme A) and (b) Co/NiFe/-Al_2O_3/NiFe electrodes (Figure 2, Scheme B).

The transport properties of ion-milled MEMEs both before and after attachment of **1** is shown in figure 3.4(a). A marked increase of 140% in current (current of ion milled tunnel junction before and after molecule attachment at 100mV was $1.35x10^{-7}$ and $3.07x10^{-7}$ Amps respectively) after attachment of molecules is observed, suggesting that current through the molecules exceeds the background tunnel current of the bare junction; bare MEME tunnel samples did not show more than a 5% increase in current with electrical stress or exposure to neat solvents used in molecular attachment processes. Unfortunately, ion-milling introduced significant thermal stresses and afforded samples that developed high current ohmic shorts after a few days.

3.3.2 Molecules on Photolithography-Liftoff Produced Molecular Electrodes.

Instability associated with ion milled MEME prompted us to investigate into whether a simple liftoff process on cross junctions could produce robust molecular electrodes of similar design. In addition to stability, there is a significant advantage of a simple, inexpensive and scalable process for device integration. Samples with Si/SiO_2(100nm), Co(8nm), NiFe(2nm), Al_2O_3(2nm), and NiFe(10nm) film thicknesses (bottom to top) were prepared by the photolithography method of figure 3.1 Scheme B. Transport studies of photolithography-liftoff produced MEME sample before and after molecule attachment, figure 3.4(b), showed similar, but more pronounced, effect on transport as seen with ion milling produced MEME sample. For the

tunnel junction produced by photolithography and liftoff process, and whose data is presented in figure 3.4 (b), current at 100mV before and after molecule attachment was $3.5x10^{-7}$ and $5x10^{-6}$ Amps respectively. These results strongly suggest that MEME samples, produced by via photolithography-liftoff based approaches, contain a sharp perpendicular side plane that is necessary for attachment of **1**.

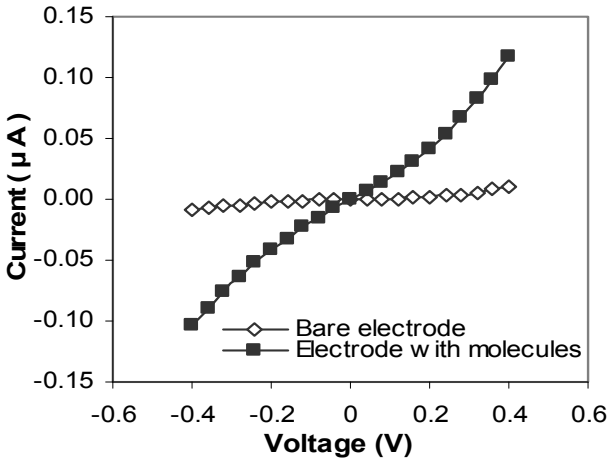

Figure 3.5: Current versus Voltage behavior of $Ta/Al_2O_3/Ta$ electrodes before and after molecular attachment.

Another key merit of the MEME electrode design strategy is the ability to incorporate a variety of metals that function as electrodes. Tantalum, a relatively unexplored metal electrode in the field of molecular electronics, was utilized to construct photolithographically-defined cross junction devices, in an attempt to improve the quality of the insulator layer of the electrodes. Photolithography-liftoff produced MEME samples with (bottom to top) Si/SiO_2 (100 nm), Ta (12 nm), Al_2O_3 (~2.5 nm), and Ta (12 nm) configurations were prepared and the transport behavior of assembled devices measured in the absence and presence of **1**, figure 3.5. Relative to bare electrodes, molecular attachment affords a ca. 28 fold increase in the measurable current, due to higher insulator film quality in the Ta system was observed; for the reported MEME current before and after molecule attachment at 100mV was $6.4x10^{-10}$ and $1.8x10^{-8}$ Amps respectively. Further current enhancement is anticipated assuming that the planar tunnel junction area can be reduced to thinner line widths, from 5 μm to 0.065 μm that is currently possible via conventional photolithographic approaches.

Molecular current is defined as the total current minus the current found for bare electrodes. Given that the electrode junctions are ca. 5 μm long, are spaced 1 nm apart, and average molecular width of **1** is ca. 2 nm, a closest-packed array of approximately 10,000

molecules can covalently attach to the exposed lengths (two sides) of the electrodes. At 50 mV applied bias, the average current per molecule was estimated to be 0.16 (±0.13) nA per molecule, for 48 photolithography-liftoff produced MEME samples, utilizing Ni and NiFe metal electrodes. The experimental molecular current was of the same order but varied in absolute magnitude between samples; a more useful measure of the variation in current per molecular between samples is to examine the log [current (amps)] of -10.01 (±0.52) values. We tentatively propose that the variation in calculated current per molecule values between samples arise from variations in tunnel junction pattern edge quality. However, these edge variations are extremely small, when compared to the current per molecule observed, and are much smaller than values reported for most molecular electrodes devices.[137,138]

3.3.2.1 Control experiments:

A series of control experiments (i) Contact angle study to ensure metal-molecule surface reaction, (ii) Effect of electrochemical treatment of electrodes in neat solutions and subsequent rinsing, (iii) Reversible molecule attachment and corresponding change in current, (iv) Attachment of short length n-butyl thio-acetate and long 20 carbon atom alkane dithiol chain and (v) Increasing alumina thickness beyond the length of molecular bridge was performed to demonstrate that the observed increase in current was due to the desired surface molecules spanning across the MEME electrode rather than experimental artifacts resulting in uncontrolled surface conduction.

To probe the presence of surface-bound molecules on NiFe electrodes contact angle measurements (using water) were preformed on bare and **1**-modified NiFe films.[118] For unpatterned thin films of NiFe, electrochemical treatment with CH_2Cl_2 solutions of **1** afforded a contact angle changes from 11º to 54°; as control experiment, bare NiFe thin films were rinsed with CH_2Cl_2 and 2-propanol under identical experimental conditions affording a modest increase in contact angles (to 34°), presumably due to alcohol and/or hydroxyl substitution. This highly water-insoluble molecule clearly functionalized the NiFe surfaces in a manner similar to previous studies.[118]

In a second series of experiments, the MEME samples were subjected to CH_2Cl_2, cycled potentiometrically in the absence of **1**, and rinsed as previously described; *no increase in current was observed* suggesting that **1** is necessary for charge transport in MEME tunnel junctions and electrochemistry performed for molecule attachment does not change the conductivity of the exposed edge tunnel junction.

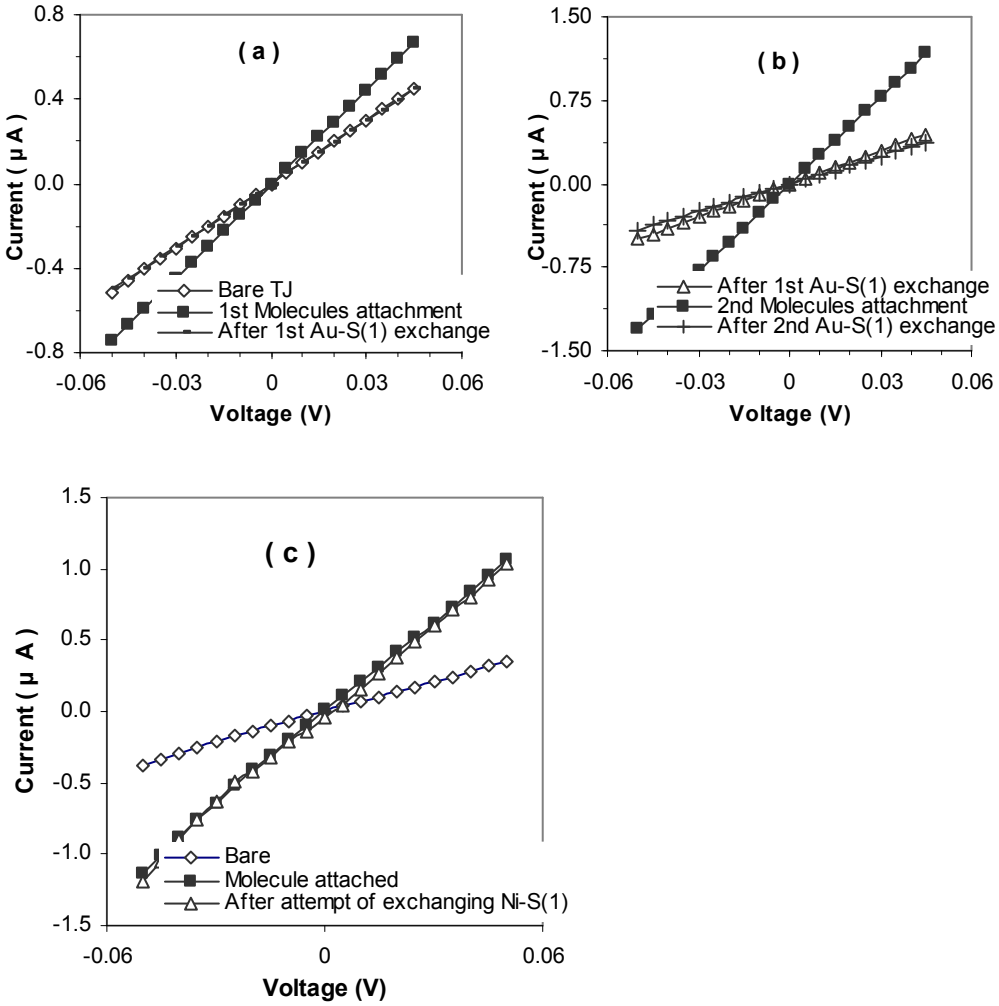

Figure 3.6: Reversible displacement of alkyl tether of **1** on Au electrode is observed upon treatment with thiol Current-Voltage characteristics of a $Ni/Al_2O_3/Au$ multilayer edge containing **1** and upon treatment with 5 mM 1-dodecanethiol. (a) Bare electrode before after molecular attachment of **1** and after thiol exchange of tether from top electrode with the thiol group of 1-dodecanethiol. (b) Repeat experiment using same sample: after first thiol exchange, **1** addition, and after second thiol exchange reaction. (c) $Ni/Al_2O_3/Ni$ molecular junction was not affected by thiol exchange reaction. Bare electrode before after molecular attachment of **1** and after the attempt to exhchange Ni-thiol bond. Au-S(1) and Ni-S(1) shows the bonding between metal and thiol group of **1**.

The most important control experiment was to show the reversibility of molecular attachment across the electrode, and hence show that there was not any serendipitous breakdown of the electrode at the time of molecular attachment. A MEME sample with Ni bottom and Au

top metal electrodes fabricated photolithography-liftoff method (Ni(10nm)/Al_2O_3(2nm)/Au(10nm) configuration). The bond enthalpies for Ni-S and Au-S are 344 and 125 kJ/mol respectively.[139,140] Since the Au-S bond is readily reversible, it was possible to remove the thioacetate linkage by mass-action in a thiol-alkane solution, to form a self-assembled monolayer of electrically insulating alkanes on the top Au metal electrode. We postulate that this should disconnect the molecule from the top electrode and reduce current to the background level of original electrode current without the molecules. Shown in figure 3.6(a) is the I-V measurement of the bare electrode, after attachment of conducting molecule, and following exchange of thiol group of alkyl tether of **1** with the thiol group of 1-dodecane thiol after exposure to a 5 mMol solution of 1-dodecane thiol in ethanol for 45 minutes. The current rose with molecular attachment then returned to the original bare electrode current level. The cycle was repeated again, figure 3.6(b), and the same behavior was exhibited, demonstrating that increase in current is due the molecular attachment across the insulator, not due to the serendipitous breakdown of the insulator. A slight increase in current for the second functional attachment was expected for an increased number of molecules due to second treatment. The same displacement experiment performed on Ni/Al_2O_3/Ni electrodes did not show the effect of thiol exchange reaction (i.e. a reduction in current) upon exposure to alkanethiol solution, figure 3.6(c). This is consistent with the thiol-Ni bond enthalpy being much stronger than Au, and hence not reversible. This series of experiments also demonstrated that the molecular current was not due to uncontrolled physisorption of molecules at the electrode surface. The use of a top Au electrode offers chemical sensing possibilities since the top lead of a tethered conducting molecule may be reversibly disconnected by coordination to a sterically bulky analyte molecule.

In our fourth control experiment we probed the effect of molecule with single thio-acetate end group that was unable to bridge the insulating film of the exposed edge tunnel junction. For this study 2 mM n-butane thio acetate solution in dicholoromethane was used to electrochemically attach the short molecules on NiFe[12nm]/Al_2O_3[2.0nm]/ NiFe[12nm] tunnel junctions. On 25 such tunnel junctions, a small increase of 17 ±16% over bare tunnel junction current due to n-Butyl thioacetate was observed indicating that uncontrolled surface chemistry is not responsible for conduction increase. For comparison bridging molecule **1** produced current increases as high as 5000% over bare tunnel junction current on the samples prepared under the same conditions. This experiment clearly suggested that just the formation of metal-thiol bond on the surface is not sufficient to affect the conduction process of exposed edge tunnel junction (MEME). We have also attached a 20 carbon long alkane with thio-acetate groups at each end to span NiFe/Al_2O_3/ NiFe samples. A 2mM solution of this molecule in dichloromethane was used

in the process. Modest current increases of 84 ±57% change (20 samples) over bare MEME current was observed consistent with the relatively poor conduction through an alkane tether bridging the insulator gap.

In the last control experiment we saw that current increase on the exposed edge of tunnel junction was only possible when the molecule was long enough to span the oxide barrier. Molecule **1,** was modified to have short *hexyl* thioacetate tethers resulting in an overall length ~2.4nm. For this study two MEME electrodes (NiFe/Al_2O_3/NiFe), first with ~2nm and the second with ~3nm Al_2O_3 barrier thickness were used. Exposed edge tunnel junction with 2nm thick Al_2O_3 (tunnel barrier thickness < molecule length) showed a clear increase in current, figure 3.7(a), but tunnel junction with 3nm thick Al_2O_3 (tunnel barrier thickness > molecule length) showed no increase in current, figure 3.7(b). This further confirms that uncontrolled surface chemistry does not provide a dominating current path.

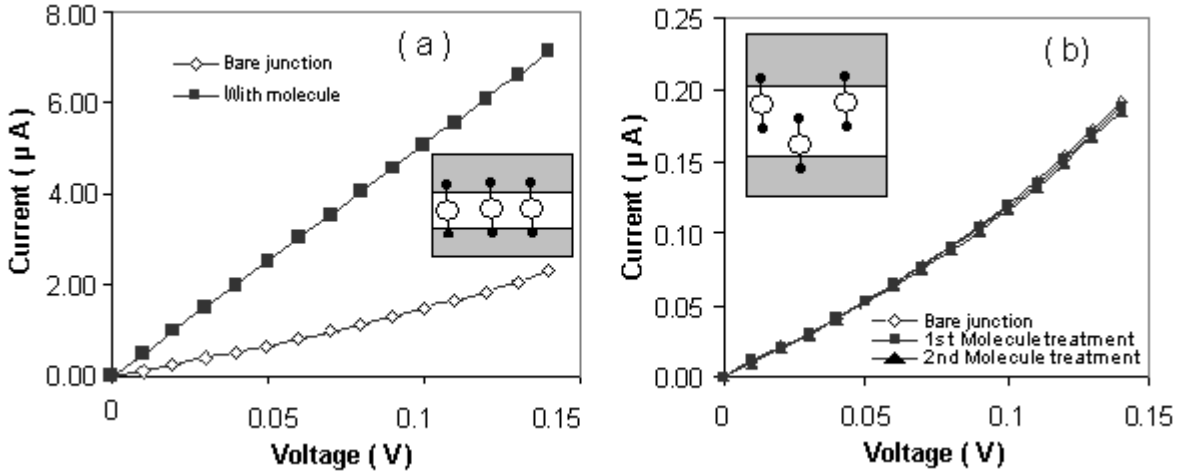

Figure 3.7: Molecule with hexyl thio acetate tether (~2.4nm long) on NiFe/ Al_2O_3/NiFe tunnel junction produced by scheme B. (a) molecule attachment on ~2nm thick tunnel barrier (shorter than molecule length) (b) attachment on a ~3nm thick tunnel barrier (thicker than molecule length).

3.4 Analysis of Electron Transport via Simmons Tunneling Model.

The electron transport properties of various MEME samples, with different insulator thickness, in the presence and absence of **1**, were analyzed via the Simmons tunnel current model. By fitting observed current density (j)-voltage (V) data to the Simmons model within a medium voltage range ($V < \varphi_B/e$) as shown below:[50]

$$j = \left(\frac{e}{4\pi^2 \hbar d^2}\right)\left\{\left(\varphi_B - \frac{eV}{2}\right)\times \exp\left[-\frac{2(2m)^{1/2}}{\hbar}\alpha\left(\varphi_B - \frac{eV}{2}\right)^{1/2} d\right] - \left(\varphi_B + \frac{eV}{2}\right)\times \exp\left[-\frac{2(2m)^{1/2}}{\hbar}\alpha\left(\varphi_B + \frac{eV}{2}\right)^{1/2} d\right]\right\} \quad (3.1)$$

where m is electron mass, d is barrier thickness, φ_B is barrier height, V is applied bias , and α is a unitless adjustable parameter, that allows for deviations from a simple rectangular barrier and effective mass of the electron.[51] Via equation 1, (setting α =1) we are able to fit the values of both barrier height and barrier thickness before and after molecule attachment for various MEME samples.

To validate the Simmons model in our system, a comparison was made between the calculated thickness of alumina (present in bare MEME tunnel junction) from the Simmons model and the physical thickness of a pattern of alumina (grown under identical conditions) as measured by AFM. Calculated and measured thicknesses of alumina were in agreement within the experimental uncertainty (2 Å). Moreover, the calculated values of barrier height of alumina used in MEME samples closely matched barrier height values found for alumina films in other studies of alumina tunnel junctions.[138] It is important to note that Simmons model, originally established for the simple tunnel barrier between two nonmagnetic metal electrodes, have been used widely. There is plenty of literature available which justify the utility of this simple model in many complex systems such as magnetic tunnel junctions and spin filters.[141]

For the modeling purposes, molecular current is defined as the total molecular electrode current after molecule attachment minus the current of the bare electrode. The bare tunnel junction area is 25 μm^2 and an effective tunnel area for molecular current is calculated in following manner. Via X-ray structural studies, **1** is approximately 1 nm wide (Fe-Ni edge), and decorate the electrode edge in a closest-packed arrangement along a 10 μm insulator line as shown in Figure 1b. Considering that the alkane tethers also occupy space, and that the cluster core is insulated from its surrounds by the coordinated ligands, the most likely conduction pathway is likely to be through the S(alkyl) chain. As a result charge enters and leaves the cluster core and tunnels through the alkyl chains, giving a total molecular tunnel area of $1\text{x}10^{-10}$ cm^2 (=10 μm x 1nm). Having obtained the current density for molecular barrier, barrier height and barrier thickness were calculated using Simmons model as shown in equation (1). In order to check the uniqueness of barrier height and barrier thickness values, curve fitting of experimental data to Simmons model was accomplished in the narrow to very wide range of barrier thickness and barrier height values. In both cases the values of barrier height and barrier thickness came out to

be the same for the best fit. Quality of curve fitting was judged in terms of the smallness of the root mean square of the ratio of experimental minus calculated to experimental current density data.

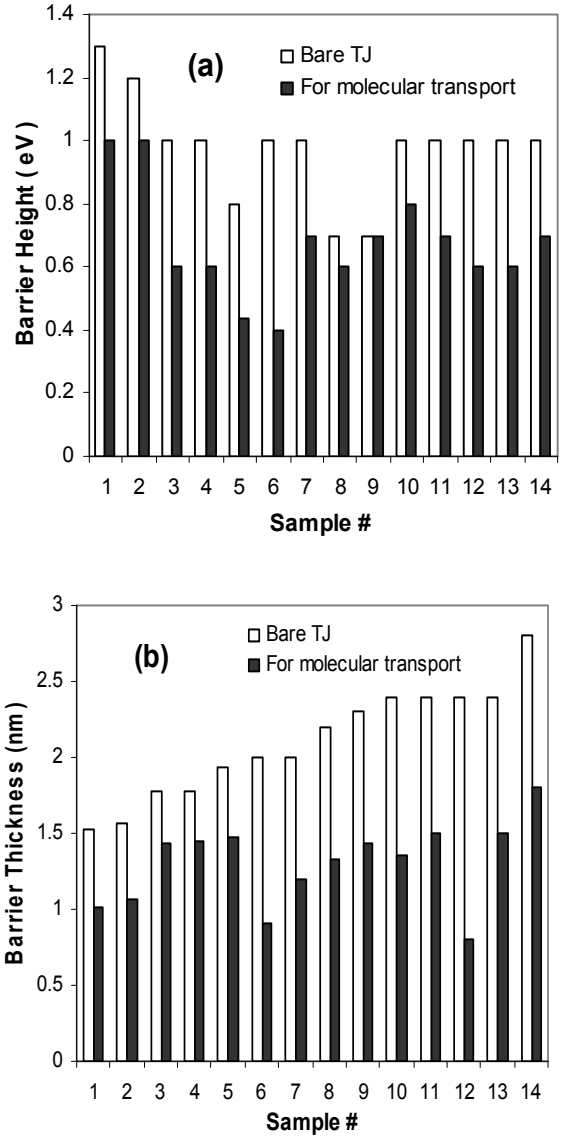

Figure 3.8: Barrier height (a) and barrier thickness (b) for photolithography-liftoff produced samples with NiFe magnetic metal electrodes (sample # 1 to 9) and non magnetic Ta metal electrodes (sample# 9 to 14).

Effective barrier heights for the molecular transport component of electrodes functionalized by **1** were calculated for a series of MEME samples with magnetic (NiFe) and non-magnetic metal (Ta) electrodes. Generally molecular barrier height values were significantly less than that of bare MEME samples with tunneling through the alumina layer. The molecular barrier height

values had significant variation with magnetic metal electrodes (0.67±0.3eV), but relatively less variation was seen with the non-magnetic Ta metal electrodes (0.74±0.16eV), for the data shown in graphs, as seen in figure 3.8(a). The scatter in current is presumably linked to spin effects of the molecule coupled to magnetic leads and is currently being studied. In figure 3.8(b), the barrier thickness (1.27 ± 0.27nm) calculated from the molecular I –V data is consistent with the expected length of an insulating decyl tether. However, the overall molecular dimensions (via X-ray) are estimated to be ca. 3 nm overall, due to 2 decyl tethers (ca. 1.2 nm length) and a $\{Fe^{III}_4Ni^{II}_4(CN)_{12}\}$ core (ca. 1 nm). The anticipated energy level diagram of the MEME before and after attachment of **1**, which resembles the energy diagram of expected for a double barrier tunnel junction,[142] is shown in figure 3.9.

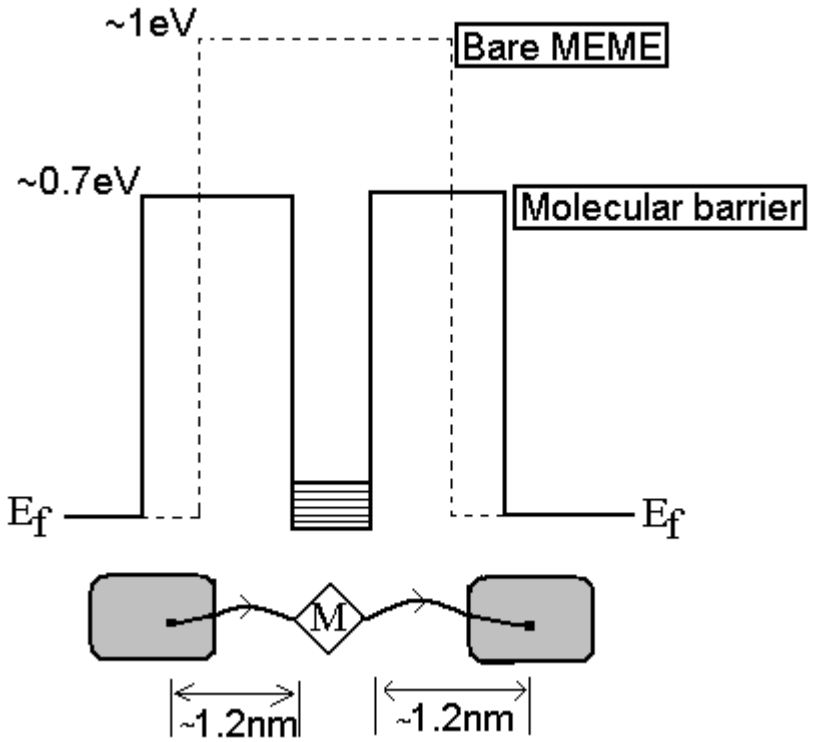

Figure 3.9. Idealized band diagram of tunnel junction before (···) and after (—) attachment of **1**. E_f Fermi energy levels of metal electrode, where ~1 eV is the barrier height of the bare tunnel junction, ~0.7 eV is the barrier height of the insulating alkane tether.

Evidence in support of molecule-mediated charge transport being the dominant conduction pathway was obtained via temperature-dependent transport studies, obtained between 25 and 100°C, using photolithography-liftoff produced MEME sample [Ta (10 nm)/Al_2O_3 (2.5 nm)/Ta (10 nm)] . Temperature effects are possible only when molecular excitation, essentially

coupled to molecular transport, can be produced at the center of molecule; the tunneling transport mechanism through the alumina insulator and alkane tether is essentially temperature independent.[51] Upon heating, the sample current increases, corresponding to a thermally activated transport process, with a ca. 0.30 (±0.02) eV activation energy barrier. This estimated activation energy barrier is consistent with activation energies expected for conformational changes[143] and calculated transport activation energies reported for other molecules.[144] The data also suggests that the transport mechanism is more complicated than a simple elastic tunneling process (thermally assisted tunneling) but is consistent with the idealized molecular geometry on the electrode surface proposed. Our molecule which has two tunnel barriers (due to alkane tethers) separated by organometallic cube with conjugated bonds, which provide density of states closer to metal electrodes Fermi level[145]. For small area double tunnel barrier system it is reported that both elastic and inelastic process contribute to the current and direct tunneling is more prominent towards lower temperature range.[146] In the transport study of several single molecular magnets transition between pure quantum tunneling (temperature independent) to thermally assisted tunneling (temperature dependent) was observed.[147] Due to adverse thermal stresses on MEME stability we are currently unable to perform cryogenic transport studies. However, the cutoff temperature for several molecular systems are close to room temperature, e.g. for terphenyl and nitroazobenzene molecules thermally activated conduction process freeze out near 10 degree C.[144] Temperature studies of these molecular junctions are ongoing and largely limited by the control of film stresses during the growth process.

Moreover, additional support for a qualitative tunneling conduction model can be inferred from the calculated value of the tunneling decay coefficient (β).[148] An exponential decrease in current ($I \propto \exp(-\beta d)$) with alkane length (d) was commonly measured. Here β was extracted from our calculated barrier heights from the Simmons model for nonmagnetic MEME samples whose barrier properties are given in **Table 3.1**. We experimentally observed a β of 0.88 (0.10) $Å^{-1}$, which was remarkably close to the observed value of $\beta = 0.85$ $Å^{-1}$ for alkane tether of similar lengths as seen in STM studies [148] of individual molecules and from self-assembled monolayers of thiol alkanes.[51,148] Here it is worth noticing that we are comparing our the value of β, which is for 10 carbon long alkane tether, with the β of 10-12 cabon long alkane studied elsewhere.

Table 3.1 Barrier thickness and height estimated via Simmons tunnel current model fits of conduction through assembled Ta/Al_2O_3/Ta multilayer edge molecular electrodes.

	Barrier Thickness (nm)	Barrier Height (eV)
Bare Electrode Tunnel Barrier	2.48 (±0.18)	0.94 (±0.13)
Molecular Tunnel Barrier	1.30 (±0.29)	0.74 (±0.16)

On the basis of experimental observations we have come up with following qualitative model for the transport through **1**. In our study molecular junction is comprised of two tunnel barrier and one region of supposedly fast transport. Time of charge transfer through the molecule has three components: [1] tunneling of electrons from the left (or right) metal electrode to the organometallic cube present in the center of molecule, [2] quick charge transport through organomettalic cube and [3] Tunneling from the organometallic cube towards right (or left) metal electrode. Expression for the total time of charge transfer (t_{Total}) through molecular junction is given by following equation :

$$t_{Total} = t_1 + t_2 + t_3 \tag{3.2}$$

t_1, t_2 and t_3 are the inverse of charge transport rate through first alkane tether, organometallic cube, and second alkane tether respectively. In the equation (3) transport rate through alkane tethers, which is based tunneling process and supposed to be the same in both alkane tethers, is expected to be much slower than transport rate through conjugated bonds enriched organometallic cube of **1**.[145] Which implies that $t_2 << t_1$ and t_3. Putting $t_1 = t_3 = 1/r(\text{alkane})$, where r(alkane) tunneling rate through

$$t_{Total} \approx \frac{2}{r(alkane)} \tag{3.3}$$

Molecular transport rate can be written as

$$Rate \propto r(alkane) \tag{3.4}$$

According to our experimental observations, molecular transport rate through **1** is governed by the slowest transport rate which is the tunneling process through alkane tethers.

3.5 Conclusions

By using the exposed face at the edge of a multilayer thin film pattern, an electrode with nm-scale distance between metal leads was reliably formed. Importantly, the critical dimension was controlled to molecular lengths with angstrom scale precision using conventional deposition processes. Since the pattern can be defined by photolithography, the economical large scale integration of molecular electrodes can be readily achieved, using the described approach. In our study, molecular electrodes with insulator thicknesses ranging from 1.5 to 2.5nm were studied. The cross junction array can utilize recently developed two terminal logic designs[130] or alternatively, the edge geometry can be incorporated into more conventional, arbitrarily addressed junctions. This edge geometry does not readily incorporate an electrostatic gate at close proximity, however, electrostatic switching of molecules typically requires extremely high electric fields (~100 MeV/cm),[143] that far exceed the breakdown point of known dielectrics. This two terminal device architecture approach has two major merits other than ease of integration. First, a wide range of materials can be introduced on alternate sides of an insulating barrier, including magnetic materials, allowing for the possibility of current modulation via spin state of the bridging metal cluster. Second, all conductive molecules reside on the exposed surface allowing for strong selective chemical interactions with analyte molecules. In principle, a bound analyte molecule can change the conformation of the conduction molecule, or force the reversible removal of a tether from a top gold contact, which may lead to the design of a reversible sensing device. Furthermore, the planar electrode geometry also provides for further conformational constraint of the molecule on the surface, which may be an important consideration in improving the molecular conduction process. The relative simplicity of this electrode geometry allows for a significant improvement in the ability to study molecular conduction and may finally enable molecules to be incorporated into large scale device architectures. We have observed that molecular electrode fabrication scheme can further simplified by avoiding the deposition of aluminum; in the next chapter we present a method in which a controlled oxidation was utilized to produce novel molecular electrodes.

Chapter 4

Molecular Scale Electrodes Fabricated By Single Step Oxidation of Photolithographically Defined Metal Electrodes

4.1 Introduction

The ability of chemical synthesis to control the electronic, magnetic and optical properties of molecules has motivated extensive research in the field of molecular devices.[8] Integrating molecules into devices by connecting the molecules between two metal electrodes remains one of the most difficult challenges to producing novel electronic, optoelectronic and spintronics devices.[8,149] To date, several schemes for producing 2-10 nm gaps have been reported.[150] Electro-migration produced break junctions and mechanical break junctions possess a nm gap between two electrodes of the same metal .[109] Several molecular transport studies exhibiting, negative deferential resistance,[149] Kondo effect[39] and current suppression,[33] have been performed with the low yield and difficult to reproduce break junctions .[103] Controlled growth of metal electrodes during a chemical vapor deposition [151] and an electrochemical process[152] was successfully demonstrated to produce nanogaps. Under these approaches the gap between two distant electrodes was reduced by amassing the electrode materials controllably.

Guo et al. have successfully produced molecular dimension gap on a single wall carbon nanotube. Oxygen plasma and chemical fictionalization were utilized, respectively, to burn a ≤10nm segment of carbon nanotube and to produce a molecular bridge between two ends of the nanogap. [153]. In molecular lithography process, multi-step and time intensive chemistry was performed to use the molecular monolayer to set the nanogap between two metal electrodes .[150] Moreover, utilization of carbon nanotube based shadow[154] and complex E-Beam alignment[155] are promising approaches for producing a nanogap between two metal electrodes.

Prevailing schemes to produce molecular dimension gaps are complicated and limited in scope as only few metals, mainly unoxidizable gold which is amenable for molecular self assembly, can be used as metal electrodes.[39] In most of the cases, it is not possible measure transport through the molecular-scale electrodes without a molecule; this factor makes many molecular studies questionable and care must be taken to avoid formation of nanoparticles with Coulomb blockade.[103] Another important issue is associated with the strategy of attaching molecules to the electrodes. Typically covalent bonds of a sheet of molecules to the bottom electrode are made by self assembly followed by direct deposition of the top metal electrode.[137] However this can complicate the molecular transport study by magnifying the effect of metal-molecule contacts and shorting defects. Uncontrolled impurities from the solution during self

assembly process and diffusion of metallic atoms into self-assembled molecular layer during top metal electrode may mask the true behavior of molecules.

A promising route to produce the molecular dimension gap between two electrodes is by controlling the thickness of a robust yet 1-3nm thick insulator between top and bottom electrodes. At the edge of the photolithographically defined junction pattern there is a vertical edge of exposed metal/insulator/metal structure. The minimum physical thickness between two electrodes is the thickness of insulator and is easily tuned to the length of molecular clusters. Covalent bonding of molecular clusters on the exposed edge of tunnel junction can establish molecular conduction channels. Critical to this approach is keeping tunneling current via insulator in the planar junction area very small allowing the molecular conduction to dominate. A scheme similar to the hypothesis of insulators giving precise thickness control is based on etching of ~4 nm silicon di-oxide insulator present between two Si or metallic layers. The etching step is followed by the shadow controlled metal depositions to shorten a nm gap between two metal or Si electrodes to produce molecular dimensions gap.[110,156] This approach is likely to suffer with irreproducibility with pattern edge line roughness and may be difficult to produce in the large array. The concept of producing molecular junctions through film thickness control, without reducing a ~4nm gap to molecular dimension by shadow metal deposition, has been successfully demonstrated in a recent work .[109],[111] The later submitted communication,[111] utilized an exposed edge tunnel junction with ~3.5nm insulator and gold top and bottom electrodes. Instead of shortening the gap between two electrodes via shadow mask metal deposition, several units of a short molecule were compounded to bridge the insulting gap between two electrodes. These molecular bridges formed a necklace around preformed tunnel junction. This resulted in >2 order increase in transport over the bare tunnel junction. However, in this approach insulator film thickness is still more than the length of molecules of interest (<3nm). For long conjugated organic molecules rotation conformation of π bonds can dramatically reduce the current. A more ideal molecular geometry is to have nm-scale tethers connecting a molecular cluster between leads. Tether lengths >1nm will have difficulty as too long a conduction barrier. One such Octa Metallic Cluster (OMC) with thiol-alkane tethers has been recently synthesized and incorporated in a.multilayer edge molecular electrode (MEME)geometry .[109] We successfully produced a gap as low as ~1.5 nm between a two metal layers on the exposed sides of a metal-alumina-metal tunnel junction. We utilized several meals, such as Ni, NiFe, Au and Ta, to produce molecular junctions. A molecular dimension gap is controlled by the thickness of aluminum deposition (and subsequent oxidation step). An exposed metal-insulator-metal face at the pattern edge is produced by the direct ion milling or liftoff step. Electrode fabrication is followed by the electrochemical

self assembly of OMC produced two arrays of molecular bridges spanning the insulator.[109] Modeling the conduction process resulted in a rate limiting step of tunneling into/out of the metallic core through alkane tethers. Interestingly, the molecular conduction process was limited by the length of the alkane tether and was rather insensitive to the tunnel barrier thickness; barrier height mainly affected the background planar area tunnel current. Ability to tune tunnel barrier thickness allows a simpler oxidation step and relaxes the requirement for ultra uniform insulator metal conformal coverage.

In this chapter we describe a simpler oxidation controlled method to produce a molecular length gap between tantalum (Ta) and an arbitrary top metal electrode. An advantage of this approach is that only one step oxidation of the bottom electrode, without depositing additional insulator or oxide forming metal film, produces the nm thick tunnel barrier. Deposition of the second metal electrode with its dimensions matching with the oxidized region of the bottom Ta layer produced a Ta/TaOx/metal junction with the exposed edges. Molecular transport studies before and after molecule attachment and a number of control experiments are utilized to demonstrate the successful realization of the new class of molecular electrodes.

4.2 Experimental Details:

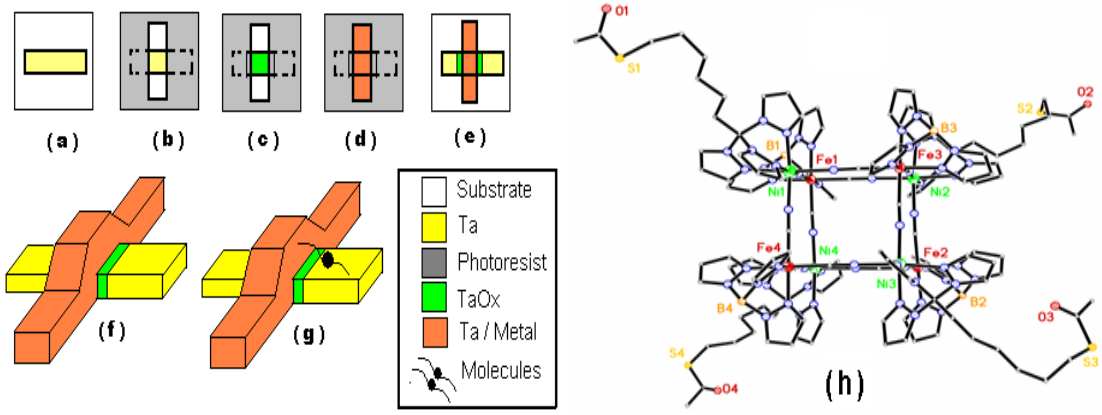

Figure 4.1: Fabrication steps: deposition of bottom electrode of ~10 nm Ta (a), opening a window in photo resist to expose selective area of bottom electrode(b), plasma oxidation to produce TaOx (c) followed by top metal electrode deposition (d). Liftoff of photoresist produced tunnel junction with exposed edges (e). A 3D image of a Ta/TaOx/M electrode before (f) and after (g) molecule attachment. X-Ray crystallograph for the octametallic molecular cluster used in this study (h).

The Ta/TaOx/M electrode fabrication scheme is summarized in figure 4.1. A (100) silicon wafer with 100nm thick thermally grown silicon di-oxide was used as a substrate and cleaned by organic solvent rinse. Sputter deposition (using AJA International sputtering machine) of the bottom Ta metal electrode was performed, with $2x10^{-7}$ torr base pressure, 100W gun power, and 1mtorr argon pressure. The following step was the photolithography (with Karl-Suss Mask aligner) for the creation of photoresist (PR) mask, using Shipley 1813, with a 5μm wide window over a Ta bottom electrode, figure 4.1(b). Soft baking of PR, performed at 110 ºC, was critical for strengthening the PR to minimize its burning in the following plasma oxidation step. Plasma oxidation of the Ta electrode through a 5μm window was performed, figure 4.1(c), within the sputtering chamber at 60 mtorr pressure of argon and oxygen mixture (Argon:Oxygen::1:1) and 20W RF substrate bias for 30-90 seconds duration .[109]

The growth rate of TaOx has two competing factors, growth due to oxidation of Ta atoms and etching due to sputtering by the bombarding ions from plasma .[157] Plasma oxidation condition was carefully optimized to have the desired thickness of high quality TaOx insulator and to burn the photoresist protection minimally. According to AFM study of oxidized patterns, the PR etch rate was found to be 30±4 nm per minute.

After the plasma oxidation process, a top metal electrode was deposited, through the same PR window as utilized for the oxidation step. This approach enables the coverage of only the oxidized Ta metal present in the exposed region within PR window, figure 4.1(d). Various metal, such as Ta, palladium (Pd) and NiFe (with Ni:Fe: 80::20), were utilized as top metal electrode. It is noteworthy that at the end of tunnel junction fabrication we observed a nonlinear tunneling electron transport on bare tunnel junction. The tunneling behavior is only possible when the top metal electrode and the unoxidized part of the Ta electrode are disconnected.

Fabrication of the bare Ta/TaOx/M electrode was followed by the molecule attachment. Two molecules, cyanide-bridged octametallic molecular complexes (OMC), $[(pzTp)Fe^{III}(CN)_3]_4$-$[Ni^{II}(L)]_4[O_3SCF_3]_4$ [(pzTp) = tetra(pyrazol-1-yl)borate; L = 1-S(acetyl)tris(pyrazolyl)decane][3] and 1,n-Dithiol Eicosane ($HS(CH_2)_{20}SH$),[158] were synthesized. Via thiol surface attachment to the metal leads, an array of OMC or Dithiol Eicosane molecules were covalently-linked onto the Ta and top metal electrodes, forming a dominant conduction pathway. Electrochemical molecular attachment [117] of the molecules to the Ta/TaOx/M electrodes via the thiol group was accomplished by the immersion of the electrodes in a dichloromethane solution of molecules (0.1mM), followed by alternating a ±100 mV bias between the two metal electrodes at a time interval of 0.002 seconds for 2 min.[109] Subsequently, the assembled devices were rinsed with dichloromethane, 2-propanol, and deionized water and dried under a nitrogen gas stream.

Immersion of the electrodes in a dichloromethane solution of molecules without the performing of the electrochemical step did not affect their transport properties. We surmise that the use of alternating voltage during the electrochemical step, in addition to removing thio-acetate protection group, helped condition the metal electrode surface by slightly etching it and subsequently favored the metal-thiol bonding.

Transport study of the Ta/TaOx/M electrodes was performed before and after the attachment of molecules using a Kiethley. Normally current-voltage measurement on Ta/TaOx/M electrodes, before and after molecule attachment, was performed between ±100 mV. However, a ±500mV range for transport studies was chosen for determining the tunnel barrier properties. It is noteworthy that chosen voltage ranges are far below the breakdown voltage potentials (~1.7V) of the bare electrodes. Typically 3-5 measurements per each I-V plot, using a 5 mV voltage step and 0.5 to 1 second time steps, were collected for each sample, to minimize possible scan to scan variation error.

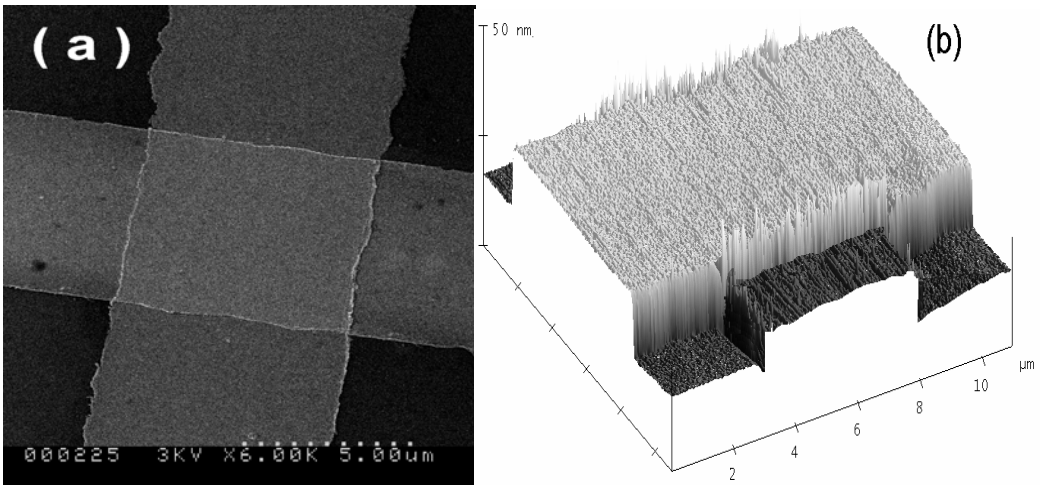

Figure 4.2: Junction characterization: (a) SEM micrograph giving top view and (b) 3D AFM view of one side of a Ta/TaOx/Ta electrode.

Structural characterization of typical Ta/TaOx/Ta electrodes by SEM, figure 4.2(a), and AFM, figure 4.2(b), showed the expected edge geometry and dimensions of the junction. Tunneling current transport study was found to be the best indicator of the tunnel junction quality. Effective barrier thickness and barrier height were measured by fitting the transport data of a bare Ta/TaOx/M electrode with the Simmons model.[159] Typical junction area ranged from 9-25 μm^2. Breakdown voltage and barrier thickness of electrodes were 1.7±0.2 V and 2-3.5 nm, respectively. The fact that tunneling current was observed meant that there was no deposition ot top metal directly on the bottom electrode and that nm-scale gaps between electrodes existed.

4.3 Results and discussion:

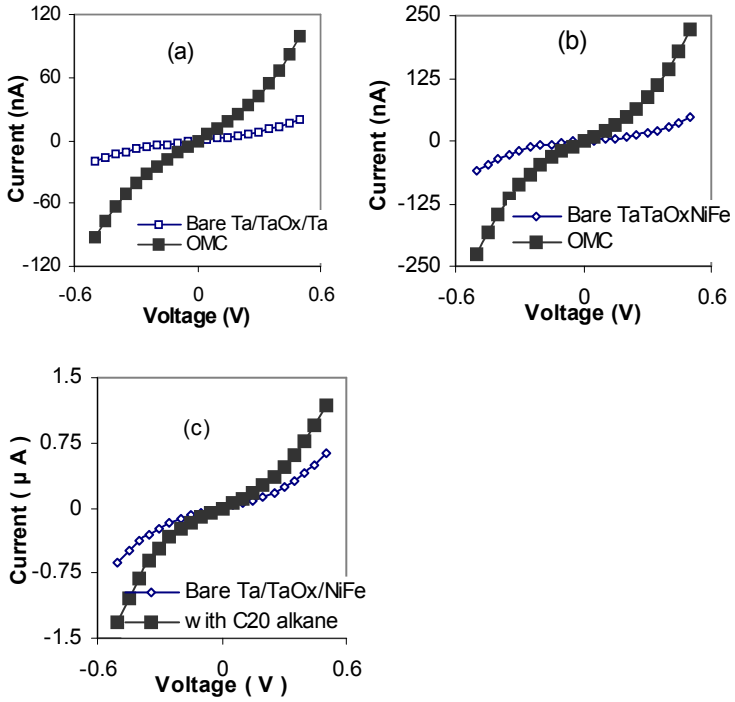

Figure 4.3: Transport before and after molecule attachment: (a) I-V before and after OMC attachment on Ta/TaOx/Ta and (b) Ta/TaOx/NiFe. (c) Ta/TaOx/NiFe before and after Dithiol Eicosane molecule attachment.

Transport of Ta/TaOx/M electrodes before and after molecule attachment was studied. The Ta/TaOx/Ta electrode exhibited a 3-5 fold increase in current due to OMC attachment, figure 4.3(a), and **Table 4.1**.

Table 4.1: The magnitude of current at 100mV of electrode in bare state and after molecular bridging.

	Bare (nA)	With molecule (nA)
Ta/TaOx/Ta [figure 3 (a)]	2.4	11.7
Ta/TaOx/NiFe [figure. 3(b)]	3.2	20.1
Ta/TaOx/NiFe [figure. 3(c)]	53	104

Molecular current is defined as total current minus bare electrode current. To show the ability of Ta/TaOx/M electrodes to produce a nanogap between dissimilar metal electrodes, the

top Ta metal electrode from the Ta/TaOx/Ta electrode was replaced with the ferromagnetic NiFe to produce a Ta/TaOx/NiFe electrode. OMC attachment on these junctions yielded a 3-7 fold increase in current over the background current, a representative example is shown in figure 4.3(b). With the utilization of NiFe as a top electrode ~30% higher current is seen.

Attachment of short length 20 carbon alkane molecules, Dithiol Eicosane, also increased the current of Ta/TaOx/NiFe by ~2 fold, figure 4.3(c). Dithiol Eicosane were found to be attaching rather easily on electrodes prepared with smaller oxidation time, 30-40 seconds, which presumably produces a smaller insulating gap between two metal electrodes within and, more importantly, at the edge of the tunnel junction. The present scheme allows the realization of a shorter insulating gap between unoxidized bottom Ta electrode and top NiFe electrode compared to Al_2O_3 deposition of insulator barrier. Consequently, this situation enables the bridging of shorter Dithiol Eicosane molecules (~2.2nm) between metal electrodes. However, generally, Ta/TaOx/NiFe junction with produced with smaller oxidation time duration exhibited higher leakage current. It is noteworthy that here barrier thickness of Dithiol Eicosane is comparable with TaOx barrier thickness; thus increase in current is due to the establishment of new relatively conductive molecular channels. The leakage current through ultrathin TaOx varied from sample to sample. Plasma oxidation is expected to produce inhomogeneous oxide;[160] it is difficult to reproduce the effect of imperfect stoichiometry on samples grown in different batches.

Approximate number of OMC's (1nm diameter) attached on Ta/TaOx/M electrodes 10um length) is ~10,000; however, due to smaller steric hindrance the number of Dithiol Eicosane molecules attached on electrodes is expected to be ~30,000. The magnitude of the current per molecule, calculated according to (total current - bare electrode current) / (# of molecules) ,[109] for OMC and Dithiol Eicosane were 12±6.7pA and 0.62±0.5pA, respectively. The current per OMC(Dithiol Eicosane) molecule with NiFe/Alox/NiFe electrodes was 160±130pA(11±7pA);[109] change of metal electrode from Ta to NiFe exhibits an increment by a factor of ~17 for OMC(Dithiol Eicosane). More than one order difference in current per molecule between two metals can be attributed to the difference in availability of number of sites for molecule attachment or metallic density of states .[161] Since Ta is easily oxidized, it also possible for a partially oxidized surface to have fewer molecular channels than the case with NiFe electrodes. However it is difficult to distinguish from contact/electrode effects and the current density calculations are based on the total exposed electrode edge area. The current per molecule (50 mV bias) of OMC across Ta/AlOx/Ta electrode,[109] (3.5±2pA), is in good agreement with the present case of the Ta/TaOx/Ta electrode (11±7pA).

4.3.1 Control experiments

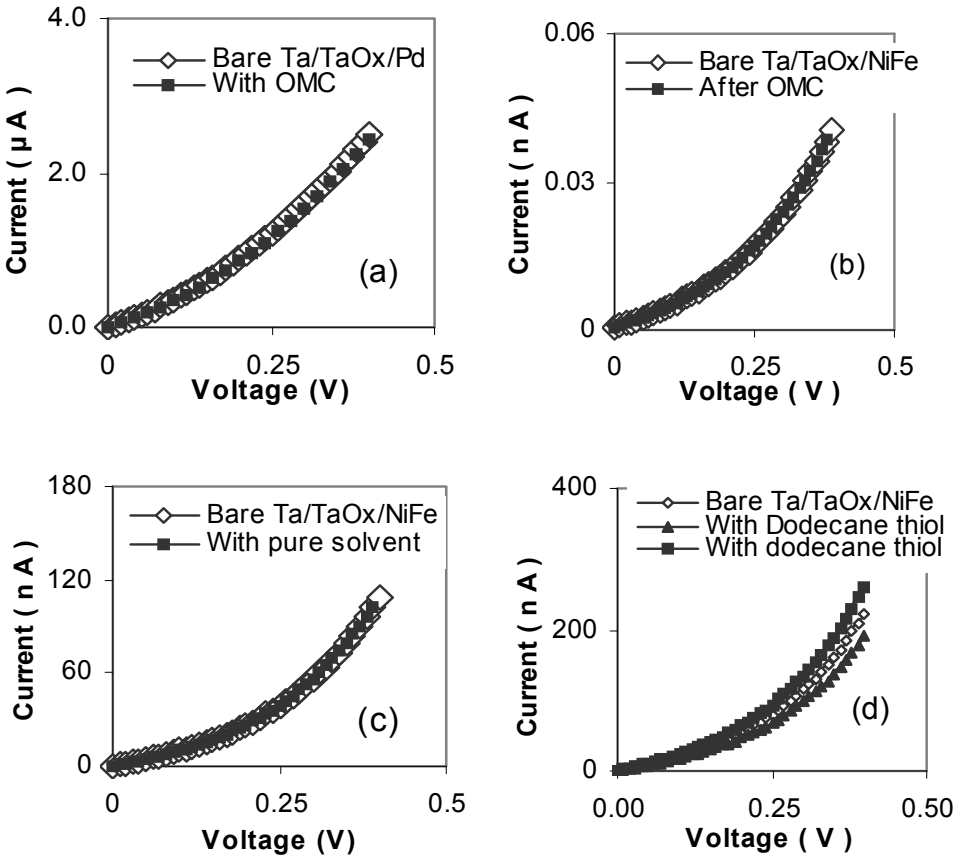

Figure 4.4: Control experiments. Ta/TaOx/M electrodes with (a) high leakage current and (b) with thick tunneling spacer, produced through PR protection with undercut profile, are unaffected by OMC attachment. (c) Electrochemical molecule attachment process in pure solvent produced no change on transport. (d) Attachment of 1,n dodecanthiol thiol molecules produced ± 15% change in the bare Ta/TaOx/NiFe electrodes transport.

A number of control experiments were performed to confirm that conduction was through molecules spanning the insulator surface of the electrodes. Electrodes with large leakage current, for instance Ta/TaOx/Pd with 200kΩ junction resistance, remained unaffected by the molecular treatment. High junction conductivity signifies the high leakage current between two metal electrodes via a presumably thinner and/or defective TaOx barrier;[162] establishment of new molecular channels will only contribute negligibly with respect to the bare junction current.

Ta/TaOx/M electrodes with a thicker tunneling barrier than the physical length of OMC did not exhibit any noticeable change in transport. To perform this experiment, the top electrode/oxide photo resist mask was made with an undercut. The idea of using undercut in PR

mask was to create a sufficiently large gap (>3nm, the OMC length) between the top metal electrode and the unoxidized part of the Ta electrode. This precludes the possibility of producing shorter OMC molecules spanning the gap to form addition molecular current. Isotropic plasma oxidation of Ta film produced a wider TaOx span as compared to the width of the top metal electrode deposited by an approximate line-of-sight deposition conditions. We were unable to resolve the lateral dimensions of the larger gap, but conclude that it is greater than 3 nm.

In the next control experiment, the possibility of any degradation of electrodes during electrochemical treatment (HCl formation) was determined. Electrochemical process, with the pure dicholoromethane solvent, did not exhibit any noticeable change in the transport of bare electrodes as shown in figure 4.4(c).

Attachment of a 1-n dodecanthiol from its 2mM solution in dicholoromethane on a Ta/TaOx/NiFe electrode nominally affected bare electrode transport (±15%), figure 4.4(d). This experiment confirms that only a long molecule that can bridge over the insulator and form metal-thiol chemical bonds are responsible for observed current increase.

4.3.2 Transport-Analysis

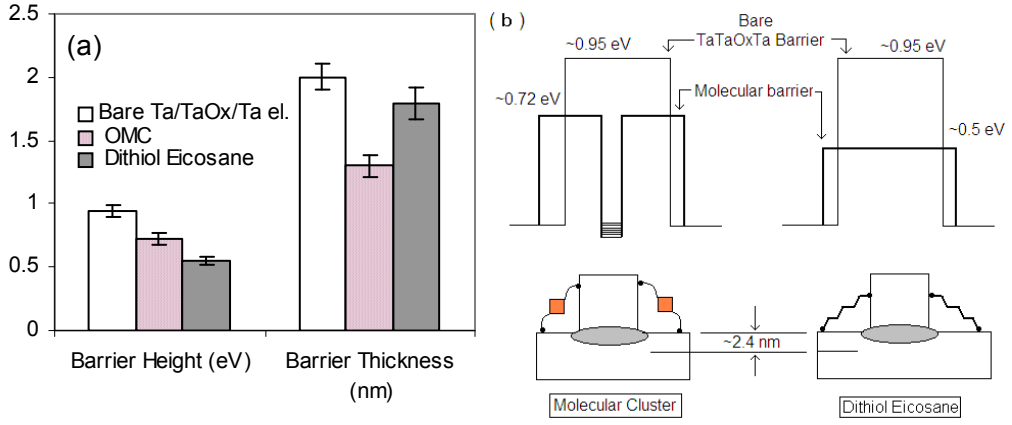

Figure 4.5: Barrier height and effective barrier thickness before and after OMC and Dithiol Eicosane attachment as calculated from Simmon's model fit to experimental data. (b) Schematic description of change in tunneling barrier specificity of bare electrode after molecule attachment.

To elucidate the molecular conduction mechanism, we have fitted current density (j)-voltage (V) data of bare and molecule attached Ta/TaOx/Ta, electrodes with the Simmons model .[159] We surmise that ~10,000 nm-scale molecules, coupled to metallic electrodes by the well defined metal-S bonds, are capable of affecting the transport of Ta/TaOx/M electrodes. The

molecular current was calculated by subtracting the bare electrodes current from the total current observed after the molecule attachment. A molecular cross section area is calculated by assuming that 10,000 OMCs, each with 1nm square, are attached along the 10μm long edge giving $1x10^{-10}$ cm^2 area for molecular current. Although a larger number of Dithiol Eicosane molecules are expected to bridge between two metal electrodes, they are expected to pack within the same physical area as calculated for the OMC molecules.

Barrier properties, barrier thickness and barrier height on the bare and molecule attached electrodes were obtained by fitting the experimental current density -voltage data with the Simmons model within a medium voltage range ($V< \varphi_B/e$) as give below[163]:

$$j = \left(\frac{e}{4\pi^2\hbar d^2}\right)\left\{\left(\varphi_B - \frac{eV}{2}\right)\times \exp\left[-\frac{2(2m)^{1/2}}{\hbar}\alpha\left(\varphi_B - \frac{eV}{2}\right)^{1/2} d\right] - \left(\varphi_B + \frac{eV}{2}\right)\times \exp\left[-\frac{2(2m)^{1/2}}{\hbar}\alpha\left(\varphi_B + \frac{eV}{2}\right)^{1/2} d\right]\right\} \quad (4.1)$$

where m is electron mass, d is barrier thickness, φ_B is barrier height, V is applied bias , and α is a unitless adjustable parameter, that allows for deviations from a simple rectangular barrier and effective mass of the electron.[163] Via equation 1, (setting α =1) we are able to fit the values of both barrier height and barrier thickness before and after molecule attachment for various Ta/TaOx/Ta samples. Tunneling decay factor (β) was also calculated using barrier height data.

The Molecular cluster possesses a relatively conducting organomettalic cube .[3] Transport rate via molecular cluster has three stages: slow tunneling rate(s) from metal electrode (OMC center) to OMC center (metal electrode) and fast transport within organometallic cube.[109] The molecular barrier thickness is expected to be equal to one alkane tether length (~1.2 nm) while total molecule length is ~3nm. The Simmons model clearly suggests that for OMC barrier thickness is ~1.3nm and barrier height of ~0.72 eV in accordance with a previous molecular transport study with the same molecule .[109] Tunneling decay factor for the transport through OMC came out to be 0.86 $Å^{-1}$ which is in agreement with the previously obtained β for the 10-12 carbon alkanes.[163] For Dithiol Eicosane molecules, similar analysis was performed. Barrier thickness, barrier height and β were 1.8±0.1nm, 0.55±0.05 eV and ~0.75$Å^{-1}$, respectively Attainment of shorter barrier thickness with regards to the physical length of Dithiol Eicosane , ~2.2nm, can be attributed to the deviation of barrier shape and mass of the electron from the ideal case.[163] Change in molecular conformation is another likely reason for the smaller barrier thickness.

4.4 Conclusion

A molecular-scale gap between two metal electrodes was successfully controlled by a single step plasma oxidation method. This simple approach only required widely available thin film deposition method and photolithography. A variety of metals can be used as the top electrode with present electrode design. The primary advantage of this methodology is that it produces a lateral-insulating gap smaller than ~2nm. This gap does not have to be precisely controlled to the molecular length so long as the molecule can bridge it and background tunnel current is sufficiently low. The present device design will directly benefit from the commercially available scaling of photolithographic line width w (5um to ~50nm), with background tunnel current being proportion to w2 and molecular current proportional to 1/w. Conduction is through the well controlled length of a molecule, allowing chemical synthesis to directly affect conduction which is not possible in polymer systems or large macromolecules where π bond conformations are dominate. This devise design allows molecules in the exposed region of the junction to easily interact with light radiation and specific chemical agent (that can affect the molecular transport) allowing the formation of molecular-photo devices and chemical sensors, respectively.

Chapter 5

TaOx Thin Film Photovoltaic Devices

5.1 Introduction

The realization of thin film based photovoltaic devices offers lucrative options for the replacement of costly silicon based solar cells.[164] A practical thin film based solar cell should be able to absorb sufficient radiation. More importantly, it should be endowed with a mechanism, akin to the inbuilt potential in the p-n junction solar cells,[165] to separate the photo-energy created electron-hole pairs. Device, based on ~100nm thick semiconducting cuprous oxide (Cu_2O) sandwiched between the two metal films have exhibited rectifying transport properties and photovoltaic effects.[166] Rectification in this case was attributed to the dissimilar metal contacts with different work functions present on the two sides of Cu_2O.[167,168] However, the maximum solar cell efficiency achieved thus far with Cu_2O based solar cell is ~2%, which is well below the predicted efficiency for Cu_2O based solar cells (20%).[168] The aim of using ~100nm thick Cu_2O,[168] primarily to enhance the light absorption, is generally defeated as it possesses atomic defects in the proportion of thickness. A higher defect density can annihilate the photo-generated electron-hole pairs before they are separated and transferred to the opposite electrodes.[164,165]

A better approach to make a metal-metal oxide-metal based solar cell is to reduce the metal oxide thickness to a few nm, yet managing to keep the light absorbance reasonably high. Recently, attempts have been made to produce a thin film photovoltaic cell using an ultrathin ~3nm niobium oxide (NbOx) based tunnel barrier, grown by the air oxidation of niobium (Nb).[169] The significant difference in the barrier heights of the two metal/insulator interfaces of the Nb/NbOx/Ag tunnel junction was attributed to the difference in the work function of the metal contacts. In spite of showing a rectifying behavior, these tunnel junctions did not show a noticeable photovoltaic effect. Previously, tunnel junctions utilizing aluminum (Al) electrodes and 3nm alumina (AlOx) with an Al/AlOx/Al configuration have exhibited ~0.9eV difference in barrier heights at two Al/AlOx interfaces.[165] This study suggested an inhomogeneous oxidation alone can produce an inbuilt potential, i.e. the difference between the two barrier heights. In our knowledge, no photovoltaic effect has been reported with the Al/AlOx/Al system. The reason why this system did not show photovoltaic effect is presumably due the absence of a mechanism to absorb the light radiation within the AlOx barrier.

In the quest of finding a significant photovoltaic effect in the metal-metal oxide-metal system, we explored the photovoltaic effect in Ta/TaOx/Ta tunnel junctions. This system is particularly promising; previous X-Ray photoelectron emission (XPS) studies of Tantalum oxide

(TaOx), grown by the thermal oxidation of a Ta metal, exhibited a graded distribution of unoxidized Tantalum (Ta) ions impurities.[160] The gradient of atomic defects within a TaOx is consistent with the oxygen diffusion model. We conjectured that a similar profile of atomic defects will appear from the plasma oxidation treatment[157] of Ta. The reason for switching to plasma oxidation instead of thermal oxidation is its easy controllability to produce ultrathin insulators. [17] We hypothesized that defects at the optimum spatial location within TaOx can absorb light radiation[170] to form electron-hole pairs. On the other hand, a gradient in defect density[162,171] can produce the difference in the barrier height between the two Ta/TaOx interfaces. Eventually unequal barrier heights[165] will produce inbuilt electric fields for the separation of electron–hole pair.[172] To realize this theme, we have produced a Ta\TaOx\Ta tunnel junction using photolithography, sputter deposition, and plasma oxidation. A highly controllable plasma oxidation process produced nm thick nonstochiometric TaOx.[171] The number of characterizations, including the transport and optical properties of TaOx, were utilized to establish these junctions as a photovoltaic device.

5.2 Experimental details:

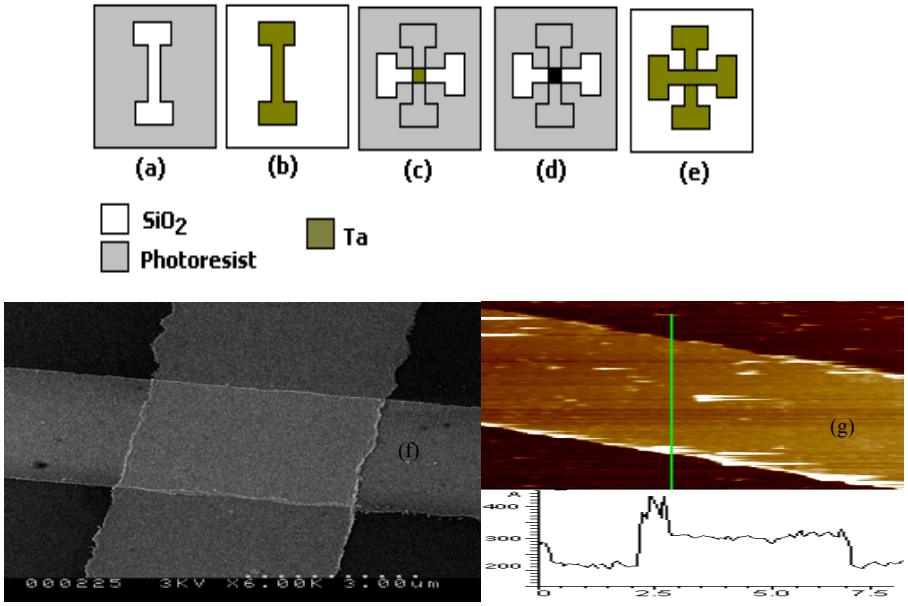

Figure 5.1: The fabrication and characterization of Ta/TaOx/Ta junction: (a) Photoresist pattern for bottom Ta layer deposition; (b) pattern after deposition of Ta film and lift-off of photoresist; (c) after the second stage photolithography; (d) plasma oxidation of Ta (dark black region shows oxidized segment) layer followed by the deposition of the top Ta electrode in the white area; (e) planar view of the complete junction after liftoff; (f) SEM micrograph of a Ta/TaOx/Ta junction, and (g) AFM study of the bottom electrode.

The fabrication steps of Ta/TaOx/Ta junctions and their characterization is illustrated in figure 5.1. Throughout this study, a Si wafer with thermally grown 100nm silicon oxide was utilized. Wafer pieces were sequentially washed in acetone, isopropyl alcohol, and DI water for 2min each and then samples were dried in the nitrogen flow.

The following steps were performed in the given order during first stage photolithography: the spin coating of a Shipley 1813 positive photoresist at 3500 rpm for 30sec, soft backing at 100ºC for 1 min, exposure for 20sec through a photomask by Karl-Suss mask aligner, the developing of a photoresist with a MF-319 developer solution for 1min, and the rinsing of the samples in DI water 5 times followed by drying in the nitrogen gas flow. The samples were then transferred to the load lock chamber of the sputtering machine (AJA Multitarget Sputtering System) using clean sample enclosures. The sputtering of ~12nm Ta was performed in the main chamber with $2x10^{-7}$ torr base pressure at 100W DC gun power and 1 mTorr Ar (99.99% purity) pressure at RT. Within 5 min of the sample's removal from the sputtering machine, it was soaked in a Shipley-1165 resist remover solution for 30min for liftoff, followed by rinsing in DI water and drying in the nitrogen flow.

The second photolithography step, using the previously mentioned photolithography protocol, to produce a cross pattern, figure 5.1(c), was performed. Next, samples were transferred to the sputtering machine. The duration of which the first Ta film remained outside of the sputtering system was 2hrs (for 90 min in contact with various electronic grade solvents and for 30min in the clean room environment).

The exposed segment of the bottom electrode through a photoresist layer was plasma oxidized to produce a ~3nm TaOx insulating layer. The thickness of TaOx was confirmed by the spectroscopic ellipsometer based thickness measurement on a simultaneously processed TaOx sample. Plasma oxidation was performed at a 20 W substrate bias and 60 mTorr pressure of 1:1 argon:oxygen mixture for 60 seconds. After the oxidation step, purging was performed with Ar for 1 hr to replace the remaining oxygen from the main chamber. Then the top ~12nm thick Ta metal electrode was deposited using the previously mentioned Ta deposition parameters through the same photoresist window. Next, the liftoff step with a Shipley-1165 resist remover produced a Ta/TaOx/Ta tunnel junction (TJ). The AFM study of TJ showed that Ta electrodes are 12±0.5nm thick and possessed 0.2±0.1nm Rq roughness. TJ area is ~25 μm^2. A typical TJ showed a breakdown voltage of 1.8±0.2V.

5.3 Results and discussion:

As prepared, Ta/TaOx/Ta tunnel junctions (TJs) exhibited an asymmetric tunneling characteristic,[173,174] figure 5.2(a), which is more apparent from the transport analysis presented elsewhere in this chapter. An asymmetric transport is rather surprising for a TJ with identical top and bottom electrode materials. This behavior can be attributed to the nonuniform composition[174,175] of the TaOx tunnel barrier.[160] Tunnel barriers produced by the plasma oxidation of a metal film are known to have a depleting amount of oxygen or an increasing amount of unoxidized metal atoms as one moves from the top to bottom of TaOx.[160,175] Depth wise, the XPS study of the TaOx[160,175] suggested the presence of stochiomiteric Ta_2O_5 on the top surface but Ta+ rich suboxides of Ta on approaching the bottom of TaOx. In the secondary mass ion spectroscopy analysis of electrochemically grown TaOx,[162] asymmetrically distributed carbon impurities were detected. This work aims to show the effect of asymmetrically distributed atomic defects without delving into defect specific details. However, Ta+ ions[162] are expected to play the key role and these type of defects are more relevant to the barrier formed by the plasma oxidation.[157]

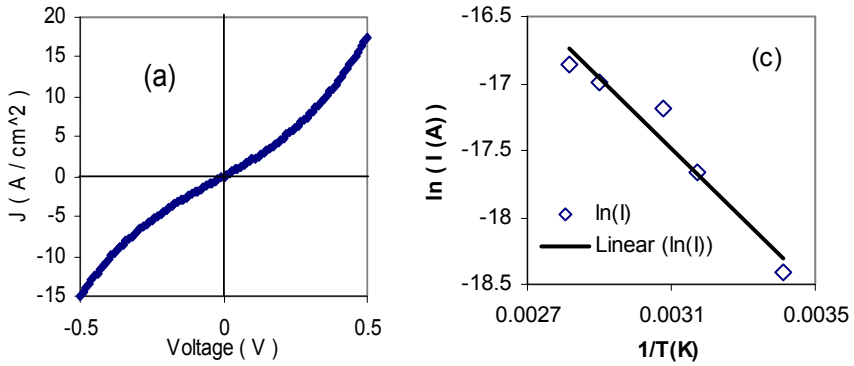

Figure 5.2: (a) RT transport study of Ta/TaOx/Ta tunnel junctions with good photovoltaic effect. (b) linear relation between logarithmic current and inverse of temperature showing thermally activated transport.

Because of the presence of defects, previous transport studies of TaOx based TJs were found to be thermally activated[162 176,177]. The Pool Frenkel type thermally activated transport that generally occurred via defect induced energy levels in TaOx, has been widely observed [177,178]. A temperature dependent transport study of our TJs indicated a thermally activated process, figure 5.2(b). It clearly indicates that defects play an active role on barrier properties and transport[162]. Thermal activation energy calculated using the Arrhenius equation was found to be 0.23±0.15V.

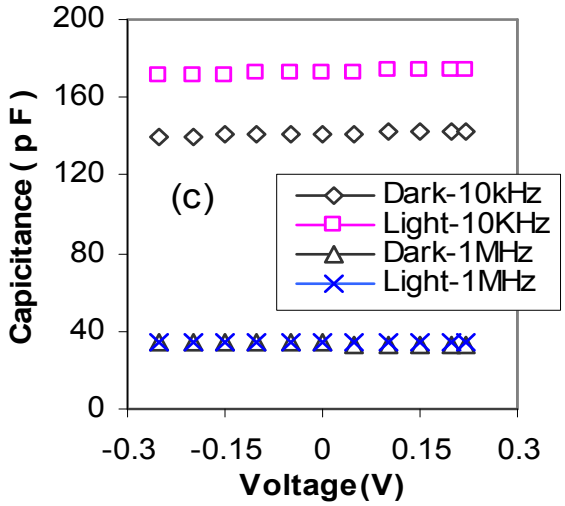

Figure 5.3: C-V study of Ta/TaOx/Ta tunnel at 10kHz and 1MHz frequencies in dark and light at 295K.

To further establish the presence of atomic defects within the barrier capacitance-voltage (C-V), measurements were performed.[178,179] The capacitance of TJs was found to vary with frequency, Figure 5.3. For instance, the capacitance of a typical TJ at 10 kHz (1MHz) was ~140(~38) pF. The capacitance of defect free tunnel junctions are invariant of frequency.[180] This study, although, clearly suggests that TaOx possesses imperfections but does not point to the position of defects within the barrier.[178] To locate the position of defects, we rely on previous XPS studies on an analogous system.[160] It is also noteworthy that for a stoichiometric Ta_2O_5 capacitor with 3nm thickness and 25μm^2 area, calculated capacitance is 3pF. However, in the present case the capacitance of TaOx is nearly one order higher and can be attributed to the defect induced states. Defects within the barrier can significantly reduce the effective distance between two electrodes and can also alter the effective dielectric constant. Furthermore, the capacitance value of TJ at 10 kHz in dark and white light irradiated TJ are, respectively, 140pF and 180pF. This study suggests that a TaOx barrier with atomic defects is photoactive as observed in the case of solar cells.[179]

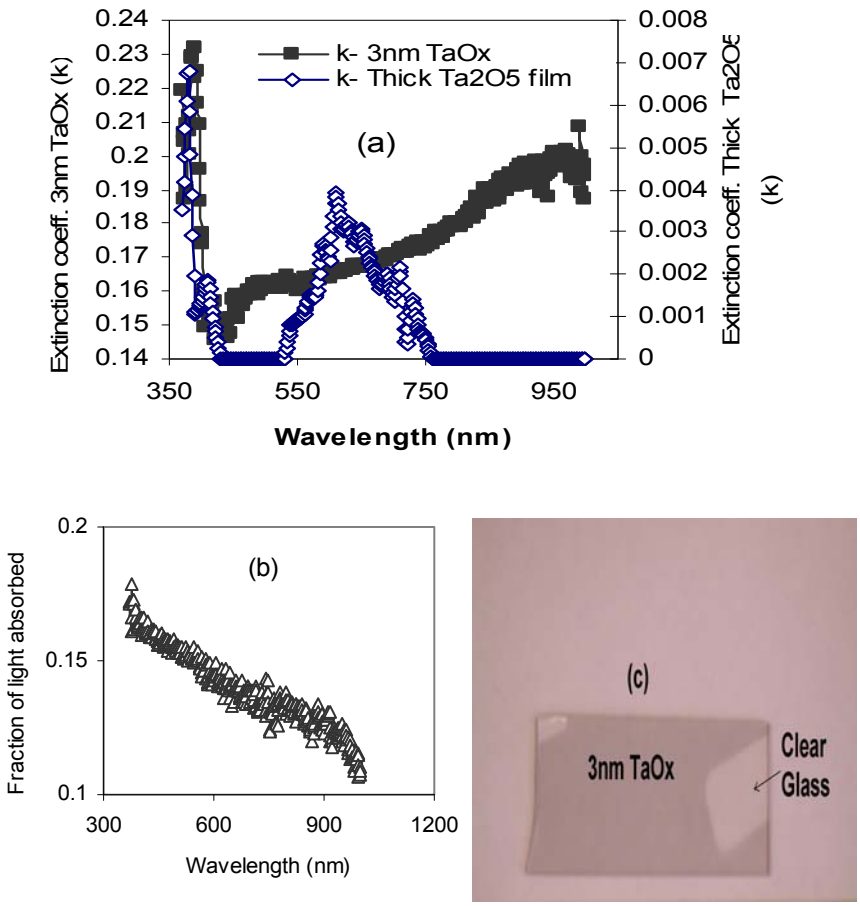

Figure 5.4: Optical properties of ~3nm TaOx: (a) Comparison between extinction coefficients data for different wavelengths between ~3nm TaOx and Thick Ta_2O_5[2]; (b) fraction of light absorbed by the ~3nm TaOx, deposited on quartz. (c) Nontransparent 3nmTaOx on glass slide exhibiting light absorption.

To analyze the optical properties of ~3nm TaOx grown on a thermally oxidized Si wafer and quartz substrate, spectroscopic ellipsometery, using a GA Woolam ellipsometer, was performed. The extinction coefficient for ~3nm thick TaOx was found to be 0.15 to 0.2 for a range of 400 to 1000 nm wavelength radiation, figure 5.4(a). It is noteworthy that stoichiometric Ta_2O_5 is transparent for a significant regime of the visible range,[2] figure3(a). Almost a 2 order higher extinction coefficient and as high as ~15 % absorbance, in figure 5.4(b) ~3nm thick TaOx indicates its strong tendency to absorb light. The deposition of ~3nm TaOx on glass produced significantly light absorbing film, as evidenced by figure 5.4(c). It is interesting to note that in our case plasma oxidation produced TaOx showed a spike in the extinction coefficient value (around 400nm) and this agrees with the similar spike observed with Ta_2O_5.[2] The magnitude of the

refractive index for TaOx in our case for ~500nm wavelength is 2.3, which is in good agreement with the value of the refractive index (2.1), as observed for the thermally grown TaOx.[178]

Photoactive Ta/TaOx/Ta with a rather asymmetric transport, motivated us to probe the photovoltaic effect[169] by conducting a transport study under the varying white light intensity. A significant amount of photocurrent and as high as 160mV open circuit voltage (Vo) was recorded, figure 5.5(a). The typical energy efficiency of the 25μm^2 Ta/TaOx/Ta TJs was found to be 8±3%. To calculate the energy efficiency, the product of the multiplication of half of the open circuit voltage and half of the photocurrent density was divided by the incident light intensity. It was observed that the value of energy efficiency did not remain constant with the change in tunneling area. Moreover, increasing tunnel junction area was concomitant with a decrease in energy efficiency. This decrease is presumably due to the enhancement of the interaction between atomic defects and light generated electron-hole pairs at other atomic defects sites.

Interestingly, Vo saturated with increasing light intensity, figure 5.5(b), and exponentially decayed with increasing temperature, figure 5.5(c). The mechanism behind the photovoltaic effect and the dependence of Vo on the light intensity and temperature is discussed elsewhere in this chapter.

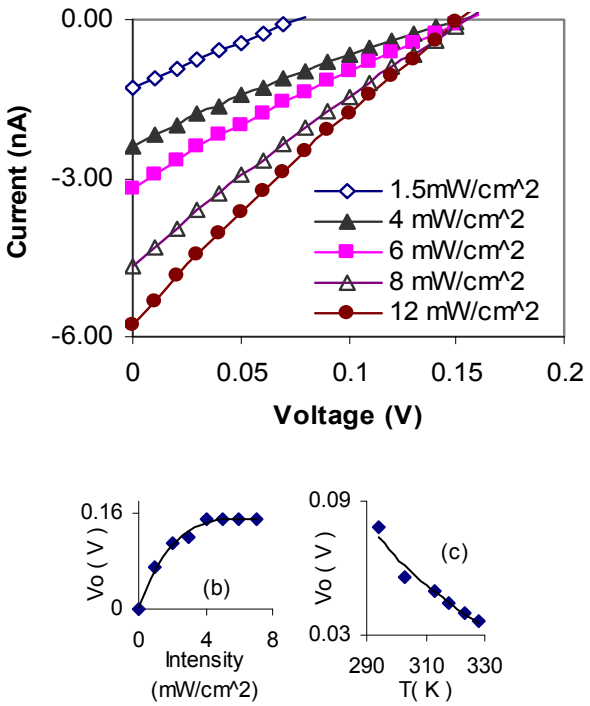

Figure 5.5: Photovoltaic effect at Ta/TaOx/Ta junction (a) Light intensity versus photo current and photovoltage (b) light intensity vs open circuit voltage and (c) temperature reducing Vo at exponential rate at 2mW/cm^2 light intensity.

To comprehend the role of atomic defects in rendering tunneling barriers asymmetric and photoactive, the transport data of as prepared TJs were fitted with Simmons[50] and Brinkman models.[173] The rationale behind using the Simmons and Brinkman model is as follows: we surmise that even though transport between two electrodes is occurring via defects sites, even then the conduction process between the electrode and an aggregate of defects is governed by the tunneling mechanism at room temperature. It is noteworthy that the usage of tunneling model in complex cases[109] has given useful insight about conduction mechanism.[173] The aim of using tunneling model here is to understand the Ta/TaOx/Ta tunnel junction qualitatively. The application of the model on transport data gave effective barrier thickness and barrier height value, **Table 5.1**.

Table 5.1: Barrier height and barrier thickness of TaOx tunnel barrier calculated from Simmons and Brinkman tunneling model.

Model	Barrier Th. (nm)	Barrier Ht.(V)	Barrier Asymmetry (V)
Simmons(+Bias/-Bias)	1.5±0.2/1.9±0.15	2.3±0.2/1.5±0.2	0.82±0.2
Brinkman	1.8±0.2	1.5±0.25	1.1±0.3

According to the Simmons model,[50] was prepared TJ possessed a thinner (thicker) barrier and a large (small) barrier height from the top (bottom) electrode side. A stochiometeric TaOx, i.e. Ta_2O_5, should have a uniform value of barrier height throughout. We surmise that the population of atomic defects, presumably unoxidized Ta (Ta+) atoms, are highest in the proximity of the bottom electrode and decreases rapidly on approaching the top electrode.[160] Such asymmetric spatial distribution of atomic defects has been concluded to lower the barrier height near the interface with a higher defect population .[177]

A previous study suggested that the appearance of the energy levels within the TaOx barrier were due to the metallic Ta impurities.[181] Atomic defects are expected to produce energy levels starting from the conduction band to the deep level, figure 5.6(c). If this assumption is true, then defects close to the Fermi level of Ta would allow tunneling via them. This effect will cause the barrier thickness to be around half of the physical thickness of TaOx. These assumptions are supported by the barrier thickness values. Effective barrier thickness values obtain by fitting the transport data with tunneling models fall within the range of 1.5-1.9 nm; TaOx physical barrier thickness, measured by the ellipsometry, was found to be ~3 nm.[176] A smaller barrier thickness is indicative of defect mediated transport.

It has been observed that the values of barrier height and barrier thickness vary with the range voltage for which transport data is chosen.[177] We have fitted the current density data to the Simmons and Brinkman model to extract barrier thickness using a 1.7 eV experimental value of the barrier height for the TaOx barrier.[182] From both models, barrier thicknesses were found to be in the range of 1.5-1.9 nm; experimentally measured barrier thickness is ~3nm. It is also noteworthy that for unrestricted fitting, where barrier thickness and barrier height were used as variables, barrier height values are in the range of 1.5-2.3 eV, which is in agreement with the experimentally measured values.[182] One surprising thing to note is that the I-V characteristics of a Ta/TaOx/Ta in our case is quite symmetric in appearance.[174] In a few cases, it was found that the transport analysis of a degraded tunnel junction after heating or intense light exposure produced a 2.5-3 nm barrier thickness and ~0.5 eV barrier height. A smaller barrier height has also been observed elsewhere.[171] The difference in barrier parameters is presumably due to the difference in the profile and density of atomic defects in a freshly prepared[160] and degraded TaOx barrier.

Qualitative mechanism of the photovoltaic effect in Ta/TaOx/Ta is presented in figure 5.6 (a-f). From the XPS studies and discussion thus far it is apparent that a higher density of atomic defects is present in the vicinity of the bottom electrode, figure 5.6(a). A graded density profile of donor type defects is expected to transform the ideal tunnel barrier, figure 5.6(b), to produce asymmetric barrier heights, figure 5.6(c) or a new energy band, figure 5.6(d). Atomic defects far from the bottom electrode are likely to have different electrostatic environment; and presumably produce deep-level and photoactive defects.

We conjectured that due to a smaller barrier height photo excited electron from the defect site in the vicinity of top electrode will move to the bottom electrode.[170] While the resulting hole on the defect level will tunnel towards the top electrode, due to a smaller tunneling distance; tunneling distance affect the tunneling rate exponentially.[50] This mechanism of separating photo-excited electron hole pairs would enable a net photovoltaic effect. This mechanism bears resemblance to the Glass model;[170] glass model was previously studied to explain the photovoltaic effects within the oxides due to defect centers.[172] Atomic defects, which are closer to the bottom electrode, will not yield a net photovoltaic effect; holes and electrons from the defect sites will reach the bottom Ta electrode and will annihilate each other, figure 5.6(e).

Alternative explanation for the photovoltaic effect in this system can be given in the following manner. Photo-excited electron from the deep level defect, closer to top electrode, will move to the defect induced energy band. From this band, photo excited electron can move to the bottom electrode. However, photo-generated hole will more to the top electrode, leading to charge separation. We have observed that as-prepared TJs open circuit voltage (Vo) saturated

once white light intensity increased beyond a threshold point of 4mW/cm^2, figure 5.4(b). The halogen lamp, used in this study, has a wide distribution of wavelengths from infrared to ultraviolet.[183] Photo-generated electron-hole pairs within photoactive regime of tunnel barrier will be swept to leads causing an accumulation of charges, ultimately defining the Vo. Magnitude of Vo is a strong function of thickness of depletion layer,[183] which is surely complicated to define in our system[160,177] but surely has a finite value which leads to a saturation of Vo. The open circuit voltage (Vo) was also observed to decrease exponentially with increasing temperature, figure 5.4(c).

To elucidate this observation it is necessary to recall that the transport through as prepared TJ was found to be thermally activated. The charge flow rate is an exponential functional of the temperature.[162] In other words, accumulated charges, defining Vo on the two leads are expected to be siphoned out at an exponential rate with increasing temperature. Therefore a corresponding decrease in Vo, dictated by the accumulated charge, is justifiable.

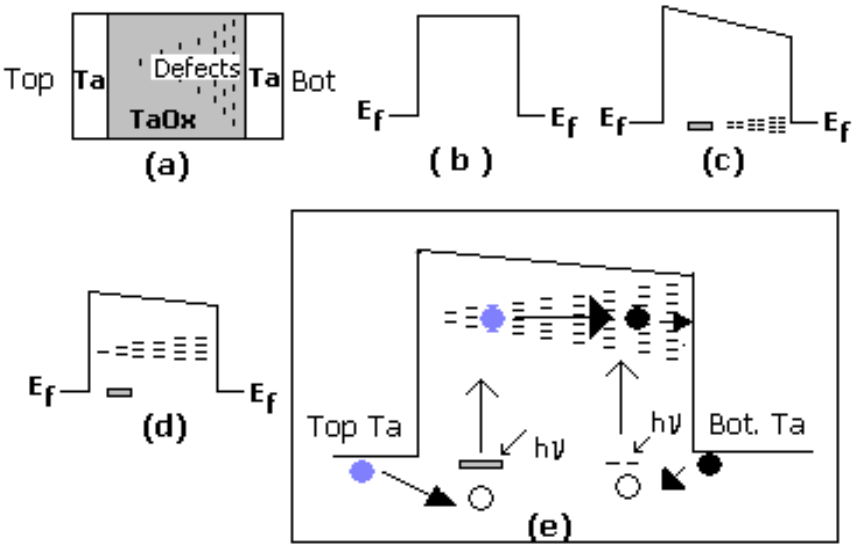

Figure 5.6: Atomic defect distribution in TaOx barrier (a), ideal tunnel barrier profile (b) large gradient in atomic defects in TaOx produced asymmetric tunnel barrier and photoactive defect states within the barrier, shown by dashed line (d). Charge separation is only possible for defect sites closer to the top electrode, but not for the defects closer to the bottom electrode (e).

The operational life of Ta/TaOx/Ta based thin film solar cell is observed to be strongly influenced by the heat treatment and exposure time to the intense light radiation. TJ used in this study started showing instabilities soon after heating above 70 ºC. Long exposure to intense white light is expected to produce effect similar to the heating; the broad band light source contained

radiation in infrared range. When a junction degraded, presumably under the influence of relaxing tensile stresses, mainly arising from heating, a drastic increase in surface roughness was observed. In our previous studies, evolution of pinhole population was clearly noticed after the heating of the cobalt/alumina (2nm) bi-layer system. This event is strongly associated with the poor facture toughness of insulating film. Due to this reason insulating layer (underlying metallic layer) fragmented (deformed plastically) under tensile stress, producing pinholes of various shapes and sizes.[184]

To verify the role of pinholes, only a bi-layer of Ta/TaOx on Si wafer was studied; avoiding top layer deposition permits direct observation of morphological changes on a TaOx layer by the AFM. In the case of the Ta/TaOx system, surface roughness increased 8-10 folds after a heat treatment at 360 K for 5 min, figure 5.7, which is consistent with the creation of pinholes on the barrier layer discussed in chapter 2. The TJs affected with pinholes generally showed a 0.8-1.2V breakdown voltage, and in many cases failed within 2-4 days on their own, presumably due to the aggravating pinhole effects. Such TJs also exhibited a 0-50mV open circuit voltage or nil photovoltaic effect.

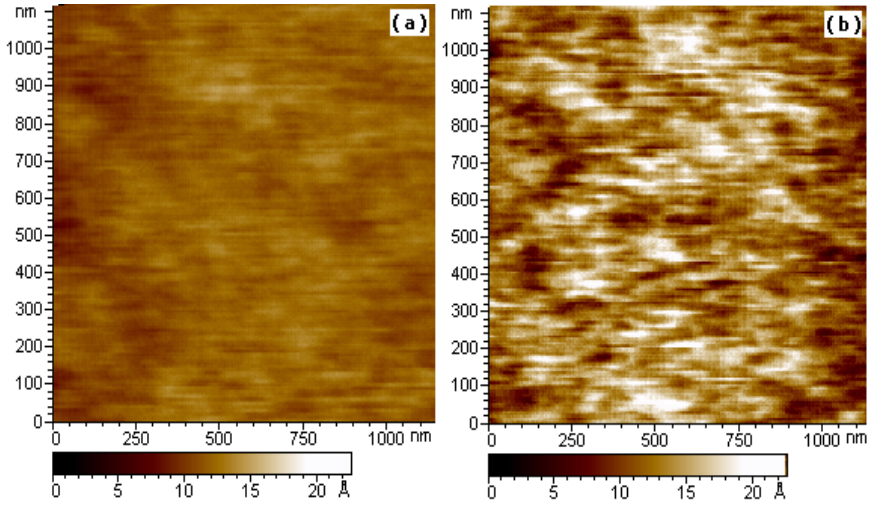

Figure 5.7: Surface morphology of Ta/TaOx bi layer before (a) and after heating (b) at 360 K for 5min.

5.4 Conclusion

In summary, graded density of atomic defects, presumably Ta+, produced an asymmetric barrier with quantum well type defect levels. Graded density of defects produced net inbuilt electric field Vo yield a photovoltaic effect on Ta/TaOx/Ta tunnel junctions. These tunnel junctions showed high vulnerability towards temperature variation and exposure to the intense light which appeared to produce pinhole type defects causing barrier failure. Ultrathin TaOx based tunnel junctions are promising candidate for producing economical solar cells. Present system is likely to be better suited for extracting energy from low intensity radiation. Variety of substrate can be utilized to produce TaOx based photocells. However, application of such system would need significant work to improve the stability and reliability. Cheaper thin film solar cells are feasible with other analogues systems with higher stability. The asymmetric doping of thicker tunnel barrier may be performed to enhance the photovoltaic effect.

Content of the present chapter also serves as an excellent control experiment for the spin dependent photo-effect we observed on magnetic molecule treated multilayer edge molecular electrodes (MEME), details in chapter 7.

Chapter 6

Molecular Cluster Induced Antiferromagnetic Coupling between Two Ferromagnetic Electrodes

6.1 Introduction:

The possibility of producing faster and energy efficient logic and non-volatile memory devices[26] using spin of an electron, spin based devices have attracted enormous interest. Magnetic tunnel junctions (MTJ) with a multilayer of ferromagnet-insulator-ferromagnet structures are one of the most promising categories of spin devices.[18] Performance of a magnetic tunnel junctions critically depends upon the magnitude of ferromagnet/insulator interfaces[18] possessing complex electronic properties and dangling bonds.[17] Ferromagnet/insulator interfaces are expected to contribute for ~90% of spin scattering in a spin valve.[18] Moreover, reproducible production of absolutely defect free insulator with angstrom scale precision over thickness, even with a state of art film deposition system is a daunting task.[17] Interestingly, it was found that change in insulating material in MTJ from alumina to magnesium oxide improved the magneto resistance ratio from ~50% to 600% with improved interlayer coupling.[18]

Organic molecules are endowed with small hyperfine splitting and spin orbit coupling as compared to insulators and semiconductors.[26] There is several advantages of using molecules in spin valve devices. Molecule length can be easily reproduced with an angstrom scale precision and molecule can be easily functionalized to chemically bond with desired metal.[9] These factors make the molecule a strong contender of conventional insulating materials.[20] Previous attempts for utilizing alkane molecule as an insulator between two Ni ferromagnetic nanowire electrodes in a nanopore geometry did not demonstrate performance advantages over conventional magnetic tunnel junctions.[16] Devices where molecules are directly sandwiched between two metallic layers are likely to be affected by impurities,[95] mechanical deformations,[35] large deviations in transport characteristics[185] and have no intrinsic molecular spin-states as transition metal complexes often do**.**

In another study with Ni break junction utilizing C_{60} molecule, a surprisingly strong exchange coupling was observed between two Ni electrodes via C_{60} molecule.[13] C_{60} molecule was believed to be in low spin state (s=1/2). High spin state molecules,[3,33] exhibiting novel transport phenomenon in a gold break junction based study,[33] are expected to produce novel transport features and magnetic couplings when employed between ferromagnetic electrodes.[14] The magnetic characterization is challenging due to fragility and irreproducibility of molecular

devices. [90] Moreover, it is difficult to use ferromagnetic electrodes in present molecular device designs.

We have recently developed a Multilayer Edge Molecular Electrodes (MEME) for forming molecular contacts between metal thin films. MEME is essentially an exposed edge tunnel junction with an insulator thickness close to the dimension of conducting molecular complexes. Thiol-functionalized metal clusters are bridged between two metal electrodes along the exposed edges forming molecular electron conduction channels.[40] The key advantage is the freedom to choose virtually any metal as an electrode, including ferromagnetic metals. Molecular dimension inter-electrode separation is set by the robust insulator,[33] which also minimizes the effect of foreign impurities and works as a diffusion barrier. Importantly, we are able to characterize the conduction of the device before and after attachment of the molecules, which is a critical control experiment and accurately measures molecular conduction through the system.

A particularly intriguing hypothesis is whether the spin-state of a molecule can affect the spin state of the metallic leads. The geometry of the molecule spanning the electrode gap can allow the exchange of spin specific electrons mediated by well defined molecular electronic states of transition metals in the clusters. Isolated dots of Ferromagnetic Multilayer Edge Molecular Electrodes (FMEME) can be magnetically characterized before and after the bridging of high spin molecular complexes. Here we present the experimental results along with a number of control studies to demonstrate the effectiveness of high spin state molecule in modifying the magnetic coupling between two ferromagnetic electrodes of a FMEME. When we used the organometallic complex[3] with (S=6) spin state as a molecular coupler, the magnetic coupling strength between two electrodes of FMEME increased dramatically to 20 ergs/cm^2. The extent of molecule induced coupling is so strong that signature of original ferromagnetic films vanished at RT even with applied fields as high as 3 Tesla.

6.2 Experimental details:

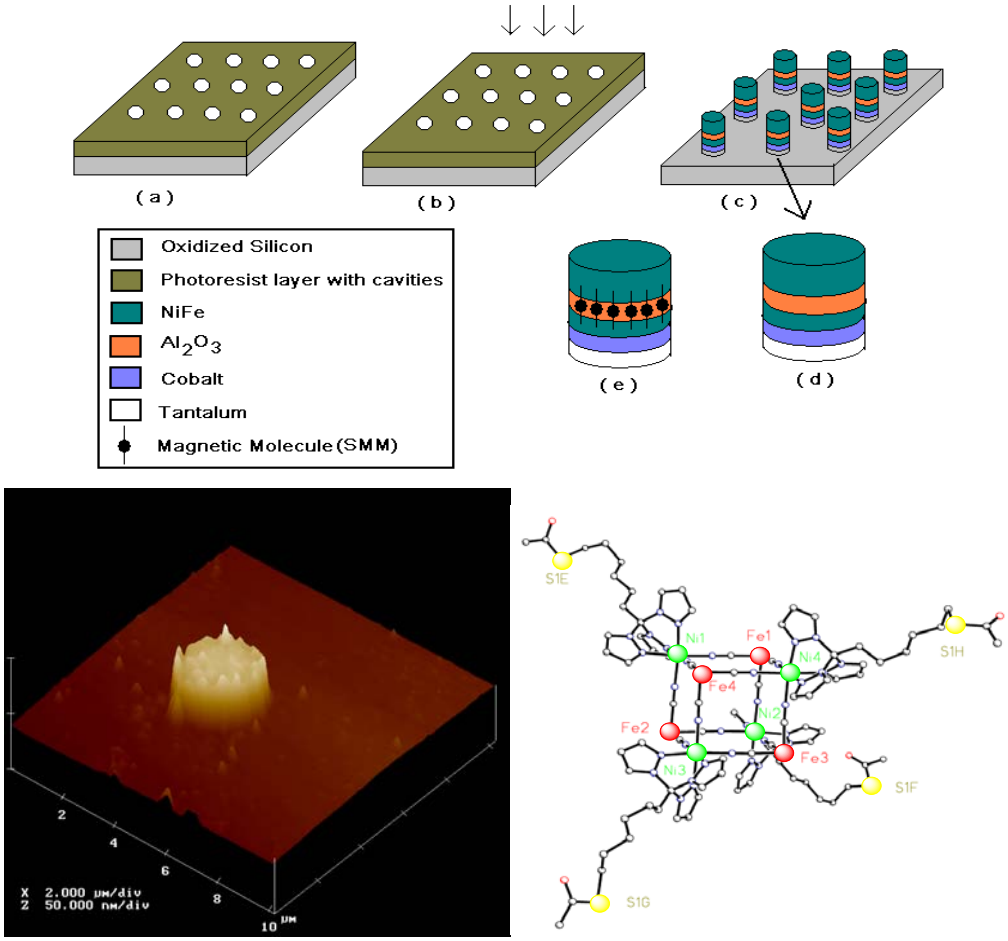

Figure 6.1: Schematic of fabrication steps for FMEME (a) photolithographically define dot array in photoresist. (b) Deposition of Ta/Co/NiFe/Al_2O_3/NiFe multilayer thin film dot, (c) liftoff to reveal pattern with exposed edges; Ta is seed layer and Co/NiFe layer is magnetically harder than NiFe. (d) Idealized multilayer electrode dots before and (e) after treatment with molecular complex. (f) 3D AFM image of a FMEME dot and (g) simplified crystal structure organometallic molecular complex.[3]

Approximately 7000 to 21000 FMEME dots were grown on thermally oxidized Si wafers to attain the detectable signal intensity during magnetization studies. FMEME dots were prepared by depositing all the films (Ta, Co, NiFe, Al_2O_3, NiFe) into a single photo resist cavity to form Ta[5nm]/Co[5nm]/NiFe[5nm]/AlOx[2nm]/NiFe[12nm] samples followed by liftoff to produce the exposed side edges. Details of photolithography, deposition steps for alumina and top and electrodes, and molecule attachment have been published elsewhere.[40] Each dot was of ~3µm diameter and dot to dot separation was 3-5µm.

Following scheme of molecule attachment was adopted to bridge the molecules on FMEME dots. A ~2.5nm long organometallic cluster (OMC) with thioacetate terminated tethers was synthesized[3] for attachment across the present electrode design. Through thiol surface attachment to metal leads, an array of OMC, $[(pzTp)Fe^{III}(CN)_3]_4[Ni^{II}(L)]_4[O_3SCF_3]_4$ [(pzTp) = tetra(pyrazol-1-yl)borate; L = 1-S(acetyl)tris(pyrazolyl)decane], were covalently linked to top and bottom electrodes to span the edge of the insulator film to form a dominant conduction pathway.[116] This molecule essentially comprises a cube of 8 edges of cyanide bridged Ni and Fe atoms (-Ni-N≡C-Fe-). There are four 10 carbon alkane tethers connected to Ni atoms of the molecule's cube at one end and to the metal electrode, with thio-acetate group, on another end.[3] The thioacetate group is a protecting group to preclude thiol reactions during the formation of an octametalic core. This thiolacetate group is readily removed during an electrochemical molecule attachment process[117] on the device to form thiol-Ni surface bonds. To attach the molecule to electrodes, a 2mM solution of OMC in dichloromethane (CH_2Cl_2) solvent was subjected to the alternating ±100mV biasing between two metal electrodes with a time interval of 0.02 seconds for a period of 2 minutes. After the molecule attachment process samples were rinsed with CH_2Cl_2, iso-propyl alcohol and DI water (18Mohm), the samples were dried.

We prepared twelve FMEME dot samples with (Ta/Co/NiFe/AlOx(2nm)/NiFe) dots in different batches. How successful molecule effect is in changing the magnetic coupling between two FM electrodes of a dot was justified by the FMR study. Twelve FMEME samples were prepared in this study. Out of twelve samples eight samples were of good quality, while four samples showed quite erratic magnetic behavior. After the treatment of magnetic molecular complex[3] three samples showed dramatic effects; conventional ferromagnetic film signals disappearing beyond the detection limit. Out of other four partially successful samples, two samples showed ~80% decrease in FMR signal intensity while rest of the two samples showed ~25% decrease in FMR signal intensity. Two samples showed negligible effect of molecular complex. Three samples in bare state itself behaved erratically, presumably due to imperfections in insulating barrier. Besides the samples of primary composition (Ta/Co/NiFe/AlOx(2nm)/NiFe), a number of other samples with different film compositions were prepared to perform control experiments.

It should be noted that our sample fabrication scheme is based on simple photolithography and thin film depositions. Quality of photoresist, photoresist profile, cleanliness of liftoff, thickness and quality of ultrathin alumina are of critical importance in producing tunnel junction dots with exposed side edge and bridgeable insulator thickness. For the sake of consistency, we have extensively studied the two similar samples, FMEME-A and FMEME-B

that showed the strong molecularly induced reorientation of thin film magnetic properties. FMEME-A and FMEME-B both possessed 14,000 dots.

The magnetization study was performed using the Quantum Design MPMS XL 7T superconducting quantum interference device (SQUID) magnetometer. The sample was then mounted on a glass rod with the help of epoxy and introduced into helium gas flushed superconducting coil of SQUID magnetometer. Samples were centered carefully to get the optimum signal intensity. The temperature during magnetization study was kept at 150K. Very low temperature (4K) was observed to damage the tunnel barrier and also made the rotation of magnetic domains in electrodes film difficult. At higher temperature noisy data were a limiting factor.

For ferromagnetic resonance (FMR) study Brucker EMX EPR spectrometer equipped with Brucker Mirowave Bridge ER 041MR and Brucker Power Supply ER 081(90/30) was utilized. Consistently ~9.7GHz microwave frequency and room temperature was used for all the experiments. A magnetic field was applied in the sample plane to study the uniform modes of thin films and multilayers. Application of the magnetic field perpendicular to the sample plane did not produce a promising distinct signal for the study of molecule effect. Before every sample cavity's spectra was checked for the background signal at 5 fold higher gain than that used for the main samples. FMR spectra of a sample did not change noticeably within the ±10º variation with respect to the magnetic field direction.

Magnetic force microscope (MFM) studies were performed using Digital instrument's multimode AFM. Highly sensitive MFM tips (supplied by Nanosensors) with the following specifications were utilized: type PPP-MFMR, tip side Cobalt coated, force constant: 0.5-9.5N/m, resonance frequency 45-115 kHz. During MFM scans the gap between tip and substrate was 10-150nm. For the high resolution and uninterrupted MFM study 100nm tip sample gap was maintained.

6.3 Results and discussion:

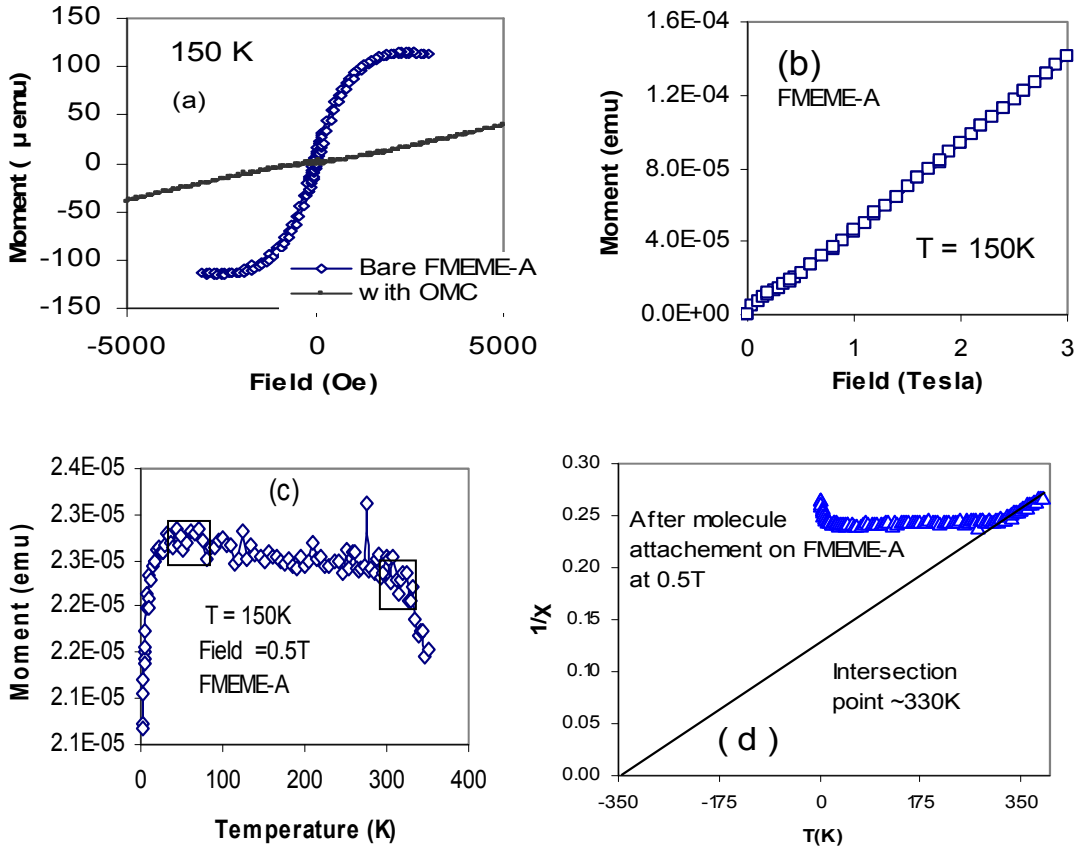

Figure 6.2: (a) Magnetization study of FMEME-A dots before and after the attachment of magnetic molecular complex. Figure (b) is magnetization of the same sample (with molecule) up to 3T at T=150K. (b) Inverse of magnetic susceptibility vs. temperature curve for the molecule treated sample used in study (a). (c) Magnetic moment vs. Temperature study on FMEME-A under 5000 Oe inplane magnetic field.

Magnetization studies were performed to elucidate the effect of molecular complex on the FMEME dots. A magnetic field was applied in the sample plane and at 150K. FMEME-A dots exhibited weak antiferromagnetic coupling via ~2nm alumina insulator and exhibited a saturation magnetization value of ~1.0×10^{-4} emu at 0.2T. The FMR study, mentioned later in this dissertation, confirms the nature of coupling to be antiferromagnetic. A little higher coercive field for magnetic dots, as compared to unpatterned structures (Fe/MgO/Fe), is expected to arise from the shape anisotropy and inter-dot dipolar interactions.[186]

Within 20 minutes of the molecular bridging on the exposed sides of dots the magnetization study were performed in the identical conditions as used for the bare sample. After cluster addition, a dramatic drop (~90%) in the magnetic moment and the appearance of linear magnetization behavior was observed, figure 6.2(a). Interestingly, magnetic moment of FMEME-A dots after molecule attachment did not saturate up to 3T magnetic field, figure 6.2(b), and even slightly surpassed the saturation magnetic moment value for the bare sample at ~0.2 T. A linear magnetization curve implies that cumulative magnetic response is either paramagnetic or antiferromagnetic. We surmised that if ferromagnetic electrodes of FMEMEs are antiferromagnetically coupled via molecular channels then a transition in magnetic moment vs. temperature study should appear.[187] We have plotted the inverse of magnetic susceptibility vs. temperature to determine the nature and magnitude of coupling via molecule, figure 6.2(d). Tangent on the part of curve which appear after the transition intersect temperature axis at -330K[187] (Neel temperature); according to Curie-Weiss law this intersection on negative temperature axis indicates the presence of strong antiferromagnetic coupling associated with the ensembles of molecule treated FMEMEs.

Another control sample molecule treated FMEME-B, which also showed linear magnetization vs. magnetic field curve, exhibited -310K Neel temperature; hence showing consistent behavior with molecule treated FMEME-A. We argue that observed transition and antiferromagnetic coupling is associated with the molecule induced strong antiferromagnetic coupling between NiFe and Co/NiFe ferromagnetic electrodes. However, we should address a plausible experimental concern that the samples could be inadvertently oxidized and render an antiferromagnetic oxide. Nearly 75% of the ferromagnetic metal on FMEME is NiFe. NiFe is known to be stable in atmospheric condition until sample is heated beyond 250ºC.[114] The possible antiferromagnetic oxides of NiFe are NiO and FeO possessing 570K and 1000K Neel temperature, respectively [187]. In a typical FMEME, Co is covered by NiFe and only exposed to the oxidative atmosphere through 5nm thick sides. The ratio of exposed area Co to protected planar area is ~0.001; cobalt oxide has a 320K Neel temperature[187] but cannot dominate the magnetic property of the whole FMEME stack.

In a control experiment, discussed later in this thesis, a purposefully oxidized FMEME dot did not markedly change the magnetic response. It is noteworthy that a decrease in magnetic moment for ~0.2T field (saturation field for the bare sample) is consistent with the antiferromagnetic alignment of the top and bottom NiFe layers.[188] From the saturation values of separate thin films (Co/NiFe and NiFe) we anticipate that the difference between ferromagnetic (additive) and antiferromagnetic alignment (subtractive) of the electrodes layers, would afford a ~

92±4% change in the magnetization values. The fact that an application of 3T of field did not switch both ferromagnetic layers to become parallel with the applied field (and reach saturation) is remarkable. The *lower limit* energy of coupling is readily estimated by utilizing the volume of anti-aligned magnetic film, moment (M_a) and applied field(H_{appl}) from the following expression:

$$E = 2.V.M_a.H_{appl} \tag{6.1}$$

Table 6.1: Calculation of energy and values of parameters utilized in calculation.

Parameters	**Values**
Magnetization of soft film(Ma)	1.2×10^{5} A/m
Thickness of soft film (ta)	1.0×10^{-8} m
Applied saturation field (Happ)	3T
FMEME dot diameter	3.0×10^{-6}m
Area	7.1×10^{-12}m^2
Volume/dot	2.0×10^{-19} m^3
No. of molecules	1.0×10^{4}
Antiferromagnetic coupling energy	1.5×10^{-13}J or 1.5×10^{-6}ergs
Energy per unit junction area	21.87 ergs/cm^2
Energy per molecule (in Jules)	1.5×10^{-17} J/molecule
Energy per molecule (in eV)	97.0 eV

It was seen that the energy/dot is on the order of micro-ergs which translates to ~20 ergs/cm^2 , when using the planar area of the electrode. This is an unprecedented value compared to the previously large value of ~0.8erg/cm^2 coupling energy between two ferromagnetic electrodes with impurity assisted defects.[95] In our case, strongly coupled molecules play the role of well defined and controllable impurities. If we use a more stringent coupling area of just the electrode edge where the molecules are (10um x 1nm) the coupling energy becomes a dramatic 16,000 erg/cm^2 corresponding to 97eV per molecule. Clearly at these unreasonable energies, the coupling must be distributed over a large number of ferromagnetic atoms. The following chapter discusses the high degree of spin polarization in the metallic leads and the role of molecular spin-state in electron conduction/filtering.

The value of 20ergs/cm^2 is also consistent with extrapolation from observed shifts in spin-flipping in the literature. According to an experimental study,[186] nearly 50 Oe shift in magnetization loop of soft magnetic layer of a tunnel junction corresponded to ~0.25erg/cm^2. Linear relation between shift in saturation field and antiferromagnetic coupling of a MTJ suggests that for a 3T shift in saturation field antiferromagnetic coupling has to be 30erg/cm.^{2} In another study, a magnetic ferromagnet/nonmagnet/ferromagnet system with 1.54erg/cm^2 antiferromagnetic coupling was calculated to saturate ~0.5 T.[189] Assuming a linear relation between coupling energy and saturation field and nominal effect of film thickness, we find that lower bound of molecule induced antiferromagnetic coupling strength is ~9 erg/cm^2. It is worth noting that molecule induced coupling is nearly 1-2 orders higher than the maximum antiferromagnetic exchange coupling seen with ~0.5 nm thick MgO insulator.[186] Bare FMEME, with 2nm thick barrier, is expected to have coupling energy several orders smaller than 1x10^{-3} erg/cm,^{2} energy for the 0.8nm thick insulator.[95]

For most hard/soft thin film systems, the B-H response shows a sharp transition as the soft layer flips as diagrammed in figure 6.4. Coupling typically shifts this to a higher field. In our system we don't see a flat response with sharp transition, but we observe a shallow linear slope. Linear magnetization curves for the system of two ferromagnetic electrodes with antiferromagnetic coupling is feasible when antiferromagnetic coupling strength (J) is significantly greater than the product of the anisotropy constant (K) and film thickness (t) for ferromagnetic films[189]: J>K*t.[189] K is typically ~10^5 erg/cm^3 for Ni and Fe.[187] Assuming a film thickness of 20 nm, we get K*t = ~0.2erg/cm^2 far below the estimated 20 erg/cm.^{2} A linear B-H response is seen in figure 6.2(b).

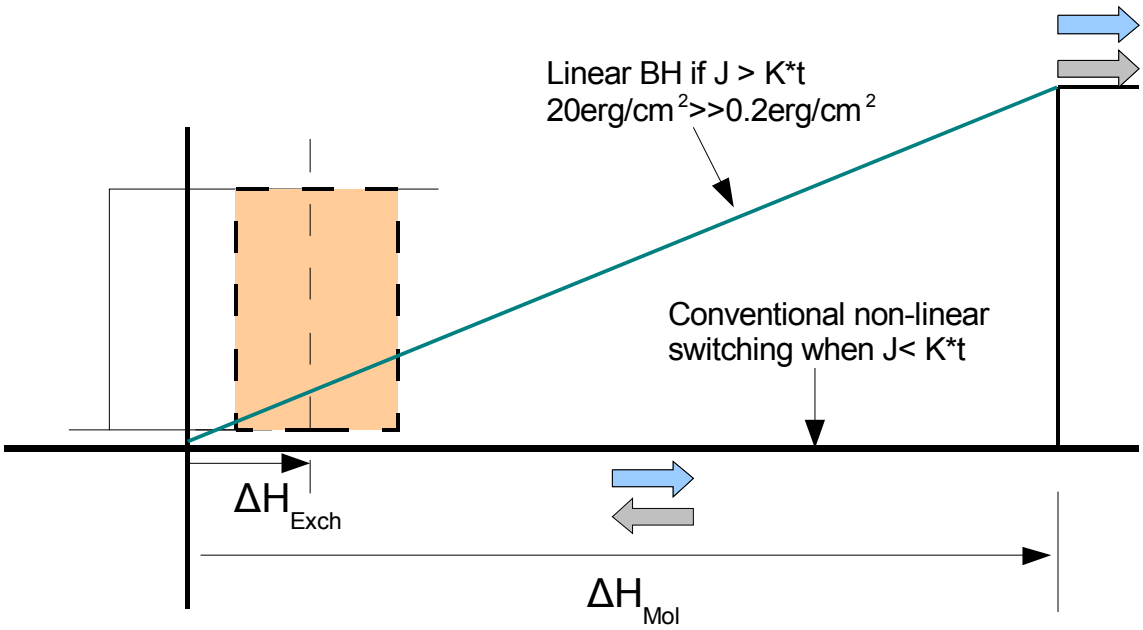

Figure 6.3: Exchange energy induced shift in magnetization loop of an electrode. ΔH_{Exch} offset is the effect of reducing MgO thin film thickness and ΔH_{Mol} is offset due to the molecular couplers.

In the control experiments unpatterned NiFe(top) and Ta/Co/NiFe (bottom) electrodes treated with molecular complex did not show dramatic change in the magnetization curve of two electrodes. Tunnel junction dots where one electrode was ferromagnetic and the other nonmagnetic after molecule bridging between two electrodes did not produce any dramatic change in the magnetization study as observed with Ta/Co/NiFe/AlOx/NiFe multilayer dots. Control experiments insinuate that one needs magnetic layers of dissimilar hardness at the molecular dimension gap to observe the effects of molecular couplers.

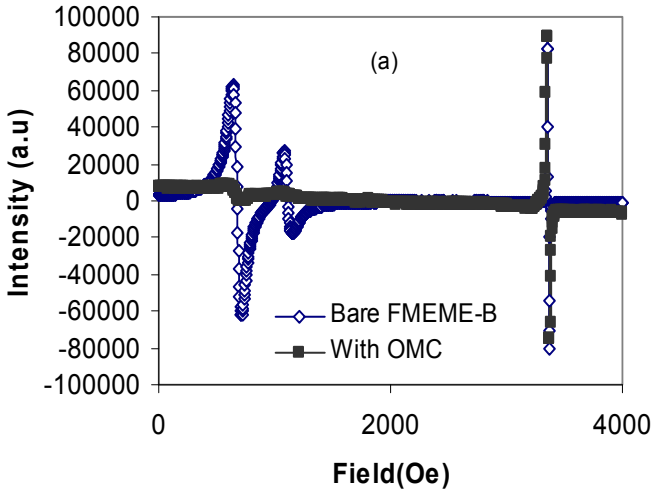
(a)
Intensity (a.u)
Field(Oe)
Bare FMEME-B
With OMC

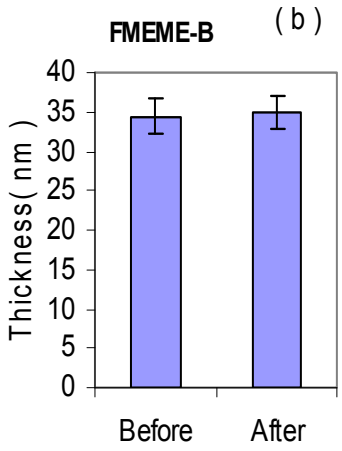
FMEME-B
(b)
Thickness(nm)
Before
After

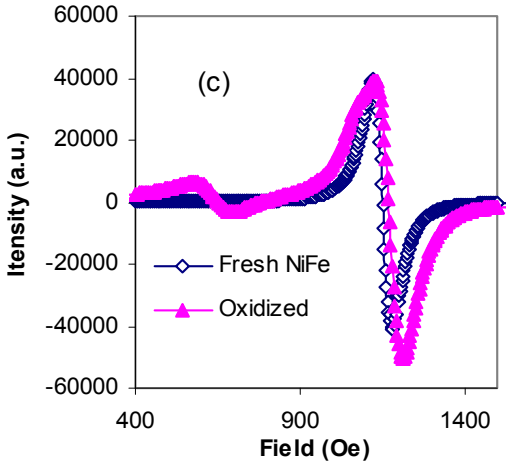
(c)
Itensity (a.u.)
Field (Oe)
Fresh NiFe
Oxidized

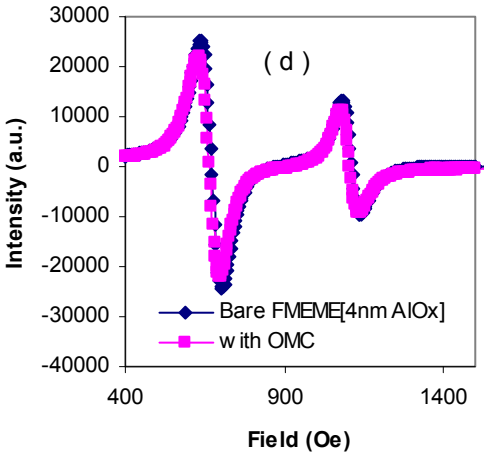
(d)
Intensity (a.u.)
Field (Oe)
Bare FMEME[4nm AlOx]
with OMC

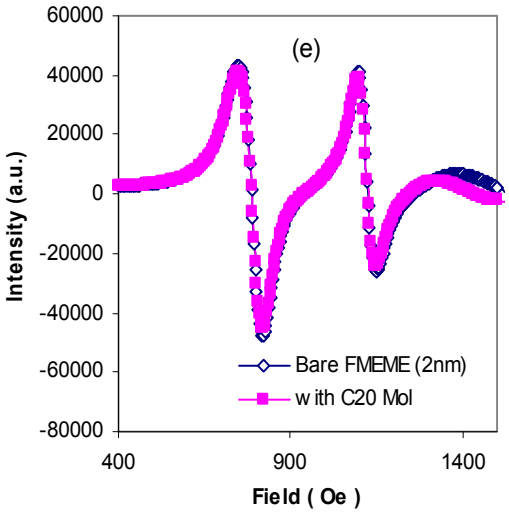
(e)
Intensity (a.u.)
Field (Oe)
Bare FMEME (2nm)
with C20 Mol

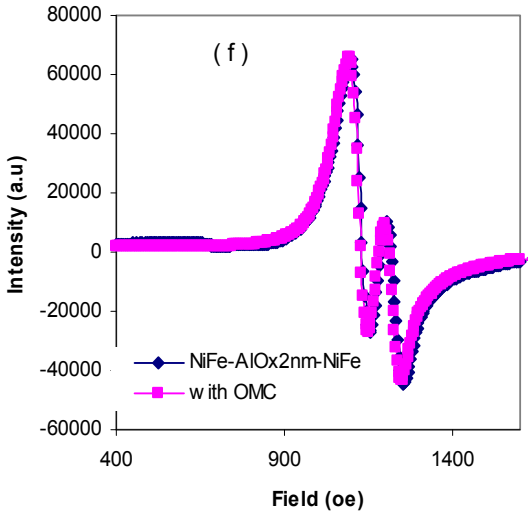
(f)
Intensity (a.u)
Field (oe)
NiFe-AlOx2nm-NiFe
with OMC

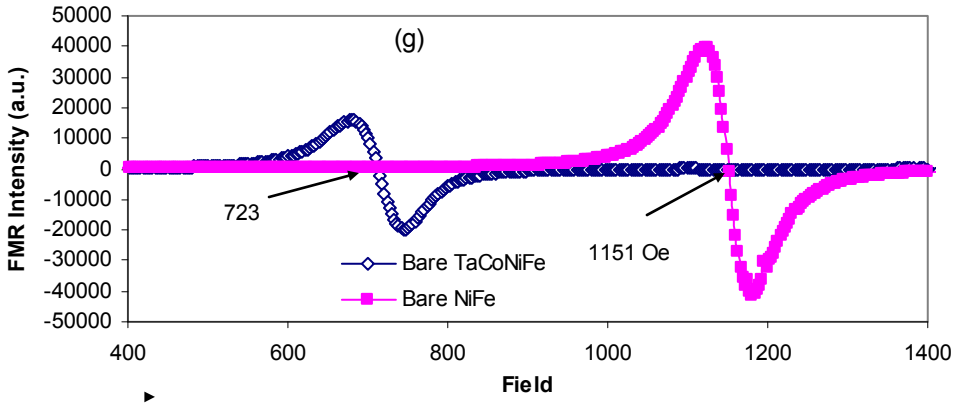

Figure 6.4: (a) FMR of a FMEME-B after treatment with molecular complex showed almost complete disappearance of uniform modes. (b) AFM thickness measurement before and after molecule treatment of the sample of which data is presented in (a). (c) FMEME with 4nm thick alumina remained indifferent towards molecule treatment due to molecule inability to bridge the gap. (d) Dithiol Eicosane molecule did not produce any significant change in FMR spectra of 2nm thick FMEME dot pattern. (e) Oxidation of 10nm thick NiFe did not make signal disappear. (f) NiFe/AlOx/NiFe response to OMC and (g) Peaks of bare NiFe and Ta/Co/NiFe films.

We have also performed FMR studies on FMEME dots before and after molecular treatment to complement magnetization studies. FMEME dots exhibited two clear modes, acoustic mode (peak with higher intensity) at ~670 Oe and optical mode (peak with smaller intensity) at 1120 Oe. The location of optical mode after the acoustic mode imply an antiferromagnetic coupling [190] between two ferromagnetic layers via ~2nm thick insulator, figure 6.4(a). Comparison of the mode position of FMEME dot sample, designated as FMEME-B, with the resonance mode position of individual ferromagnetic layers, studied in identical conditions, revealed following information. Acoustic mode (optical mode) was close to the mode position of NiFe(TaCoNiFe) layer; the difference between acoustic mode(optical mode) position and isolated NiFe(TaCoNiFe) mode position was 40-70(30-50)Oe.

Surprisingly, bridging of molecular complex between two ferromagnetic layers of FMEME dots, with previously used procedure,[40] yielded the disappearance of the two modes. FMR study of the molecule-treated FMEME-A dot sample, on which magnetization studies were performed, also showed complete disappearance of the modes; consistent with the study shown in figure 6.3(a).

Theoretically, it was calculated that such mode disappearance is only possible when antiferromagnetic coupling strength between two ferromagnetic layers cross a critical limit; in this case spin flip occurs. Two ferromagnetic layers in such case behave like one unless the applied magnetic field is of the order of strong antiferromagnetic coupling energy.[191] To make sure that severe damage to the sample (i.e. complete etching of magnetic dots) is not the reason for the FMR signal disappearance, the thickness of dots were monitored before and after molecular treatment. Thickness measurement by the AFM showed unnoticeable statistical difference in the heights of dots. More than 140 dots at near corners and in the central parts were studied to give the statistical heights distribution before and after molecule attachment figure 6.4(b). The similar thickness of FMEME dots before and after molecule treatment insinuates that both etching and significant oxidation (volume expansion) did not occur. High magnification optical microscopy with polarized light could be used for the confirmation of sample integrity. SEM and AFM were also performed on selected samples in agreement with optical microscopy. In some cases a small population of dots (5-10%) underwent partial to complete damage during electrochemical treatment. Electrochemical damage is the topic of appendix A2 of this thesis. FMR study of such samples did not exhibit more than 10% change in signal intensity due to molecule treatment that induced observable damage.

To check the possibility that unnoticed oxidation of dots produced antiferromagnetic oxides, e.g. NiO and FeO, thus leading to the disappearance of FMR modes NiFe ferromagnetic electrode were purposefully plasma oxidized to revealed the distinct and expected mode of bulk ferromagnet. Hence surface oxides can not be the reason for the FMR mode disappearance. After plasma oxidation of NiFe and additional resonance peak at 800 Oe, figure 6.4(c). We attribute this addition peak to the oxidized NiFe enabling near surface NiFe to behave differently than the intact NiFe.

Central to the primary hypothesis is that the molecule spanning the electrode gap is responsible for the coupling between layers. The molecules simply residing on the surface (not spanning between two films) would not induce coupling. Individual ferromagnetic layer, as used in a typical FMEME dot, were given the same molecular treatment from the same molecular solution, as used for the FMEME dots. The FMR study showed no shift in mode position or any dramatic reduction in the mode intensity after molecular treatment. A number of other control experiments were performed to validate our hypothesis that only magnetic molecular bridges on the exposed edges of FMEME dots are producing extremely strong antiferromagnetic coupling. If the insulator layer thickness of FMEME dots is more than the molecule length, then the molecule can not bridge the gap and hence no change in FMR signal due to molecule treatment will result.

We indeed observed that FMEME dots prepared with 4nm thick alumina barrier did not show any significant change in FMR signal after magnetic molecule treatment, figure 6.4(d). A smaller overlap of two modes of FMEME dots with 4nm thick barrier confirms that we indeed used a thicker barrier in this study; the thinner the barrier, the more the overlap. To answer this question we bridged the dithiol-eicosane molecule a 20 carbon alkane molecule without transition metal core) on the FMEME dots with ~2nm alumina thickness. FMR signal did not show noticeable change due to alkane molecule treatment, figure 6.4(e).

Another test of the hypothesis is to change the composition of the electrode metal to be dimagnetic or symmetric soft ferromagnetics. NiFe/AlOx/Au and NiFe/Al_2O_3/NiFe were studied before and after magnetic molecule treatment. No dramatic change in FMR signal was observed after the attachment of the molecular complex to bridge the two metals. In the case of diamagnetic gold antiferromagnetic coupling is not possible and the ferromagnetic layer behaves normally. In the case of NiFe/AlOx(2nm)/NiFe, shown in figure 6.4(e), no dominate hard layer is present (i.e. Co) to initiate ordering. Due to the similar magnetic properties of the NiFe layers, two modes of bare sample are not very distinct as is in the Co/NiFe/Al2O3/NiFe samples.

From the experimental efforts presented thus far we conclude that strong antiferromagnetic coupling is specific to the magnetic molecular complex (organometallic complex) and FMEME dots with Co/NiFe and NiFe ferromagnetic electrodes. Magnetic moment per atom for Co(5nm)/NiFe(5nm) and NiFe 10nm are ~1.95μ_B and ~2.2μ_B ,respectively.[192] Moreover, magnetic properties of NiFe in Co/NiFe are strongly influenced by the Co seed layer[193]. Our FMR study shows the resonance mode at different mode positions for the each electrodes material.

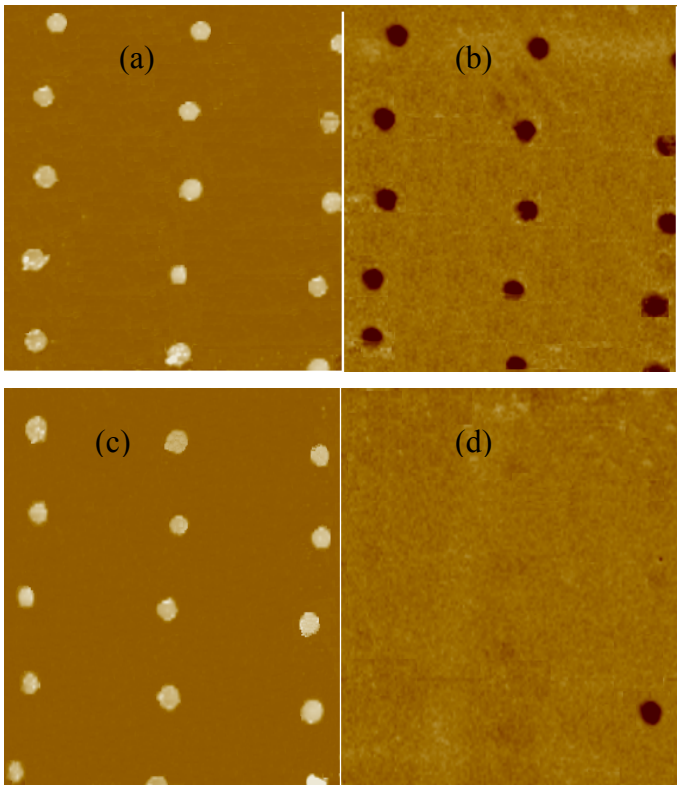

Figure 6.5: Topography (a) and magnetic image (b) of bare FMEME-B. Same sample after the treatment with molecular complex show clear topography (c) but disappearance of magnetic contrast on the majority of the dot positions (d).

Magnetic Force Microscopy can also confirm the spatial location of magnetic moments. Magnetic imaging of FMEME dots were carried with AFM. MFM study presented here is on FMEME-B sample; sample on which FMR study, shown in figure 3(a), before and after molecule attachment was performed. Before molecule attachment FMEME-B dots exhibited unambiguous magnetic images, figure 6.5(b), corresponding to their physical location and dimensions, figure 6.5(a).

After magnetic molecule attachment, most of the dots showed nil to negligible contrast in the magnetic images, figure 6.5(d), consistent with B-H, FMR data of antiferromagnetism. The topography data of the MFM also demonstrated that the dots were not chemically etched/damaged or oxidized. Separation between a Co coated MFM cantilever and the sample was 100nm for both imaging. Fresh MFM cantilever were utilized to avoid the loss of the magnetic signal due to abraded magnetic layer on old tips. The very same MFM cantilever, showing loss of magnetic signal on molecule treated FMEME dots, showed clear magnetic images of identical bare FMEME dot sample in the identical experimental condition, thus is not a

measurement artifact. The fact that we could image a single dot in figure 6.5(d) also demonstrates that MFM was properly tuned for the null result of the other 14 dots in the image frame. Loss of magnetic contrast was observed on ~90% the dots studied by the MFM.

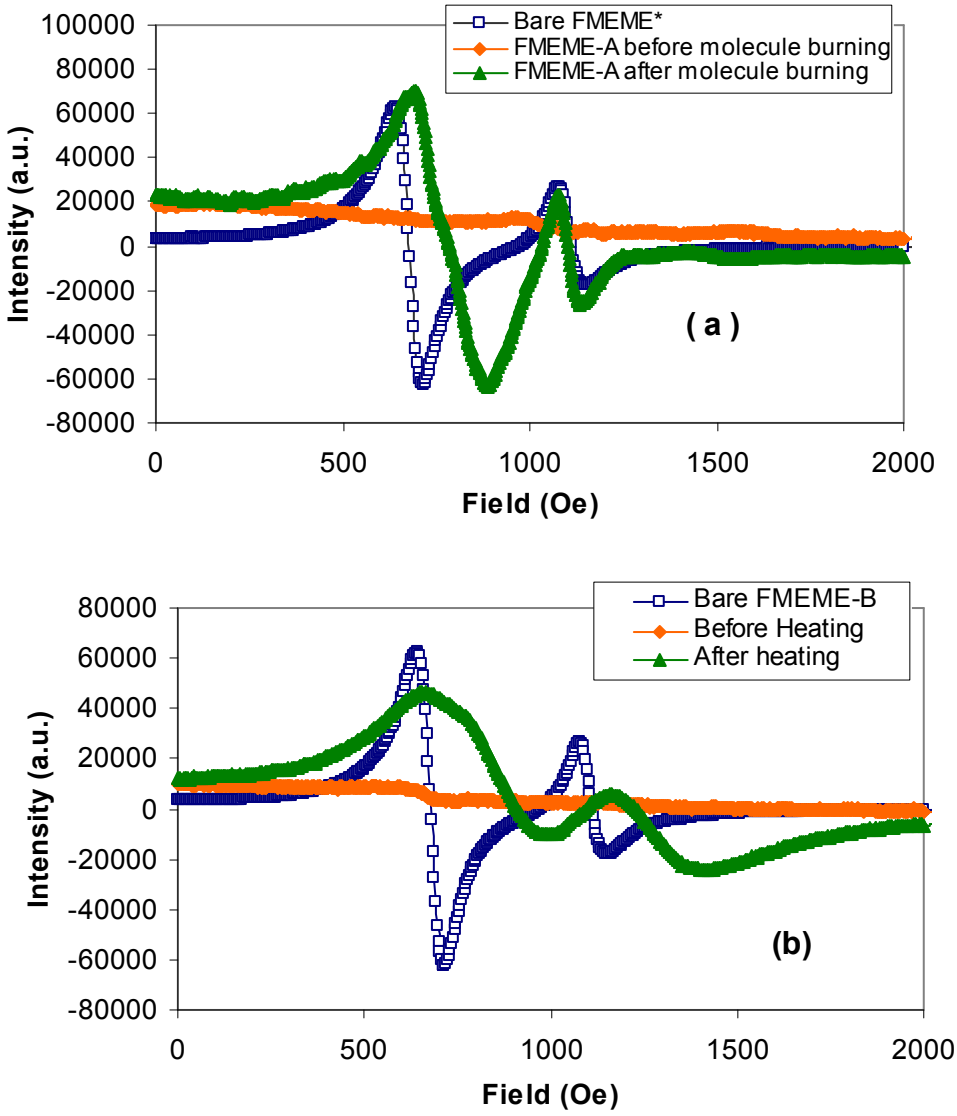

Figure 6.6: (a) FMR spectra of the FMEME-A sample before and after burning of molecules in oxygen plasma, this is the sample on which magnetization studies were performed. FMR of bare state FMR data is from different sample with identical multilayer configuration. (b) FMR spectra of the FMEME-B sample before and after heating to 390K. Note this is the sample on which FMR study showed mode disappearance after molecule attachment.

A ferromagnetic metal posses both majority and minority spin density of states; loss of magnetic contrast at FMEME dot sites at RT indicates evolution of spin bands under the effect of strong magnetic molecular coupling. Two ferromagnetic layers appear to have a significantly higher difference in density of states for the spin up and spin down electrons than 42(45)% for Co(Ni or Fe).[17]

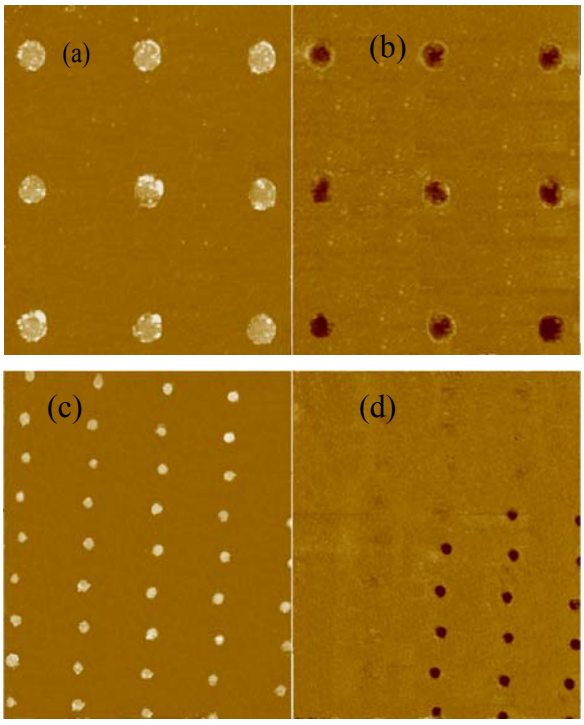

Figure 6.7: (a) Topography and (b) magnetic image of FMEME-A dot sample after the plasma oxidation of previously AF coupled array. (c) Topography and (d) magnetic image of molecule complex treated FMEME-B after heating to damage the dot's tunnel barrier.

A critical control experiment is to show the reversibility of the strong AF ordering. This would demonstrate that the observations of small magnetic signal are not due to sample damage. Two kinds of reversible experiments were performed. In the first reversible approach, molecular bridges were burnt in the oxygen plasma (50W, 60mTorr mixture of 1:1 Ar:O_2 mixture). For this study the same sample FMEME-A on which magnetization and FMR study exhibited dramatic change, was utilized. FMR study after plasma treatment showed the reappearance of unambiguous FMR modes in the spectra, hence proving that the molecule effect is indeed reversible. Importantly, position and shape of the two modes are in agreement with the acoustic and optical modes of a bare FMEME sample, figure 6.6(a). It should be mentioned that we did not perform the FMR study on FMEME-A sample before molecule attachment since it was the object of B-H studies.

We also performed a MFM study and observed clear magnetic images, figure 6.7(b), that commensurate with the topography, figure 6.7(a), of corresponding dots. Thus the ferromagnetic response of the multilayers was restored after the removal of the coupling organometallic complexes. We did observed partial damage to the dots after plasma treatment, mainly near edges of the dots. We attribute these damages to the stress induced flaying of dot material due to the volume expansion inherent with oxidation. This experiment also provides strong support to our argument that the accidental oxidation of the sample at any stage can not make the magnetic mode disappear in FMR study. Oxidation is a diffusive process and will be restricted to surfaces of the dot. Most of the ferromagnetic material is not oxidized and observed in the FMR study, figure 6.6.

Another method to demonstrate the reversibility of the strong AF coupling is to damage the insulating barrier of FMEME dots to allow competing magnetic coupling via high density pinholes and defects[186] or simply short circuit any spin polarization. We have observed that heating induced tensile stresses fragments the ultra-thin alumina layer.[194]

For this study we chose the same sample on which FMR modes magnetic image contrast previously disappeared after the treatment with magnetic molecular complex, sample FMEME-B. The sample was heated at 390K for 30min in flowing helium ambience, to avoid unintentional oxidation. The sample was cooled to room temperature and was subjected to FMR study. FMR spectra of this sample showed clear broad resonance mode; start and end point of mode position is within the combined range of mode positions for the two ferromagnetic layers. We attribute the broadened resonance mode to the emergence of wide range of coupling strength between two ferromagnetic electrodes via defective insulator.[190] The MFM study, figure 6(d-e), showed that FMEME-B sample possessed a sizeable number of dots showing clear magnetic contrast (ferromagnetic). However, large number of dots still showed negligible magnetic contrast (antiferromagnetic) and can be attributed to the significant number of dot insulator barriers surviving the heat treatment.

The ~4 orders increase in magnitude of antiferromagnetic coupling between two ferromagnetic electrodes induced by the transition metal complex is dramatic and unprecedented. When accounting for the small area of molecular contacts, the coupling is many orders of magnitude above previous experimental observation and theoretical prediction. Certainly this report is based on the previously described experimental observations and careful control experiments; however, there is significant importance to discussing the mechanisms of molecular coupling and the plausibility of this remarkable observation. From our previous study of the MEME using the same organometallic molecular cluster (OMC) we found that the conduction

mechanism was primarily 1) tunneling from metal electrode to oranometalic core by tunneling through alkane tether that acts as a tunnel barrier 2) rapid electron transfer within the organometallic Ni-CN-Fe cube and 3) tunneling through alkane tether to the other electrode. Well defined spin-states in the organometallic Ni-CN-Fe cube would determine electron spin-conduction and possibly provide a mechanism for coupling. A relatively small number of molecules at the edge of the junction can affect a large volume of ferromagnetic metal atoms.

Apart from experimental evidence, theoretical study[46] also supports the evolution of strong influence of molecular channels on our tunnel junction with 7μm^2. Theoretical study treating transport via tunneling barrier and atomic impurity on equal footing revealed the following information. A single atomic impurity at 0.75nm distance from the metal electrodes of a 1.5nm thick barrier could dramatically change the spin polarized transport in a magnetic tunnel junction of 0.01μm^2 planar area. Extrapolating this result for 10μm^2 junction area, one would need 10,000 atomic impurities in the center plane of the tunnel barrier; it is a difficult task to control the position of atomic defects for any useful application.

Assuming our molecule plays the role of an atomic impurity, we find that the ~10,000 molecules we are attaching via alkane tethers is a sufficient number, in the light of theoretical calculation, for the 10μm^2 junction area. A molecular core, ~0.7nm wide, is 1.2 nm away from the metallic electrode; a similar gap was used in the theoretical calculation. It is noteworthy that unlike impurities we are able to control the position, i.e. around the center of the insulating barrier, of the molecular core with the help of alkane tethers. Alkane tethers possess smaller barrier height than that of alumina barrier; charge exchange via molecular channels is expected to be significantly better than alumina or any other inorganic insulating barrier. Since our molecules are placed outside the tunneling barrier, we have the distinct advantage of comparing the effect of molecules with that of a good quality tunnel barrier. Exchange coupling of magnetic tunnel junction is effectively described by the Slonczewski's model, with following expression.[186]

$$J = \frac{\varphi_B k^3 (k^2 - k_\uparrow k_\downarrow)(k_\downarrow - k_\downarrow)^2 (k_\downarrow + k_\uparrow)}{\pi^2 d^2 (k^2 + k_\uparrow^2)^2 (k^2 + k_\downarrow^2)^2} e^{-2k.d} \qquad (6.2)$$

Here, d and φ_B are the barrier thickness and barrier height, respectively, of the insulating medium between two spin polarized electrodes, whereas, $k_\downarrow$ and $k_\uparrow$, are the wave vectors of the spin down and spin up electrons of the ferromagnetic layers. The wave vector of an electron in the insulating regime is k and is given by a relation, $k=\sqrt{(2.\varphi_B.m.\hbar^{-2})}$. Here, m is the effective mass of the electron and ħ is Planck's constant.

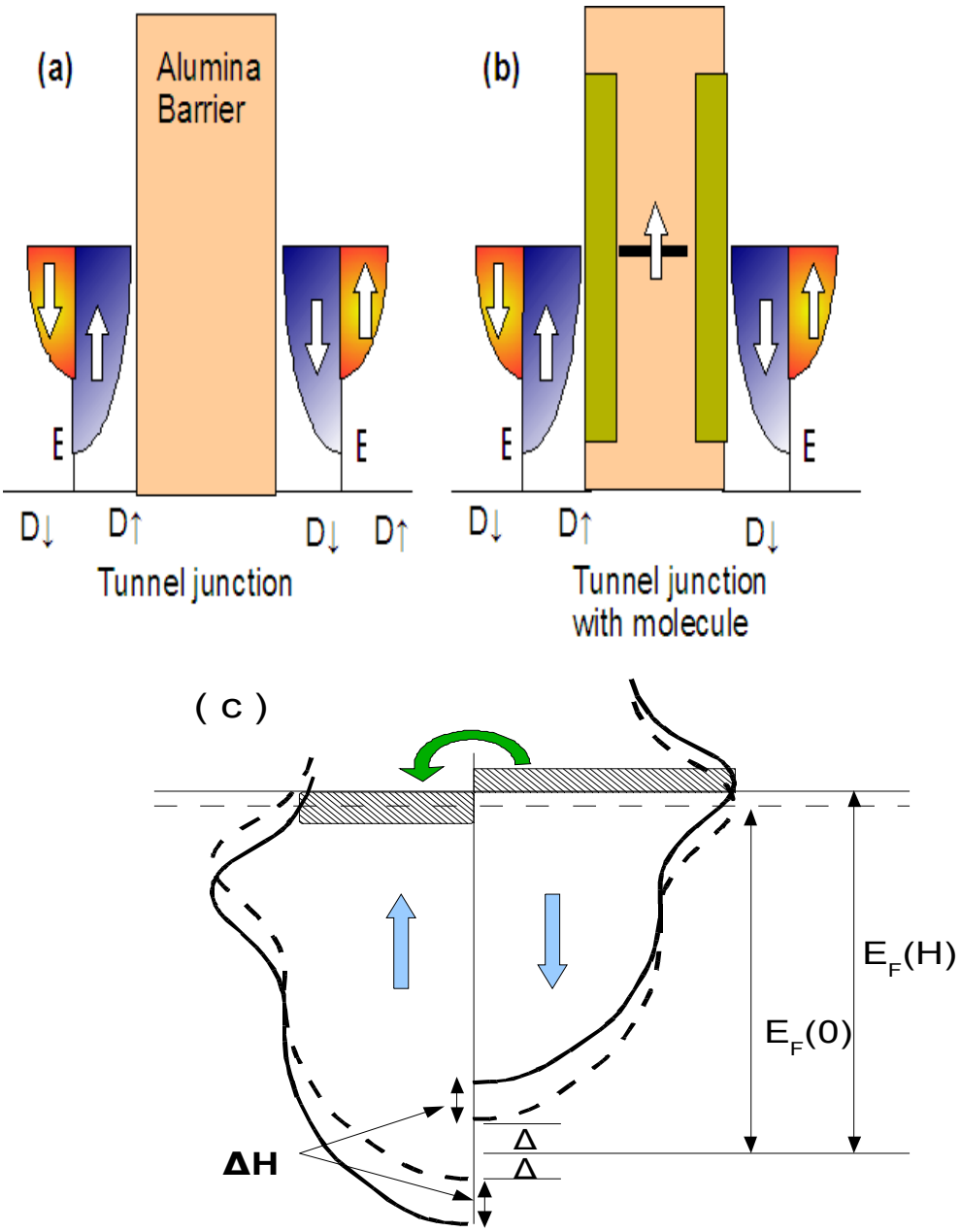

Figure 6.8: (a) Band diagram of a bare FMEME tunnel junction (b) FMEME with molecular bridges and (c) molecule induced readjustment of spin population in magnetic electrodes.

We assume that molecular complex, which has net spin state, behaves like a spin polarized electrode and hence reduces the effective barrier thickness from 2nm to 1nm(distance between center of the molecule core to the metal electrode edge). From eqn1, exchange coupling expression can be simplified to $J\sim(1/d^2).\exp(-2k.d)$.[186] Assuming the barrier height of 1eV, it is easy to see reduction in barrier thickness from 2nm to 1nm produces 5 orders stronger exchange coupling strength. Moreover, the coupling energy between two metal electrodes changes monotonically with thickness.[186] This simple calculation can be applied to exchange coupling due to atomic defects within tunnel barrier.[95] It was found that an impurity level present around the center of tunnel barrier and providing local density of states close to the metal electrode's Fermi level increased coupling strength by up to ~3 orders.[95] It is worth noticing that in our case, molecules also provide local density of states around the center of the tunnel barrier as confirmed by the molecular transport study for the same molecular complex in the MEME geometry.[40]

There are few major points to justify why the molecular complex in the present case produce an extremely strong antiferromagnetic exchange coupling. It is well established that molecular levels overlap with a continuum of metallic levels to undergo broadening;[55] broadening significantly increase the charge transport rate to and from the molecular levels.[35] Increased probability of exchange of charge via molecular channels is expected to significantly enhance the superexhange type interaction between ferromagnetic electrodes via molecule.[49]

It is worth noting that if molecule possess non-degenerate energy levels for the spin up and spin down electrons then, in addition to enhancing the magnetic coupling molecule can also serve as a spin filter between two spin reservoirs.[195] How a molecule is bonded to the metal electrode can dramatically effects the molecular transport and exotic phenomena.[35] It was found that the cobalt phthalocyanine (CoPc) molecule exhibited ~ 200 K Kondo temperatures when molecule interaction to the Au electrode was changed from physiosorption to covalent type. Moreover, alkane tethers used in our case to covalently bridge the molecule to the metal electrodes are much more effective electron channels than the vacuum gap[37] and a barrier height of only 0.8eV seen.

Exchange coupling via molecule can be tremendous if the spin state of a molecule interacts with the ferromagnetic electrodes. Physio-sorbed C_{60} molecule, in s =1/2 spin state, produced unprecedented coupling strength between two magnetically asymmetric Ni electrodes of a break junction.[13] The strong exchange coupling via molecule was believed to produce ~70T magnetic field in the vicinity of molecular junction. Under the influence of this strong magnetic field, the molecular level produced ~16mV Zeeman splitting.[13] The extent of splitting was proportional to the product of molecule coupling energy with electrodes and spin polarization of

the ferromagnetic electrode. It is worth noticing that huge Kondo splitting at cryogenic temperatures was observed due to one C_{60} molecule and more importantly with microscopic Ni electrodes.[13] The molecule mediated inter-electrode coupling is only expected to be a local effect and which can affect the molecular levels to manifest unprecedented Kondo splitting. Here we argue that in our case we have utilized two ferromagnetic electrodes having the effective area comparable with that reported by Pasupathi et al[13]. In the previous study, ferromagnetic electrodes were made of different hardness using shape anisotropy effect, but in our case we used different compositions. In the present study, the major difference with regards to the work of Pasuppathi et al., is that we covalently (not physio-sorption) attached ~10,000 high spin state magnetic molecular complex; a much stronger effect than that of a single molecule is expected.[97] Moreover, spin transport to and from the molecular complex is to occur via organic alkane molecule dominant spin channels; organic molecules are well known to be more efficient spin channels than other conventional insulators and semiconductors.[27] We are not aware of the exact spin state of our molecule when bridged between two metal electrodes. Our molecular complex exhibited S=6 spin state at 10K and S=3 spin state at 77K in the bulk form.[3] We surmise that after attaching the molecule to two ferromagnetic leads; it will possess a spin state of more than one. In particular, the process of conducting spin selective molecules through a cluster would likely induce spin ordering with the ferromagnetic electrodes. It is noteworthy that molecular charge state that could not be stabilized in free molecules was observed in the vicinity of metallic electrodes.[39] For instance s=1/2 spin state of the vanadium complex, was only observed after placing them between two gold metal electrodes.[39]

Our magnetic studies, especially MFM, strongly suggest a significant change in the density of states of the spins in two ferromagnetic layers. We surmise that molecule induced exchange coupling produced a strong magnetic field that not only split the molecular levels but also acted upon ferromagnetic atoms attached to them or in close proximity. This can induce Zeeman splitting to enhance the splitting between spin up and spin down electron density. This effect in turn can produce a difference in chemical potential under the effect of magnetic field. Spin dependent exchange coupling via molecule is shown to produce an effective magnetic field.[13] In the context of our multi-molecular system where two ferromagnetic electrodes are anti-parallel to each other, for the exchange induced magnetic field (B), the following form can be utilized.[13]

$$B \approx \frac{a\sum_{n=1}^{N}(P_T\Gamma_{nT} - P_B\Gamma_{nB})}{g.\mu_B} \qquad (6.3)$$

Here, N is the total number of molecules bridging the gap between ferromagnetic layers, $P_T(P_B)$ is the degree of spin polarization of the top (bottom) ferromagnetic layer, and Γ_{nT} (Γ_{nB}) is the coupling energy of the n^{th} molecule with the top (bottom) layer. g and μ_B denote the gyromagnetic ratio for the molecule and Bohr magnetron, respectively.

In order to estimate the magnitude of B, we can consider N=10,000, aP is 0.15[92] and $g\mu_B$ ~115μV/T.[31] Generally molecular coupling energy is ~10 meV.[13] Assuming a conservative range for the difference in coupling energy is 0.001-0.01 mV, for this we obtain B in the range of ~100-1000T. In a previous study,[13] the effect of extremely high molecule induced exchange field was clearly observed in the form of unprecedented Kondo level splitting. We surmise that same field/splitting energy also acts on ferromagnetic electrodes in the vicinity of molecular junctions. This produces strong Zeeman splitting which in turn will produce readjustment of spin density of states according to the molecule induced equilibrium. Here we wish to mention explicitly that magnetic field arising from molecule-mediated interlayer exchange coupling is only a local field. We are unable to explain how this local field can affect the spin polarization or stoner splitting of a microscopic magnetic electrode.

In the MFM study, we had an unambiguous signature of dramatic change in spin polarization at individual electrodes due to molecular complexes. We believe that the evolution of highly spin polarized magnetic layers is primarily due to the large Zeeman splitting energy produced by the molecular complexes. According to the calculation of Slonczewski[94], the degree of spin polarization of tunneling electrons depends on the height of the tunneling barrier. With the higher barrier, one recovers the classical expression of spin polarization; but for the small barrier height, spin polarization can be dramatically different.[17,94] A discussion on spin polarization of bare and molecule treated FMEME is furnished in chapter 7.

6.4 Conclusion:

We have found that magnetic molecular channels bridged over the insulator gap on exposed sides of a magnetic tunnel junction strongly influenced the coupling strength between two ferromagnetic electrodes of the host tunnel junction. Dramatic antiferromagnetic coupling energies of at least 20ergs/cm^2 are seen using the entire planar junction area (7um^2). If only the molecular junction area is considered, then the coupling can be 3-orders of magnitude higher. The process is reversible with the removal of molecular coupling and only hard/soft

ferromagnetic electrode systems work. The phenomenon is seen by B-H, FMR and MFM studies. Recent theoretical studies, predicting the strongly correlated states between molecule and ferromagnetic leads[97], and utilizing variational spin density of state of ferromagnetic electrodes strongly coupled to quantum dot, can represent our system.[99] However, the unprecedented magnitude of the coupling (especially if one considers only the molecular junction area) many atoms must be involved with the coupling and the conduction electrons may be an important part of the coupling mechanisms. Molecular spin devices formed by bridging of high spin molecule, with well defined atomic orbitals, on the sides of a magnetic tunnel junction are expected to show dramatic change in spin dependent transport and would likely be the source of or a product of the observed dramatic magnetic coupling.

Chapter 7

Dramatic Current Suppression and Magnetic Ordering Induced By Molecular Junctions

7.1 Introduction:

The reduction of electronic device dimensions to incorporate molecules as the active element allows the utilization of well defined molecular electronic states that can be systematically tuned and exactly reproduced in bulk quantities by synthetic chemistry.[49] In addition to the challenges of integrating reliable electrodes with molecular scale dimensions, the large separation of electronic states requires very large applied bias for electrostatic gating.[143] Thus, it is desirable to examine alternative forms of molecular switching based on optical excitation, chemical coordination (sensing), or magnetic field.[26] Spin electronics (spintronics) involve the manipulation of the spin state of the electron in devices[19,196] that generally results in significant resistance changes with the reorientation of magnetic domains at device junctions. Diamagnetic organic molecules possess weak spin-orbit and hyperfine interactions and consequently exhibit spin coherence lengths and times that are greater than those seen in semiconductors and metals.[19,8] Several molecule-based magnets are reported to exhibit photoinduced magnetic ordering at room temperature,[8] allowing for the design of magneto optical devices. Petrove *et al.* have predicted that in the case of an antiferromagnetically ordered molecular wire, the inter-electrode tunnel current can be regulated via the application of a magnetic field over the wide regions of the 7-8 orders of the current magnitude.[30] For a system of organic molecules and magnetic electrodes, the possibility of realizing a ~700% magneto resistance ratio,[19] and the observation of Berry phase blockade[32] have been theoretically demonstrated. The initial experimental realization of molecular spin devices has been accomplished by inserting molecular metal coordination compounds into the region between the gold break junction electrodes.[103] In such studies, the Coulomb blockade[31] and Kondo effect[31,39] have been observed at low temperature. Interestingly, the transport of the single molecular magnet, with a S=10 spin state, in gold breakjunction was shown to be dependent on the spin ladder states of the molecule; these devices exhibited negative differential current and complete current suppression phenomenon.[33] Nickel ferromagnetic breakjunction with C_{60} molecule revealed a ~16meV Kondo level splitting in negligible magnetic field.[13] Preceding theoretical calculation explained the enormous splitting to be caused by the spin fluctuation-induced molecule-mediated inter-electrode exchange coupling.[92] Spin fluctuation based exchange a coupling has been demonstrated, experimentally and theoretically, to affect the Tc of 2D ferromagnetic layers coupled by the nonmagnetic spacer.[197]

We aimed to produce robust and high yield molecular spin devices using high spin molecules and ferromagnetic electrodes. A readily scalable process for molecular electrodes incorporating a wide variety of metals, including ferromagnetic films, has been recently reported.[40] In this approach, a metal/insulator/metal thin film structure is patterned by photolithography to reveal an exposed edge at the side of the junction. Here covalently attached molecular complexes can span across the insulator layer on the surface of the exposed vertical sides of the pattern connecting the top and bottom metallic electrodes becoming the dominant current path. The key merit of this Multilayer Edge Molecular Electrode (MEME) is that it is technologically easy to match film thickness to the critical dimension of molecular length (~2-3 nm). The conduction mechanism is primarily tunneling from the first metal electrode through an insulating alkane chain tether into the metal cluster core and followed by subsequent tunneling to the second electrode. This arrangement emphasizes the available molecular states for conducting into, thus allowing the study of a primary hypothesis that the well defined spin state of the transition metal complex[3] will modulate current across the junction between magnetically ordered ferromagnets. However, the remarkable observation reported here is that when molecular clusters are chemically linked to F-MEMEs, there is a dramatic decrease in the device current (3-6 orders of magnitude) concomitant with a strong molecule-induced antiferromagnetic coupling. This observation is over the entire junction (molecular channels and the planar tunnel junction) and is far above typical changes exhibited by Tunneling Magneto Resistance (TMR) devices.[18] Described here are the current transport, temperature, optical excitation, magnetic force microscopy (MFM), and magnetization studies of the Molecular Magnetic Junction (MMJ), with particular emphasis on control experiments to demonstrate the phenomena.

7.2 Device fabrication and physical characterization:

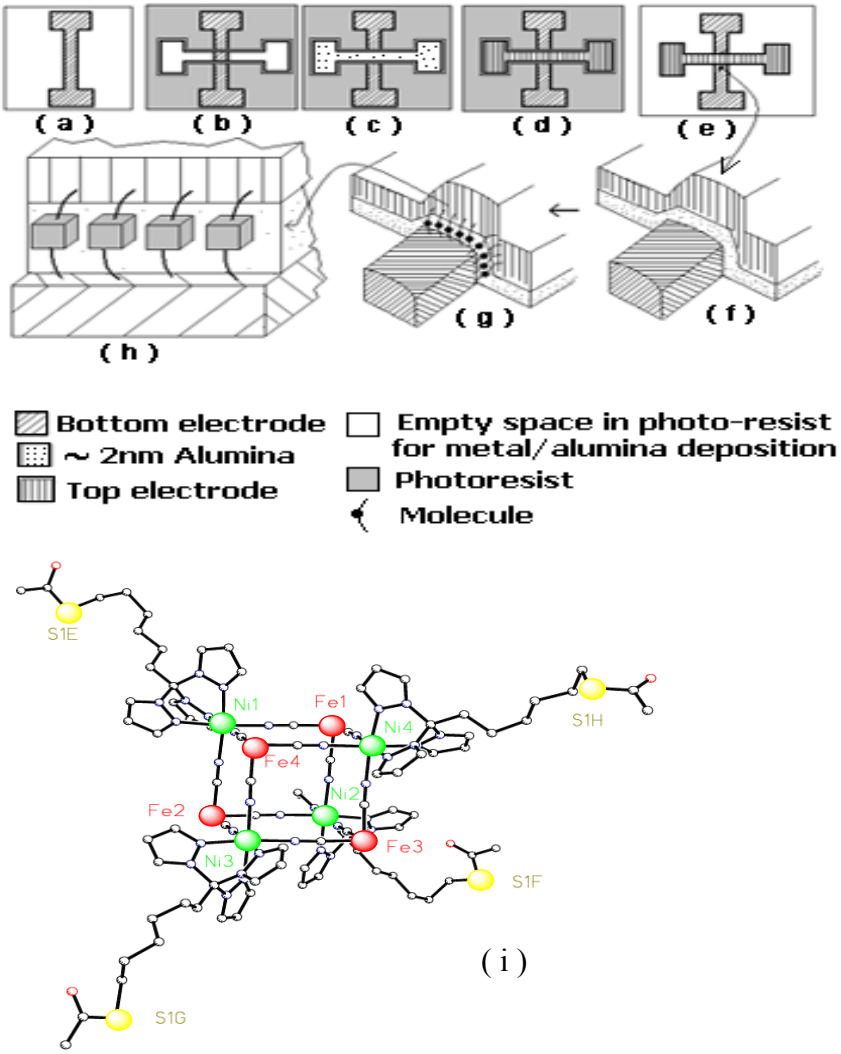

Figure 7.1: Multilayer edge molecular electrode fabrication scheme: lift-off approach. (a) Deposition of bottom metal electrode [Ta(5nm)/Co(5nm)/NiFe(5nm)] followed by (b) creation of photoresist window for alumina and top metal electrode deposition. (c) Deposition of ~2nm thick alumina, (d) top metal electrode NiFe(12nm) deposition, and (e) lift-off producing exposed edhe F-MEME. View of typical exposed side edge (f) before and (g) after molecular cluster attachment. (h) Idealized cross-junction edge with chemisorbed clusters. *Note: Clusters chemisorb to all exposed metal surfaces and only those spanning the insulator gap are electrically relevant.* (i) Organometallic molecular cluster.

The photolithography-liftoff produced F-MEME[40] with Ta(5 nm)/Co(5 nm)/NiFe(5 nm)/Al_2O_3(~2 nm)/NiFe(10 nm) configuration were initially studied, figure 7.1(a-f). The NiFe (20 wt% Ni) layer, which interacts with molecular bridges, possesses the elemental form of Ni and oxides of Fe inambient conditions; NiFe do not get oxidized unless heated above 250 ºC.[114] An array of paramagnetic molecular clusters, $[(pzTp)Fe^{III}(CN)_3]_4[Ni^{II}(L)]_4[O_3SCF_3]_4$ [(pzTp) = tetra(pyrazol-1-yl)borate; L = 1-S(acetyl)tris(pyrazolyl)decane][3], figure 7.1(i), were covalently-linked onto the electrodes (NiFe) electrochemicaly via sulfur atoms linkers.[117] F-MEME fabrication method and the molecule attachment process are detailed elsewhere.[40] The center of the magnetic molecular cluster (MMC) is a cube with alternating Ni and Fe centers at each corner bridged by cyano groups. The thioacetate terminated ligands reside on the Ni centers, figure 7.1(c) and allow for the covalent bonding (Ni-S) of the cluster to the ferromagnetic NiFe leads. At temperatures below 10 K, the cluster contains ferromagnetically coupled low-spin Fe^{III} (S = ½) and Ni^{II} (S = 1) centers, affording an S = 6 magnetic ground state.[3]

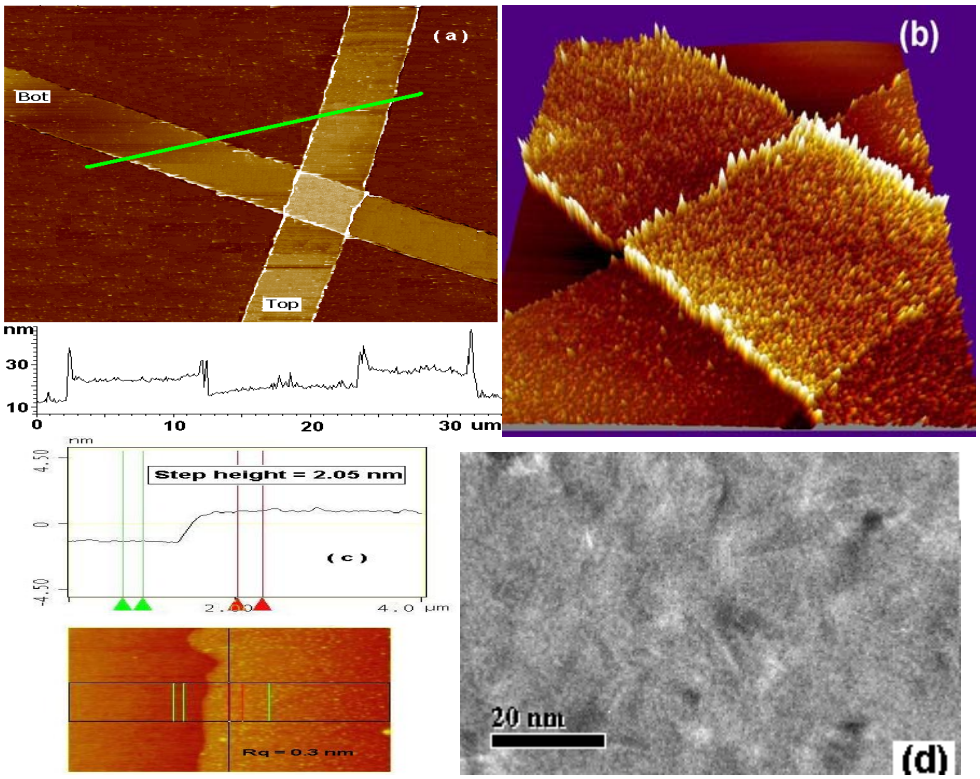

Figure 7.2: Characterization of F-MEME (a) AFM micrograph of a photolithography-liftoff produced tunnel junction with exposed metal-insulator-metal side edges. (b) 3D image of a MMJ showing the exposed edge where molecules are hosted (c) AFM showing Al_2O_3 film to be ~2nm and roughness Rq= 0.3nm (d) TEM image of Si_3N_4(50nm)/Co(7nm)/NiFe(3nm)/Al_2O_3(2nm) clearly showing pinhole free Al_2O_3 covering bottom ferromagnetic electrode.

FMEMEs used in this study were characterized by AFM (Digital Instrument Multimode AFM, and Molecular Imaging Pico Plus AFM), and a 200kV field emission analytical transmission electron microscope (JEOL JEM-2010F), figure 7.2(a-d). TEM characterization of the side edges of the F-MEME could not be performed due to the difficult sample geometry. However, surface morphology of 2nm thick Al_2O_3 barrier deposited on the bottom electrode was judged by the TEM and AFM, figure 7.2(c-d). Both types of measurements suggested a pinhole free conformal coverage of Al_2O_3 on the Co/NiFe bottom electrode. Transport property and breakdown studies were the ultimate tests of barrier integrity. Al_2O_3 barrier thickness in completed tunnel junctions was also calculated by fitting the observed current to the Simmons model,[50] which was in agreement with the thickness measured by AFM. A high quality alumina insulator is critical to MEME formation because it sets the separation between two metal electrodes to the molecular length scale and keeps the leakage or background current low,[194] thus enabling the observation of molecular current. Mechanical stress induced barrier failures[124] (producing ohmic device characteristics) are the primary failure mechanism for these devices; significant efforts are made to minimize these deleterious stresses.[194] A typical FMEME has a 5x5 μm^2 cross junction area, >100-500 kΩ tunneling resistance, and hosts ~10,000 MMCs on its edges.

7.3 Transport measurement methods and apparatus:

All transport measurements were conducted on a Keithley-2430 1KW Pulse source meter (μA to nA range) and a Keithley-6430 Sub-Femtoamp source meter equipped with a Keithley preamplifier (sub fA range). For all transport measurements, samples were placed directly on an electrically grounded chuck residing within a grounded and dark Micromanipulator S8 Desktop Station box. Electrical contacts to the metal electrodes were made using Micromanipulator arm and probes. Also, bi- and triaxial cables were utilized to connect source meters to samples. The source meter performance was compared to output values obtained on an Agilent 4155 B Semiconductor Parameter Analyzer.

A current was measured while applied bias was simultaneously swept in the ±100 mV range for transport, ±500mV range for tunnel barrier parameter extraction, and ±2.5V range for electrical breakdown study, respectively. In general, applied biases are well below the device breakdown potential (~ 2V). Three to five measurements were carried out and averaged for I-V data plots. A 2-5mV bias step and 0.5-1s intervals between two bias steps were used to avoid sweep rate dependent variation. The periodic accuracy verification of I-V measurements were accomplished using resistors of known values (e.g. 10GΩ, 1MΩ). To minimize possible probe

charging between measurements deliberate electrical shorting prior to electrode pad contact was performed. Low temperature transport measurements of stable F-MEME were performed after wire bonding them on the cryogenic insert (Janis Research) for immersion into liquid nitrogen. The sample temperature was determined using a Cryogenic Controller Inc. (Model 62).

Photo-activated transport on MMJ samples was performed with a calibrated Microlite FL3000 model white light source, equipped with fiber optics light channel. Light intensity from the source was also measured by a Model 820 A Digital Photometer (Gamma Scientific Inc).

7.4 Results:

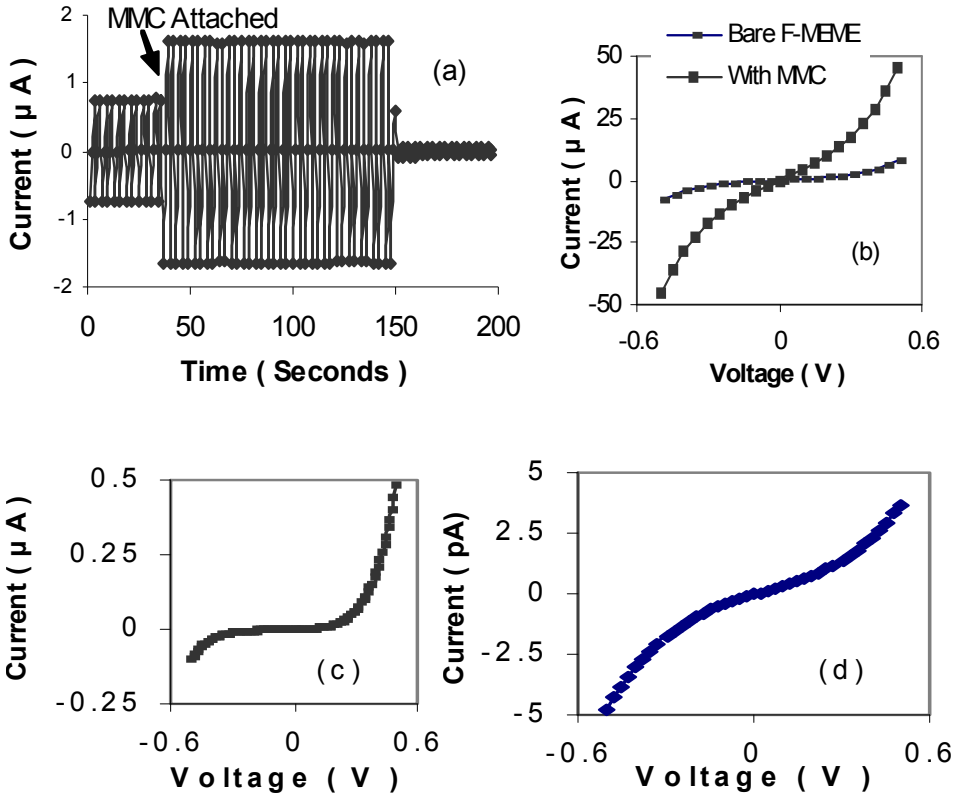

Figure 7.3: (a) Device current at ± 100mV before and after immersing of F-MEME in MMC solution. On a typical MMJ (b) initial high (μA) current state with additional molecular current path, (c) intermediate nA state within a few hours of attachment and (d) lowest pA current states after long incubation, low temperature or strong in-plane applied field.

The magnetic molecular clusters are attached to F-MEME by the cyclic electrochemical[24] reaction, as illustrated in figure 7.3(a). An increase in current is expected after the attachment of the molecules when new current paths are created, figure 7.3(b). However, after several minutes the current dramatically reduces to a level far below that of the current through the planar area of the electrode junction (background current) on the representative F-MEME. In most of the cases, the higher μA current levels observed (2-5 μA at100 mV) were stable for several hours. Surprisingly after 4-48 h (after molecular attachment), the nA device current level (1-5 nA at 100 mV) became stable. Generally, an asymmetric I-V curve was observed in the nA current range for these devices, figure 7.3(c). It is important to note that the convention used to describe the experimental behavior is that bias is applied to the top electrode and the bottom functions as the ground. Thus the asymmetry favors electron injection from the bottom Co/NiFe electrode (similar to what is seen in the following photo excitation study) rather than the top NiFe electrode. The nA current range remained stable at RT when the MMJs were subjected to frequent transport studies. However, incubating the molecular junctions for a week without performing transport studies, followed by the application of an in-plane 0.45T magnetic field or cooling to 77 K, produced a device state in the ~pA current range (0.5-10 pA at 100 mV), figure 7.3(d). In summary, three current states were observed on MMJ 1) high current (μA) due to additional molecular conduction paths 2) intermediate (nA) current and 3) lowest (pA) current state after the application of magnetic field, low temperature, or long incubation time.

7.4.1 Control experiments:

The dramatic current reductions observed require a mechanism to effectively turn-off the metal/insulator/metal current path in the planar area of the device, presumably through magnetic ordering effects induced by the molecule. Consequently significant numbers of control experiments were conducted in an effort to establish that the observed current reduction is due to appended molecules rather than experimental artifacts.

7.4.1.1 Statistical Observation of F-MEME Current Reduction after Molecular Attachment:

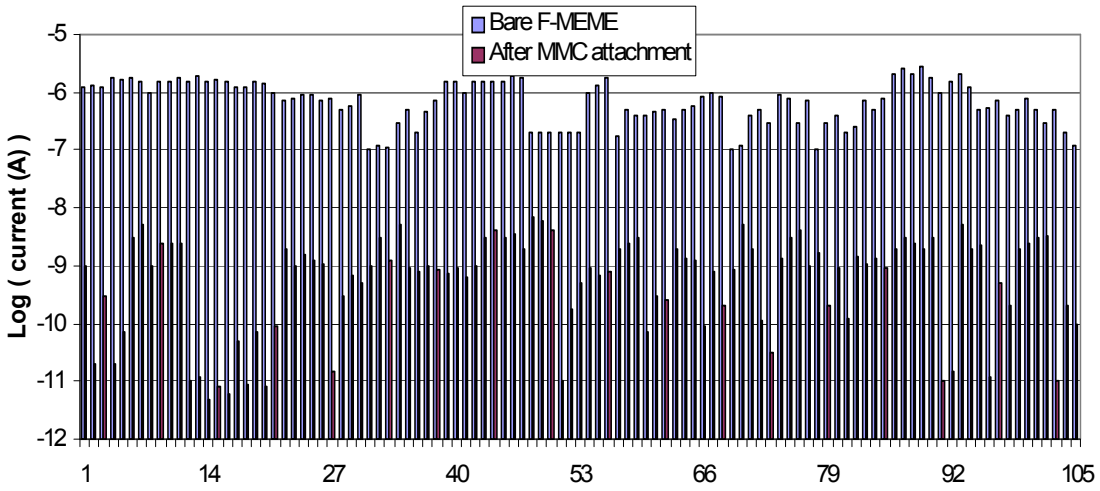

Figure 7.4: Experimental tunnel currents of bare and MMC-functionalized F-MEME (100 mV, 48 hrs).

Over the last 20 months 105 ferromagnetic-multilayer edge molecular electrode (F-MEME) samples have been prepared and their transport behavior characterized. Treatment of each F-MEME with CH_2Cl_2 solutions of magnetic molecular cluster (MMC) afford devices initially with high tunnel current values (~μA) that approach a low current state (nA to pA) after hours to days, figure 7.4. Once low current state is attained, electrical transport remains in an nA current state for more than 14 months (6 samples selected for control study). To statistically verify this unexpected behavior the tunnel current (at 100mV bias) of 105 bare and MMC-functionalized F-MEMEs (48 hr incubation, N_2 ambient, RT) are provided, Figure 4. For approximately 90% of F-MEMEs, junction current dramatically increases when bare electrodes are treated with MMC while the remaining devices immediately afford low tunnel current values; within 4 to 24 hours lowered current values (nA range) are observed for all electrodes functionalized with MMC at room temperature. After 48 hours, the data clearly suggests that electrodes treated with MMC exhibit significantly lower tunnel current values ($1.4 \pm 1.5 \times 10^{-9}$ A) in comparison with bare electrodes ($8.6 \pm 5.6 \times 10^{-7}$ A).

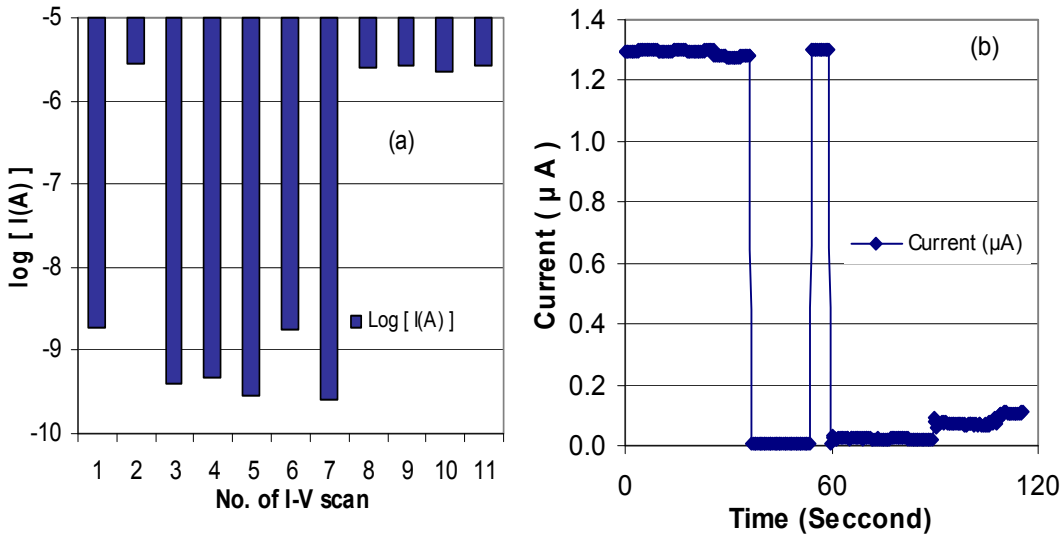

Figure 7.5: Changing current state of MMJ: (a) A MMJ shifting from low to high current state with repeating I-V measurement. (b) Another MMJ shifting from high to low current state.

It is noteworthy that an F-MEME after molecule attachment shifted back and forth between the low and high current state for 24-48 hrs. For instance, one MMJ shifted to high current state on repeating I-V. Another MMJ, in higher current state after the molecule attachment, shifted to the low current state during the transport study at 50mV. Most of the magnetic molecular junction exhibited this behavior. Results in figure 7.5 suggest that an electrical connection to the junction is intact.

Generally, higher quality F-MEMEs (lower leakage current) switched to low current state more quickly. We postulate that the parallel current through defects in the tunnel barrier (outside of the molecular conduction path) interfere with the formation of magnetic domain structures within the magnetic electrodes, that presumably afford low tunnel current states. Pinhole in the tunnel barriers is known to produce ferromagnetic interlayer coupling.[186] F-MEMEs treated with various solvents did not exhibit appreciable changes in tunnel current values up to two weeks relative to background. Thermal and mechanical stresses present in F-MEMEs quickly caused failure due to rapid electrical shorting (e.g., junction resistance < 20kΩ)[194] regardless of whether the electrodes have been treated with sulfur containing molecules.

7.4.1.2 Molecular Reach vs. Tunnel Barrier Thickness

To probe the possibility that uncontrolled surface conduction is responsible for the unusual experimental conduction behavior, we prepared electrodes with varying insulator layer (Al_2O_3) thicknesses,[40] while keeping all other factors identical. From X-ray crystallographic data, we estimate the sulfur-sulfur contact to be ~2.6 nm for MMC and we engineered F-MEMEs with alumina layer thicknesses ranging from 2.0 to 4.0 nm. The Al_2O_3 barrier thicknesses were measured via AFM and Simmons fitting of the tunnel current of bare electrodes prior to treatment with MMC, figure 7.6(b). We observe that F-MEMEs with 4 nm barrier thickness did not exhibit change in transport after the treatment with MMC, Figure 6(a),[40] unlike the dramatic change seen with F-MEMEs with 2 nm barrier, figure 7.6(b). However, when the Al_2O_3 layer thickness is smaller than the distance between the sulfur-sulfur contacts, the tunnel current is 4-20 times larger and diminishes rapidly with increasing time, approaching nA values after approximately seven hours.

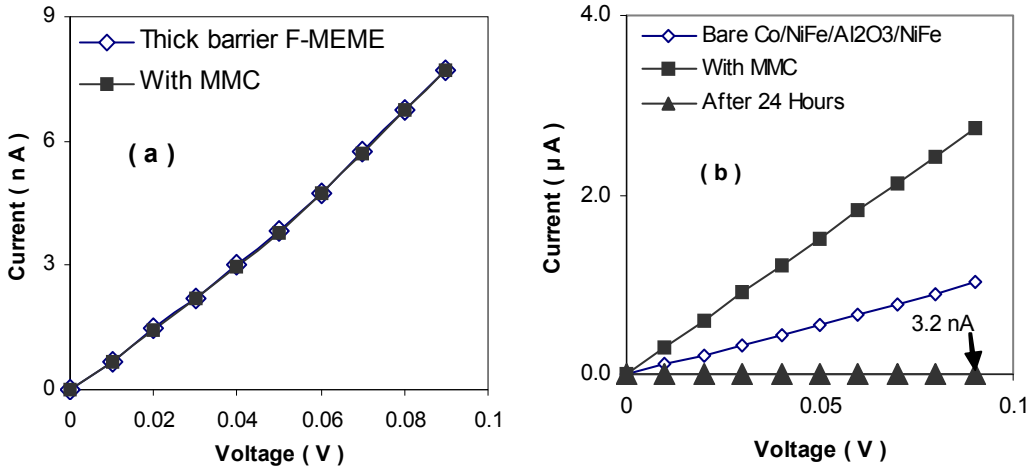

Figure 7.6: Electrical behavior of F-MEME treated with MMC. (a) I vs. V plot for F-MEMEs with 3.5 nm Al_2O_3 barrier. (b) Response of MMC on F-MEME with 2 nm barrier thickness.

7.4.1.3 Device current state with 1,20-Dithioeicosane treatment:

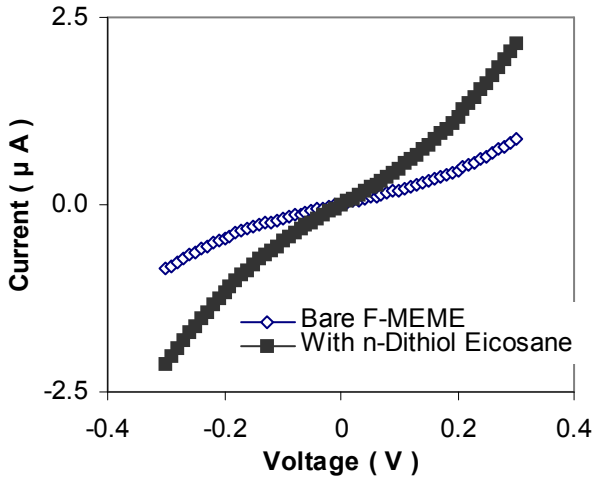

Figure 7.7: Voltage dependence of current for bare and 1,20-dithioeicosane functionalized F-MEME.

To probe if molecules containing unpaired electrons in transition metal centers are necessary to exhibit low tunnel current states, a series of F-MEMEs was treated with diamagnetic 1,20-dithioeicosane, which is long enough to span a 2 nm Al_2O_3 insulator gap to produce molecular conduction channels. The treatment (same process as used for MMC attachment) of F-MEME with 1,20-dithioeicosane[40] (2 mM) followed by washing in dichloromethane(20mL), 2-propanol (20 mL) and DI water(40mL) and then the drying of samples under an N_2 gas stream, afforded a series of devices containing chemisorbed diamagnetic dithiols. The F-MEME electrodes exhibited significant increases in tunnel current, not the dramatic current suppression as observed after attachment of MMC, figure 7.7.

7.4.1.4 Electrode composition and molecular junction transport behavior:

The reproducible and dramatic changes in tunnel current values (nA or pA state) are found only when magnetic molecular clusters (MMC) and ferromagnetic metals are present. In particular, the dramatic current reduction is only seen for [Co(10-x nm)/NiFe(x nm)/-Al_2O_3(~2.0nm)/NiFe(8-12nm)] F-MEMEs functionalized with MMC**.** Here x varies between 3-5 nm**.** In our magnetic measurement we have observed that the coercive field for the bottom electrode is nearly 5 fold higher than that for the top NiFe electrode. In the ferromagnetic resonance study also we observed that the top and bottom electrodes behave quite differently. The resonance mode position for the bottom electrode (Co/NiFe) and top electrode (NiFe) were found to be at 720 Oe and 1140 Oe, respectively. Bare F-MEME is found to exhibit weak

antiferromagnetic coupling via insulator. Extensive details of magnetic studies of F-MEME and the effect of MMC on its magnetic attributes are presented in chapter 6. We have observed that changes in the configuration of the top and bottom electrodes produce a dramatic effect on the molecular cluster response. It was found that the composition of an F-MEME's magnetic electrodes was critical in enabling a molecular spin device's current switchability by the magnetic field. Details of the effect of electrode composition on the molecular spin device are furnished in appendix A6**.** We observed that if the top and bottom electrodes are of the same ferromagnetic metal, current suppression could not stabilize. For instance, F-MEMEs with both electrodes made up of NiFe, just produced a stable current increase, figure 7.8. The ferromagnetic resonance study exhibited that this configuration does not show highly distinctive modes for the top and bottom electrodes, suggesting a stark difference in the magnetic property of this F-MEME with respect to the F-MEME with a Co/NiFe bottom electrode. The difference in the coercivity of two magnetic electrodes was found to be critical for observing Kondo splitting of C_{60} based molecular junction[13] and tunneling magneto resistance.[18]

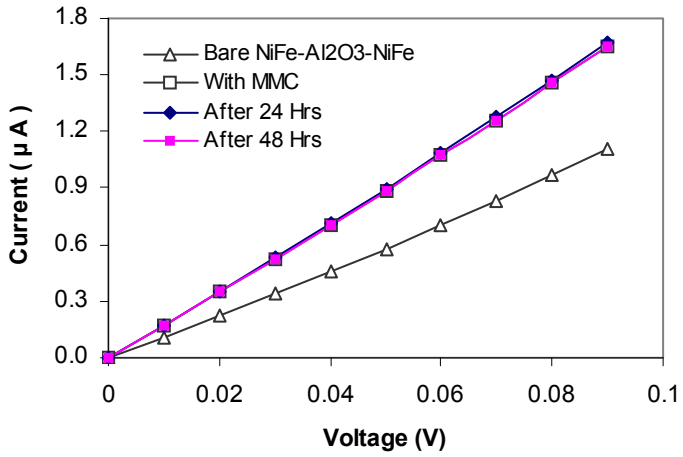

Figure 7.8: Tunnel current vs. voltage behavior for NiFe(12)/Al_2O_3(2)/NiFe(12).

We have also prepared a series of nonmagnetic [Ta(12 nm)/Al_2O_3(2.5 nm)/Ta(12 nm)] electrode junctions to investigate the apparent requirement that ferromagnetic electrodes are necessary for the dramatic current reduction.[40] The treatment of these electrodes with either 1,20-dithioeicosane or MMC did not show the dramatic changes in tunnel current (nA or pA state) relative to background values.[7] Combining the results of these two systems suggests that in order to produce the dramatic change in transport (nA or pA current state), MMCs are required to be attached across ferromagnetic F-MEMEs (Co/NiFe/Al_2O_3/NiFe).

7.4.1.5. Chemical and Oxidative Stability of F-MEMEs

To further investigate the effects of sulfur-containing molecules on electrical transport behavior, a series of electrodes was treated with organic thiols of varying chain lengths. In two experiments, electrodes were treated with CH_2Cl_2 solutions of either 1-butanethiol (2mM) or 1-dodecanethiol (5mM), which afforded negligible changes in F-MEME transport (~17 %), relative to a bare F-MEME's current value. Furthermore, the observed tunnel currents are far below those seen for electrodes decorated with MMC (300-5000% increase) or 1,20-dithioeicosane. We postulate that short alkanethiols (C_4–C_{10}) cannot span the insulator gap to assist in conduction.

To further probe the stability of the electrodes and the role of surface oxides in transport behavior, we purposefully oxidized several electrodes with plasma of various energies. Oxygen plasma (20W RF; $P(O_2)$=50mtorr) treatment (conditions) or heating of electrodes to 100ºC in air for 10 minutes did not significantly alter the transport properties relative to freshly prepared samples. However, increasing the plasma energy (100W RF, $P(O_2)$=50mtorr) quickly induced catastrophic tunnel barrier failure; that is likely due to significant charging of the samples during plasma treatment or the generation of thermal stresses. The formation of surface oxides at or near ambient conditions does not appear to significantly alter the F-MEME transport properties. Even an improvement in the switching field of the tunneling magneto resistance device was observed after a plasma treatment of ion milled magnetic tunnel junction.[198] Interestingly, we observed that the burning of molecules by the oxygen plasma from the circumference of F-MEME dots reversed the molecule effect; the bare sample's magnetic modes were recovered, chapter 6.

7.4.1.6 Quality of exposed edge of F-MEME for molecule attachment (Ion Milling vs. Lift-off based F-MEME Fabrication):

The exposed side edge of F-MEME is crucial for allowing molecules to bridge over the insulator gap. Producing an exposed metal/insulator/metal junction by another fabrication route and having the same current reduction/magnetic ordering effects can be viewed as a supportive experiment for the conclusions of this work. Given that Ar ion milling is an established method for generating exposed edges of multilayer films normal to their growth planes, we prepared several F-MEMEs using the ion milling approach, figure 7.9(b). Engineering protocols and conditions are identical to those described for electrodes using lift-off approaches except for ion-milling of the multilayer edge.[40] During the ion beam milling (using FISCHIONE 1010 ion mill), samples are cooled by liquid N_2 to minimize photoresist hardening. TEM studies have confirmed that a uniform and sharp edge is obtained on ion-milled magnetic tunnel junctions.[10] We observed that F-MEME samples, prepared with ion milling, possessed an exposed edge; a sharp exposed

edge allowed the MMC attachment. The MMC attachment resulted in the identical transport response, figure 7.9(c), as seen with the samples with lift-off produced exposed edges, Figure 9(a). However, thermal stresses introduced in samples during milling and/or cooling resulted in severe tunnel junction instabilities, poor reproducibility, and short device lifetimes.[199] Further discussion about exposing the edge of F-MEMEs for molecule attachment is given in appendix A1.

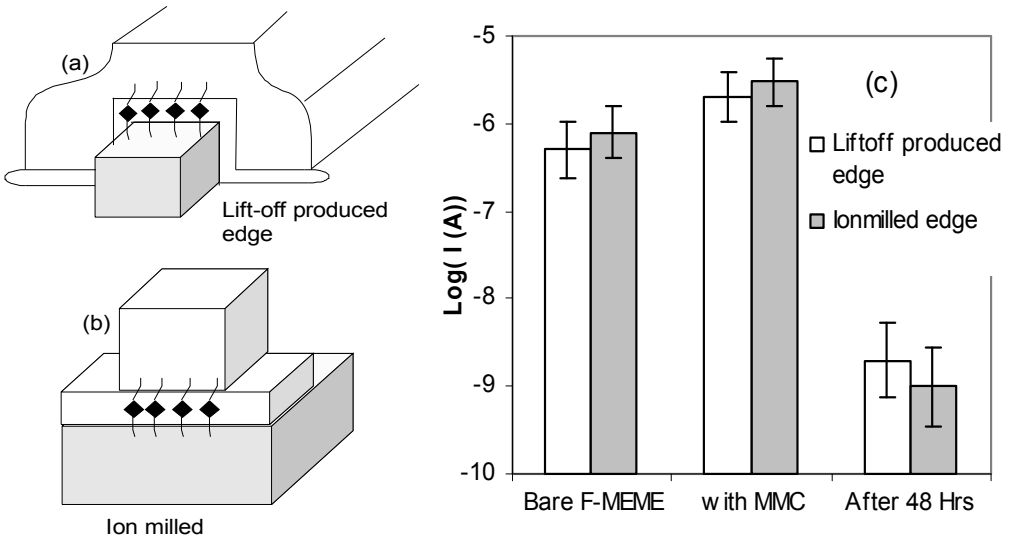

Figure 7.9: Comparative study of current at 100mV before and after MMC attachment on F-MEME produced by liftoff and ion milling methods.

7.4.1.7 Bottom electrode stability:

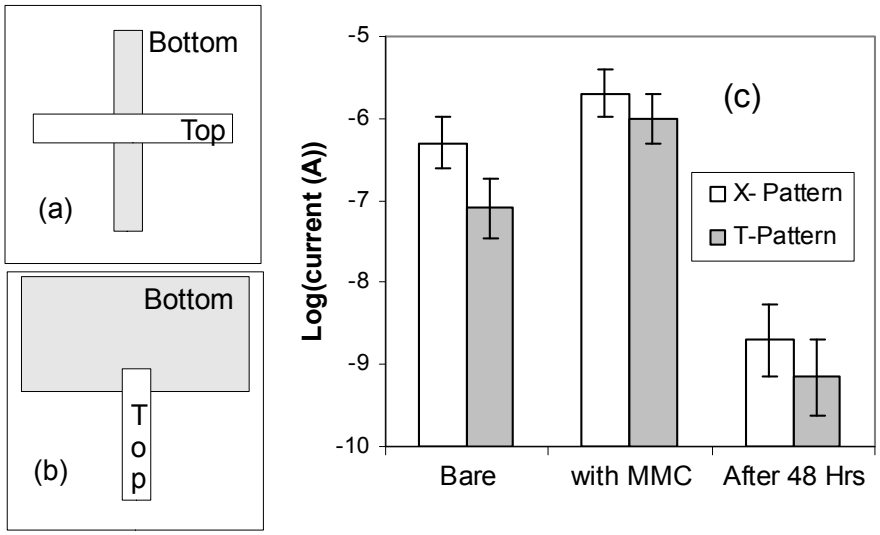

Figure 7.10: Effect of changing F-MEME design from cross (X) pattern (a) to T –junction (b) on magnetic molecular response (c).

A serious experimental difficulty is that on numerous samples, severe electrochemical etching occurred during the molecule functionalization step (appendix A2). The damage was highly dependent on initial pattern quality and not seen on the samples with Co/NiFe bilayer pattern. The bottom electrode of F-MEME contains 50-75% of Co and is under the NiFe layer. We have observed that Co exhibited <2nm/min dissolution rate in the molecular solution during the electrochemistry step used for the molecule attachment. However, 3-5 nm NiFe over Co provides excellent stability. Unpatterned Co/NiFe bilayers did not show noticeable dissolution in an electrochemical step performed for 30 min with aggressive molecular solution and up to the ±500mV bias step (usually ±100mV bias for 2min are applied during molecular treatment). To make sure that any unnoticeable damage to the bottom electrode, the most sensitive part in our device, is not producing current suppression, we performed the following control experiment. F-FMEME devices with a wide bottom electrode (10x3 mm^2 instead of 0.005mm^2) were produced. With the T-shape design, figure 7.10(b), we have clear advantages over the X-shape junction: etching or mechanical damage away from the junction cannot disconnect the bottom electrode. Moreover, the T-shape junction also produced a lower leakage current, presumably due to the inclusion of one edge of the bottom electrode in the junction area; tunnel junction edges are known to be the weakest point of ultrathin tunnel barrier based junction and generally produce device failure.[199] We indeed observed the same response of MMC on the individual T-shape junction as seen with the X-pattern, figure 7.10(c). In, addition 0.1mM molecular solution of MMC in tetra hydro furan (THF) solvent was also prepared to check whether any unknown chemistry specific to di-chloromethane solvent was behind the current suppression. We found that molecule treatment from this solution reproduced the current suppression on both T-shape and X-pattern F-MEME. From this study in conjunction with the fact that molecule treated F-MEMEs can switch current state, figure 7.5, we conclude that current suppression is not caused by any damage to junction or electrodes. However, due to the narrow parameter range and the variability of alumina thickness on a large area sample, it is quite inefficient to prepare a large volume of T-shape junctions.

7.4.2 Effect of temperature light and magnetic field:

7.4.2.1 Effect of temperature:

Variation in temperature dramatically affected the transport of magnetic molecular junctions (MMJs), figure 7.11. At high temperatures (400 K), magnetic ordering and transport of MMJs changed significantly. In a study three MMJs, initially in nA current state at RT, were heated to 400K and then cooled to RT; current measured at RT on all three junctions showed that the current value increased to 2-5μA levels at 100mV. Such an increase is also possible when a tunnel junction undergoes breakdown of a tunnel barrier. Upon cooling to 77 K, three junctions exhibited lowest pA current state, which may be due to two reasons: (a) MMJs transport is dominated by the defects in tunnel barrier showing the Pool-Frenkel[37] type mechanism, (b) magnetic electrodes resumed the magnetic ordering required to exhibit low current state, lost by MMJs during heating to 400K temperature. Interestingly, after warming the MMJs from 77K to 298 K, three MMJs under study persisted in the low-current state (nA-pA), and no device reached the original μA current state. Three control samples remained in nA current state or lower for more than 30 days until the second heating of MMJ to 400 K was performed. This observation unambiguously suggests that the role of defects in changing current state with temperature variation is highly unlikely. Switching an MMJ among three current states is consistent with the loosing and reinstating of molecule enabled magnetic ordering.

The effect of thermal cycles on bare junction transport was studied to ensure that the bridging of MMC on F-MEME is required to enter low current state (nA or pA states). The cooling of a bare F-MEME to 77K did not induce low current state, figure 7.11(b). The annealing of a bare F-MEME at 450 K for 30 min modestly decreased current of bare electrodes. Slow heating rate (5 K/Min), similar to what we used for the heating of three MMJs, was utilized. Presumably, improvement in tunnel barrier during annealing[17] is the reason behind reduction in the current of a bare F-MEME, figure 7.11(c). Heating performed at a faster rate, 1-10 K/sec, in ambience condition, produced either no change in transport or a permanent current increase due to tunnel barrier breakdown. This is opposed to the case of electrodes treated with MMC in which thermal annealing disrupts the low current state (nA or pA) to get into the high current state (μA). The heat treatment of F-MEME with MMC switching from nA state to μA (high temperature) and then to pA state (77K) reoccurred on an MMJ, Table 7.1. In the case of a tunnel barrier with atomic defects, such as TaOx, transport was found to be temperature dependent and was following the Pool-Frenkel type mechanism.[178] We have found that after returning to the RT from the heating and cooling step, generally the device resumed its starting current level, unlike MMJs where different current levels were observed with respect to temperature.

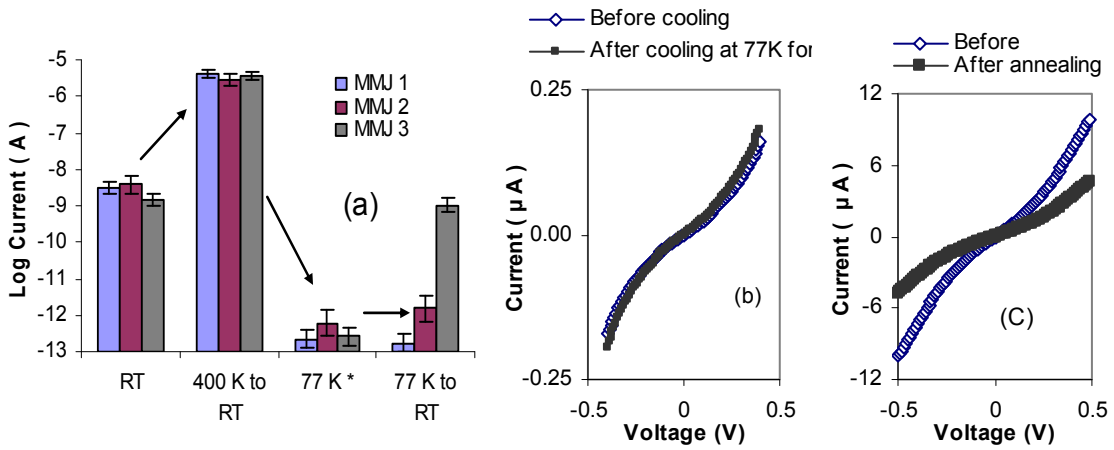

Figure 7.11: (a) Effect on device transport after heat treatments of three different MMJ samples. Measurements made at room temperature (RT) except for * marked study that was made at 77K. (b) Electrodes cooled to 77K (45 min.) and then heated to 300 K (1-5 ºC min^{-1}), and (c) Impact of annealing time and temperature on *I* vs *V* behavior of F-MEME.

Table 7.1: Effect of heating -cooling cycle was studied twice on the same MMJ.

	1st cycle	2nd cycle
At RT	$3.8\pm1x10^{-9}$	$2.0\pm1.0\ 1x10^{-9}$
After annealing at 150 C for 10 min & cooling to RT	$3.2\ \pm1x10^{-6}$	$5.0\pm2.01x10^{-6}$
After cooling to 77K	$\sim5\ \pm2\ 1x10^{-13}$	$\sim4\pm2x10^{-13}$
After warming up from 77K to RT	$\sim1\text{-}10\ 1x10^{-12}$	$\sim1\text{-}10\ 1x10^{-12}$

7.4.2.2 Effect of light:

As illustrated in figure 7.12(a), the photo excitation of MMJs in the intermediate (nA) state showed preferential current at 0V bias. The photocurrent direction is consistent with electron flow from the bottom (Co/NiFe) electrode. Since there is no Schottky barrier or other means of producing inbuilt electric field within the barrier due to the symmetrical tunnel barrier and molecule,[1] there should not be a driving force to preferentially allow for a net flow of electrons/holes from the bottom to the top electrode, unless selective photoexcition of spin-oriented electrons in the ferromagnetic films of the MMJs, have more favorable states to tunnel into the top electrode. The flux of photons (~100 mW white light) over the entire 5x5 μm^2 area of the MMJs would correspond to the 0.8 nA of observed current with ideal conversion (100%). Since the area of molecules at the edge of the pattern is $\sim10^3$ less, it is unlikely that the observed photocurrent is due to the photoexcitation of electrons present within the tethered cluster, since

photon flux is far below the experimental electron current. This assumption is consistent with a mechanism involving unselective photoexcitation of electrons in the magnetically unaligned top (NiFe) electrode experiencing higher resistance, when migrating towards the magnetically ordered bottom (Co/NiFe) electrode, to produce a net current. The photo-voltage on MMJ was 52± 5.6mV.

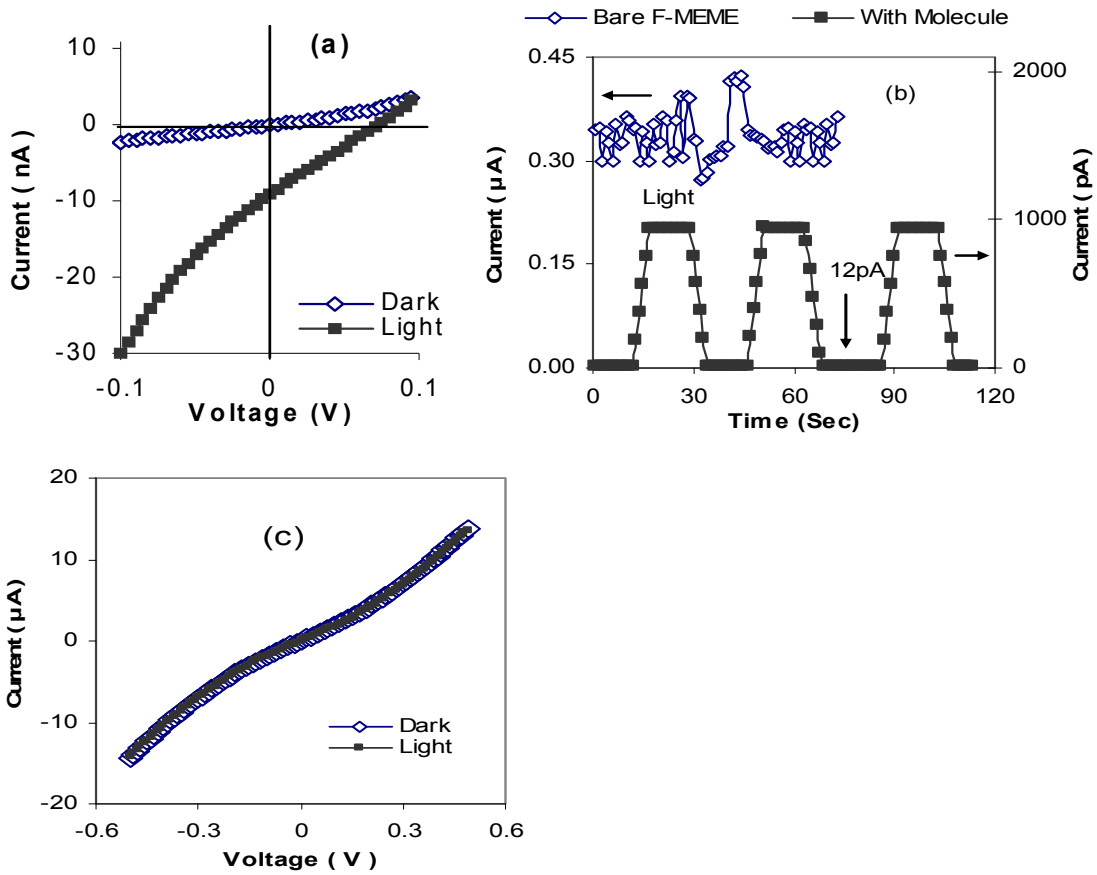

Figure 7.12: (a) Photocurrent of MMJ in nA current state and (b) *I* vs *V* data of F-MEME + dithiol eicosane electrode in the absence and presence of white light radiation.

It is noteworthy that for MMJs in the µA state, presumably with a small degree spin polarization of both electrodes due to thermal energy, current states do not show photocurrent. Generally in the pA current state, effect of white light radiation was found to be negligible. However, in a few case a MMJ, showing ~10pA current level at 100mV, exhibited an unambiguous photo effect. The example in figure 7.12(b) is from an F-MEME which showed a noisy I-V during the off and on state of white light. After molecular treatment this F-MEME showed unambiguous signature of photo-activated transport, figure 12(b). In this study 50mV constant voltage was applied on F-MEME, before and after molecule attachment. Photo activated transport on molecule attached F-MEME with V= 0V, was noisy and indistinct. It seems that in

the nA current state, an MMJ possesses optimum difference in the spin polarization or magnetic ordering of two electrodes at RT to produce photocurrent under light radiation. A discussion on the effect of magnetic molecular cluster on the spin polarization of magnetic electrodes is presented elsewhere in this chapter.

Insignificant photocurrent effects are observed in the absence of the chemisorbed MMC clusters or with organic (diamagnetic) molecules tethered across MMJ. It was observed that photo current was only obtained when magnetic molecules were self assembled across the F-MEME device. No photo current was observed on F-MEME + dithiol eicosane, figure 7.12(c), and NiFe/AlOx(2nm)/NiFe+MMC systems. Failed tunnel junction (with low ohmic resistance) also did not produce the photo current presumably due to a parallel conduction path through defects of non spin oriented electrons. However, we have seen photovoltaic effect in Ta(12nm)/TaOx(2nm)/Ta(12nm) tunnel junctions; graded density of atomic defects within a TaOx barrier not only enhanced the light absorption capability of ~2.5nm TaOx, but also produced an inbuilt electric field. We found that such photovoltaic effect is very transient with respect to the change in temperature, and exposure duration to white light. Whereas, photovoltaic effect on MMJ was found to be stable for several months; it did not vanish or change even after 30min of high intensity light radiation. Sensitivity of photovoltaic effect of MMJ towards a magnetic field also supports its origination from the molecule induced magnetic ordering of electrodes. The application of inplane magnetic field, which generally switched the MMJ's current to lower level, diminished the photo current to become negligible. However, photo effect re-appeared as MMJ resumed the nA current state. Photocurrent on Ta/TaOx/Ta was indifferent to magnetic field effect; with degrading TaOx barrier photocurrent became negligible irreversibly.

7.4.2.3 Effect of magnetic field:

Transport of the ferromagnetic multilayer edge molecular electrode (F-MEME) before and after the MMC attachment was studied, in the magnetic field varying between ±300 Gauss and after the magnetization by the static 0.45T magnetic field. For the application of weak in-plane magnetic field, bare F-MEME generally did not show a sharp magneto current change up to 250 Gauss. Presumably, it is due to the inability to pin the magnetization of one layer and rotate the magnetization of another layer independently. We obtained clear loop during the magneto-transport study, figure 7.12(a). Interestingly, it was found that after the attachment of magnetic molecular cluster a F-MEME exhibited almost similar magneto-transport loop in high and low current state, figure 7.12(b-c). However, data was significantly noisy in the transient high current

state of the MMJ, figure 7.12(b). Transports study right after the magnetization of bare F-MEME in 0.45T in-plane magnetic field exhibited no difference in tunnel junction for the lower bias but observable difference after 0.25V, figure 7.12(d). Strong in-plane magnetization fields (0.45T, 1h) applied to MMJs in nA current states, reduced the experimental current to pA levels, figure 12(e). These studies suggest: (a) MMJ does not behave like a Juliar type spin valve,[94] where resistance decreases due to electrode alignment in the applied field direction.[18](b) MMJ transport is sensitive towards the magnetic field and (c) switching between two current levels is not abrupt.[18] Since this is a layered thin film structure, magneto-restriction is not expected to significantly change the tunnel barrier thickness, as may be seen in other TMR lateral point junction devices.[200]

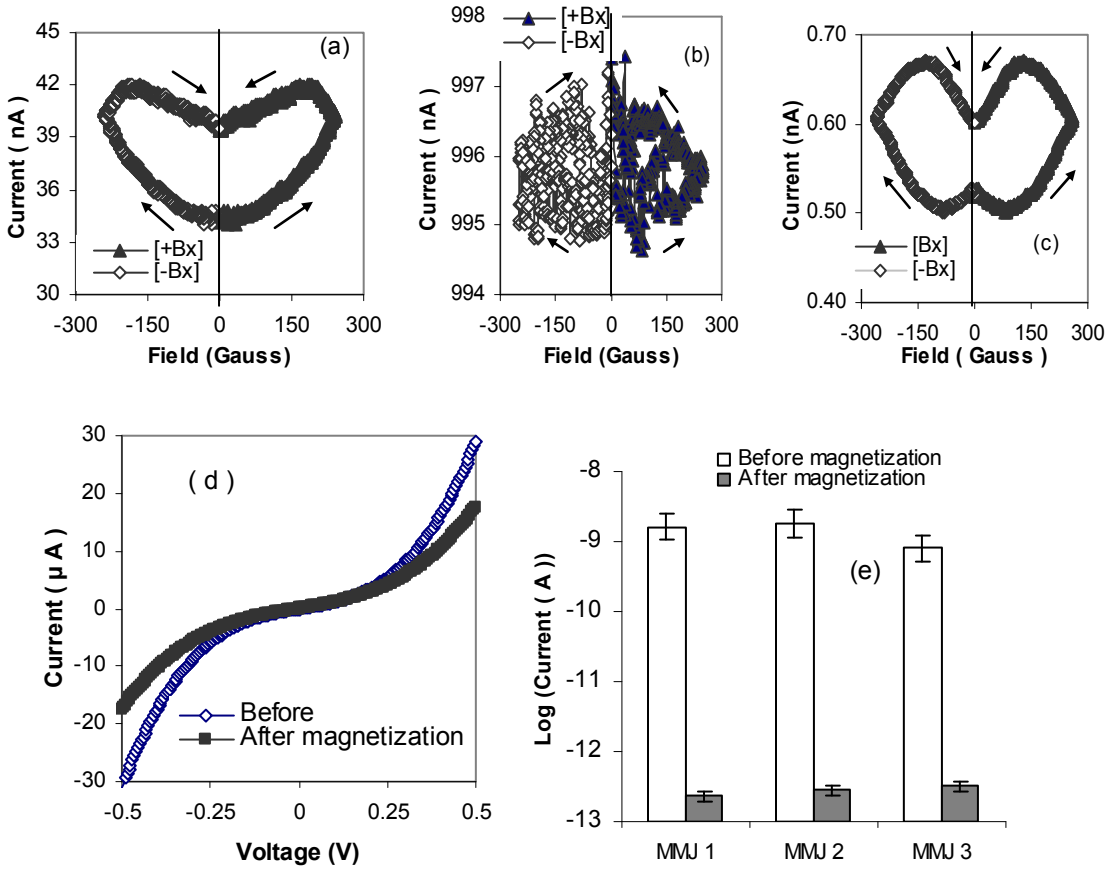

Figure 7.13. Effect of small (<300 Gauss) and large (4.5 kGauss) magnetic field. At 50mV current measurement while inplane magnetic field is changing between ±250 Gauss for bare F-MEME (a), F-MEME with MMC in high (b) and low (c) current state. Arrows represent start and end of a magnetization step. Transport study before and after magnetization, in 4500Gauss inplane field for 1 hour, of bare F-MEME (d) and MMC treated F-MEME.

7.4.3 MFM and magnetization study

In order to test the hypothesis that magnetic molecular clusters induce strong magnetic ordering in the electrodes and concomitantly decrease the device current, MFM, magnetization and ferromagnetic resonance measurements were performed as described in chapter 6. Firstly, we explored the difference in magnetic ordering of two electrodes when a junction settled in a low current state. MFM, which exhibit relative magnetic moments of electrodes in terms of magnetic image color contrast [196], reveled that magnetic images of two electrodes exhibited unambiguous higher contrast, figure 13(b) as compared to electrodes of bare F-MEME, figure 7.13(a). It is easy to see that in the junction area net contrast is smaller; it is presumably due to the fact that oppositely aligned magnetic layers, separated by 2nm Alumina, produce net magnetic signals which are the difference of the net magnetic moments of two electrodes. MFM contrast on microscopic leads over a large area signifies the strong molecule- mediated interaction between two electrodes. When we performed the MFM study on the F-MEME dots after molecule attachment, we found that most of the dots exhibited almost nil magnetic contrast under the identical experimental conditions, for details see chapter 6. In figure 7.13 (c) the rightmost dot is showing usual color and is unaffected by the molecular channels. We have also observed that different magnetic ordering near the junction area, with respect to rest of the electrode, affects the electrode resistance, appendix A2.

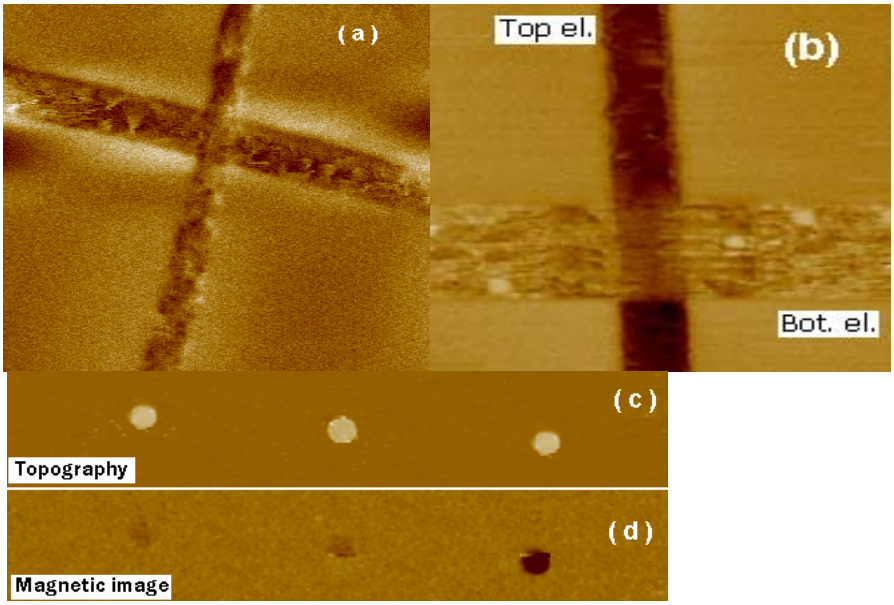

Figure 7:14:. Magnetic force microscopy image of a bare F-MEME (a) and after the molecule attachment and in sub pA state (b). Morphology (c) and magnetic image (a) of three F-MEME dots after magnetic molecular cluster attachment.

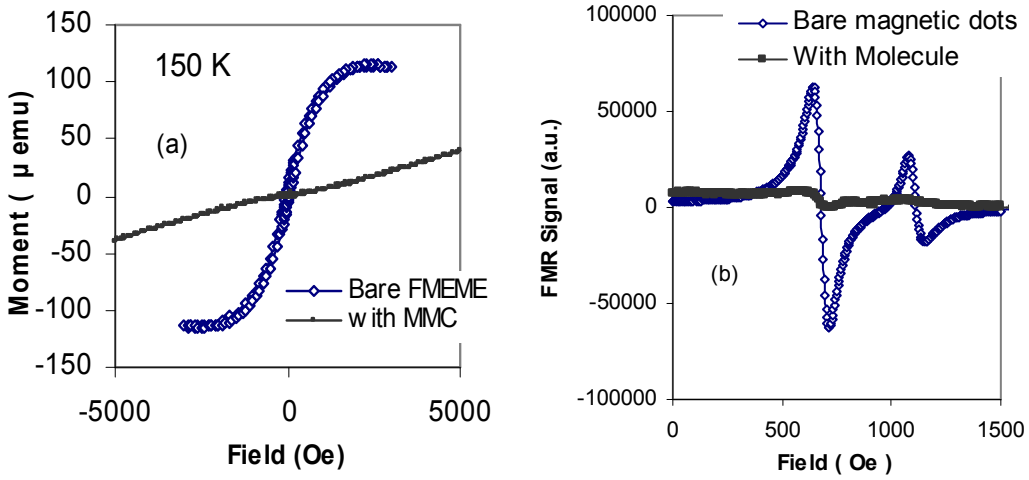

Figure 7.15. (a) Magnetization study of F-MEME dot pattern before and after MMC attachment at 150K. (b) Ferromagnetic resonance study of F-MEME before and after magnetic molecule attachment at RT.

To further probe the reason behind the difference in magnetic contrast of two electrodes after MMC attachment on F-MEME, magnetization and ferromagnetic resonance measurements were performed. Samples with F-MEME dots (~7000-14,000 dots each of ~3 μm diameter and [Ta/Co/NiFe/AlO_x/NiFe] configuration) were prepared in order to maximize the signal intensity from ferromagnetic metals. Details of magnetization and ferromagnetic resonance study on F-MEME dot patterns are furnished in chapter 6. Both studies clearly suggest the emergence of extremely strong antiferromagnetic coupling between ferromagnetic electrodes of F-MEME due to molecule attachment. Before addition of molecules, the dots were weakly antiferromagnetic, exhibiting a saturation magnetization value of ~1.0×10^{-4} emu. After cluster addition, a dramatic drop in the magnetic moment was observed (~90%) consistent with antiferromagnetic alignment of the top and bottom NiFe layers.[188]

In ferromagnetic resonance study two modes, acoustic and optical, of F-MEME dots almost disappeared from the spectra when magnetic molecular clusters were bridged on the exposed edges of the F-MEME dots. A related theoretical study has shown that when interlayer ferromagnetic coupling between two layers crosses a critical limit then, two layers get aligned antiparallel to each other. In this situation, the weaker mode flattens out and the stronger mode shifts to higher resonance field.[191] We conjecture that new resonance position for the molecule treated F-MEME dots is beyond the range of magnetic field we could study on our samples. From

our magnetic study we conclude that magnetic molecular cluster induced antferromagnetic coupling, which in turn contributed towards producing ~6 orders of current suppression.

7.5 Discussion:

We have observed 3-6 orders current suppression on ferromagnetic-multilayer edge molecular electrode (F-MEME), typically a magnetic tunnel junction, after the attachment of magnetic molecular clusters (MMC). Spin dependent transport of a magnetic tunnel junction strongly depends on the relative direction of magnetizations and degree of spin polarization of two electrodes.[18] Since current suppression is observed for the complete device comprising molecular transport channels and ~25μm^2 tunnel junction area, we surmise that it is only possible when two ferromagnetic electrodes are anti-parallel to each other and highly spin polarized. Other possibilities of defining current suppression, in terms of quantum interference among tunneling paths within a molecular magnet[30] and antiferromagnetic ordering on a molecular channel allowing >6 order resistance change due to magnetic field,[30] cannot describe the shutting down of transport via planar junction.[32]

In a magnetic tunnel junction, comprising ferromagnetic layers with~40% spin polarization,[196] sufficient population of minority spins is present close to the Fermi level.[17] Minority spin can produce significantly high transport even when majority spins of two ferromagnetic electrodes are in an anti-parallel state.[26] In magnetic characterization of F-MEME, details in chapter 6, we have observed that MMC produced strong antiferromagnetic inter-layer exchange coupling. Strong interlayer coupling was also found to decrease the magnetic contrast of F-MEME dots. Disappearance of magnetic contrast[196] is consistent with the cancellation of magnetization of one layer by the magnetization of another layer, at 2nm distance. In order to calculate the value of spin polarization, required to observe ~3 order current decrease in the present case, we assume that the highest current level after molecule attachment on F-MEME current level is similar to the case when two electrodes are parallel to each other; after MMC attachment F-MEME current is 3 order smaller at RT and two ferromagnetic electrodes are anti-aligned. Current of a magnetic tunnel junction in parallel (I_P) and antiparallel state (I_{AP}) of electrode can be given by $I_P \propto (D_\uparrow^2 + D_\downarrow^2)$ and $I_{AP} \propto 2.D_\uparrow.D_\downarrow$, respectively.[81] Where $D_\uparrow$ and $D_\downarrow$ are the density of spin up and spin down electron in the magnetic electrode; expression for spin polarization (P) is $(D_\uparrow - D_\downarrow)/(D_\uparrow + D_\downarrow)$. For I_P= 1μA and I_{AP}=1nA, value of P comes out to be >99.999 %. This level of spin polarization is completely unprecedented and would be an important breakthrough for spin-electronics.

What makes a regular ferromagnet highly spin polarized? What is the energy cost involved and from where is it sourced? These are the important questions to answer. Total energy of a ferromagnet is the sum of Heisenberg energy, dipolar energy, magnetic anisotropy energy and Zeeman energy.[191] The last term, Zeeman energy, also depends upon the external energy.[46] Degree of spin polarization in bulk ferromagnetic metals is essentially defined by the energy gap between spin-up and spin-down bands, known as Stoner splitting and it is akin to Zeeman splitting.[191,196] For instance, in Fe stoner splitting and spin polarization are ~1.4eV and ~40%, respectively.[196] Enhancement of spin polarization will require a larger splitting; for larger splitting one has to supply required energy by external means, generally in the form of a magnetic field.[46] However, it is worth noticing that we did not apply magnetic field on molecule treated F-MEME to produce any energy splitting. It is believed that interlayer coupling effectively acts as an external field.[201] Our molecule provided localized density of states amid tunnel barrier; molecular transport analysis suggested that for molecular channels barrier thickness was found to be ~1.2nm, as opposed to 2nm barrier thickness of bare F-MEME.[40] In this case, molecular array appear to work as an additional electrode inserted at the center of alumina barrier, barrier thickness after molecule attachment is ~1nm. According to Slonczewski's model[94] interlayer exchange coupling (J) via insulator is given by[186]:

$$J = \frac{\varphi_B k^3 (k^2 - k_\uparrow k_\downarrow)(k_\downarrow - k_\downarrow)^2 (k_\downarrow + k_\uparrow)}{\pi^2 d^2 (k^2 + k_\uparrow^2)^2 (k^2 + k_\downarrow^2)^2} e^{-2k.d} \qquad (7.1)$$

Here, $k_\uparrow$ and $k_\downarrow$ are the wave vector for the spin up and spin down electron in ferromagnet, wave vector for the electron in tunneling barrier is given by $k = \sqrt{2.\varphi_B.m}/\hbar$, where, φ_B is barrier height, m is mass of electron and $\hbar$ is plank's constant. For the NiFe(80% Fe) metal, which is in direct contact of molecular channels, we conjectured that using bulk parameters for the Fe is reasonable. For Fe, $k_\uparrow \approx 1.09 Å^{-1}$ and $k_\downarrow \approx 0.43\ Å^{-1}$.[186] The distance between the two nearest electrodes is d. According to our previous study the barrier thickness (Barrier height) for the alumina and molecular barrier are 2nm (1eV) and 1.2nm (0.8eV), respectively. This relation clearly produces ~4 orders enhancement, from -7.36×10^{12} erg/cm^2 to -7.33×10^{16} erg/cm^2, in coupling energy when barrier thickness (barrier height) was reduced from 2nm (~1eV) to 1.2nm (~0.74eV). It should be noted that calculated values very different from the experimental values and only appear useful for the qualitative understanding. We find it difficult to conclude that calculated increase by ~4orders is the reason behind dramatic change in transport and magnetic

properties of F-MEME; in the experimental studies, reducing down the MgO barrier thickness to 0.5nm though produced a significantly strong, yet measurable, antiferromagnetic coupling, but no remarkable change in magnetic properties of the magnetic electrodes was reported.[186]

The important point to note is that change in interlayer exchange coupling strongly depends on the nature of the spacer. Semiconductor spacers have shown interlayer exchange coupling strength to a much higher extent than that seen with insulator of similar thickness.[186] Slonczewski's model did not incorporate the important details, such as the degree of spin-orbit coupling and hyperfine splitting of the barrier, in calculating interlayer exchange coupling.[17] Spin orbit-coupling and hyperfine splitting are significantly different for organic molecules in comparison with insulators.[26,27] Another important aspect which can make a strong difference is barrier height of the spacer between the two nearest densities of state partaking in transport. Barrier height between molecular level and metal Fermi level is observed to be affected by the image charges on the metallic electrodes, induced by the charged molecule.[35]

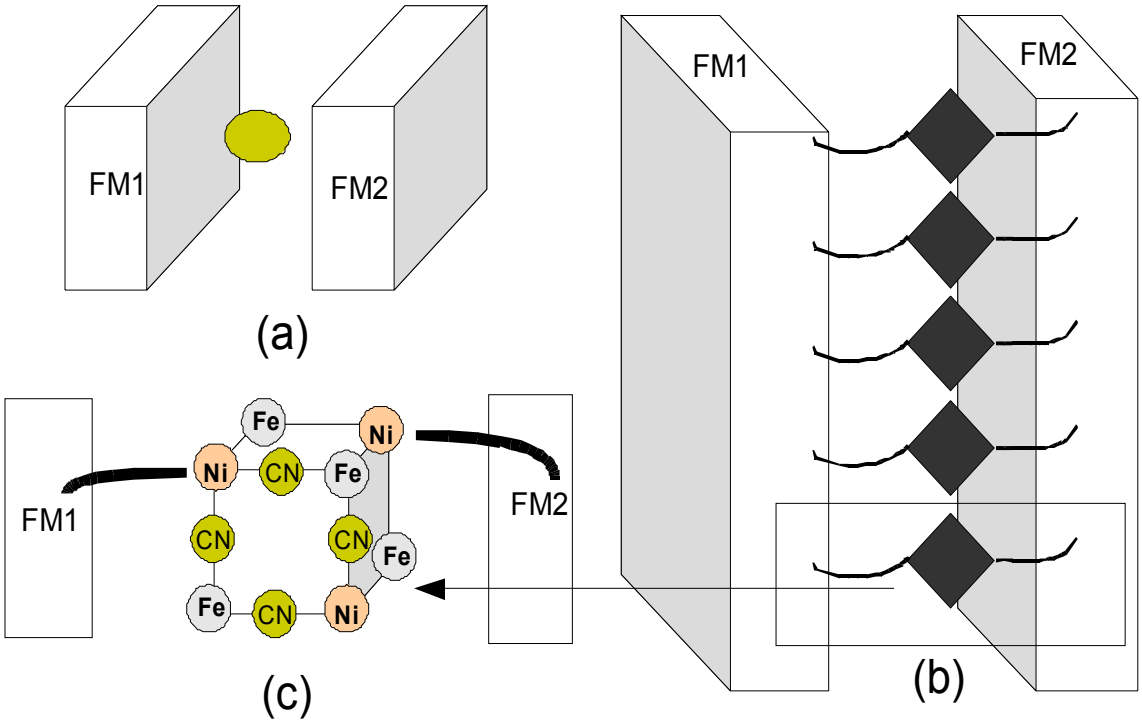

Figure 7.16: (a) An impurity between two metal electrodes, (b) molecule between two metal electrodes but only at the edges. (c) One slice of (b) showing molecule between two electrodes, molecules structure is simplified for clarity, all the ligands, H bonds CN bond (other than the front face of cluster cube) omitted.

A recent study discussing the role of atomic impurities around the center of the tunnel barrier, figure 7.16(a), producing energy level close to the Fermi level, exhibited an enhancement

in exchange coupling energy by ~3 orders.[95] It was shown that the effect of impurities on the magnetic tunnel junction transport is additive in nature.[95,202] Importantly, it was found that spin transport is indifferent towards the lateral coordinates of impurities, in the plane parallel to the electrodes.[202]

We surmise that 10,000 magnetic molecular clusters attached on the exposed edge of the F-MEME are akin to well defined impurities, whose position can be precisely controlled, figure 7.16(b-c). Since the molecule in our case also expected to possess a net spin state,[3] a strong antiferromagnetic coupling is expected to arise from the spin dependent hybridization of molecular level with the spin density of states of ferromagnetic electrodes.[56] Experimental observation of large Kondo splitting, in C_{60} molecule between two ferromagnetic electrodes, was explained in terms of a magnetic field arising from the spin-fluctuation induced exchange coupling between two ferromagnetic electrodes via molecular level.[13] Spin fluctuations have also been observed to play an important role in modifying the magnetization of 2D ferromagnetic layers coupled by a nonmagnetic layer; however;[197] in our case each ferromagnetic electrode is ~10nm thick and hence does not fit well to 2D description. Strong interlayer exchange is likely to modify the band arrangement of ferromagnetic electrodes;[99] theoretical calculation to quantify the effect of magnetic molecular cluster on the spin polarization of ferromagnetic electrodes is beyond the scope of this work.[99,201] However, according to our estimation, lower bound of molecule-induced strong antiferromagnetic coupling between two electrode is ~20 erg/cm^2; which is ~ 2 orders higher than the maximum exchange coupling observed via an 0.5nm thick insulator.[186] In summary, there are a number of promising theoretical works[97,99] which deals with the correlation between spin of metal electrodes and spin of molecules which can provide a basis for the explanation for the observed high spin polarization in this study.

We have also attempted to calculate spin polarization using Slonccczewski's model as given below.[17]

$$P = \frac{(k^{\uparrow} - k^{\downarrow})(k^2 - k^{\uparrow}k^{\downarrow})}{(k^{\uparrow} + k^{\downarrow})(k^2 + k^{\uparrow}k^{\downarrow})} \tag{7.2}$$

This model connects the spin polarization to the barrier height of tunneling barrier. Our previous study suggests that molecular transport is dominated by the alkane tunneling barrier possessing ~0.8eV barrier height; tunneling to and from the core of molecule via alkane tether was found to be the slowest step.[40] The value of polarization, assuming the same effective mass of electrons for the alumina and tunneling barrier and using the rest of the parameters as mentioned in the calculation of exchange energy, we found that value of spin polarization for the alumina barrier

(~1eV) and alkane barrier (~0.74eV) was -12% and -20%, respectively. We see that this model predicted significantly different spin polarization before and after molecule treatment. However, we are unable to explain the origin of extremely large degree of spin polarization due to molecular clusters, 99.99%, using this conventional approach. Thus it becomes very important to look at the available electronic states of the conducting metal cluster.

The cluster core is composed of alternating Ni(II) and Fe(III) metals at the corners of a cube bridged by a cyano group that induces ferromagnetic ordering at ~10K. Importantly both the Ni and Fe have available electronic states, of only one spin orientation, to tunnel into, figure 7.17(c). Ni(III) and Fe(IV) are not stable oxidation states, so only electron addition to the cluster (i.e. electron transfer not hole transfer) is plausible. In particular the Fe(III) can be reduced to Fe(II) to have a stable conduction state (with well defined spin state) before the electron can tunnel out of the system to the second electrode. From electrochemical data on the molecular clusters in solution, it was found that the oxidation potential of the Fe(II)/Fe(III) couple is 0.32 V vs. Ag/AgCl electrode. The cluster also shows a 200mV charging energy to access the next oxidation state. The resulting relative band structure from known work functions is shown in figure 7.18. Two features are of particular importance. 1st the charging energy of the 4+ molecule brings the molecular HOMO down 0.8V, and is very close to the metal leads Fermi level. Secondly since the oxidized states are not stable, the electrons cannot leave the cluster, hence while in equilibrium the Fermi level of the HOMO must be at or below the Fermi level of the metals resulting in band bending of the alkane barriers. A particular interesting phenomena is that when the molecule has an added electron charge, the energy will be raised ~200mV. This is not too far from the observed thermal activation energy of 300mV seen in chapter 3. This geometry, well defined spin states, and dynamic energy level changes allow for the cluster to act as a spin filter or pump, possibly accounting for the high degree of spin polarization.

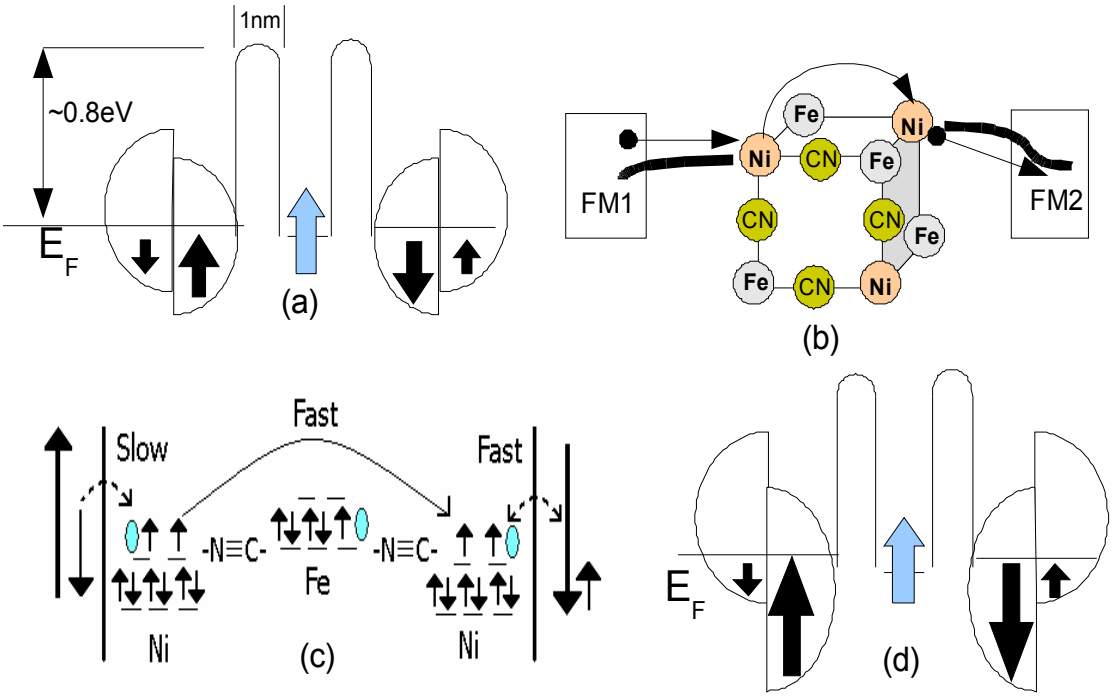

Figure 7.17: via molecular state. Right after MMC attachment molecular device in μA current level (a), exchange of spin polarized electron between two electrodes via molecule (b) electronic level description of molecule producing spin polarized electrodes (c) resultant spin polarized ferromagnetic electrodes in nA/pA current sate of molecular junctions.

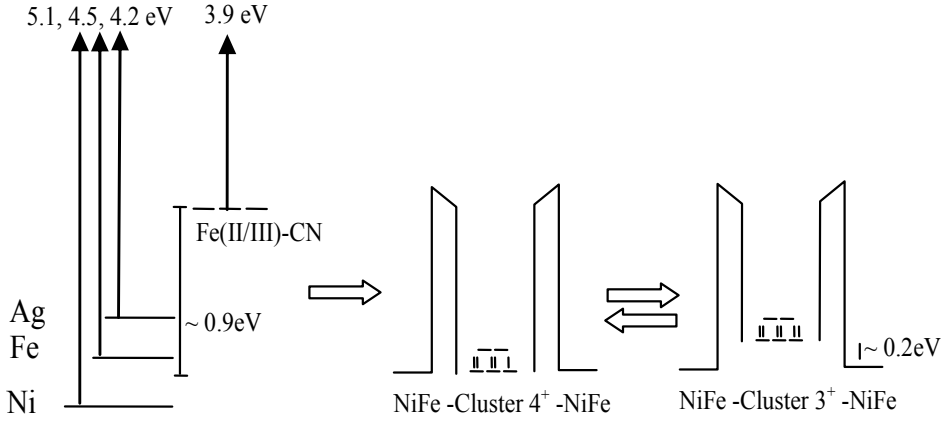

Figure 7.18: (a) Approximate band diagram deduced from electrochemical redox potentials. (b) A charging energy of 0.2eV/charge is seen for the cluster, thus for 4+ cluster, the energy level is reduced ~0.8eV. Since oxidation of Ni(II) and Fe(III) is not possible, band bending would bring molecular to Fermi-levels of contacts. Only a single Fe(II/III) d-orbital state is shown for clarity. Charging of cluster during conduction would raise energy level ~0.2eV above ground state.

Dramatic change in magnetic and transport properties of F-MEME is only seen when magnetic molecular cluster with well defined spin state was bridged along exposed edges, figure 7.17 (b). Two Ni atoms of the core cube of MMC are expected to connect to the Ni atoms of ferromagnetic layers via alkane barrier, in an ambient condition NiFe was shown to possess oxidized Fe and elemental Ni.[114] An alkane tether, being an organic molecule, is known to possess long spin coherence length and time, hence making spin exchange between ferromagnetic electrodes via molecular levels much more effective than that via alumina.[26] Bare F-MEME possessed weak antiferromagnetic coupling; we surmise that two Ni atoms of cluster core, directly connected to the ferromagnetic electrodes, have empty space for the spin down electron only, as shown in figure 7.17(c) . Electrode, where spin down (spin up) electron are in the majority, will transfer the electron spin to the Ni of molecular core with a higher (lower) rate.[17,18] Since two Ni atoms are coupled to each other through superexchange[9] CN- and Fe atom of the core, a net spin polarized flux is expected to flow from one electrode to another unless an equilibrium, producing highly spin polarized ferromagnetic layers, is reached, figure 7.17 (d). We surmise that summing the spin-dependent wave-function overlap[92] of two electrodes via 10,000 molecular clusters produces a magnitude of overlap sufficient to produce situation for super exchange.[9] Under this condition, new equilibrium will require two electrodes to be anti-parallel with each other and with a high degree of spin polarized.[46]

7.6 Conclusion

We have successfully prepared molecular spin devices by attaching the magnetic molecular cluster on the exposed edge of a multilayer edge molecular electrode. 10,000 molecular bridges between two ferromagnetic electrodes of a 25μm^2 planar junction area, suppressed the current by 3-6 orders below the leakage of bare tunnel junction. High degree of spin polarization and unprecedented molecule induced antiferromagnetic coupling is found to be the basis of dramatic change in transport. External energy forms, light, heat and magnetic field, produced unambiguous effect on transport. Spin dependent hybridization of the magnetic electrodes with the well defined spin state of the molecular cluster, appears to be the driving force behind the drastic change in spin polarization. To make molecular device switchable between two or more current states different configurations of the multilayer's and the use of molecular clusters are recommended. Our design, involving photolithography and widely-available thin-film deposition method, offer a new opportunity to produce robust and highly versatile molecular spin devices efficiently and economically.

Chapter 8

Conclusion

This dissertation showed the successful realization of novel molecular spin devices using a multilayer edge molecular electrode (MEME) design. MEMEs were prepared by customizing a classic tunnel junction structure by spanning insulator film with molecular complexes at the exposed face of patterns. The key steps of MEME fabrication are: (a) fixing the molecular dimension gap between two thin film metal electrodes, (b) producing exposed edge(s) where distance between two meal electrodes is equal to the thickness of ultrathin insulator and (c) bridging of desired molecular channels between two metal electrodes of MEME to transform it into a molecular device, figure 8.1.

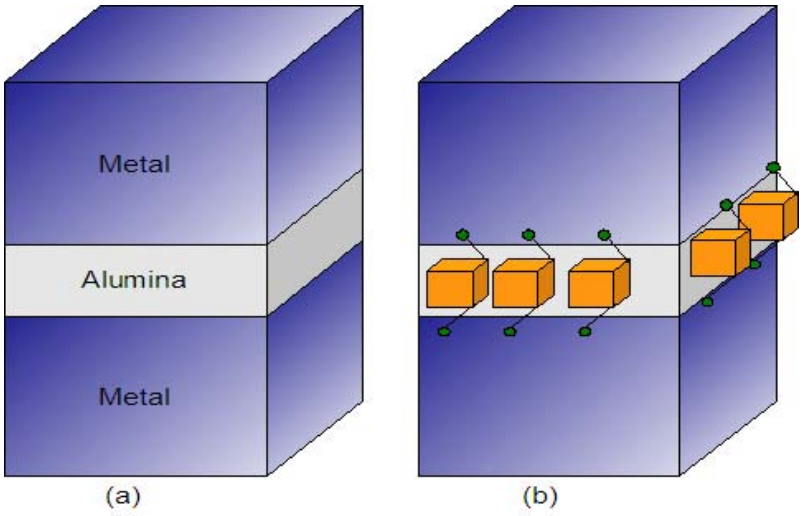

Figure 8.1: A MEME before (a) and after (b) the bridging of magnetic molecular clusters.

8.1 Advantages of MEME devices

(i) Determining the true charge and spin transport characteristic of a molecule: Since we prepare a robust tunnel junction prior to the bridging of molecular channels on the exposed edge, one can compare the transport characteristics of the molecule with respect to the transport attributes of the host MEME tunnel junction. This attribute is one of the foremost drawbacks of present molecular devices.

(ii) Easy approach to produce molecular dimension gap: In this work we used thin film deposition and oxidation to produce insulator of molecular dimension gap. Thin film deposition and oxidation are highly matured and controllable to

produce Angstrom-scale precision. A summary of other strategies to produce nano-gap is provided in chapter 4.

(iii) Economical and integrable device-fabrication scheme: For the MEME fabrication we only utilized photolithography and thin film deposition as primary tools. These tools are widely available around the world and regularly used in semiconductor technology. Any practical device resulting, such as molecular spin valve, from our approach is expected to reach the commercial stage rapidly. Institutions not equipped with hi-tech equipments can perform research using MEME design to contribute in the advancing field of molecular electronics.

(iv) Freedom to choose a variety of metal electrodes: MEME tunnel junction can include any metal on which a good quality ultrathin insulator can be grown. This study used NiFe, Ta, Cu, Pd, Au, and Si. It should be noted that most of the reported molecular devices utilize Au as a primary electrode metal, due to its ability to mechanically deform into break junctions and its inherently clean surface.

(v) Molecular electronics to molecular spintronics: In this dissertation we have prepared a large number of molecular spin devices simply by using ferromagnetic metals as top and bottom metal electrode coupled with a transition metal cyano-cluster. This enabled us to make novel molecular spin devices for the first time and subsequent observations of a number of surprising phenomenons arising from metal-molecule interaction.

(vi) Molecule being on the exposed part of MEME can interact with light and chemical: Molecules on a MEME are in the exposed region where light radiation and foreign chemical can reach. In the chapter 3, a new form of chemical sensing was demonstrated with the chemical displacement of top electrode contact. This attribute adds enormous applications for photo-active molecular devices, e.g., molecular photovoltaic cells, and chemical and biosensors.

8.2 Achievements of the present doctoral study:

i. Multilayer edge molecular electrodes were prepared. Two key challenges were: (a) to grow high quality alumina, (b) and to expose the edge(s) of MEME for the bridging of molecular channels. In order to grow the high quality alumina effect of mechanical stresses on the electrical properties and the device life was extensively studied, chapter 2. Using the optimized condition for the growth of alumina, MEME were prepared, chapter 3. For exposing the edge of a tunnel junction, two approaches were adopted. In one approach a tri-layer with metal-insulator-metal pattern was ion milled to produce an atomically sharp vertical cut. At the ion milled produced edge a minimum gap between two electrodes was equal to the insulator film thickness. However, due to the stresses introduced during ion milling, this approach was only used for performing the control experiments. In another approach, photolithography-liftoff was utilized, chapter 3. In this methodology a bottom metal electrode alumina and top metal electrode were deposited through the same photo resist window. The idea was to keep the lateral dimension of the alumina and the top electrode the same; in this case the minimum gap between the two metal electrodes is equal to the thickness of ultrathin alumina insulator, figure 8.1(b).

ii. Simplification of MEME fabrication scheme: The success of a MEME fabrication scheme is critically dependant on the thickness, quality and the edge profile of the alumina insulator. We produced a simpler version of MEME electrodes just by oxidizing bottom electrode TaOx through well controlled plasma oxidation method, chapter 4. Under this approach, the need for depositing Al was replaced with the utilization of an nm thick segment of bottom electrode of an oxidizable metal, Ta in the present case. Rest of the fabrication was the same as for photolithography-liftoff produced MEME. Though the overall device current was lower due to Ta contacts, the molecular transport mechanism from this scheme corroborated with the MEME based on alumina insulator.

iii. Photovoltaic effect of Ta/TaOx/Ta: During our attempts to produce TaOx based molecular electrodes, it was found that Ta/TaOx/Ta junction showed significant photovoltaic effect with ~9% energy efficiency, Chapter-5. A ~3nm TaOx with high graded density of atomic defects was found to show remarkably high light absorbance. The graded density profile of atomic defects in TaOx produced an inbuilt electric field to separate the electron-hole pairs, produced at a defect site within TaOx barrier. However, TaOx based photo-effect was found to be transient; heating and prolong high intensity light exposure deteriorated the energy conversion efficiency. Significant process optimization will be needed to make use of this simple and economical approach for producing thin-film photovoltaic device.

iv. Molecular coupling of ferromagnetic metal electrodes: It is widely known that molecular energy levels, charge state and charging energy change significantly when a molecule is placed in a nanogap between two metal electrodes. We obtained unambiguous evidences which confirm that molecules in a nanogap between two magnetic metals produced dramatic change in the transport and magnetic properties of magnetic electrodes at room temperature, chapter 6. SQUID based magnetization, ferromagnetic resonance and magnetic force microscopy showed that magnetic molecular clusters when attached to the patterned magnetic dots of Co/NiFe/AlOx/NiFe thin films produced an extremely strong unprecedented antiferromagnetic coupling between two ferromagnetic electrodes. Molecules induced strong antiferromagnetic coupling on the edge region of a dot pattern that propagated over the complete planar area of the electrode, presumably due to the inter-atomic Heisenberg exchange coupling inherent within ferromagnetic thin films. The coupling energy is an unprecedented 20 ergs/cm^2 for the entire junction and could be several orders of magnitude higher if only the molecular junction area is considered. The extremely large energetics for molecular coupling suggests that there is likely an important role of spin-polarized electrons

delocalized through out the electrodes, chapter 7. We were unable to untangle the exact mechanism behind this observation; dedicated quantum mechanical calculations are required to elucidate the phenomenon we observed. However, there are a number of groups who are exploring the similar effects in analogous system of strongly coupled quantum dots.

v. Molecular spin devices with 6 orders of magnitude resistance change: The ultimate aim of this doctoral study was to produce magnetic molecular junction showing molecule spin state dependent magneto resistance. In our journey to reach this aim we have came across several new insights and phenomenon. One of most striking observation was the ~6 orders current suppression due to the bridging of molecular clusters along the edges of a ~25 μm^2 magnetic tunnel junction at room temperature, chapter 7. This observation was on MEME dot with Co/NiFe/AlOx/NiFe configuration; dots with the same configuration underwent dramatic change in magnetic properties due to the magnetic molecular cluster. We found a strong correlation between the magnetic and transport properties of Co/NiFe/AlOx/NiFe, with and without molecular clusters. Numerous control experiments were performed to check the validity of our observation of molecule induced current suppression. High current state of the device could be reached by thermal treatment and low current state by incubation time, low temperature (77K) treatment, and strong applied field. We were unable to switch between current states with only the application of magnetic field to F-MEME devices with Co/NiFe/AlOx/NiFe configuration. However, we did find other configurations of MEME with softer magnetic layers that were more amenable for the magnetic field based switching but were difficult to study due to inherent instabilities, appendix A6.

8.3 Suggestions for future work:

i. During this doctoral study a simple and highly versatile molecular electrode fabrication scheme was realized. However, the cost of simplicity was the prolong struggle with the variability in process parameters. For instance, deposition rates of crucial films in sputtering, photo resist quality, and properties of molecules were found to change with time. A summary of the crucial issues for MEME fabrication electrode is given in appendix A.1. An effective way of keeping track of the variations in the parameters and their control will make MEME yield higher.

ii. Mechanical stress generated during ion milling was initially observed as a limiting factor in utilizing ion milling for the molecular electrode fabrication. A slower milling rate with a more suitable ion miller may be helpful in resurrecting this approach.

iii. Because damage or etching was observed for numerous samples during electrochemical attachment of the molecular clusters, it is necessary to further repeat key results and perform conclusive control experiments on active devices. The observation of such extreme magnetic coupling and magnetic polarization require a high level control on experimental parameters to discount any chance of experimental artifact. In particular for cross-junction devices, the integrity of top and bottom electrodes needs to be independently monitored while the device is in any of the low current states. In previous samples, line breaks prevented this. Although the 6x6 array of cross junctions allows for large numbers of samples to be screened, defects can couple devices in an uncontrolled manner (usually high current shorts). Isolated cross-junctions need to be examined for control experiments.

iv. For a deeper understanding of molecular conduction mechanism a low temperature study of molecular junctions comprising magnetic molecular cluster and nonmagnetic metal electrodes is critical. In particular we can measure the activation energy of the charging process of electrons tunneling into the molecular cluster.

v. Reducing the electrode planar area of the multilayer edge molecular electrodes is promising for producing low leakage current and magnetic field switchable molecular junctions. Smaller area magnetic features are typically less stable and more readily switched.

vi. Specially designed molecules for photo activated transport or current switchability is a potential research direction for converting MEME in optical devices. In particular, molecules that upon photoexcitation vacate and make available spin-state orbital would be able to act as a switchable spin filter.

vii. Molecules attached to multilayer edge molecular electrodes with an affinity for bio molecules or gases can help in transforming these electrodes into chemical and bio sensors. This can be achieved by either affecting the conduction through the molecule by shifting energy levels or by reversibly displacing one of the electrode tethers by steric bulk.

viii. Attempting various permutations of molecules and metal electrode configuration is likely to produce new insights about molecular charge and spin transport.

APPENDICES

Appendix A1

Key Parameters for Reproducing Multilayer Edge Molecular Electrodes.

For the successful realization of multilayer edge molecular electrode it is important to keep the track of following: (a) insulator film thickness (b) photoresist profile and photoresist quality for the clean lift off. (c) Molecular solution or molecules.

(a) Insulator film thickness: In our study we have mainly utilized alumina, formed by the plasma oxidation of a pre-deposited layer of aluminum. In the sputtering machine aluminum (Al) deposition rate is significantly different for the fresh and old target. Reason is associated with the nature of sputtering for the gun design we are utilizing and the sample position. Al is only removed from a circular region around the middle point of a target radius. Besides this, it was noticed that aluminum thickness is very sensitive towards the sample position (with respect to gun), gun angle and the substrate height. Aluminum deposition rate changes frantically for 1-2 minutes after the opening of the gun's shutter. A sudden hit or bump into the sputtering chamber during deposition also create unstable deposition conditions. Aluminum deposition is the critical step and hence should be done with stable plasma and consistent parameters. A periodic check of alumina thickness is highly recommended. Cross contamination, eroding Al target due to sputtering changes the sputtering rate. A reliably calibrated AFM was found to be helpful in measuring ~2 nm scale thickness.

(b) Photoresist quality is an important matter where exposed edge of a multilayer is produced through photolithography –liftoff method. It was experienced that the new photoresist or photoresist well before expiry date, produced higher yield of molecular junctions. Generally with the old photoresist, after liftoff photoresist persisted at the edge(s) of molecular junctions, precluding molecule to access the metal-insulator-metal exposed edge for establishing the molecular channels, figure A1.1. The edge profile of alumina grown in a photoresist cavity produced by a fresh photoresist, figure A1.2(a), produced minimal spike or notches on the side edges. Notch free edges of alumina helped maintaining the minimum gap between two metal electrodes equal to the insulator thickness. On the other hand expired or bad quality of photoresist produced over-cut profile at the photoresist edge leading to the creation of notches, figure A1.2(c). Notches make the effective distance between two electrodes to be more than the actual thickness of the alumina. For the good quality lift an undercut developing procedure and good quality photoresist are required.

It was found that exposing the sides of multilayer edge molecular electrode for the molecule attachment also depends on the photoresist thickness, used for the alumina and the top metal electrode. Dependence on photoresist thickness is associated with the directionality of aluminum flux reaching the substrate with photoresist layer. Aluminum flux reaches on the sample in a solid angle of ~46º, figure A1.3(a). This description hold good for the sputtering machine we utilized. Sample with a window in thick photoresist (~1μm) produced a failed tunnel junction; when an alumina grown in thick PR window is not covering the bottom electrode metal then subsequent deposition of top metal electrode directly touches the bottom electrode, figure A1.3(b-c). Reducing the photoresist thickness to 0.1μm yielded a series of good quality tunnel junction with ~1.8V break down voltage, figure A1.3(d-e).

(c) Magnetic molecular complex solution: Fresh molecular solution in dichloromethane solvent was effective in producing molecular junction. It was difficult to attach molecule with 1-2 month old solution. Dichloromethane produce hydrochloric acid under light. It was also noted that fresh molecular (1-2 months old) solution produced a shiny, smooth and continuous (rough and discontinuous) film at the end of electrochemistry step. Good quality molecules almost instantly dissolved in dichloromethane and THF solvent.

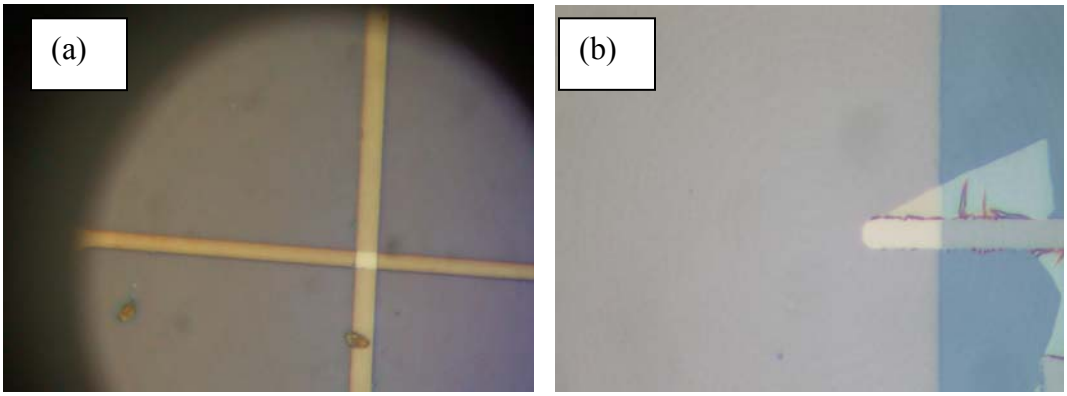

Figure A1.1: Micrograph of (a) a complete cross junction after the clean liftoff photoresist (b) persisting photoresist after 12 hours of liftoff along the edges top electrode where molecules were supposed to be hosted.

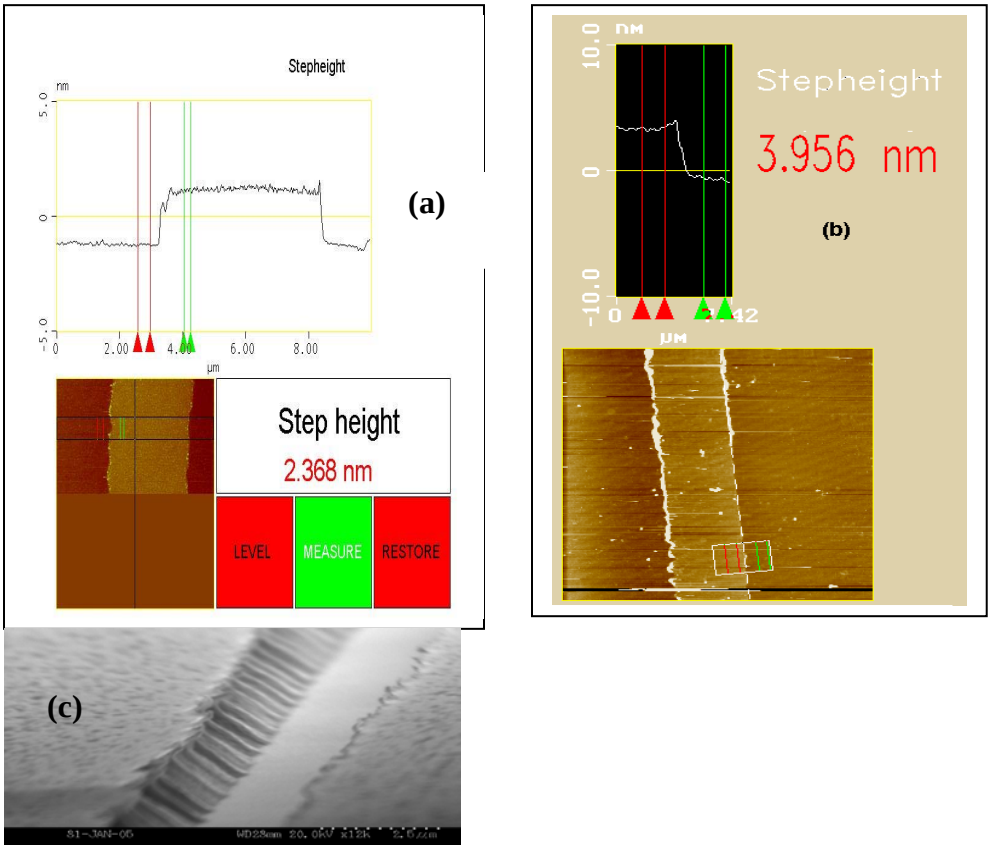

Figure A1.2: Step height measurement of alumina grown (a) with moderately eroded aluminum target (b) with heavily eroded aluminum target. (c) Photoresist profile to be avoided.

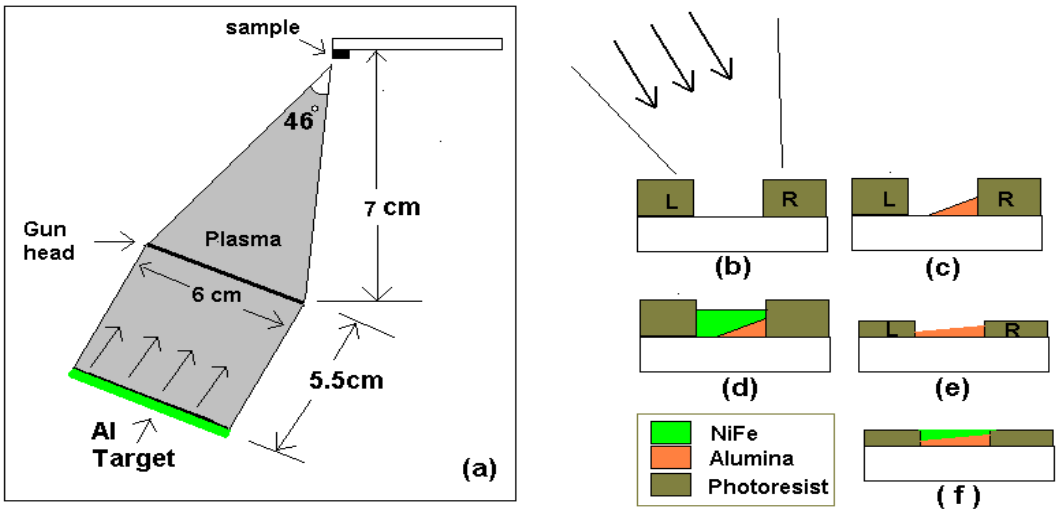

Figure A1.3: Effect of directionality of Al plasma and photoresist thickness: (a) In the sputtering chamber aluminum plasma hit the sample in a solid angle of ~46º degree (according to gun geometry and sample position). (b) Aluminum plasma impinging in a 1-2 µm thick photoresist window, (c) shadow effect of [L] photoresist wall avoiding the complete coverage of bottom metal electrode, (d) deposition of the top electrode make direct contact with bottom electrode to yield a failed tunnel junction. (e) 100-150nm thick photoresist wall allow aluminum plasma to cover bottom electrode more uniformly, moderate shadow effect is still likely (f) top electrode will not touch the bottom electrode.

Appendix A2

Stability of Bottom Metal Layers.

Multilayer edge molecular electrodes where cobalt metal was present in the bottom electrode at numerous occasion damages were observed after the electrochemical molecule treatment. We have carefully studied the damages to the junctions and their causes. There were mainly two type of devices configuration, dots and cross junction pattern, were studied. It was observed that when Co thickness was in higher side (7-12nm) damage to the bottom electrode was severe. We worried if etching of dots and cross junction may produce the effect which we found due to the molecules. Typical nature of damage to the dots and cross junction is showed in figure A2.1, and figure A2.2.

In the present study mainly, NiFe, Co and Ta metals were utilized. Chemical etching rates of the NiFe and Ta in the molecular cluster solution of dichloromethane solvent were too small to determine. However, Cobalt has <2nm/min dissolution rate in the molecular solution (in dichloromethane solvent). Cobalt also dissolves in regularly used MF-319 developer (~5nm/min). A layer of Co (5-7nm) under a protecting layer of 3-5nm of NiFe showed excellent stability against both, molecular solution in dichloromethane solvent and MF-319 developer. Aged molecular solution was found to be more aggressive, presumably due to the build up of hydrochloric acid getting produced from the light exposure of dichloromethane solvent. We generally performed molecular attachment through two electrode electrochemistry. Metals pads are found to be more aggressively attacked by the molecular solution in the vicinity of electrode contact point on metal pads.

A number of control experiments were performed to obviate the doubt that etching or material removal could cause the main findings (molecule induced magnetic ordering and current suppression). Current suppression phenomenon was observed with a molecular solution in THF solvent. Molecular solution in THF solvent was observed to be safe for the Co metal.

In some cases, it was found that multilayer got damaged near the edges. This observation was seen with those samples for which no undercut developing treatment was employed and over-exposure and over-developing conditions were used during photolithography; these conditions does not produce abrupt photoresist edges. After the multilayer deposition and liftoff, a photoresist layer is expected to persist. This photoresist layer undergo lift-off during electrochemical molecular treatment with aggressive molecular solution.

Here we present a case study to distinguish the nature of damages to the multilayer edge molecular electrodes from the lift-off of persisting thin PR under multilayer and from the

molecular solution. After a 6 minutes long electrochemical molecular treatment with a one year old molecular solution, a 100 μm dot of Ta/Co/NiFe/AlOx/NiFe was found to be damaged along the perimeter. One can see the ears/fold at the dot edge and a damaged area forming a uniform 2μm wide ring. Given to the fact that during photolithography step no method to produce undercut profile was applied, a photoresist profile of _/ shape along the edges will form; organic molecular solution has strong tendency to dissolve photoresist layer and hence will cause the damage seen in, figure A2.1(a). A 12nm thick Co, the only etchable part in our multilayer after the identical molecular treatment as used for the 100 μm dot did not produce any preferential damage along the edges.

An array of ~4 μm dots of Ta/Co/NiFe/AlOx/NiFe configuration after the treatment the aggressive molecular treatment partially or fully damaged the 10-15% of total dots; general appearance of dot population is shown in figure. A2.1(c). Ferromagnetic resonance study of dot pattern after the molecular treatment produced clear high intensity magnetic modes, (details of FMR in chapter 6). FMR modes unambiguously confirmed the presence of magnetic layers, figure A2.1(d). It is worth noting that magnetic dot samples on which FME modes disappeared after molecule treatment were found to be safe. AFM and optical microscopy were performed to monitor the sample quality. More importantly we could do reversible experiments which discard the possibility of etching away of all the dots, details in chapter 6.

Bottom electrode (Co/NiFe) is an important part of our multilayer edge molecular electrode. We attempted to produce the bottom electrode by the etching method. A stack of Co/NiFe was etched to produce 5μm wide bottom electrode. In number of cases, mainly when Co thickness was over 8nm, bottom electrodes were found to be damaged in localized area, figure A2.2(a-d). However, we did not find any cross junction where current suppression and damage to bottom electrode were concomitant. Moreover, we observed current suppression on tunnel junction was made up of Ta/Co/NiFe configuration; damage to Co/NiFe away from the junction does not affect the bottom electrode continuity as Ta is significantly inert towards molecular solution we used. Moreover, current suppression was also realized with few mm wide bottom electrode, idea was to keep the avid any disconnection due to any accidental damage arising from mechanical and chemical in nature.

Typical methodology used to make electrical contact with tunnel junction during molecular attachment is shown in figure A2.3(b). Figure A2.3(a) shows the actual micrograph of a cross junction array.

On an F-MEME with Co/NiFe/Alox/NiFe where molecular treatment produced current suppression bottom electrode resistance was noticed to be changing by orders. For instance in pA state of a molecular junction, the transport measurements through a bottom electrode were performed by electrically contacting opposite ends of bottom electrode. First few I-Vs appear in nA current state, however repeating of transport study produced the usual μA current level. However, junction transport remained unaffected. Change in bottom electrode transport can be due to improper electrical contact to the pads or there can be a zone on bottom electrode affected by the presence of cross junction in low current state. Such zone may produce high spin scattering for the in electrode spin transport. However, at this point we do not have conclusive proof to substantiate later hypothesis. The importance of this result is that it suggests that bottom electrode, the most sensitive part of a molecular junction, is electrically continuous, figure A2.4.

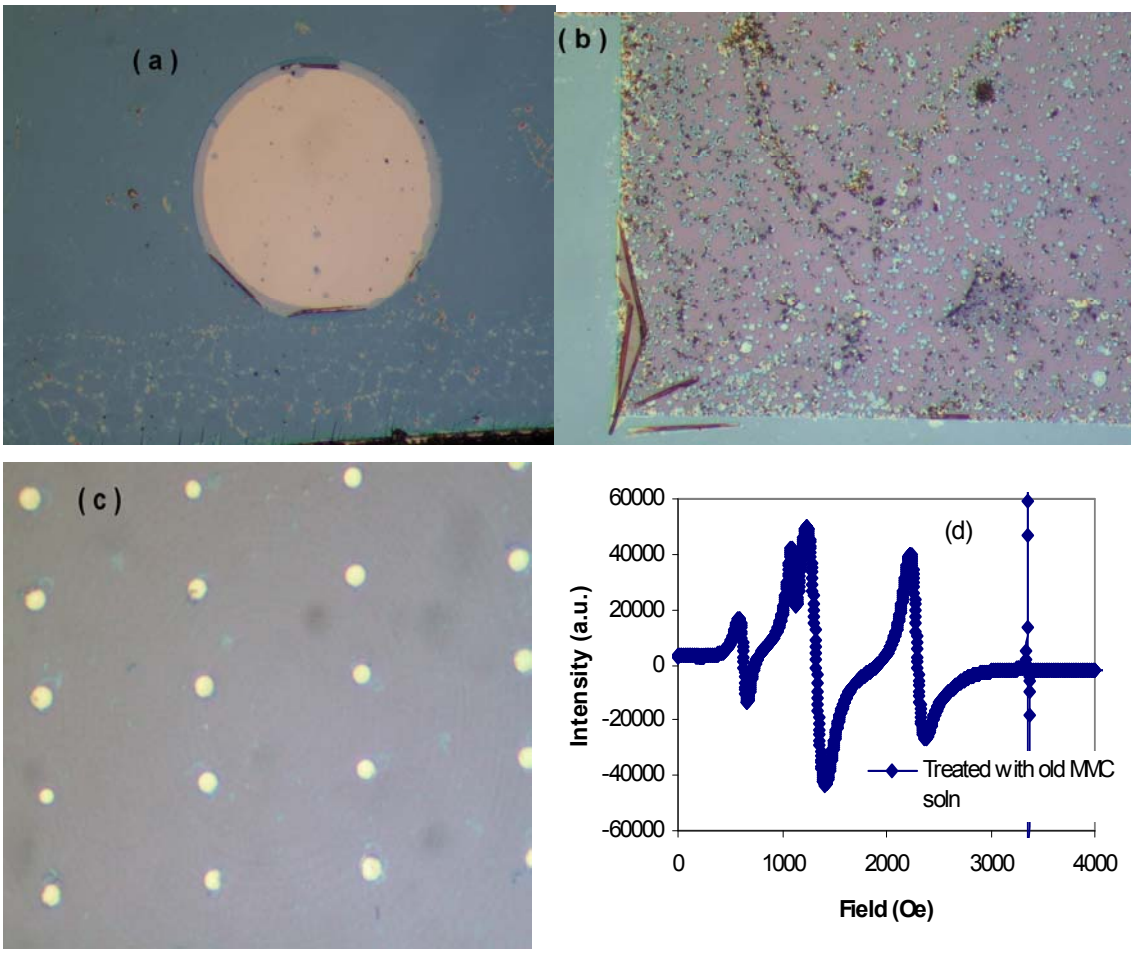

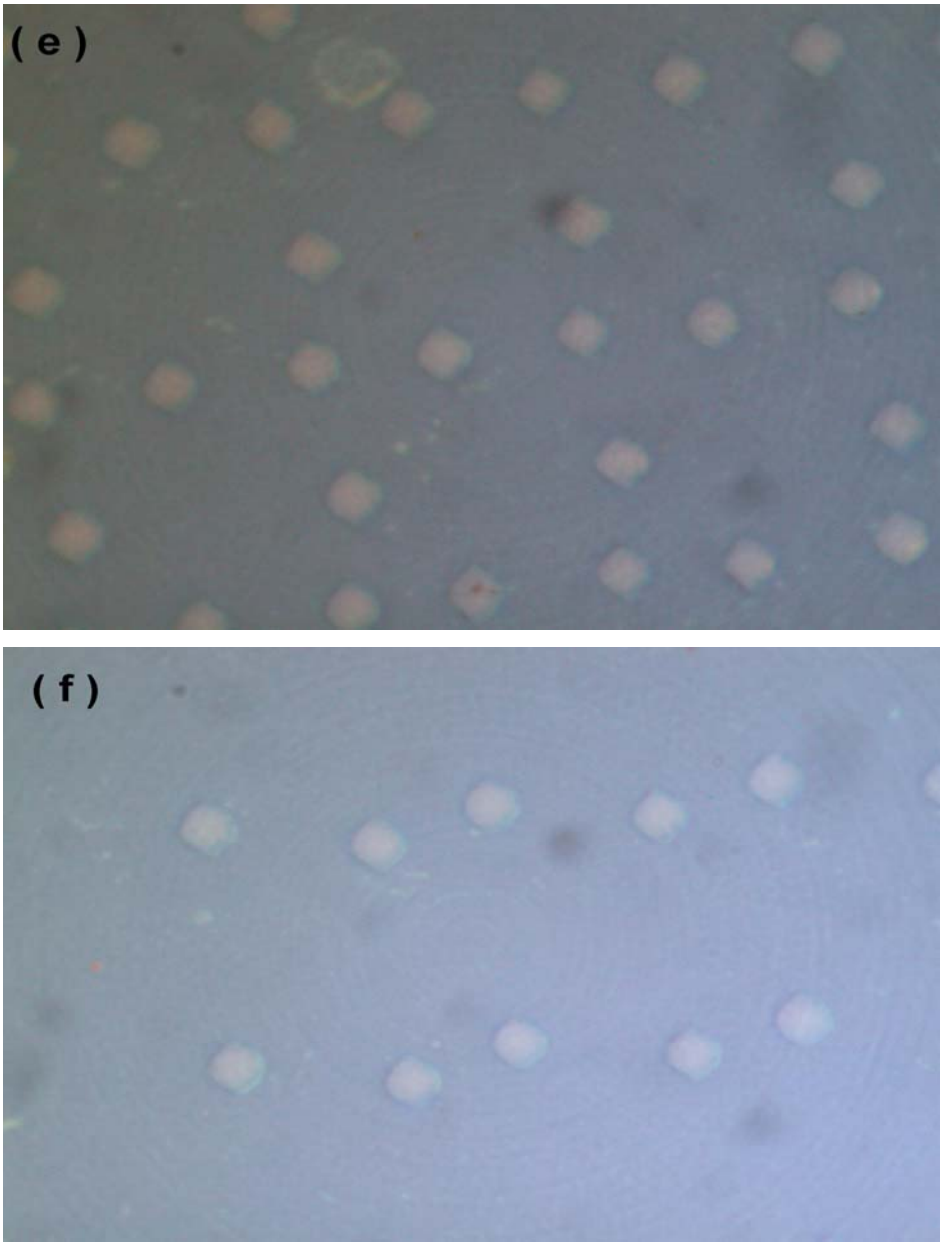

Figure A2.1: (a) ~2μm damage along perimeter of a 100μm Ta/Co/NiFe/AlOx/NiFe dot after 6 min of electrochemical molecular treatment with 1 year old molecular solution, (b) bare 12nm thick Cobalt after 20min of electrochemical treatment with same solution as used in (a), (c) 4μm diameter Ta/Co/NiFe/AlOx/NiFe after exactly the same molecular treatment as used in (a), (d) FMR spectra of dots shown in(c). (e) a cross junction whose bottom electrode was prepared by the electrochemical etching of bottom electrode (Co/NiFe).

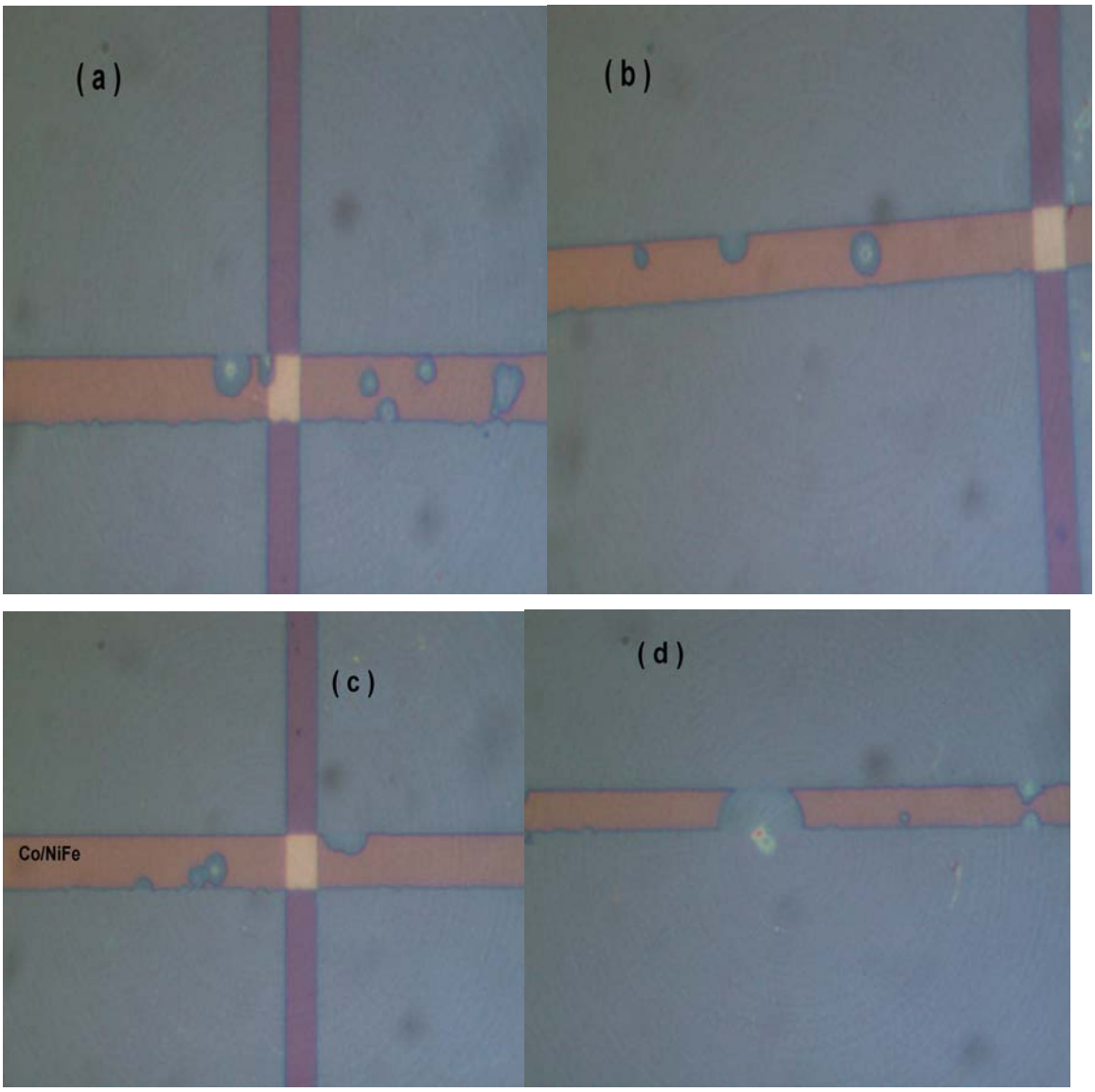
(a)
(b)
(c)
Co/NiFe
(d)

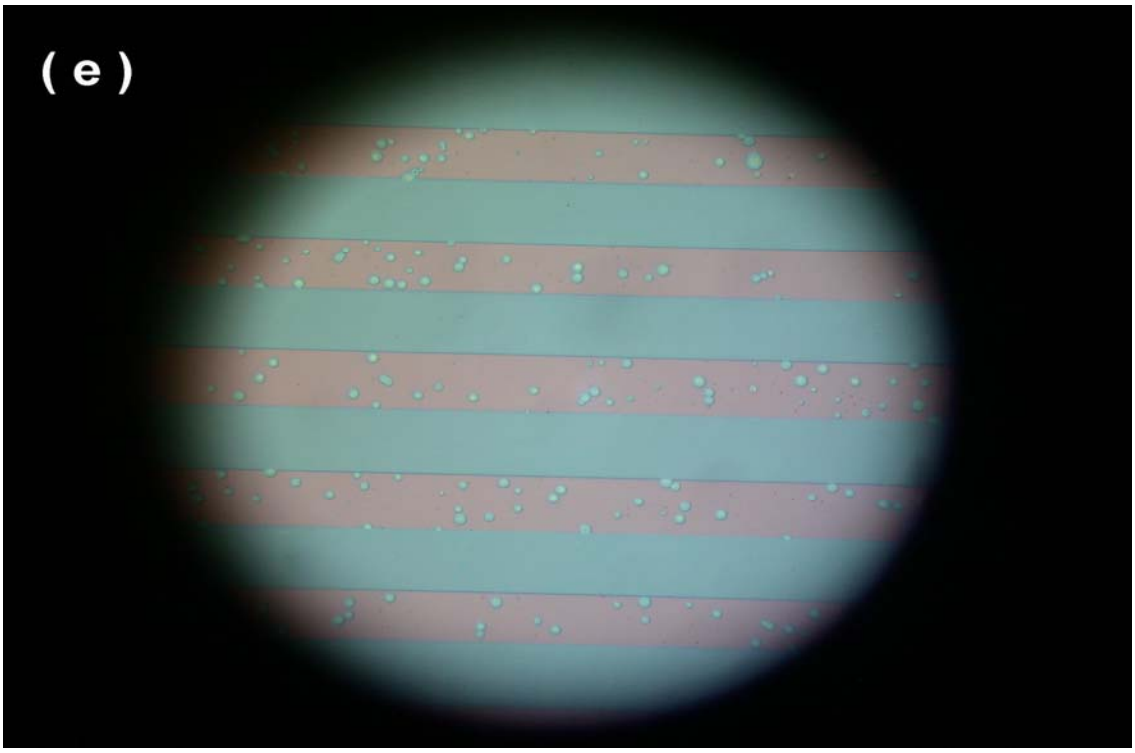

Figure A2.2 various examples of damaged electrode of a magnetic tunnel junction grown with Co/NiFe configuration. (a-d) are of typical cross junctions (e) is the bottom electrodes each of 100μm width. All the bottom electrodes were prepared by the chemical etching of a Co/NiFe stack. None of the junction showed in this study showed the current suppression.

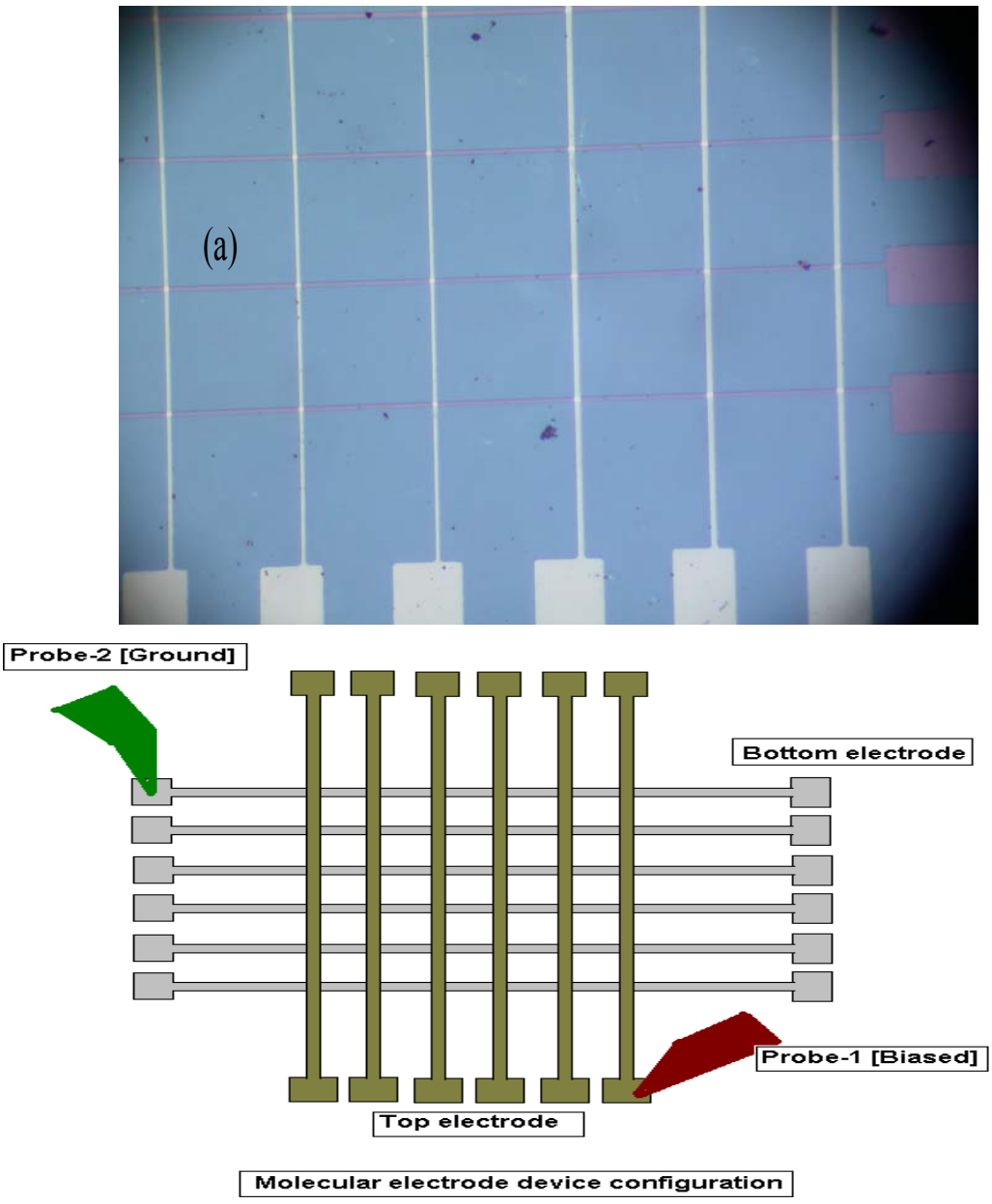

Figure A2.3: (a) Micrograph of an array of a typical cross junction pattern used in molecular electrode fabrication scheme. (b) Schematic of a complete 6x6 cross junction pattern. Probe positions show that the top (bottom) electrode was biased (grounded). During molecular attachment shown position of two electrical probes were used, while all the central region remain submerged in the molecular solution.

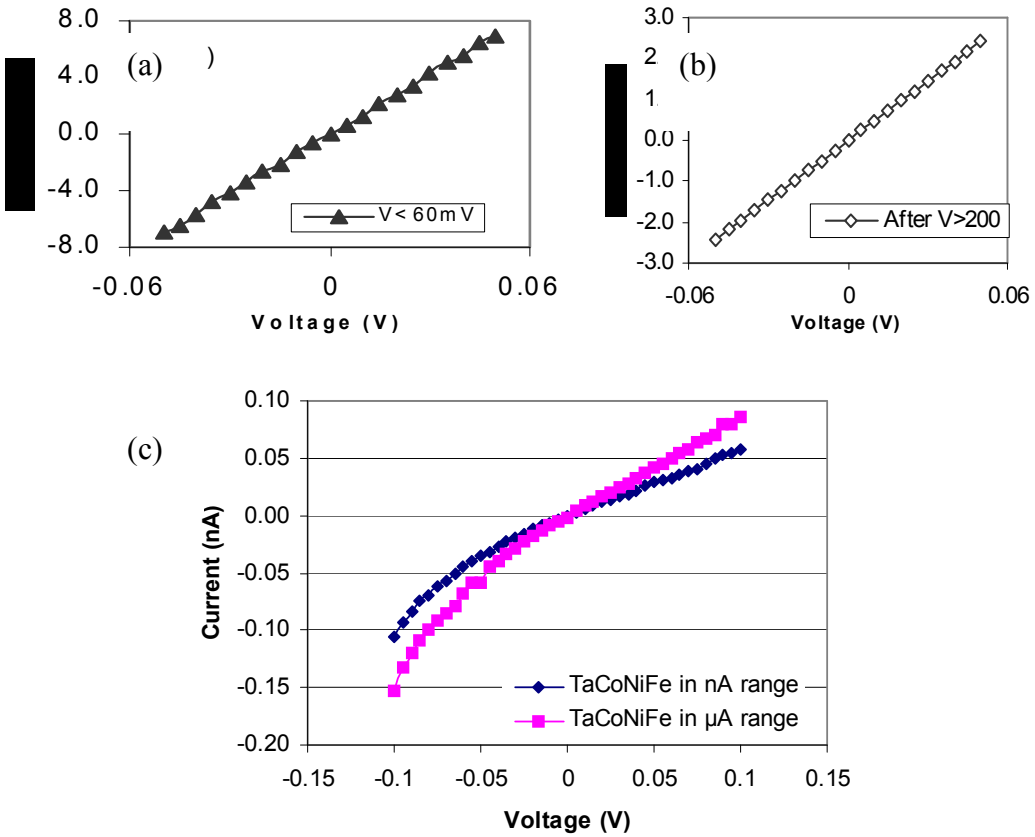

Figure A2.4: Resistance of bottom electrode Ta/Co/NiFe shown in figure 5 (b). I-V below 100mV (a) and after forcing current by applying 200mV on the same electrode Figure 5(b).
Junction current before and after changing the bottom electrode current by 3 orders with high bias application.

Appendix A3

Fabrication of semiconductor-molecule-metal junction using multilayer edge molecular electrode design

A Si/AlOx/NiFe based molecular junction was prepared. A p-type silicon wafer with 1-50 Ω resistivity and thermally grown 100nm silicon di oxide was utilized. After defining a 5µm window in photoresist, SiO_2 was etched with BOE solution. Soon after etching of oxide samples were put in vacuum for the deposition of AlOx and NiFe layer through a photoresist window, across the silicon pattern. Deposition parameters used are same as mentioned in chapter 2. Lastly, electrochemical molecule attachment was perfumed to produce silicon-molecule-metal junction. Unambiguous increase in transport was noticed after the bridging of molecular channels. In order to make electrical contact with silicon, electrical probes were directly touched to the opposite side of AlOx/NiFe pattern.

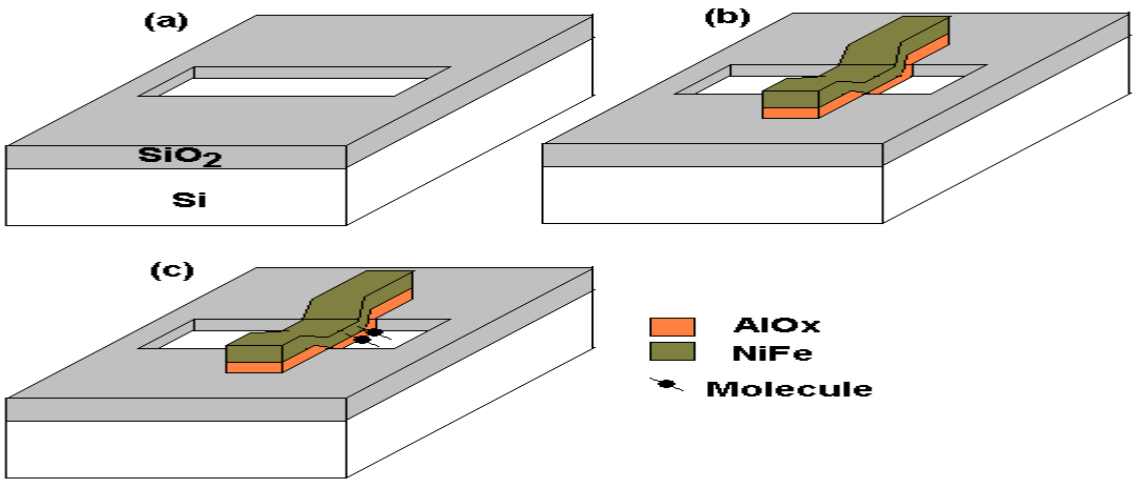

Figure A3.1: Fabrication scheme (a) etch away a window in the SiO2 layer present over Si wafer. (b) Deposit ~2nm alumina and NiFe metal electrode (c) attach molecules.

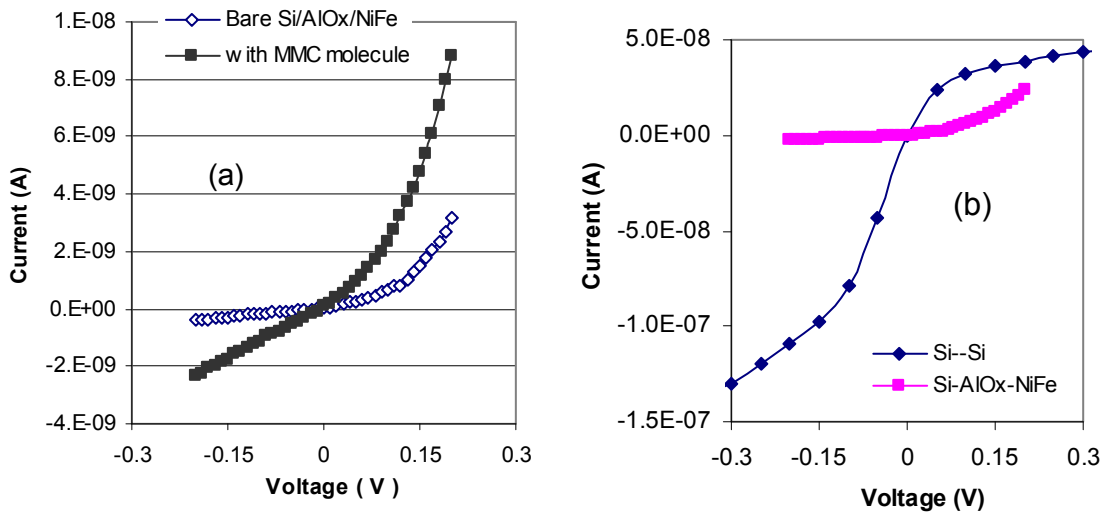

Figure A3.2: (a) Effect of molecule creating additional molecular conduction channels along the edge of Si/AlOx/NiFe junction. (b) I-V characteristics of a bottom silicon electrode and the Si/AlOx/NiFe junction. (Note resistance of junction is higher than that of silicon electrode.

Appendix A4

Conducting probe AFM study of magnetic molecular cluster self assembled on NiFe

Conducting probe AFM study of monolayer of magnetic molecular cluster: Aim of this experiment was to measure the current per molecule and to estimate the density of states profile of the magnetic molecular cluster. A gold coated contact mode AFM cantilever was utilized to study the electrochemically assembled monolayer of magnetic molecular cluster (MMC) on the 10nm thick NiFe layer. For this 0.1mM MMC solution in dichloromethane was utilized. Electrochemistry parameters were the same used in chapter-2 and 3. After self assembly process sample was rinsed with dichloromethane, ethyl alcohol and DI water. Connection to the AFM cantilever was checked before and after measurement with a known resister of 1GOhm. In the present case voltage was sourced from the AFM tip (cantilever served as a source). This study indicates that possibly electron charging energy to the single or few molecular clusters is above 1V.

A conductance gap was observed between -1.8V to 1.2V range. A 1nA current level is reached at 1.4V; current increase steeply after. Current increases from 1.1 to 7.8nA when voltage increased from 1.42 to 1.64V. Current per molecule of magnetic molecular cluster on a multilayer edge molecular electrode (MEME) is 0.16(±0.13) nA at 100mV. Molecular transport on a MEME

is approximately linear or show weak tunneling behavior. The corresponding current per magnetic cluster for the MEME with NiFe electrode at 1.4V is 2.2 nA, figure A4.1.

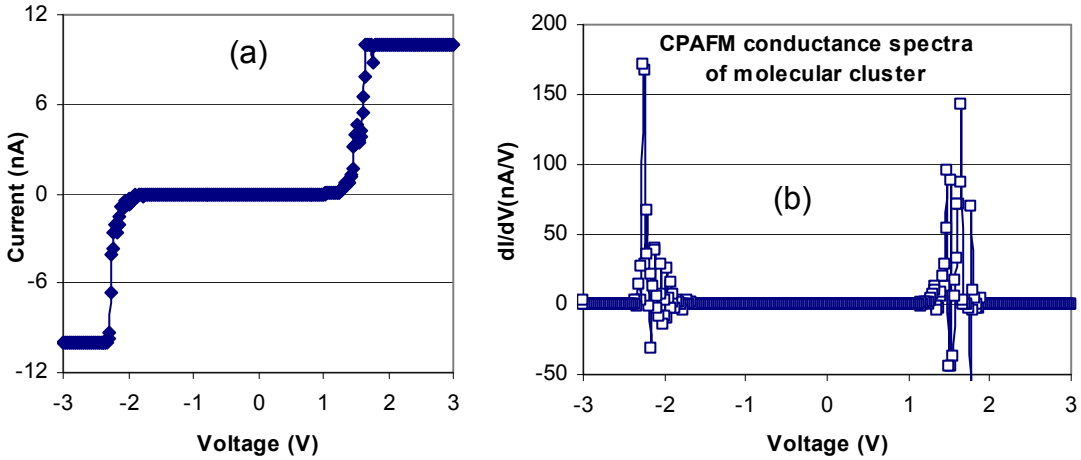

Figure A4.1: (a) Conducting probe AFM based I-V study of magnetic molecular cluster electrochemically self assembled on the NiFe metal (b) Conductance vs. voltage graph of molecular cluster.

Appendix A5

Magnetization study of NiFe/AlOx/Pd, TaCoNiFe/AlOx/Pd, NiFe and Ta/Co/NiFe with and without treatment with organometallic cluster.

The magnetization study of multilayer edge molecular electrodes with one ferromagnetic layer was performed. Effect of magnetic molecular clusters was found to be quite different for the magnetic electrodes embedded in tunnel junction as compared to the case when they were isolated. Magnetic moment of NiFe/Alox/Pd (TaCoNife/AlOx/Pd) reduced (increased) after the bridging of magnetic molecular clusters, figure A5.1 (a-b). Magnetic molecular clusters did not affect magnetization of unpatterned NiFe and TaCoNiFe layers, figure A5.1 (c-d).

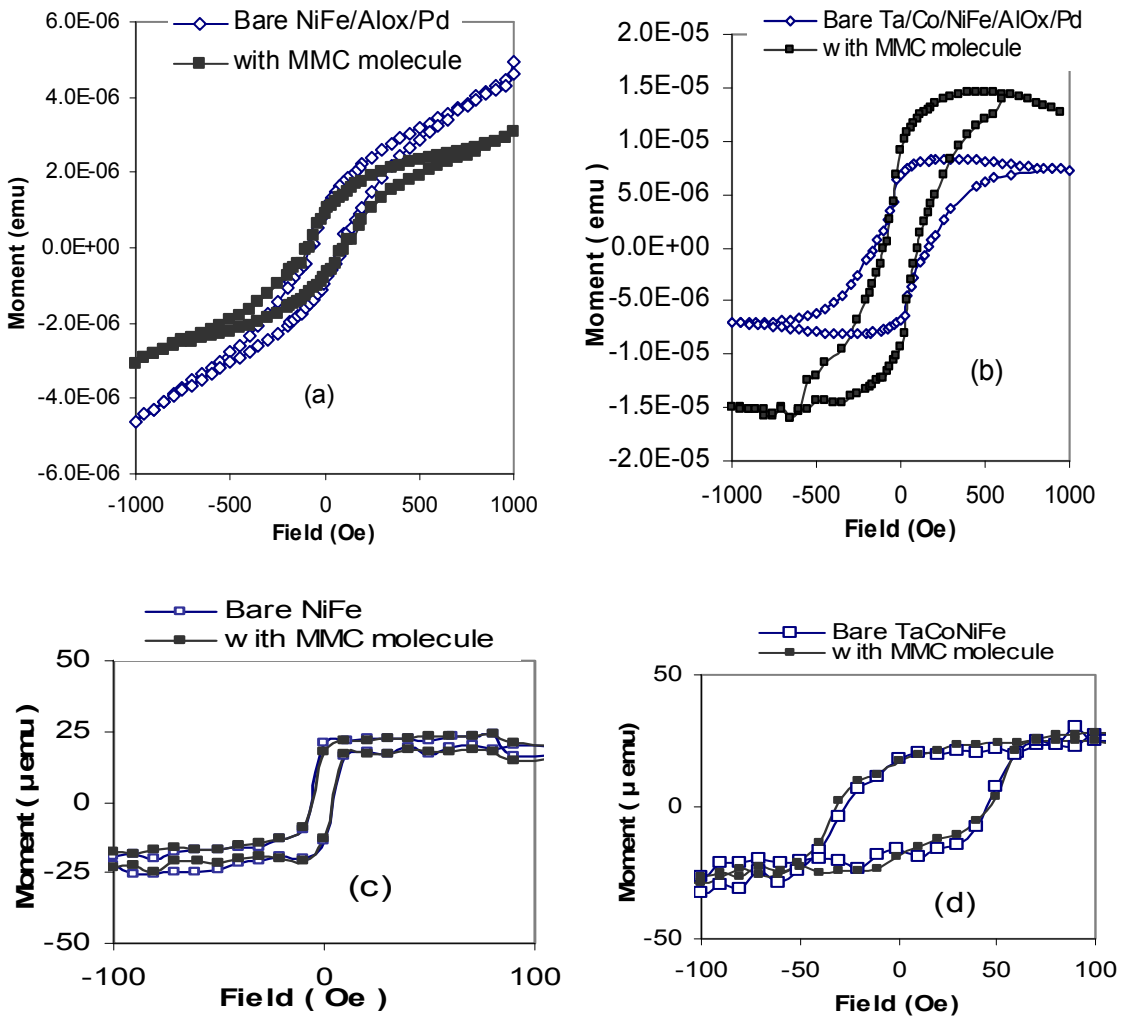

Figure A5.1. Magnetization study with and without molecule of (a) NiFe/AlOx/Pd (b) Ta/Co/NiFe/AlOx/Pd (c) un-patterned NiFe and (d) un-patterned TaCoNiFe.

Appendix A6

Molecular Spin Device with Different Configurations of Ferromagnetic Electrodes

Three configurations of ferromagnetic-multilayer edge molecular electrode were utilized to form molecular spin devices. Three configurations are:

(a) NiFe(10nm)/AlOx(2nm)/NiFe(10nm)

(b) Ta(5nm)/Co(5nm)/NiFe(5nm)/AlOx(2nm)/NiFe(10nm)

(c) Ta(5nm)/Co(5nm)/NiFe(5nm)/AlOx(2nm)/NiFe(5nm)/Ta(5nm)

Magnetic measurements and transport behavior of the entire three configurations were found to be quite distinct. Following are the details of representative behavior of each configuration.

FMR study show that NiFe(10nm)-AlOx(2nm)-NiFe(10nm) configuration showed two resonance modes at 1126 and 1223 Oe. Smaller mode (optical mode) lying after taller mode (acoustic mode) implies that nature of inter-layer coupling via alumina is antiferromagnetic, figure 1(a). Resonance mode for single NiFe electrode of 10nm thickness appears at 1150Oe. After the bridging of magnetic molecular clusters, current (at 100mV) of NiFe/Alox/NiFe increased from 0.2μA to 3μA. Magnetization of this molecular electrode by the 0.45T, in-plane magnetic field for 30min forced a low current state, 0.1μA at 100mV, figureA6.1(c). Repeating I-V or leaving the device for sometime exhibited retrieval of high current state,
3.6μA at 100mV.

FMR spectra of Ta/Co/NiFe/AlOx/NiFe(Ta/Co/NiFe/AlOx/NiFe/Ta) contained higher intensity peak (lower intensity peak) appear at lower magnetic field suggesting antiferromagnetic (ferromagnetic coupling between two ferromagnetic layer, figure A6.2(a) and figure A6.2(b). Bridging of MMC molecules on bare Ta/Co/NiFe/AlOx/NiFe(Ta/Co/NiFe/AlOx/NiFe/Ta) reduces (increases) the magnetic moment, figure A6.2(d)(figure A6.2(c)). Two magnetization studies suggest that the two configurations behave almost opposite to each other. In the transport study, magnetic molecular cluster forced the current suppression on tunnel junctions with Ta/Co/NiFe/AlOx/NiFe configuration (details in chapter7). When bridged between the two ferromagnetic electrodes of the Ta/Co/NiFe/AlOx/NiFe/Ta, magnetic molecular cluster produced several current levels. Although current level tended to settle at lower levels than the background current, but molecular junctions did not settle to the same low current state, figure A6.3(a). With this configuration magnetic field could be used to switch the device current state from one level to another. One device, whose current level initially was at pA level, figure A6.3(d), shifted to μA level with the repeating magneto resistance study, figure A6.3(c). A summary of various current stages seen on the magnetic molecular junction is in, figure A6.3(e). Many time a current state

changed with just the repetition of the I-V/MR measurements. A low current state set by the magnetic field could be perturbed by repeating I-Vs, as seen with the case of NiFe-AlOx-NiFe.

On another F-MEME with Ta/Co/NiFe/AlOx/NiFe/Ta configuration, prepared in different batch application of permanent in-plane magnetic field at RT was found to switch the device current from μA current level to pA current state, figure A6.4.

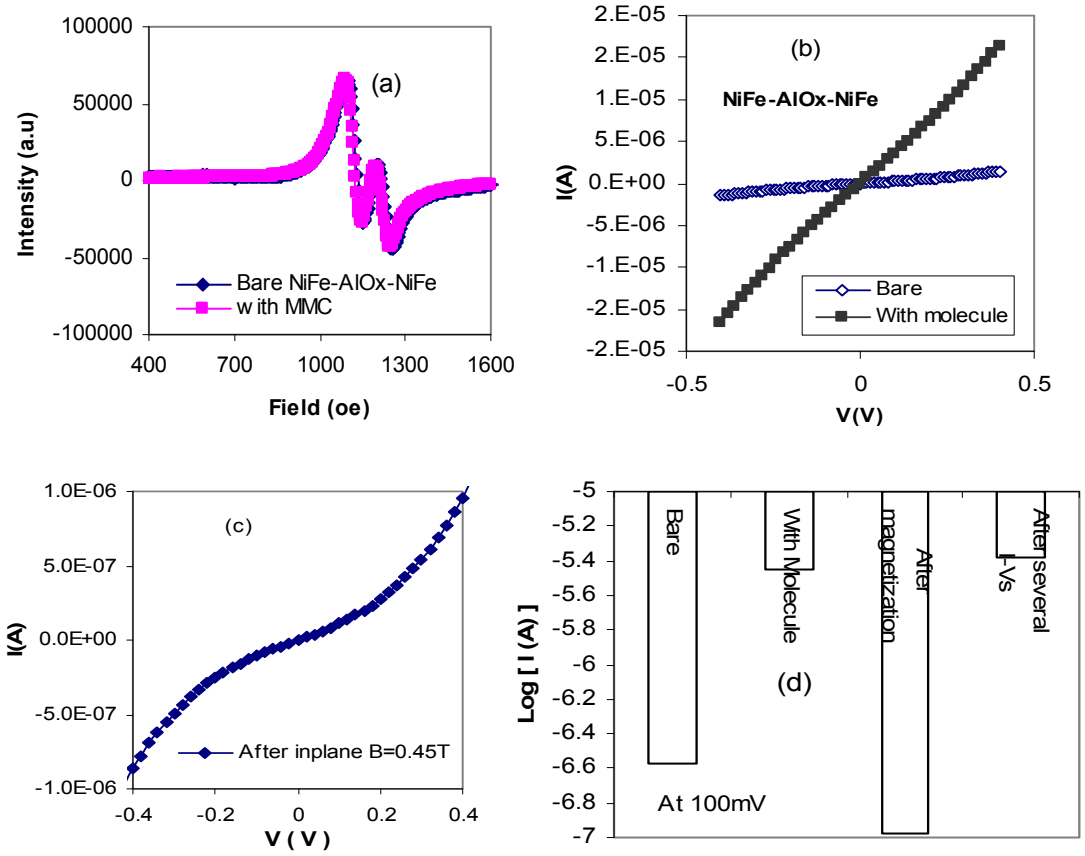

Figure A6.1: (a) FMR response of NiFe/AlOx/NiFe, (b) I-V before after establishment of molecular conduction channels (c) after 0.45T in plane magnetization molecular device settling into two order smaller current (d) summary of current value at 100mV in various stages of NiFe/AlOx/NiFe.

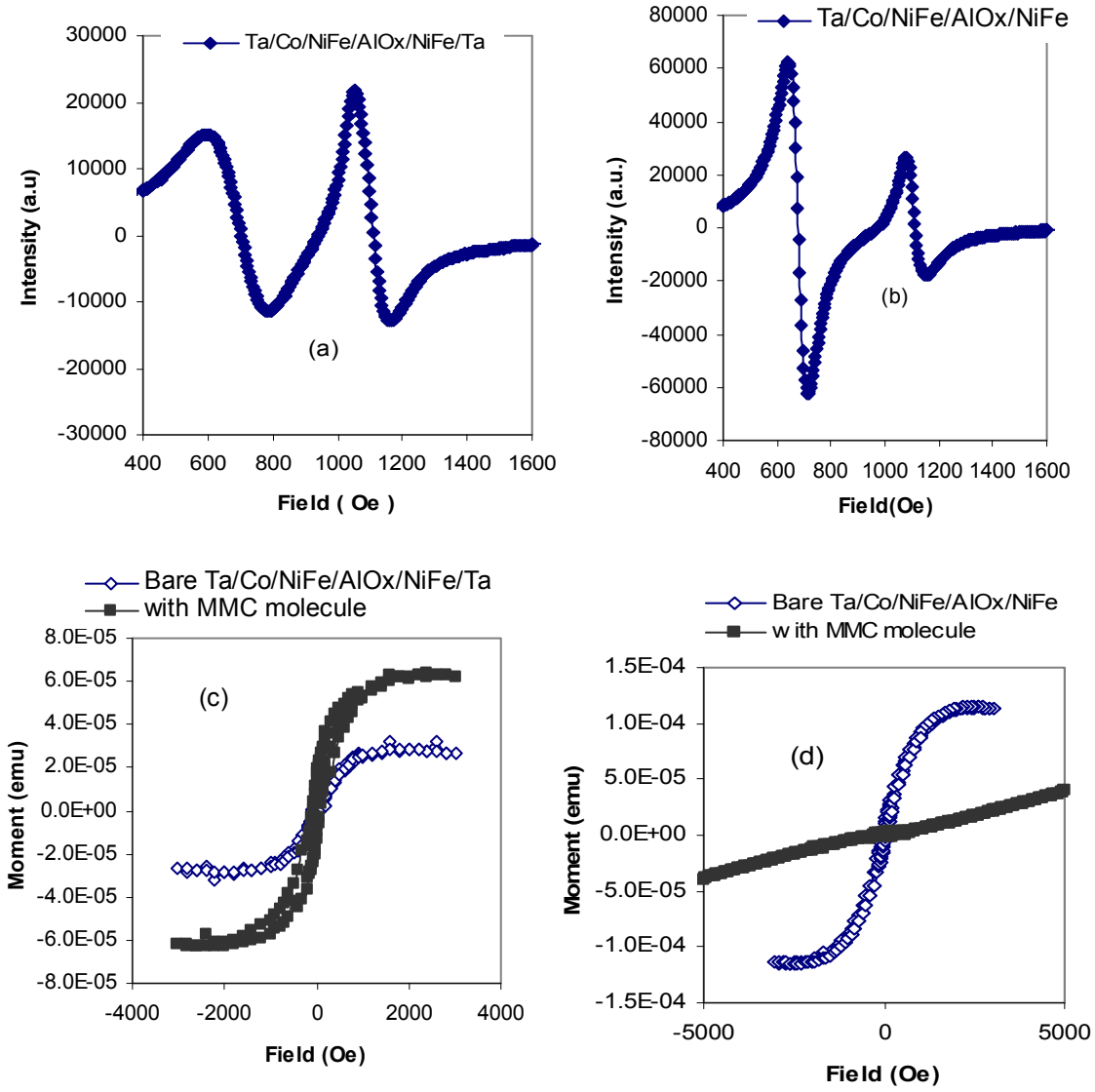

Figure A6.2. FMR response of bare TaCoNife/AlOx/NiFe/Ta (a) and Ta/Co/NiFe/AlOx/NiFe (b). SQUID magnetic measurement of with and without molecule of TaCoNife/AlOx/NiFe/Ta (c) and Ta/Co/NiFe/AlOx/NiFe (d).

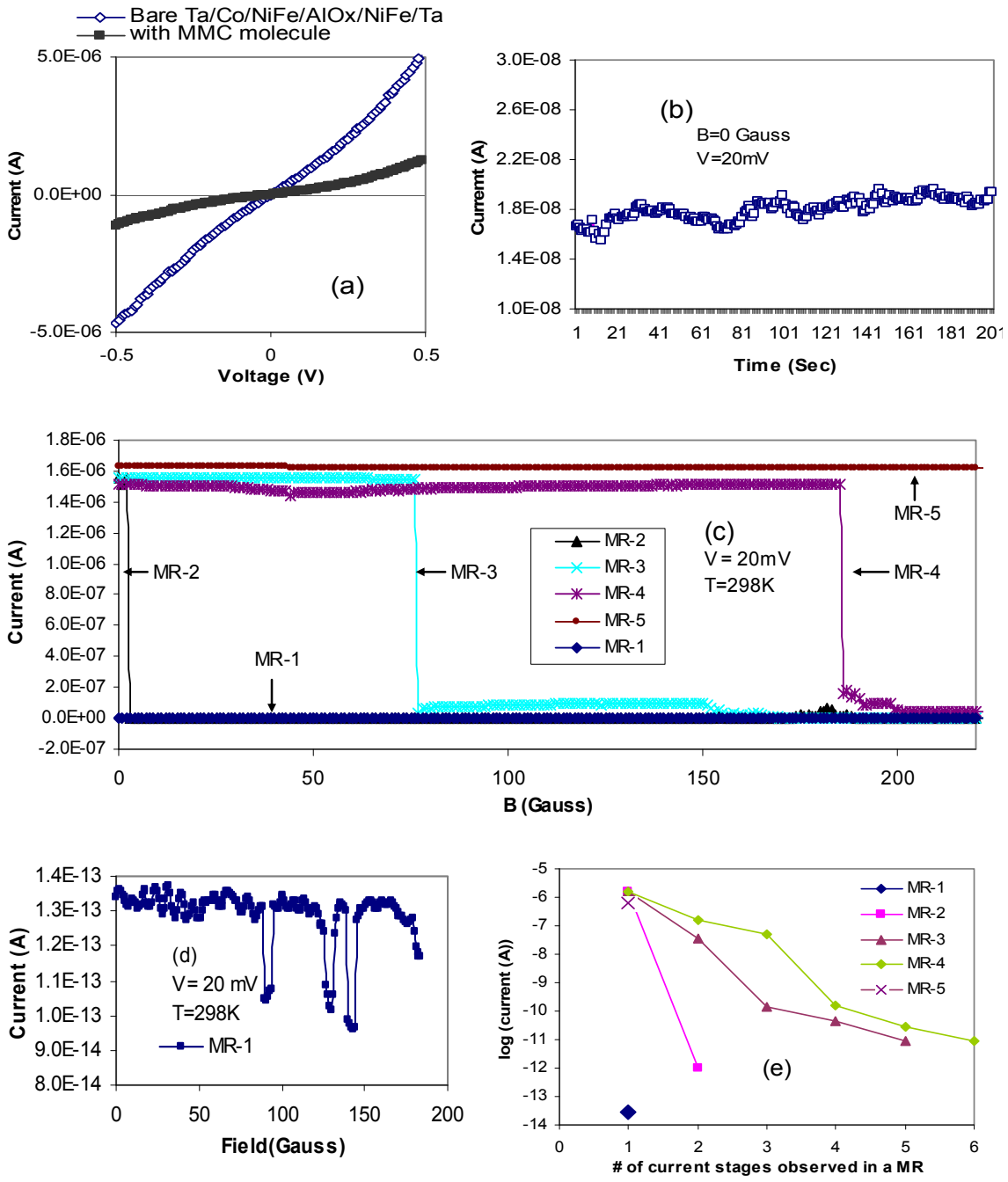

Figure A6.3: (a) Effect of the attachment of magnetic molecular clusters on the transport of bare TaCoNiFeAlOxNiFe/Ta (b) Stability of a current level at 20mV in zero magnetic field. (c) Switching of current state from 0.1pAto 1μA level due to the magnetic field (d) starting current level, during magneto resistance (MR) study. (e) Number of current levels observed during a magneto resistance (MR) study.

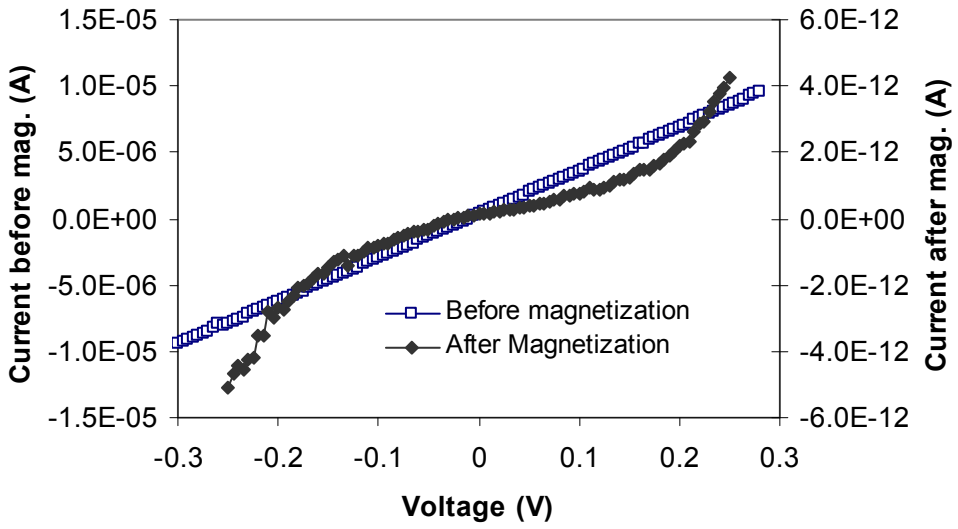

Figure A6.4: Magnetic molecular cluster treated TaCo/NiFe/AlOx/NiFe/Ta before and after magnetization by an in-plane 0.45T magnetic field at RT.

Appendix A7

Low Temperature Study of Magnetic Molecular Cluster Treated Ta/Co/NiFe/AlOx/NiFe Ferromagnetic Multilayer Edge Molecular Electrodes (F-MEME)

A few F-MEMEs showed dramatic current suppression (of ~6 orders) after the bridging of magnetic molecular clusters on the exposed edge. Three MMC treated F-MEME were subjected to low temperature transport study up to 77K. Current of all the junctions settled into pA state. However, I-V spectra were accompanied by the sharp peaks, figure A7.1(a-c). These peaks appeared at various positions on voltage axis; peaks were found to occur more frequently at few specific positions, e.g. 0.2V and 0.3V, figure A7.1(d). Highest number of spikes or peaks was observed at 0.3V. According to our calculation molecular transport with MMC treated Ta/AlOx/Ta exhibited ~0.3V activation energy, chapter 3. It is likely that 0.3V peak is arising from a vibration mode or change in conformation at the core of the molecule. We are unable to pinpoint the origin of 0.2V peak. It is quite likely that molecule assume several charge states during an I-V. These peaks persisted after the warming of F-MEME sample up to room temperature; intensity of peaks was found to be in nA range. However, these peaks were not observed after the few hours at RT.

To minimize the role of noise, duration of each I-V was kept to be 1hour. I-V studies were performed with Keithely-6430 sub femtoamp source meter equipped with preamplifier.

Minimum noise condition was maintained by doing I-V in from the surrounding. Samples were mounted on a superconducting insert. To maintain a 77K temperature a Dewar filled with liquid nitrogen was utilized. To avoid the reasons that electrical connections, wiring and instrument is producing spikes/peaks in I-V of MMC treated F-MEME another tunnel junction in identical condition was studied. A nonmagnetic Ta/TaOx/Ta tunnel junction, possessing Pool Frenkel type atomic defects, exhibited temperature dependent transport and reached the pA current level at 77K. No spike or peak was observed in I-V of Ta/TaOx/Ta junctions. Temperature dependent transport of our molecular device was found to be quite difficult; ultrathin alumina stability is sensitive towards the thermal stresses.

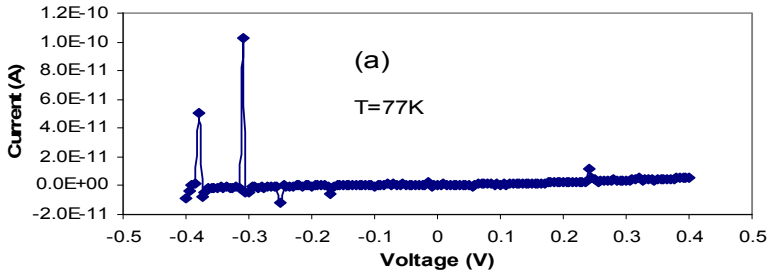

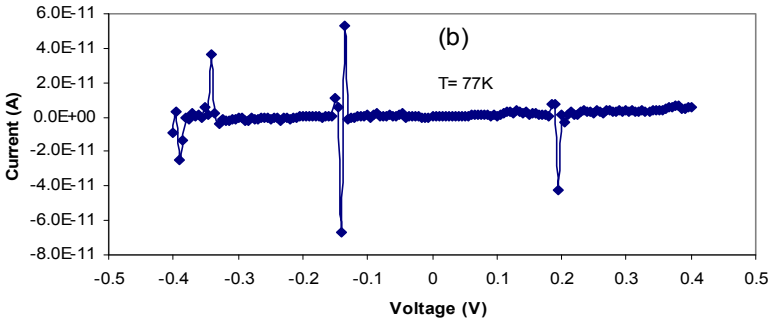

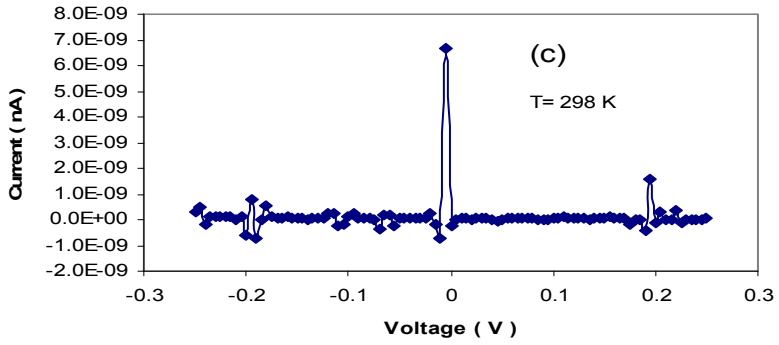

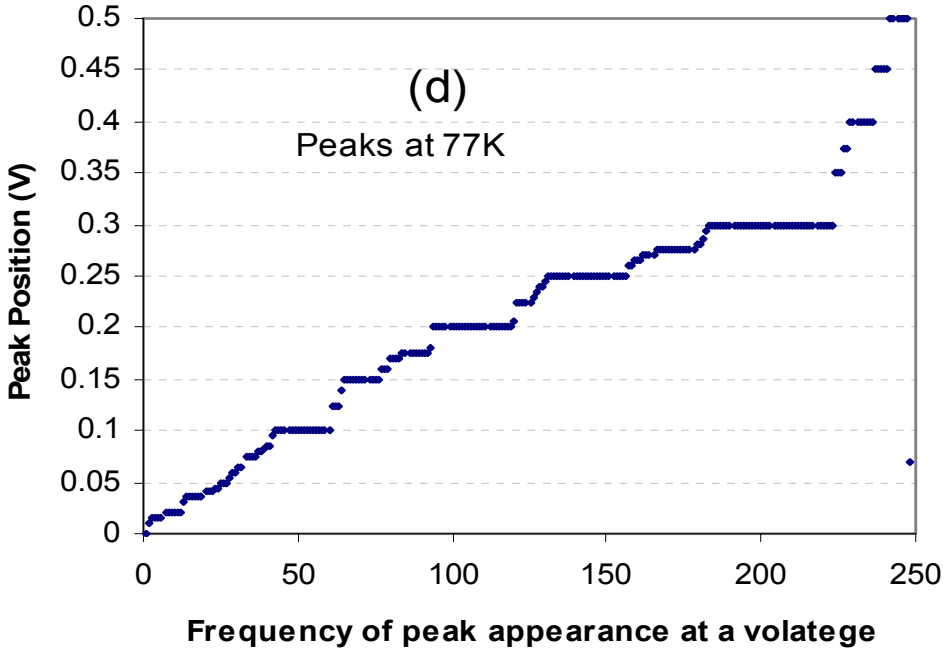

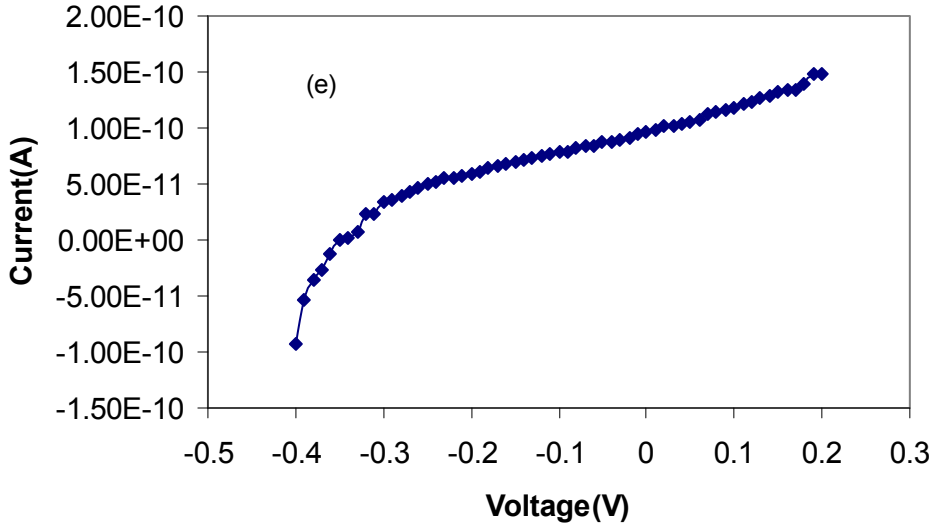

Figure A7.1: Peaks in I-V scan of molecule treated Co/NiFe/AlOx/NiFe at 77K (a) and (b). Peaks in I-V spectra of a molecular junction warmed up to 77K (c). Peak position vs. frequency graph for the peaks observed at 77K. (d) Peak position vs. frequency.(e) I-V of a molecular junction after warming up to room temperature from 77K, no peak is observed but a slight offset of I-V origin.

Appendix A8

Labview Programs for Transport and Magneto Resistance Studies

Source meter KE2430

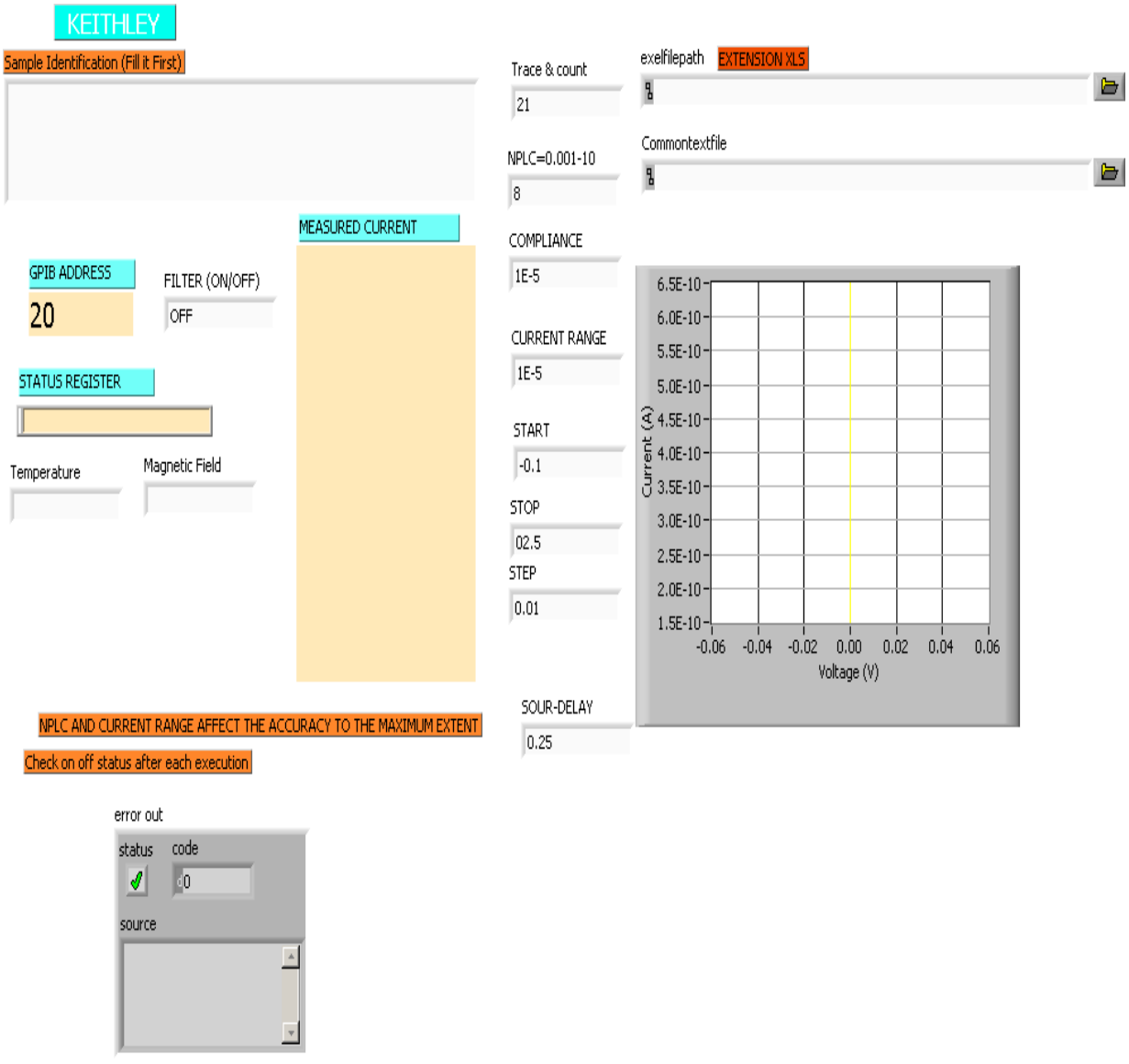

Program for Magneto Resistance Study:

Source Meter KE6430: For Continuous I-V Studies

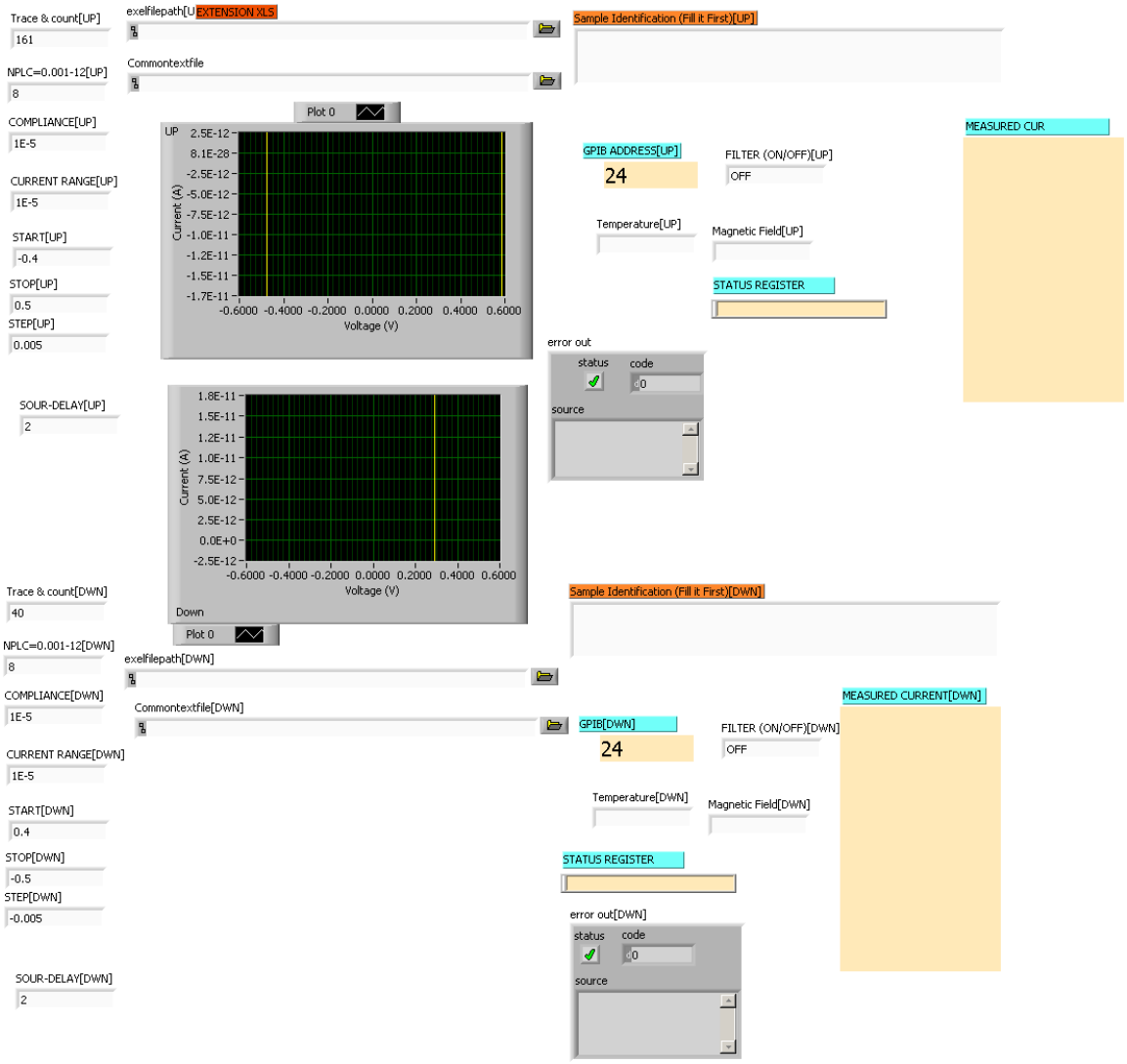

REFERENCES

[1] I. Zutic, J. Fabian, and S. C. Erwin, "*Bipolar spintronics: Fundamentals and applications"* Ibm Journal Of Research And Development **50,** 121-139 (2006).

[2] C. R. Barnes, "*The proposed Cambrian-Ordovician global boundary stratotype and point (GSSP) in Western Newfoundland, Canada"* Geological Magazine **125,** 381 (1988).

[3] D. F. Li, S. Parkin, G. B. Wang, G. T. Yee, R. Clerac, W. Wernsdorfer, and S. M. Holmes, "*An S=6 cyanide-bridged octanuclear (Fe4Ni4II)-Ni-III complex that exhibits slow relaxation of the magnetization"* Journal Of The American Chemical Society **128,** 4214-4215 (2006).

[4] C. Joachim, J. K. Gimzewski, and A. Aviram, "*Electronics using hybrid-molecular and mono-molecular devices"* Nature **408,** 541-548 (2000).

[5] R. L. Carroll and C. B. Gorman, "*The genesis of molecular electronics"* Angewandte Chemie-International Edition **41,** 4379-4400 (2002).

[6] A. Aviram and M. A. Ratner, "*Molecular Rectifiers"* Chemical Physics Letters **29,** 277-283 (1974).

[7] M. A. Reed, C. Zhou, C. J. Muller, T. P. Burgin, and J. M. Tour, "*Conductance of a molecular junction"* Science **278,** 252-254 (1997).

[8] A. J. Epstein, "*Organic-based magnets: Opportunities in photoinduced magnetism, spintronics, fractal magnetism, and beyond"* Mrs Bulletin **28,** 492-499 (2003).

[9] J. R. Heath and M. A. Ratner, "*Molecular electronics"* Physics Today **56,** 43-49 (2003).

[10] C. Joachim and M. A. Ratner, "*Molecular wires: guiding the super-exchange interactions electrodes between two electrodes"* Nanotechnology **15,** 1065-1075 (2004).

[11] D. K. James and J. M. Tour, "*Electrical measurements in molecular electronics"* Chemistry Of Materials **16,** 4423-4435 (2004).

[12] S. A. Wolf, D. D. Awschalom, R. A. Buhrman, J. M. Daughton, S. von Molnar, M. L. Roukes, A. Y. Chtchelkanova, and D. M. Treger, "*Spintronics: A spin-based electronics vision for the future"* Science **294,** 1488-1495 (2001).

[13] A. N. Pasupathy, R. C. Bialczak, J. Martinek, J. E. Grose, L. A. K. Donev, P. L. McEuen, and D. C. Ralph, "*The Kondo effect in the presence of ferromagnetism"* Science **306,** 86-89 (2004).

[14] E. G. Petrov, I. S. Tolokh, and V. May, "*Magnetic field control of an electron tunnel current through a molecular wire"* Journal Of Chemical Physics **108,** 4386-4396 (1998).

[15] E. G. Emberly and G. Kirczenow, "*Molecular spintronics: spin-dependent electron transport in molecular wires"* Chemical Physics **281,** 311-324 (2002).

[16] J. R. Petta, S. K. Slater, and D. C. Ralph, "*Spin-dependent transport in molecular tunnel junctions"* Physical Review Letters **93** (2004).

[17] J. S. Moodera, J. Nassar, and G. Mathon, "*Spin-tunneling in ferromagnetic junctions"* Annual Review Of Materials Science **29,** 381-432 (1999).

[18] S. Parkin, "*Spin-polarized current in spin valves and magnetic tunnel junctions"* Mrs Bulletin **31,** 389-394 (2006).

[19] A. R. Rocha, V. M. Garcia-Suarez, S. W. Bailey, C. J. Lambert, J. Ferrer, and S. Sanvito, "*Towards molecular spintronics"* Nature Materials **4,** 335-339 (2005).

[20] S. Sanvito and A. R. Rocha, "*Molecular-spintronics: The art of driving spin through molecules"* Journal Of Computational And Theoretical Nanoscience **3,** 624-642 (2006).

[21] E. Holmstrom, L. Nordstrom, L. Bergqvist, B. Skubic, B. Hjorvarsson, I. A. Abrikosov, P. Svedlindh, and O. Eriksson, "*On the sharpness of the interfaces in metallic multilayers"* Proceedings Of The National Academy Of Sciences Of The United States Of America **101,** 4742-4745 (2004).

[22] F. Meier, V. Cerletti, O. Gywat, D. Loss, and D. D. Awschalom, "*Molecular spintronics: Coherent spin transfer in coupled quantum dots"* Physical Review B **69** (2004).
[23] J. P. Launay, "*Long-distance intervalence electron transfer"* Chemical Society Reviews **30,** 386-397 (2001).
[24] L. Cheng, J. P. Yang, Y. X. Yao, D. W. Price, S. M. Dirk, and J. M. Tour, "*Comparative study of electrochemically directed assembly versus conventional self-assembly of thioacetyl-terminated oligo(phenylene ethynlyene)s on gold and platinum surface"* Langmuir **20,** 1335-1341 (2004).
[25] E. Y. Tsymbal, O. N. Mryasov, and P. R. LeClair, "*Spin-dependent tunnelling in magnetic tunnel junctions"* Journal Of Physics-Condensed Matter **15,** R109-R142 (2003).
[26] W. J. M. Naber, S. Faez, and W. G. van der Wiel, "*Organic spintronics"* Journal Of Physics D-Applied Physics **40,** R205-R228 (2007).
[27] M. Ouyang and D. D. Awschalom, "*Coherent spin transfer between molecularly bridged quantum dots"* Science **301,** 1074-1078 (2003).
[28] M. Verdaguer, "*Rational synthesis of molecular magnetic materials: a tribute to Olivier Kahn"* Polyhedron **20,** 1115-1128 (2001).
[29] M. N. Leuenberger, F. Meier, and D. Loss, "*Quantum spin dynamics in molecular magnets"* Monatshefte Fur Chemie **134,** 217-233 (2003).
[30] E. G. Petrov, I. S. Tolokh, A. A. Demidenko, and V. V. Gorbach, "*Electron-Transfer Properties Of Quantum Molecular Wires"* Chemical Physics **193,** 237-253 (1995).
[31] J. Park, A. N. Pasupathy, J. I. Goldsmith, C. Chang, Y. Yaish, J. R. Petta, M. Rinkoski, J. P. Sethna, H. D. Abruna, P. L. McEuen, and D. C. Ralph, "*Coulomb blockade and the Kondo effect in single-atom transistors"* Nature **417,** 722-725 (2002).
[32] M. N. Leuenberger and E. R. Mucciolo, "*Berry-phase oscillations of the kondo effect in single-molecule magnets"* Physical Review Letters **97** (2006).
[33] H. B. Heersche, Z. de Groot, J. A. Folk, H. S. J. van der Zant, C. Romeike, M. R. Wegewijs, L. Zobbi, D. Barreca, E. Tondello, and A. Cornia, "*Electron transport through single Mn-12 molecular magnets"* Physical Review Letters **96,** 206861 (2006).
[34] R. M. Metzger, "*Unimolecular electrical rectifiers"* Chemical Reviews **103,** 3803-3834 (2003).
[35] Y. Selzer and D. L. Allara, "*Single-molecule electrical junctions"* Annual Review Of Physical Chemistry **57,** 593-623 (2006).
[36] A. Nitzan, "*Electron transmission through molecules and molecular interfaces"* Annual Review Of Physical Chemistry **52,** 681-750 (2001).
[37] R. L. McCreery, "*Molecular electronic junctions"* Chemistry Of Materials **16,** 4477-4496 (2004).
[38] A. Nitzan and M. A. Ratner, "*Electron transport in molecular wire junctions"* Science **300,** 1384-1389 (2003).
[39] W. J. Liang, M. P. Shores, M. Bockrath, J. R. Long, and H. Park, "*Kondo resonance in a single-molecule transistor"* Nature **417,** 725-729 (2002).
[40] P. Tyagi, D. F. Li, S. M. Holmes, and B. J. Hinds, "*Molecular Electrodes at the Exposed Edge of Metal-Insulator-Metal Trilayer Structures"* Journal Of The American Chemical Society **129,** 4923-4928 (2007).
[41] J. C. Cuevas, J. Heurich, F. Pauly, W. Wenzel, and G. Schon, "*Theoretical description of the electrical conduction in atomic and molecular junctions"* Nanotechnology **14,** R29-R38 (2003).
[42] A. Salomon, D. Cahen, S. Lindsay, J. Tomfohr, V. B. Engelkes, and C. D. Frisbie, "*Comparison of electronic transport measurements on organic molecules"* Advanced Materials **15,** 1881-1890 (2003).

[43] L. Senapati, R. Pati, and S. C. Erwin, "*Controlling spin-polarized electron transport through a molecule: The role of molecular conformation"* Physical Review B (Condensed Matter and Materials Physics) **76,** 024438 (2007).

[44] M. Dorogi, J. Gomez, R. Osifchin, R. P. Andres, and R. Reifenberger, "*Room-Temperature Coulomb-Blockade From A Self-Assembled Molecular Nanostructure"* Physical Review B **52,** 9071-9077 (1995).

[45] A. D. Zhao, Q. X. Li, L. Chen, H. J. Xiang, W. H. Wang, S. Pan, B. Wang, X. D. Xiao, J. L. Yang, J. G. Hou, and Q. S. Zhu, "*Controlling the Kondo effect of an adsorbed magnetic ion through its chemical bonding"* Science **309,** 1542-1544 (2005).

[46] P. Seneor, A. Bernand-Mantel, and F. Petroff, "*Nanospintronics: when spintronics meets single electron physics"* Journal Of Physics-Condensed Matter **19** (2007).

[47] H. J. Davies, "*The Physics of Low Dimensional Semiconductors"* Cambridge University Press (1998).

[48] Y. Q. Xue and M. A. Ratner, "*Theoretical principles of single-molecule electronics: A chemical and mesoscopic view"* International Journal Of Quantum Chemistry **102,** 911-924 (2005).

[49] C. Joachim and M. A. Ratner, "*Molecular electronics: Some views on transport junctions and beyond"* Proceedings Of The National Academy Of Sciences Of The United States Of America **102,** 8801-8808 (2005).

[50] J. G. Simmons, "*Generalized Formula For Electric Tunnel Effect Between Similar Electrodes Separated By A Thin Insulating Film"* Journal Of Applied Physics **34,** 1793-& (1963).

[51] W. Y. Wang, T. Lee, and M. A. Reed, "*Mechanism of electron conduction in self-assembled alkanethiol monolayer devices"* Physical Review B **68** (2003).

[52] G. V. Nazin, S. W. Wu, and W. Ho, "*Tunneling rates in electron transport through double-barrier molecular junctions in a scanning tunneling microscope"* Proceedings Of The National Academy Of Sciences Of The United States Of America **102,** 8832-8837 (2005).

[53] Y. Selzer, L. T. Cai, M. A. Cabassi, Y. X. Yao, J. M. Tour, T. S. Mayer, and D. L. Allara, "*Effect of local environment on molecular conduction: Isolated molecule versus self-assembled monolayer"* Nano Letters **5,** 61-65 (2005).

[54] X. Y. Zhu, "*Charge transport at metal-molecule interfaces: A spectroscopic view"* Journal Of Physical Chemistry B **108,** 8778-8793 (2004).

[55] S. Datta, "*Electrical resistance: an atomistic view"* Nanotechnology **15,** S433-S451 (2004).

[56] J. Martinek, M. Sindel, L. Borda, J. Barnas, J. Konig, G. Schon, and J. von Delft, "*Kondo effect in the presence of itinerant-electron ferromagnetism studied with the numerical renormalization group method"* Physical Review Letters **91** (2003).

[57] S. W. Wu, G. V. Nazin, X. Chen, X. H. Qiu, and W. Ho, "*Control of relative tunneling rates in single molecule bipolar electron transport"* Physical Review Letters **93** (2004).

[58] N. P. Guisinger, M. E. Greene, R. Basu, A. S. Baluch, and M. C. Hersam, "*Room Temperature Negative Differential Resistance through Individual Organic Molecules on Silicon Surfaces"* Nano Lett. **4,** 55-59 (2004).

[59] D. V. Averin, A. N. Korotkov, and K. K. Likharev, "*Theory Of Single-Electron Charging Of Quantum-Wells And Dots"* Physical Review B **44,** 6199-6211 (1991).

[60] D. Segal, A. Nitzan, W. B. Davis, M. R. Wasielewski, and M. A. Ratner, "*Electron transfer rates in bridged molecular systems 2. A steady-state analysis of coherent tunneling and thermal transitions"* Journal Of Physical Chemistry B **104,** 3817-3829 (2000).

[61] J. M. Seminario, C. E. De La Cruz, and P. A. Derosa, "*A Theoretical Analysis of Metal-Molecule Contacts"* J. Am. Chem. Soc. **123,** 5616-5617 (2001).

[62] R. H. M. Smit, Y. Noat, C. Untiedt, N. D. Lang, M. C. van Hemert, and J. M. van Ruitenbeek, "*Measurement of the conductance of a hydrogen molecule"* Nature **419,** 906-909 (2002).

[63] N. Nilius, T. M. Wallis, and W. Ho, "*Localized molecular constraint on electron delocalization in a metallic chain"* Physical Review Letters **90** (2003).

[64] B. Q. Q. Xu, X. L. L. Li, X. Y. Y. Xiao, H. Sakaguchi, and N. J. J. Tao, "*Electromechanical and conductance switching properties of single oligothiophene molecules"* Nano Letters **5,** 1491-1495 (2005).

[65] B. Q. Xu and N. J. J. Tao, "*Measurement of single-molecule resistance by repeated formation of molecular junctions"* Science **301,** 1221-1223 (2003).

[66] X. Y. Xiao, B. Q. Xu, and N. J. Tao, "*Measurement of single molecule conductance: Benzenedithiol and benzenedimethanethiol"* Nano Letters **4,** 267-271 (2004).

[67] M. Mayor, H. B. Weber, J. Reichert, M. Elbing, C. von Hanisch, D. Beckmann, and M. Fischer, "*Electric current through a molecular rod - Relevance of the position of the anchor groups"* Angewandte Chemie-International Edition **42,** 5834-5838 (2003).

[68] J. Reichert, R. Ochs, D. Beckmann, H. B. Weber, M. Mayor, and H. von Lohneysen, "*Driving current through single organic molecules"* Physical Review Letters **88** (2002).

[69] S. Kubatkin, A. Danilov, M. Hjort, J. Cornil, J. L. Bredas, N. Stuhr-Hansen, P. Hedegard, and T. Bjornholm, "*Single-electron transistor of a single organic molecule with access to several redox states"* Nature **425,** 698-701 (2003).

[70] W. F. Brinkman, R. C. Dynes, and J. M. Rowell, "*Tunneling Conductance of Asymmetrical Barriers"* Journal of Applied Physics **41,** 1915-1921 (1970).

[71] N. B. Zhitenev, H. Meng, and Z. Bao, "*Conductance of small molecular junctions"* Physical Review Letters **88** (2002).

[72] H. Park, J. Park, A. K. L. Lim, E. H. Anderson, A. P. Alivisatos, and P. L. McEuen, "*Nanomechanical oscillations in a single-C-60 transistor"* Nature **407,** 57-60 (2000).

[73] A. N. Pasupathy, J. Park, C. Chang, A. V. Soldatov, S. Lebedkin, R. C. Bialczak, J. E. Grose, L. A. K. Donev, J. P. Sethna, D. C. Ralph, and P. L. McEuen, "*Vibration-assisted electron tunneling in C-140 transistors"* Nano Letters **5,** 203-207 (2005).

[74] L. H. Yu, Z. K. Keane, J. W. Ciszek, L. Cheng, M. P. Stewart, J. M. Tour, and D. Natelson, "*Inelastic electron tunneling via molecular vibrations in single-molecule transistors"* Physical Review Letters **93** (2004).

[75] B. C. Stipe, M. A. Rezaei, and W. Ho, "*Single-molecule vibrational spectroscopy and microscopy"* Science **280,** 1732-1735 (1998).

[76] M. Turek and K. A. Matveev, "*Cotunneling thermopower of single electron transistors"* Physical Review B **65** (2002).

[77] A. Nitzan, J. Jortner, J. Wilkie, A. L. Burin, and M. A. Ratner, "*Tunneling time for electron transfer reactions"* Journal Of Physical Chemistry B **104,** 5661-5665 (2000).

[78] M. Julliere, "*Tunneling Between Ferromagnetic-Films"* Physics Letters A **54,** 225-226 (1975).

[79] A. Iovan, S. Andersson, Y. G. Naidyuk, A. Vedyaev, B. Dieny, and V. Korenivski, "*Spin Diode Based on Fe/MgO Double Tunnel Junction"* Nano Lett. (2008).

[80] P. M. Tedrow and R. Meservey, "*Spin-Dependent Tunneling Into Ferromagnetic Nickel"* Physical Review Letters **26,** 192-& (1971).

[81] S. Takahashi and S. Maekawa, "*Effect of Coulomb blockade on magnetoresistance in ferromagnetic tunnel junctions"* Physical Review Letters **80,** 1758-1761 (1998).

[82] H. C. Nam, H. Shim, S. K. Kim, and K. B. Cho, "*Thickness Dependence of Magnetic Coupling Strength and Thermal Stability in a Spin-Dependent Tunnel Junction "* Phys. Stat. Sol. (a) **201,** 1708-1711 (2004).

[83] M. Bode, M. Getzlaff, and R. Wiesendanger, "*Spin-polarized vacuum tunneling into the exchange-split surface state of Gd(0001)"* Physical Review Letters **81,** 4256-4259 (1998).

[84] E. Y. Tsymbal, Oleinik, II, and D. G. Pettifor, "*Oxygen-induced positive spin polarization from Fe into the vacuum barrier"* Journal Of Applied Physics **87,** 5230-5232 (2000).

[85] P. Crespo, R. Litran, T. C. Rojas, M. Multigner, J. M. de la Fuente, J. C. Sanchez-Lopez, M. A. Garcia, A. Hernando, S. Penades, and A. Fernandez, "*Permanent magnetism, magnetic anisotropy, and hysteresis of thiol-capped gold nanoparticles"* Physical Review Letters **93,** 087204 (2004).

[86] L. H. Yu and D. Natelson, "*Transport in single-molecule transistors: Kondo physics and negative differential resistance"* Nanotechnology **15,** S517-S524 (2004).

[87] M. R. Buitelaar, T. Nussbaumer, and C. Schonenberger, "*Quantum dot in the Kondo regime coupled to superconductors"* Physical Review Letters **89** (2002).

[88] M. S. Choi, D. Sanchez, and R. Lopez, "*Kondo effect in a quantum dot coupled to ferromagnetic leads: A numerical renormalization group analysis"* Physical Review Letters **92** (2004).

[89] S. Doniach, "*Kondo Lattice And Weak Antiferromagnetism"* Physica B & C **91,** 231-234 (1977).

[90] L. H. Yu and D. Natelson, "*The Kondo effect in C-60 single-molecule transistors"* Nano Letters **4,** 79-83 (2004).

[91] R. Cohen, K. Stokbro, J. M. L. Martin, and M. A. Ratner, "*Charge transport in conjugated aromatic molecular junctions: Molecular conjugation and molecule-electrode coupling"* Journal Of Physical Chemistry C **111,** 14893-14902 (2007).

[92] J. Martinek, Y. Utsumi, H. Imamura, J. Barnas, S. Maekawa, J. Konig, and G. Schon, "*Kondo effect in quantum dots coupled to ferromagnetic leads"* Physical Review Letters **91** (2003).

[93] D. Goldhaber-Gordon, H. Shtrikman, D. Mahalu, D. Abusch-Magder, U. Meirav, and M. A. Kastner, "*Kondo effect in a single-electron transistor"* Nature **391,** 156-159 (1998).

[94] J. C. Slonczewski, "*Conductance and exchange coupling of two ferromagnets separated by a tunneling barrier"* Physical Review B **39,** 6995 (1989).

[95] M. Y. Zhuravlev, E. Y. Tsymbal, and A. V. Vedyayev, "*Impurity-assisted interlayer exchange coupling across a tunnel barrier"* Physical Review Letters **94** (2005).

[96] W. Wetzels, G. E. W. Bauer, and M. Grifoni, "*Exchange effects on electron transport through single-electron spin-valve transistors"* Physical Review B **74** (2006).

[97] A. Hubsch, J. C. Lin, J. Pan, and D. L. Cox, "*Correlated hybridization in transition-metal complexes"* Physical Review Letters **96** (2006).

[98] H. Shimada, K. Ono, and Y. Ootuka, "*Driving the Single Electron device with a Magnetic Field"* J. App. Phys. **93,** 8259 (2000).

[99] M. Sindel, L. Borda, J. Martinek, R. Bulla, J. Konig, G. Schon, S. Maekawa, and J. von Delft, "*Kondo quantum dot coupled to ferromagnetic leads: Numerical renormalization group study"* Physical Review B **76** (2007).

[100] J. J. Henderson, C. M. Ramsey, E. del Barco, A. Mishra, and G. Christou, "*Fabrication of nanogapped single-electron transistors for transport studies of individual single-molecule magnets"* Journal Of Applied Physics **101,** 09E102 (2007).

[101] M. H. Jo, J. E. Grose, K. Baheti, M. M. Deshmukh, J. J. Sokol, E. M. Rumberger, D. N. Hendrickson, J. R. Long, H. Park, and D. C. Ralph, "*Signatures of molecular magnetism in single-molecule transport spectroscopy"* Nano Letters **6,** 2014-2020 (2006).

[102] S. Voss, M. Fonin, U. Rudiger, M. Burgert, and U. Groth, "*Experimental observation of a band gap in individual Mn-12 molecules on Au(111)"* Applied Physics Letters **90,** 133104 (2007).

[103] A. A. Houck, J. Labaziewicz, E. K. Chan, J. A. Folk, and I. L. Chuang, "*Kondo effect in electromigrated gold break junctions"* Nano Letters **5,** 1685-1688 (2005).

[104] Y. Luo, C. P. Collier, J. O. Jeppesen, K. A. Nielsen, E. Delonno, G. Ho, J. Perkins, H. R. Tseng, T. Yamamoto, J. F. Stoddart, and J. R. Heath, "*Two-dimensional molecular electronics circuits"* Chemphyschem **3,** 519-+ (2002).

[105] M. A. Reed and J. M. Tour, "*Computing with molecules"* Scientific American **282,** 86-93 (2000).

[106] M. Galperin, A. Nitzan, S. Sek, and M. Majda, "*Asymmetric electron transmission across asymmetric alkanethiol bilayer junctions"* Journal Of Electroanalytical Chemistry **550,** 337-350 (2003).

[107] X. D. Cui, A. Primak, X. Zarate, J. Tomfohr, O. F. Sankey, A. L. Moore, T. A. Moore, D. Gust, L. A. Nagahara, and S. M. Lindsay, "*Changes in the electronic properties of a molecule when it is wired into a circuit"* Journal Of Physical Chemistry B **106,** 8609-8614 (2002).

[108] D. J. Wold and C. D. Frisbie, "*Fabrication and characterization of metal-molecule-metal junctions by conducting probe atomic force microscopy"* Journal Of The American Chemical Society **123,** 5549-5556 (2001).

[109] P. Tyagi, D. F. Li, S. M. Holmes, and B. J. Hinds, "*Molecular electrodes at the exposed edge of metal/insulator/metal trilayer structures"* Journal Of The American Chemical Society **129,** 4929-4938 (2007).

[110] S. W. Howell, S. M. Dirk, K. Childs, H. Pang, M. Blain, R. J. Simonson, J. M. Tour, and D. R. Wheeler, "*Mass-fabricated one-dimensional silicon nanogaps for hybrid organic/nanoparticle arrays"* Nanotechnology **16,** 754-758 (2005).

[111] G. J. Ashwell, P. Wierzchowiec, C. J. Bartlett, and P. D. Buckle, "*Molecular electronics: connection across nano-sized electrode gaps"* Chemical Communications**,** 1254-1256 (2007).

[112] P. H. Townsend and T. A. Brunner, "*Elastic Relationships In Layered Composite Media With Approximation For The Case Of Thin-Films On A Thick Substrate"* Journal Of Applied Physics **62,** 4438-4444 (1987).

[113] D. R. Franca and A. Blouin, "*All-optical measurement of in-plane and out-of-plane Young's modulus and Poisson's ratio in silicon wafers by means of vibration modes"* Measurement Science & Technology **15,** 859-868 (2004).

[114] W. Bruckner, S. Baunack, M. Hecker, J. Thomas, S. Groudeva-Zotova, and C. M. Schneider, "*Oxidation of NiFe(20 wt.%) thin films"* Materials Science And Engineering B-Solid State Materials For Advanced Technology **86,** 272-275 (2001).

[115] Y. S. Song, S. J. Park, T. W. Kim, and C. W. Chung, "*Influence of wet chemical cleaning on properties of magnetic tunnel junction stack for magnetic RAM"* Electrochemical And Solid State Letters **7,** C64-C66 (2004).

[116] P. Tyagi, D. F. Li, S. M. Holmes, and B. J. Hinds, "*Molecular Electrodes at the Exposed Edge of Metal/Insulator/Metal Trilayer Structures"* Journal Of The American Chemical Society **129,** 4929-4928 (2007).

[117] C. E. Inman, S. M. Reed, and J. E. Hutchison, "*In situ deprotection and assembly of S-tritylalkanethiols on gold yields monolayers comparable to those prepared directly from alkanethiols"* Langmuir **20,** 9144-9150 (2004).

[118] Z. Mekhalif, F. Laffineur, N. Couturier, and J. Delhalle, "*Elaboration of self-assembled monolayers of n-alkanethiols on nickel polycrystalline substrates: time, concentration, and solvent effects"* Langmuir **19,** 637-645 (2003).

[119] W. Oepts, H. J. Verhagen, R. Coehoorn, and W. J. M. de Jonge, "*Analysis of breakdown in ferromagnetic tunnel junctions"* Journal Of Applied Physics **86,** 3863-3872 (1999).

[120] H. Li, J. L. Sun, and L. P. Huang, "*Effects of ductile cobalt on fracture behavior of Al2O3-TiC ceramic"* Materials Science And Engineering A-Structural Materials Properties Microstructure And Processing **323,** 17-20 (2002).

[121] T. L. Anderson, "*Fracture Mechanics: Fundamental and Applications"* Fracture Mechanics: Fundamental and Applications (CRC Press Boston) (1995).
[122] R. F. Egerton, P. Li, and M. Malac, "*Radiation damage in the TEM and SEM"* Micron **35,** 399-409 (2004).
[123] C. Herring and J. K. Galt, "*Elastic And Plastic Properties Of Very Small Metal Specimens"* Physical Review **85,** 1060-1061 (1952).
[124] D. Kim, B. Heiland, W. D. Nix, E. Arzt, M. D. Deal, and J. D. Plummer, "*Microstructure of thermal hillocks on blanket Al thin films"* Thin Solid Films **371,** 278-282 (2000).
[125] K. S. Yoon, J. H. Park, J. H. Choi, J. Y. Yang, C. H. Lee, C. O. Kim, J. P. Hong, and T. W. Kang, "*Performance of Co/Al2O3/NiFe magnetic tunnel junctions prepared by a two-step rf plasma oxidation method"* Applied Physics Letters **79,** 1160-1162 (2001).
[126] J. Chen, M. A. Reed, A. M. Rawlett, and J. M. Tour, "*Large on-off ratios and negative differential resistance in a molecular electronic device"* Science **286,** 1550-1552 (1999).
[127] C. P. Collier, E. W. Wong, M. Belohradsky, F. M. Raymo, J. F. Stoddart, P. J. Kuekes, R. S. Williams, and J. R. Heath, "*Electronically configurable molecular-based logic gates"* Science **285,** 391-394 (1999).
[128] J. K. N. Mbindyo, T. E. Mallouk, J. B. Mattzela, I. Kratochvilova, B. Razavi, T. N. Jackson, and T. S. Mayer, "*Template synthesis of metal nanowires containing monolayer molecular junctions"* Journal Of The American Chemical Society **124,** 4020-4026 (2002).
[129] D. I. Gittins, D. Bethell, D. J. Schiffrin, and R. J. Nichols, "*A nanometre-scale electronic switch consisting of a metal cluster and redox-addressable groups"* Nature **408,** 67-69 (2000).
[130] R. Beckman, E. Johnston-Halperin, Y. Luo, J. E. Green, and J. R. Heath, "*Bridging dimensions: Demultiplexing ultrahigh-density nanowire circuits"* Science **310,** 465-468 (2005).
[131] N. A. Melosh, A. Boukai, F. Diana, B. Gerardot, A. Badolato, P. M. Petroff, and J. R. Heath, "*Ultrahigh-density nanowire lattices and circuits"* Science **300,** 112-115 (2003).
[132] H. Gossner, F. Wittmann, I. Eisele, T. Grabolla, and D. Behammer, "*Vertical Mos Technology With Sub-0.1-Mu-M Channel Lengths"* Electronics Letters **31,** 1394-1396 (1995).
[133] L. D. Qin, S. Park, L. Huang, and C. A. Mirkin, "*On-wire lithography"* Science **309,** 113-115 (2005).
[134] J. Berg, P. Lundgren, P. Enoksson, and S. Bengtsson, "*Low frequency noise in silicon nanogaps"* Applied Physics Letters **87** (2005).
[135] S. M. Dirk, S. W. Howell, S. Zmuda, K. Childs, M. Blain, R. J. Simonson, and D. R. Wheeler, "*Novel one-dimensional nanogap created with standard optical lithography and evaporation procedures"* Nanotechnology **16,** 1983-1985 (2005).
[136] F. Maya, A. K. Flatt, M. P. Stewart, D. E. Shen, and J. M. Tour, "*Formation and analysis of self-assembled monolayers from U-shaped oligo(phenylene ethynylene)s as candidates for molecular electronics"* Chemistry Of Materials **16,** 2987-2997 (2004).
[137] H. B. Akkerman, P. W. M. Blom, D. M. de Leeuw, and B. de Boer, "*Towards molecular electronics with large-area molecular junctions"* Nature **441,** 69-72 (2006).
[138] D. M. Jeon, J. W. Park, D. H. Lee, S. Y. Yoon, D. H. Yoon, and S. J. Suh, "*Annealing effect on the barrier properties and TMR of magnetic tunneling junctions fabricated in various oxidation conditions"* Journal Of Magnetism And Magnetic Materials **272-76,** 1956-1958 (2004).
[139] D. R. Lide, 79 ed., edited by D. R. Lide (1998-1999).
[140] C. M. Ruan, T. Bayer, S. Meth, and C. N. Sukenik, "*Creation and characterization of n-alkylthiol and n-alkylamine self-assembled monolayers on 316L stainless steel"* Thin Solid Films **419,** 95-104 (2002).

[141] J. S. Moodera, X. Hao, G. A. Gibson, and R. Meservey, "*Electron-Spin Polarization In Tunnel-Junctions In Zero Applied Field With Ferromagnetic Eus Barriers"* Physical Review Letters **61,** 637-640 (1988).

[142] B. Ricco and M. Y. Azbel, "*Physics Of Resonant Tunneling - The One-Dimensional Double-Barrier Case"* Physical Review B **29,** 1970-1981 (1984).

[143] M. Di Ventra, S. T. Pantelides, and N. D. Lang, "*The benzene molecule as a molecular resonant-tunneling transistor"* Applied Physics Letters **76,** 3448-3450 (2000).

[144] F. Anariba and R. L. McCreery, "*Electronic conductance behavior of carbon-based molecular junctions with conjugated structures"* Journal Of Physical Chemistry B **106,** 10355-10362 (2002).

[145] S. Piccinin, A. Selloni, S. Scandolo, R. Car, and G. Scoles, "*Electronic properties of metal-molecule-metal systems at zero bias: A periodic density functional study"* Journal Of Chemical Physics **119,** 6729-6735 (2003).

[146] D. V. Averin and Y. V. Nazarov, "*Virtual Electron-Diffusion During Quantum Tunneling Of The Electric Charge"* Physical Review Letters **65,** 2446-2449 (1990).

[147] C. S. Park, "*Crossover between pure quantum and thermally assisted tunneling in a molecular magnet with tetragonal symmetry"* Journal Of Magnetism And Magnetic Materials **267,** 281-288 (2003).

[148] X. D. Cui, X. Zarate, J. Tomfohr, O. F. Sankey, A. Primak, A. L. Moore, T. A. Moore, D. Gust, G. Harris, and S. M. Lindsay, "*Making electrical contacts to molecular monolayers"* Nanotechnology **13,** 5-14 (2002).

[149] A. Troisi and M. A. Ratner, "*Molecular signatures in the transport properties of molecular wire junctions: What makes a junction "molecular"?"* Small **2,** 172-181 (2006).

[150] G. S. McCarty, "*Molecular lithography for wafer-scale fabrication of molecular junctions"* Nano Letters **4,** 1391-1394 (2004).

[151] C. S. Ah, Y. J. Yun, J. S. Lee, H. J. Park, D. H. Ha, and W. S. Yun, "*Fabrication of integrated nanogap electrodes by surface-catalyzed chemical deposition"* Applied Physics Letters **88,** 133116 (2006).

[152] B. Kim, S. J. Ahn, J. G. Park, S. H. Lee, Y. W. Park, and E. E. B. Campbell, "*Temperature-dependent molecular conduction measured by the electrochemical deposition of a platinum electrode in a lateral configuration"* Applied Physics Letters **85,** 4756-4758 (2004).

[153] X. F. Guo, J. P. Small, J. E. Klare, Y. L. Wang, M. S. Purewal, I. W. Tam, B. H. Hong, R. Caldwell, L. M. Huang, S. O'Brien, J. M. Yan, R. Breslow, S. J. Wind, J. Hone, P. Kim, and C. Nuckolls, "*Covalently bridging gaps in single-walled carbon nanotubes with conducting molecules"* Science **311,** 356-359 (2006).

[154] N. Chopra, W. T. Xu, L. E. De Long, and B. J. Hinds, "*Incident angle dependence of nanogap size in suspended carbon nanotube shadow lithography"* Nanotechnology **16,** 133-136 (2005).

[155] M. A. Guillorn, D. W. Carr, R. C. Tiberio, E. Greenbaum, and M. L. Simpson, "*Fabrication of dissimilar metal electrodes with nanometer interelectrode distance for molecular electronic device characterization"* Journal Of Vacuum Science & Technology B **18,** 1177-1181 (2000).

[156] L. F. Sun, S. N. Chin, E. Marx, K. S. Curtis, N. C. Greenham, and C. J. B. Ford, "*Shadow-evaporated nanometre-sized gaps and their use in electrical studies of nanocrystals"* Nanotechnology **16,** 631-634 (2005).

[157] A. T. A. Wee, S. X. Wang, and K. Sin, "*In-situ characterization of oxide growth for fabricating spin-dependent tunnel junctions"* Ieee Transactions On Magnetics **35,** 2949-2951 (1999).

[158] N. Nakamura, K. Uno, and Y. Ogawa, "*Icosane-1,20-dithiol"* Acta Crystallographica Section E-Structure Reports Online **57,** o505-o507 (2001).
[159] J. G. Simmons, "*Generalized Formula For Electric Tunnel Effect Between Similar Electrodes Separated By A Thin Insulating Film"* Journal Of Applied Physics **34,** 1793 (1963).
[160] E. Atanassova and D. Spassov, "*X-ray photoelectron spectroscopy of thermal thin Ta2O5 films on Si"* Applied Surface Science **135,** 71-82 (1998).
[161] J. M. Seminario, C. E. De la Cruz, and P. A. Derosa, "*A theoretical analysis of metal-molecule contacts"* Journal Of The American Chemical Society **123,** 5616-5617 (2001).
[162] T. Hirai, H. Morita, and M. Tasaka, "*Current-voltage characteristics and conductivity of metal-insulator-metal (Ti/TaOx/Ta) type thin-film diode"* Japanese Journal Of Applied Physics Part 1-Regular Papers Short Notes & Review Papers **39,** 657-661 (2000).
[163] W. Y. Wang, T. Lee, and M. A. Reed, "*Mechanism of electron conduction in self-assembled alkanethiol monolayer devices"* Physical Review B **68,** 035416 (2003).
[164] M. A. Green, "*Third generation photovoltaics: solar cells for 2020 and beyond"* Physica E-Low-Dimensional Systems & Nanostructures **14,** 65-70 (2002).
[165] S. M. Sze, "*Physics of Semiconductor Devices, 2nd Edition, John Wiley & Sons"*.
[166] L. O. Grondahl, "*The copper-cuprous-oxide rectifier and photoelectric cell"* Reviews Of Modern Physics **5,** 0141-0168 (1933).
[167] M. Nolan and S. D. Elliott, "*The p-type conduction mechanism in Cu2O: a first principles study"* Physical Chemistry Chemical Physics **8,** 5350-5358 (2006).
[168] A. Mittiga, E. Salza, F. Sarto, M. Tucci, and R. Vasanthi, "*Heterojunction solar cell with 2% efficiency based on a Cu2O substrate"* Applied Physics Letters **88,** 163502 (2006).
[169] E. N. Grossman, T. E. Harvey, and C. D. Reintsema, "*Controlled barrier modification in Nb/NbOx/Ag metal insulator metal tunnel diodes"* Journal Of Applied Physics **91,** 10134-10139 (2002).
[170] A. M. Glass, D. V. D. Linde, D. H. Auston, and T. J. Negran, "*Excited-State Polarization, Bulk Photovoltaic Effect And Photorefractive Effect In Electrically Polarized Media"* Journal Of Electronic Materials **4,** 915-943 (1975).
[171] P. Rottlander, M. Hehn, O. Lenoble, and A. Schuhl, "*Tantalum oxide as an alternative low height tunnel barrier in magnetic junctions"* Applied Physics Letters **78,** 3274-3276 (2001).
[172] A. A. Kaplyanskii, S. A. Basun, U. Happek, R. S. Meltzer, and G. M. Salley, "*Photoionization related phenomena in doped insulators: The role of inversion site symmetry of impurity centers"* Radiation Effects And Defects In Solids **155,** 1-9 (2001).
[173] W. F. Brinkman, R. C. Dynes, and J. M. Rowell, "*Tunneling Conductance Of Asymmetrical Barriers"* Journal Of Applied Physics **41,** 1915-& (1970).
[174] C. de Buttet, M. Hehn, F. Montaigne, C. Tiusan, G. Malinowski, A. Schuhl, E. Snoeck, and S. Zoll, "*Low-resistance magnetic tunnel junctions with an MgO-Al2O3 composite tunnel barrier: Asymmetric transport characteristics and free electron modeling of a self-limited oxidation bilayer"* Physical Review B **73,** 104439 (2006).
[175] M. F. Gillies, A. E. T. Kuiper, R. Coehoorn, and J. Donkers, "*Compositional, structural, and electrical characterization of plasma oxidized thin aluminum layers for spin-tunnel junctions"* Journal Of Applied Physics **88,** 429-434 (2000).
[176] E. Suzuki, D. K. Schroder, and Y. Hayashi, "*Carrier Conduction In Ultrathin Nitrided Oxide-Films"* Journal Of Applied Physics **60,** 3616-3621 (1986).
[177] P. Rottlander, M. Hehn, and A. Schuhl, "*Determining the interfacial barrier height and its relation to tunnel magnetoresistance"* Physical Review B **65,** 054422 (2002).
[178] N. Novkovski, "*Conduction and charge analysis of metal (Al, W and Au)-Ta2O5/SiO2-Si structures"* Semiconductor Science And Technology **21,** 945-951 (2006).

[179] V. P. Singh and J. C. McClure, "*Design issues in the fabrication of CdS-CdTe solar cells on molybdenum foil substrates"* Solar Energy Materials And Solar Cells **76,** 369-385 (2003).

[180] K. Kukli, T. Aaltonen, J. Aarik, J. Lu, M. Ritala, S. Ferrari, A. Harsta, and M. Leskela, "*Atomic layer deposition and characterization of HfO2 films on noble metal film substrates"* Journal Of The Electrochemical Society **152,** F75-F82 (2005).

[181] L. S. Dorneles, R. L. Sommer, and L. F. Schelp, "*Tunnel magnetoresistance in NiFe/TaOx/Al2O3/Co junctions with a thin TaOx layer"* Journal Of Applied Physics **91,** 7971-7973 (2002).

[182] Y. Jeliazova, M. Kayser, B. Mildner, A. W. Hassel, and D. Diesing, "*Temperature stability of thin anodic oxide films in metal/insulator/metal structures: A comparison between tantalum and aluminium oxide"* Thin Solid Films **500,** 330-335 (2006).

[183] Z. Luo and J. Gao, "*Rectifying characteristics and photovoltaic effect in heterojunctions of La0.9Sr0.1MnO3/Nb-doped SrTiO3"* Journal Of Applied Physics **100,** 056104 (2006).

[184] P. Tyagi, D. F. Li, S. M. Holmes, and B. J. Hinds, "***Fabrication of Stable Molecular Electrode Using Patterned Edge of a Metal/Insulator/Metal Junction"*** Nanotechnology, 2006. IEEE-NANO 2006. Sixth IEEE Conference **1,** 70-73 (2006).

[185] J. Sune, I. Placencia, N. Barniol, E. Farres, F. Martin, and X. Aymerich, "*On The Breakdown Statistics Of Very Thin Sio2-Films"* Thin Solid Films **185,** 347-362 (1990).

[186] J. Faure-Vincent, C. Tiusan, C. Bellouard, E. Popova, M. Hehn, F. Montaigne, and A. Schuhl, "*Interlayer magnetic coupling interactions of two ferromagnetic layers by spin polarized tunneling (vol 89, art no 107206, 2002)"* Physical Review Letters **89** (2002).

[187] C. Kittel, *Intorduction to Solid State Physics*, 7th ed. (John Wiley & Sons, Inc, New York, 1996).

[188] R. R. Gareev, L. L. Pohlmann, S. Stein, D. E. Burgler, P. A. Grunberg, and M. Siegel, "*Tunneling in epitaxial Fe/Si/Fe structures with strong antiferromagnetic interlayer coupling"* Journal Of Applied Physics **93,** 8038-8040 (2003).

[189] S. O. Demokritov, "*Biquadratic interlayer coupling in layered magnetic systems"* Journal Of Physics D-Applied Physics **31,** 925-941 (1998).

[190] J. Lindner and K. Baberschke, "*Ferromagnetic resonance in coupled ultrathin films"* Journal Of Physics-Condensed Matter **15,** S465-S478 (2003).

[191] A. Layadi, "*Ferromagnetic resonance modes in coupled layers with cubic magnetocrystalline anisotropy"* Journal Of Applied Physics **83,** 3738-3743 (1998).

[192] I. L. Soroka, R. Brucas, V. Stanciu, P. Nordblad, and B. Hjorvarsson, "*Enhanced magnetic moment at the interfaces in Fe81Ni19/Co superlattices"* Journal Of Magnetism And Magnetic Materials **277,** 228-235 (2004).

[193] C. C. Yu and A. K. Petford-Long, "*Effect of ferromagnetic layer structure on the magnetization process in NiFe/Co/Al-O/NiFe and Co/NiFe/Al-O/NiFe junctions"* Journal Of Applied Physics **85,** 5753-5755 (1999).

[194] P. **Tyagi**, B. Hinds, D. F. Li, and S. M. Holmes, "*Insulator Film Thickness to Fix the Spacing between Electrodes to Molecular Length Scale"* International Conference on Nano/Micro Engineered and Molecular Systems, NEMS '07. 2nd IEEE **1,** 191-194 (2007).

[195] X. Hao, J. S. Moodera, and R. Meservey, "*Spin-Filter Effect Of Ferromagnetic Europium Sulfide Tunnel Barriers"* Physical Review B **42,** 8235-8243 (1990).

[196] M. J. T. Michael Ziese, *Spin Electronics (Lecture Notes in Physics)* (Springer Verlag, 2001).

[197] K. Baberschke, "*Why are spin wave excitations all important in nanoscale magnetism?"* Physica Status Solidi B-Basic Solid State Physics **245,** 174-181 (2008).

[198] M. Yoshikawa, E. Kitagawa, S. Takahashi, T. Kai, M. Amano, N. Shimomura, T. Kishi, S. Ikegawa, Y. Asao, H. Yoda, K. Nagahara, H. Numata, N. Ishiwata, H. Hada, and S.

Tahara, "*Reduction of switching field distributions by edge oxidization of submicron magnetoresistive tunneling junction cells for high-density magnetoresistive random access memories"* Journal Of Applied Physics **99** (2006).

[199] W. Oepts, H. J. Verhagen, D. B. de Mooij, V. Zieren, R. Coehoorn, and W. J. M. de Jonge, "*Observation and analysis of breakdown of magnetic tunnel junctions"* Journal Of Magnetism And Magnetic Materials **199,** 164-166 (1999).

[200] W. F. Egelhoff, L. Gan, H. Ettedgui, Y. Kadmon, C. J. Powell, P. J. Chen, A. J. Shapiro, R. D. McMichael, J. J. Mallett, T. P. Moffat, M. D. Stiles, and E. B. Svedberg, "*Artifacts in ballistic magnetoresistance measurements (invited)"* Journal Of Applied Physics **95,** 7554-7559 (2004).

[201] P. J. Jensen, K. H. Bennemann, P. Poulopoulos, M. Farle, F. Wilhelm, and K. Baberschke, "*Enhanced induced magnetization in coupled magnetic trilayers in the presence of spin fluctuations"* Physical Review B **60,** R14994-R14997 (1999).

[202] L. Sheng, D. Y. Xing, and D. N. Sheng, "*Theory of impurity resonant tunnel magnetoresistance"* Physical Review B **69** (2004).

Vita

Pawan Tyagi was born on 13th of April, 1975 in Meerut, India. He received his Bachelor of Technology degree in Metallurgical and Materials Engineering from Indian Institute of Technology, Roorkee (formerly Univ. of Roorkee) in 1998. Next he served as a quality control engineer at Midhani, India. At Midhani he specialized in nondestructive testing methods and earned Level-2 certificate in ultrasonic testing. In 2000 he joined Indian Institute of Technology Kanpur to pursue a Mater of Technology degree at Materials and Metallurgical Engineering.

To pursue a career in teaching and research Pawan Tyagi joined PhD program at Chemical and Materials Engineering, University of Kentucky in 2002. During his research as a graduate student he has been associated with center of nanoscience and technology (CeNSE). He has been awarded a certificate of honor for his role in improving the functioning of CeNSE in 2005.

He has received numerous travel awards to attend international conferences and academic activities. During his stay at University of Kentucky, he was an active member of Green thumb environmental group. Pawan Tyagi has also represented chemical and materials engineering department at Graduate Student Congress for 2007-2008 session. He is currently working as postdoctoral fellow in Prof. David Gracias's lab at John Hopkins University.

Pawan Tyagi possesses a multidisciplinary background. He specializes in fabrication and characterization of micro/nano magnetic/electronic devices and nanostructures. His future interests are:

- Novel concepts and devices for energy production.
- Molecular spintronics devices and the study of novel magnetic nanostructures.
- Electronic devices (e.g. devices with molecules, nanowires and nanotubes).
- Chemical and biological sensing (with the main emphasis on neurosensors)
- Biomedical devices

PUBLICATIONS

[Published/Accepted]

1. **Pawan Tyagi**, B.J. Hinds, D.F. Li, S. Holmes, "Fabrication of Molecular Electrodes on the Exposed Edge of Metal-Insulator-Metal Structure," *Journal of American Chemical Society,* 2007, 129, 4929-38.

2. **Pawan Tyagi**, B.J. Hinds, D.F. Li, S. Holmes, **"**Insulator Film Thickness to Fix the Spacing between Electrodes to Molecular Length Scale" IEEE NTC Review of Advances in Micro, Nano, and Molecular Systems. (Accepted) (Also presented at 2nd IEEE International Conference on Nano/Micro Engineered and Molecular Systems, 2007. NEMS '07.)

3. **Pawan Tyagi**, B.J. Hinds, D.F. Li, S. Holmes, **"**Fabrication of Stable Molecular Electrode Using Patterned Edge of a Metal/Insulator/Metal Junction" In refereed proceedings of Sixth IEEE conference on Nanotechnology, 2006. IEEE-NANO 2006. Volume 1, 17-20 June 2006, 70 – 73.

[Submitted]

4. **Pawan Tyagi**, B.J. Hinds, D.F. Li, S. Holmes, "Role of Mechanical Stresses in Fabrication of Molecular Electrodes on the Exposed Edge of Multilayer Structure," **(**IEEE Transaction on Nanotechnology).

[In preparation]

5. **Pawan Tyagi**, D.F. Li, S. Holmes, B.J. Hinds "Molecular Scale Electrodes from the Controlled Oxidation of the Cross Junction Geometry". (Nanotechnology).

6. **Pawan Tyagi**, D.F. Li, S. Holmes, B.J. Hinds "Molecular Cluster Induced Antiferromagnetic Coupling between Two Magnetic Electrodes".

7. **Pawan Tyagi**, D.F. Li, S. Holmes, B.J. Hinds "Dramatic Current Suppression by Magnetic Molecular Junction".

8. **Pawan Tyagi** and B.J. Hinds, "TaOx Thin Film Photovoltaic Devices".

9. Bing Hu, **Pawan Tyagi**, Nitin Chopra, B.J. Hinds, "Zinc Oxide Nanowire Growth at the Exposed Edge of Si/Al2O3 Multilayer Patterns for nm-Scale Shadow Lithography".

PAPERS PRESENTATION IN CONFERENCES

1. **Pawan Tyagi**, B.J. Hinds, D.F. Li, S. Holmes, "Large Current Suppression and Dramatic Magnetic Ordering by Molecular Channels on the Exposed Edge of Magnetic Tunnel Junction" , Materials Research Society, November 26-29, 2007, Boston, USA

2. B.J. Hinds, **Pawan Tyagi** "Dramatic Resistance Increase and Magnetic Ordering with Magnetic Molecular Electrodes" Molecular Conduction & Sensing Workshop July 18-20, 2007, Purdue University.

3. **Pawan Tyagi**, B.J. Hinds, "Dramatic Resistance Increase and Magnetic Ordering with Molecular Spin Valve Electrodes" Electronic Materials Cconference-2007, University of Notre Dame.

4. **Pawan Tyagi**, B.J. Hinds, D.F. Li, S. Holmes, "Fabrication of Molecular Electrodes on Exposed Edge Tunnel Junction", American Physical Society, March Meeting 2007, Denver, Colorado.

5. B.J. Hinds, **Pawan Tyagi**, D.F. Li, S. Holmes, "Molecular Spintronics Electrodes" American Physical Society March Meeting 2007, Denver, Colorado.

6. **Pawan Tyagi**, B.J. Hinds, D.F. Li, S. Holmes, "Insulator Film Thickness to Fix the Spacing between Electrodes to Molecular Length Scale" IEEE- Nano/Micro Engineered and Molecular Systems -2007 Bangkok, Thailand.

7. **Pawan Tyagi**, B.J. Hinds, D.F. Li, S. Holmes "Scheme of Preparing Molecular Electrode at the Exposed Edge of Tunnel Junction Structure EPSCOR -2006, Louisville.

8. **Pawan Tyagi**, B.J. Hinds, D.F. Li, S. Holmes , "Fabrication of Molecular Electrode at the Exposed Edge of Tunnel Junction Structure", IEEE-Nano-2006, Cincinnati

9. **Pawan Tyagi**, B.J. Hinds, D.F. Li, S. Holmes, "Molecular Electrodes at the Exposed Edge of Metal-Insulator-Metal Junctions" Electronic Materials Conference 2006. University of Pennsylvania, College Park.

10. **Pawan Tyagi**, B.J. Hinds, D.F. Li, S. Holmes., "Mechanical Stress Induced Instabilities in Tunnel barriers", Electronic Materials Conference -2005. University of California, Santa Barbara.

MEMBERSHIP

- ACS (American Chemical Society)
- APS (American Physical Society)
- ISNT (Indian Society of Non Destructive Testing) life member.

AWARDS AND ACHIEVEMENTS

1. Certificate of honor for the contribution/improvement in the functioning of Center of Nanoscience and Engineering (CeNSE), University of Kentucky July-2004
2. **Secured 17th National Rank** in Graduate Aptitude Test for Engineers (GATE)-2000 (National level test for master program with scholarship in India).
3. Achieved prestigious **Level-2** certificate in Ultrasonic Testing, from American Society of Nondestructive Testing-June/2000.
4. Achieved prestigious **Level -2** "Fluorescent and Normal Liquid Penetration Testing" from Indian Society of Non Destructive Testing- May/1999.
5. NSF funded travel award from University of Illinois Urbana Champaign to attend summer school on **Quantum Monte Carlo Simulations**-2008, Italy Trieste.
6. Student travel awards from (a) GaAsMantech organization in 2001 (b) Electronic Material Conference 2005-2007 (c) University of Kentucky in 2005-2007.
7. "Adventurer of the Year Award" from Himalayan Explorer Club, 1997, IIT Roorkee.
8. **Six** gold medals in rowing competitions from1996 to1998, IIT-Roorkee, India.